Lost landslides: Rock-avalanche occurrence and fluvial censoring processes on South Island, New Zealand

Rupert H.T. Bainbridge

Ph.D.

2017

Lost landslides: Rock-avalanche occurrence and fluvial censoring processes on South Island, New Zealand

Rupert H.T. Bainbridge

A thesis submitted in partial fulfilment of the requirements for the award of Doctor of Philosophy of the University of Northumbria at Newcastle

This research was undertaken in the
Department of Geography
Faculty of Engineering and Environment

Date: 11/2017

Abstract

Rock-avalanches (RAs) are a large (typically >10^6 m^3) and extremely rapid (30 >100 m/s) type of landslide. RAs pose a significant hazard as they can runout over long distances and generate secondary hazards such as tsunami and unstable, cross-valley dams. Previous research on the distribution of rock-avalanche deposits (RADs) on the South Island, New Zealand has suggested that there are fewer deposits than would be expected for a seismically active, high-mountain region. This is due to their removal from the sedimentary record (censoring) by fluvial erosion, glacial entrainment, vegetation cover, sub-aqueous occlusion and deposit misidentification. Censoring of deposits skews magnitude-frequency relationships of RA occurrence and hinders hazard planning. This research examines processes acting to fluvially censor RADs on the South Island. 268 known, and 47 possible RADs were identified to provide the first RAD inventory for the entire South Island. The temporal distribution of RADs indicates censoring of the record over the Holocene. >500 year intervals exist between RA events from 12,000 to 2,000 years ago; A more complete record is shown for the last 1,000 to 100 years with intervals of >50 - <150 years. The last 100 years shows phases of co-seismic RAD generation, a period of RAD quiescence and a recent increase in aseismic RAD occurrence. The spatial distribution of RADs suggests that the West Coast, Fiordland and Nelson could have experienced fluvial censoring of deposits. The sediment routing characteristics of catchments in these regions, where the majority of rivers have direct pathways from RADs to the ocean, suggest that fluvially reworked RAD material could be stored within alluvial flats and braidplains.

Agglomerate grains (microscopic grains which are diagnostic of RAs) were used to identify fluvially reworked RAD material. Grains were detected in dam-breach flood terraces up to 1km downstream of known RADs. Contemporary river sediment samples showed no agglomerate presence, this suggests that 1) agglomerates break down under extended fluvial transport, 2) they are not supplied to river systems outside of flood events, 3) agglomerates become diluted by other river sediment or 4) they become buried in discrete sedimentary layers. In order to investigate the redistribution of coarse RAD material within South Island rivers, a micro-scale flume model was developed. Using ultra-violet sand as a novel analogue for a RAD, the redistribution of material through an idealised South Island catchment could be examined. The model showed that RAD material is deposited in discrete aggradational layers in dam proximal locations. Downstream, the sedimentary signal is rapidly diluted by ordinary river sediment flux.

The research shows that the RAD record for the South Island is incomplete and that fluvial censoring is prevalent within the West Coast, Nelson and Fiordland. The agglomerate tracing method can be used to identify the presence of RADs in fluvial systems proximal to RADs but the signal is undetectable after ~1km from the deposit. Both field sampling and flume modelling show that localised flood derived aggradational layers, close to deposit locations, will archive reworked RAD material. These results have important implications for understanding the magnitude and frequency of RADs within New Zealand and other similar high-mountain, tectonically active regions of the globe.

Table of contents

List of figures

Chapter 4

Chapter 5

List of tables

List of abbreviations

AF – *Alpine Fault*

DEM – *Digital elevation model*

D_{50} – *Median grain-size value of the grain-size distribution; 50% of the material is coarser and 50% of the material is finer*

EIL – Earthquake induced landslide

ESA – *Eastern Southern Alps*

FI - *Fiordland*

Fr – Froude number

GCP – *Ground control point*

GSD – *Grain size distribution*

GSF – *Grain size fraction*

LGM – *Last glacial maximum*

LINZ – *Land Information New Zealand*

LRISP – *Land Resource Information Systems Portal*

MA – *Marlborough*

MM – *Modified Mercalli*

MFZ – *Marlborough Fault Zone*

NEL -*Nelson*

NZ – *New Zealand*

OSL – *Optically stimulated luminescence*

OT – *Otago*

RAD(s) – *Rock-avalanche deposit(s)*

RA(s) – *Rock-avalanche(s)*

Re – Reynolds number

RGB – *Red, Green, Blue*

RMS – *Root mean squared*

SA – *Southern Alps*

SAMD – *Southern Alps main divide*

SEM – *Scanning electron microscope*

SE – *Secondary electron*

SfM – *Structure from Motion*

UV – *Ultra violet*

We – Weber number

WSA – *Western Southern Alps*

Acknowledgements

I would first like to thank my supervisors, Dr. Stuart Dunning, Prof. John Woodward and Dr. Mike Lim for their input and support throughout this project. Stu, thanks for instigating the project in the first place and listening to my digressions on various topics before getting me back onto the straight and narrow. John, you have been instrumental in actually getting me to the point of finishing the thesis; thank you for helping me focus down on the final product as it were! Mike, thank you for coming on board mid-PhD and providing guidance and advice on a project already well into its journey.

Also at Northumbria University, I have to give my thanks to the technicians Lesley Dunlop, Dave Thomas, Rebecca Payne and Will Thomas for their help in the Geography labs (especially at short notice). Dr. Pietro Maiello was integral to helping me with analysis on the SEM; his patience with training, microscope fixing and general advice for sample preparation was invaluable and I appreciate all the time he gave to help. Thanks also to Lisa Harrison for her advice with running the flume model.

I would like to acknowledge the support of the Digital Globe Foundation who supplied aerial imagery for some of the fieldsites and the British Society for Geomorphology for their support of my New Zealand fieldwork with the Postgraduate Research Grant. Special mention here to my good friend Kate Bazeley (Laaa) for her help in the field; I dragged you through some rainy and muddy places for samples, again! Thanks for helping out and keeping me company ☺ Also on the New Zealand side, I would like to thank Prof. Tim Davies, Cathy Higgins and Jenny Ladley for help with fieldsites, equipment and a comfortable field station to stay in! Tim, thank you also for your interest in the project and emails with new rock-avalanches for the inventory!

Thank you to everyone in the PGR office for your friendship, support and making the last few years great, in and out of university! Kate and Mark, we started together and (kind of) finished together, all the best to you both; thank you for being a sounding board so many times and making the office seem a bit saner. Tom, Pete, Steph, Clare, Bradley, Jack and Sina, thanks for all the great times over the years; it won't feel the same not having us all together to plan ridiculous trips or let our hair down at Cosy's. Looking forward to catching up with you all soon...Devon II I think.

Finally, I'd like to thank The Ladz (+ honorary members Truemanshow & Estevez), Mum, Dad, my brother Ed, and the rest of the family for being there for the last few years through the good and the bad. I can always count on you for some moral support and a good session setting the world to rights. Without everyone's help I could not have finished the project, I am grateful to you all!

Declaration

I declare that the work contained in this thesis has not been submitted for any other award and that it is all my own work. I also confirm that this work fully acknowledges opinions, ideas and contributions from the work of others.

Any ethical clearance for the research presented in this thesis has been approved. Approval has been sought and granted by the University Ethics on 18/12/13.

I declare that the Word Count of this Thesis is **44,965** words

Name: Rupert H T Bainbridge

Signature:

Date: **06/11/17**

Aoraki/Mt Cook on the South Island, the tallest peak in New Zealand. In 1991 a 2.4 x 10^6 m^3 rock-avalanche fell from the eastern flank of the mountain down the Hochstetter ice fall and onto the Tasman Glacier. After two field-seasons of having Mt. Cook shrouded in cloud whenever I visited, I finally managed to see its peak on the last day of a conference trip in 2015. It was well worth the wait! The New Zealand landscape has certainly provided constant entertainment during my fieldwork.

Chapter 1

Introduction

1.1 Rock-avalanches

Landslides are failures and movement of a rock mass, sediment or soil under the influence of gravity (Clague, 2013). They are a major geological hazard around the world and include very small (~10 m^3) to very large movements (≥10^8 m^3; Hancox and Perrin, 2009; Hungr et al., 2013; Varnes, 1978). Rock-avalanches (RAs) are a subset type of landslides that are large (typically >10^6 m^3), extremely rapid (30 - >100 m/s), often hypermobile, flow-like movements of dry, granular material that result from the disintegration of a rock-mass (Dunning, 2006; Hermanns, 2013; Pudasaini and Miller, 2013; Dufresne et al., 2016a, 2016b). They generate distinctive deposit morphology and sedimentology which have recently been used to examine the transport and emplacement processes at work when RAs occur (Dufresne et al., 2016a).

Rock-avalanche deposits (RADs) have been observed in almost every major mountain range around the world. As a non-extensive list encompassing six continents this includes; the Argentinian and Chilean Andes (Sepúlveda and Moreiras, 2013), Tien Shan and Pamir Mountains in Kyrgyzstan (Havenith et al., 2003; Strom and Korup, 2006; Hewitt et al., 2008; Robinson et al., 2014), the Himalayas (Hewitt, 2011; Blöthe et al., 2015), Norwegian fjords (Blikra et al., 2005, 2006), European Alps (Schoeneich et al., 2008; Fischer et al., 2012), Moroccan Atlas mountains (Hughes et al., 2014), Greenland (Kelly, 1980; Pedersen et al., 2002), the USA (Schulz et al., 2008; Stock and Uhrhammer, 2010; Bessette-Kirton and Coe, 2016; Castleton et al., 2016) and New Zealand's Southern Alps (Whitehouse and Griffiths, 1983; Hancox et al., 1997; Korup, 2003; Allen et al., 2011).

RAs have immediate detrimental impacts on the physical environment and infrastructure; they have also been directly responsible for loss of life including the 1962 Nevados Huascaran, Peru RA which killed ~4000 people (Plafker and Ericksen, 1978) and the Hattian Bala RA in northern Pakistan which killed ~1000 people (Dunning et al., 2007). Secondary geo-hazards such as tsunamis (Ward, 2001; Blikra et al., 2005; Masson et al., 2006; Robinson and Davies, 2013) or relatively unstable landslide dams which develop lakes upstream (Costa and Schuster, 1988; Korup, 2002; Ermini and Casagli, 2003; Evans et al., 2006; Korup and Tweed, 2007; Hancox and Perrin, 2009; Korup et al., 2010) can be generated when RAs collapse into water bodies or narrow mountain valleys respectively.

This makes RAs an important landscape process to understand and predict as they pose a hazard to life and infrastructure at considerable distances from the deposit. Predicting the hazards posed by RAs around the world requires detailed inventories of deposits and source areas to allow magnitude-frequency relationships to be examined. Unfortunately, landslide inventories are often incomplete; this has been shown to be the case in studies around the world regardless of the scale at which research studies are conducted. Global examples include, catchment scale research by Geertsema and Clague, (2006) in British Columbia, Van Den Eeckhaut and Hervás (2012) examining national landslide databases in Europe, Hewitt et al., (2008) examining mountain range scale inventories in the Himalayas, and Allen et al., (2011) examining a regional RAD inventory in the Southern Alps, New Zealand. Incomplete landslide inventories are produced when deposits are eroded or obscured from the sedimentary record by censoring processes such as fluvial erosion, glacial entrainment, vegetation cover, sub-aqueous occlusion and deposit misidentification (Korup, 2005b; Evans et al., 2006; Allen et al., 2011; Smith et al., 2012; Dunning et al., 2015;). Calculations of landslide magnitude-frequency relationships, an important aspect of landslide hazard quantification, are aided by having more complete landslide inventories (Evans et al., 2006).

Research has progressed on quantifying the censoring of deposits via glacial and subaqueous censoring processes. Dykstra, (2012) used bathymetric maps and sub-bottom profiling of Milford Sound, NZ to reveal 26 previously undetected $>10^6$ m^3 landslides, whilst Dunning et al., (2015) used ground penetrating radar to examine the rapid sequestration of a RAD into the Grand Plateau ice field in NZ. However, little research attention has been paid to quantifying the loss of RADs through fluvial censoring processes. As fluvial censoring is the only censoring process to actively rework material from the deposit, rather than passively transport or obscure, it would be necessary to trace fluvially reworked RAD sediment within the river system in order to detect censored deposits. Tracing of fluvially reworked RAD material and inference of a censored deposit could be achieved through the detection of agglomerates (microscopic grains which are diagnostic of RAs; Reznichenko et al., 2012), in river sediment; this is further explored in Chapter 3. Therefore, key themes explored within this thesis will be 1) the evidence for fluvial censoring of RADs within NZ and, 2) how diagnostic sedimentology of RADs can be used to infer their presence within river systems. The following chapter will review our current knowledge of RA generation, deposit morphology, deposit sedimentology and censoring processes, as well as their impacts on mountain river systems.

1.2 RA preconditioning, preparatory and triggering factors

The timing of RAs is dependent on the interplay of preconditioning, preparatory and triggering factors (Table 1.1; Glade and Crozier, 2004; McColl, 2012, 2015; McColl

Table 1.1 Preconditioning, preparatory and triggering factors associated with the generation of RAs around the world (Glade and Crozier, 2004; McColl, 2012, 2015)

Factors	Preconditioning	Preparatory	Trigger
Lithology	Always		
Intact rock strength	Always		
Rock mass quality	Always		
Joint characteristics	Often		
Structure (e.g. bedding)	Often		
Pre-glacial erosion	Often		
Pre-existing stresses	Often		
Debutressing		Sometimes	Sometimes?
Glacial erosion		Often	Unknown
Sheet jointing		Often	Often
Static fatigue		Always	Unknown
Seismicity		Unknown	Often
Climatic changes:			
Water		Unknown	Often
Permafrost		Sometimes	Often?
Weathering		Always?	Unknown

and Davies, 2013). Preconditioning factors are inherent rock-mass properties that primarily control the stability of a rock-slope. Preparatory factors are exterior influences to the rock mass, which reduce the stability of a given slope over time but do not cause failure or movement. Triggering factors turn a slope from being ‘marginally stable’ to being ‘actively unstable’, causing collapse.

1.2.1 Preconditioning factors

Preconditioning factors include local lithology, intact rock strength, rock-mass quality and joint characteristics (Hewitt et al., 2008). The intact rock strength determines the threshold height and angle that a slope can maintain before failure by a triggering factor. The lithology (e.g. hard basaltic rocks or softer mudstones) and slope geometry, such as fall height and gradient, can influence the type of landslide produced (McColl, 2012, 2015). Joints and bedding discontinuities within the rock mass can impact the

structural strength depending on if they are dipping into or out of the slope (Glade and Crozier, 2004). Outward dipping structures provide structural weaknesses, failure plains and permeable layers where material can be weakened and dislodge from the slope. Inward dipping or horizontal structures provides stability to the slope and can allow steep cliff formation (McColl, 2015).

1.2.2 Preparatory factors

Preparatory factors shift the stability of the slope from 'stable' to a 'marginally stable' state (Glade and Crozier, 2004). Some preparatory factors may operate over long time periods such as tectonic uplift, weathering and climate change (Glade and Crozier, 2004); whilst others can be short term changes such as glacial erosion, rainfall infiltration, sheet joint formation, static fatigue and glacial debuttressing (McColl, 2015). Some preparatory factors can also be triggering factors and vice versa (Popescu, 1994; McColl, 2012, 2015).

A major control on RA generation in mountain regions is the occurrence of high-angled, oversteepened slopes (Fischer et al., 2012). Slopes may become oversteepened through regional tectonic uplift, glacial rebound and slope undercutting by fluvial, glacial and marine erosion (McColl, 2015). This oversteepening leads to areas of topography that exceed the stable threshold slope angles for that intact rock mass. Blöthe et al. (2015) term volumes of material above threshold slope angles 'excess topography'. In the Himalayas, these areas of excess topography are mostly found near or below median elevations for the mountain range along major fluvial and glacial gorges. Himalayan rock slope failures are typically generated in these excess topography zones (Blöthe et al., 2015).

Changes in stress fields within a given rock mass can begin to destabilise slopes. Tectonic uplift can cause the formation of stress-induced rock mass jointing. Climate change is also capable of driving processes that alter rock stress fields. This includes sheet joint formation when compressive stresses from glacier ice on the rock mass are released during deglaciation (Table 1.1; McColl, 2012), as well as modifying slope hydrology and adjusting weather patterns; all of which could reduce slope stability (Evans et al., 2006; Allen et al., 2008; Krautblatter and Moore, 2014). Ballantyne et al., (2014) show a higher rate of catastrophic rock-slope failures clustering 1.6-1.7ky after glacial retreat. They infer this time lag is a response to stress release by deglacial unloading which leads to rock mass strength degradation through the development of failure planes. Linked to deglaciation is the process of glacial debuttressing. Glaciers provide a force onto the base of a slope which then buttresses the slope. If glacial ice is removed, the unloading process can reduce the stability of the slope for subsequent trigger factors

(McColl, 2012). The time since deglaciation of a landscape has also been shown to be a factor in the occurrence of slope failures.

In the European Alps there is a growing concern for the triggering of rock slope failures due to climate warming. Evidence suggests that permafrost degradation (trigger factor) associated with warming temperatures (preparatory factor) has led to reduced stability of rocks masses (Krautblatter and Moore, 2014; Haeberli et al., 2015) as permafrost acts to bind highly fractured rock material together (Bodin et al., 2015). In the Southern Alps (SA) of NZ, there is currently insufficient evidence to show that extremely warm temperatures are triggering increased rockfall activity (Allen and Huggel, 2013). Within the mountain ranges of the South Island the distribution of permafrost appears to be limited to zones above ~2000 m a.s.l. in the Southern Alps and above ~2150m a.s.l. in the Inland Kaikoura Range to the north-east (Sattler et al., 2016). This constitutes a relatively small high-mountain zone compared to the areal extent of mountain ranges within the South Island. Allen et al. (2011) show that many bedrock landslides are occurring within the lower boundaries of permafrost areas and in zones of recent glacier recession. However it is not yet possible to link the occurrence of these landslides with the degradation of permafrost, atmospheric warming and perennial ice melt, as the effects of these factors are hard to distinguish from tectonic and other climatic forcing in NZ (Allen et al., 2011).

1.2.3 Triggering factors

Commonly triggering factors are external forces on the rock mass such as earthquakes, rainfall and permafrost degradation. Permafrost degradation has already been discussed in relation to preparatory factors. Rainfall can be a preparatory or triggering factor and has been cited as both for RADs (Hancox and Thomson, 2013). Rainfall will have a greater impact on RAD generation depending upon the intensity of a given rainfall event and the rock-mass properties, i.e. lithology and permeability. In the Himalayas pre-historic RAs have been attributed to intensified monsoons and increases in bedrock porewater pressure (Dortch et al., 2009). Heavy rainfall events before earthquakes are also thought precondition slopes and considerably increase the number of landslides produced (Hancox, 2010).

On plate boundaries where terrain is actively uplifting there is also a high-likelihood of earthquakes which may trigger RADs (e.g. Himalayas, Southern Alps, Andes). Earthquakes that are >M6, with depths of <45km and shaking intensities of ≥MM9 (Modified Mercalli) are thought to be capable of co-seismically triggering RAs (Hancox et al., 2002; Cox and Barrell, 2007). Rock masses subjected to earthquake shaking can experience ground acceleration producing instantaneous shear stresses which overcome the rock strength, propagate fractures through the rock mass and increase porewater

pressure; all of which may trigger slope failure (McColl, 2015). Earthquake induced shaking can also be viewed as a preparatory factor mechanism. It is also thought that if slopes do not fail during earthquakes then they may have been sufficiently weakened so that further earthquake shaking will produce more slope failures (Parker et al., 2015).

Some slope failures occur without any noticeable trigger mechanism (McSaveney, 2002; Korup, 2006a; McSaveney et al., 2015). Whilst rainfall and earthquakes are often thought of as the main triggers for slope failures a lack of a known triggering factor is surprisingly common. Events with no known trigger could be associated with gradual weakening of the rock mass, which lowers the rock mass strength below that which can be overcome by gravitationally induced stress (Glade and Crozier, 2004).This is examined by Rosser (2010) who suggests that damage to a hillslope is cumulative. Therefore extrinsic environmental forcing events (preparatory factors), such as storms or earthquakes, as well as long term effects such as weathering, which do not make a slope fail serve to only cumulatively weaken a rock mass. Eventually the rock mass reaches a critical threshold of stability and fail catastrophically without any apparent trigger (Rosser, 2010).

1.3 RAD morphology and sedimentology

Morphologically, RADs typically display hummocky surface features, sometimes arranged linearly in a radial pattern (McColl and Davies, 2011; Barth, 2014), can have lobate flow fronts and long run-out distances (Davies and McSaveney, 1999; Evans, 2008). Sedimentologically they are characterised by three major facies, (1) boulder carapace, (2) body facies and (3) basal facies (Fig. 1.1; Dufresne et al., 2016a; Dunning and Armitage, 2011).

The carapace is an ~1-10m thick surface feature consisting of angular, open-framework boulders (Weidinger et al., 2014), which can account for up to 30% of the thickness of the deposit (Dunning et al., 2005). Typically the carapace facies thins with greater distance from the RA source and provides much of the over-burden pressure which drives the intense comminution of material within the body and basal facies (Weidinger et al., 2014; Dufresne et al., 2016a). It has been anecdotally suggested by Dufresne et al., (2016a) that topographic confinement of RAs during motion may influence the comminution of the carapace material and that more confined run-out paths may produce smaller carapace material.

The carapace overlies the body facies, a mostly fine grained layer which often comprises the majority of the deposit (Fig. 1.1; Dufresne et al., 2016a; Dunning et al., 2006). The body facies often retains the lithological stratigraphy from the source area

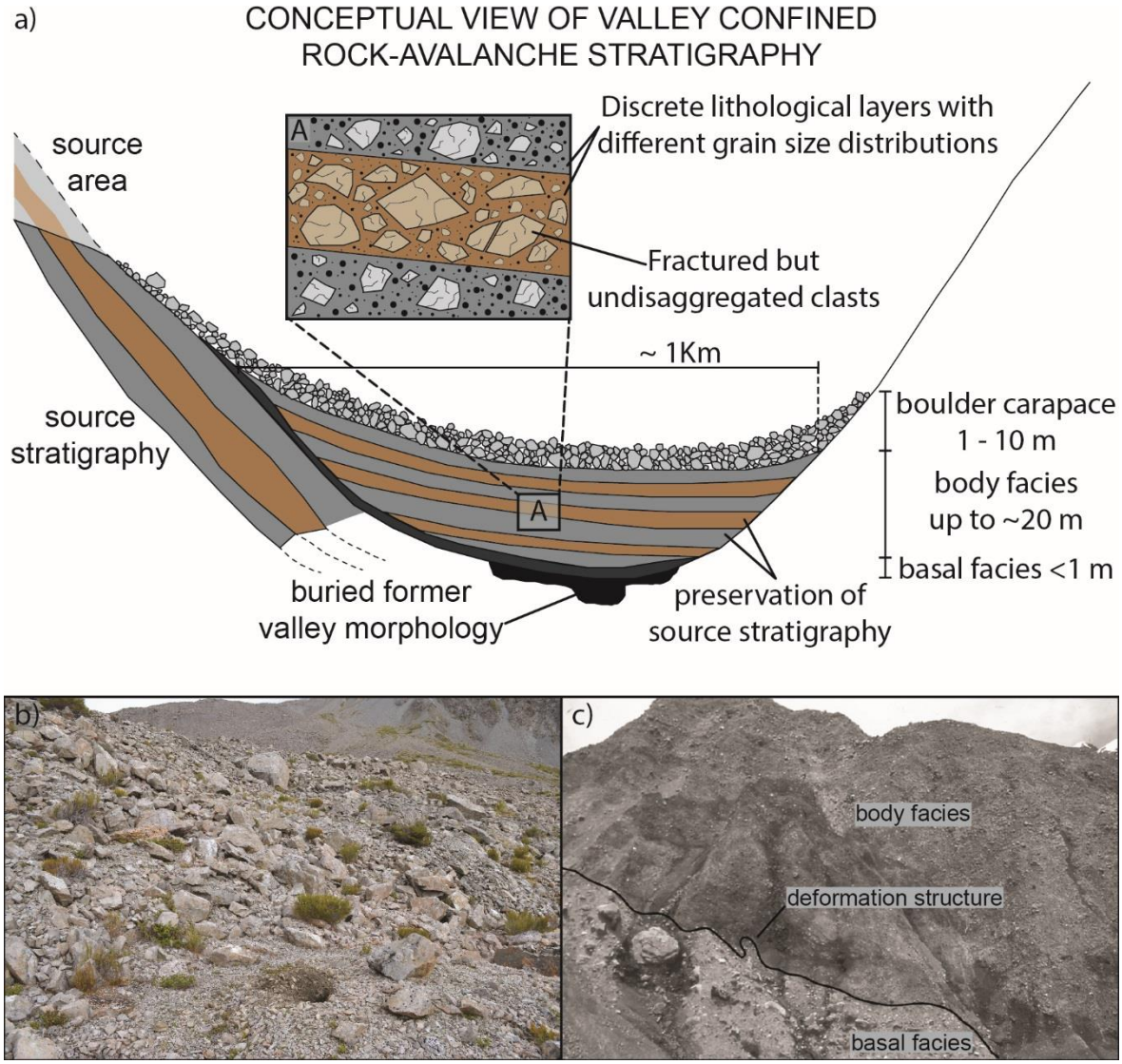

Fig. 1.1 a) Conceptual view of RAD stratigraphy within a valley confined setting based upon descriptions of deposits in Dufresne et al., 2016a; Dunning and Armitage, 2011; Harrison et al., 2015; Wang et al., 2013, the inset A shows a zoomed section of the RAD indicating changes in the grain size distribution of the deposit depending upon the separation of discrete lithological layers; b) Photograph of the Falling Mountain RAD, NZ boulder carapace; c) Photograph of the body and basal facies of the Falling Mountain RAD from Dunning et al., (2005).

(Dunning and Armitage, 2011; Dufresne et al., 2016a) as stretched sub-horizontal banding (Dunning et al., 2005).

Given this stratigraphic preservation, variations in grain-size and the presence of highly-fractured but undisaggregated clasts have been observed depending on the lithological zonation in RADs (Fig. 1.1aA; Dufresne et al., 2016a; Dunning and Armitage, 2011; Hewitt, 2009a; Weidinger et al., 2014).

The basal facies underlies the deposit and represents a zone where the RA has interacted and incorporated material from existing valley substrate during motion (Fig. 1.1). This facies is rarely exposed (unless RADs have been deeply incised by rivers) as it is typically buried under the rest of the deposit (Dunning and Armitage, 2011). The facies

often contains deformation structures such as faulting, folding and shear bands (Dufresne et al., 2016a). Evidence of substrate entrainment in RADs can be observed as material mixing, dyke formation and rip-up clasts (Hewitt, 2009a; Dufresne et al., 2016a). Additionally, substrate material that has been altered by the passing RA can be included in this facies such as material mobilised in front of the RA and modified bedrock structures (Dunning and Armitage, 2011).

RAs in the literature often have a minimum volume of ≥ 1 x 10^6 m^3, this is an approximate threshold under which the hypermobility processes, which drive the distinct deposit sedimentology associated with this type of landslide, are not usually seen (Davies and McSaveney, 2009). Hypermobility results in the excessive runout length often observed with RADs, which is further than would be expected for dry granular material under normal frictional conditions (Davies and McSaveney, 2009; Hungr et al., 2013). This excessive runout can vary between deposits given the morphological and geological differences encountered by RAs during motion. However, the runout distance of a rock avalanche appears to be related to initial rock mass volume, that is to say, larger initial rock mass volumes will produce greater runout distances (Davies and McSaveney 1999; Rait and Bowman, 2010). This has been accepted within the rock-avalanche research community since the seminal work by Hsu (1975) which first quantified this phenomenon (Fig. 1.2). The hypermobility phenomenon has been linked to many different processes such as air cushioning, frictionite formation, acoustic fluidisation, basal lubrication and dynamic fragmentation (Davies et al., 1999; Hungr, 2006; Rait et al., 2012; Pudasaini and Miller, 2013). Hypermobility of RAs is still an active area of research, however the process of dynamic fragmentation is a promising theory as it explains hypermobility whilst accounting for the production of large quantities of fine grained material in RADs (Davies et al., 1999; McSaveney and Davies, 2006; Davies and McSaveney, 2009; Rait et al., 2012).

Processes occurring during RA motion provide an extreme environment for the comminution of the source material and generation of fine grained sediment in the final deposit (Davies and McSaveney, 2009). Initially joint-controlled blocks collapse from the source area, these blocks disintegrate along pre-existing joints (Davies and McSaveney, 2002; Evans et al., 2006). The block collapse transitions into a dynamically disintegrating rock mass with apparent behaviour similar to that of a granular flow (Rait and Bowman, 2010). This dynamic fragmentation of the rock mass is driven by shear, compressional and confining stress fields within the RA flow which elastically deform clasts and grains (Davies et al., 2007). The deformation of material within the ‘flow’ drives fragmentation of clasts along newly generated failure surfaces, not pre-existing rock-mass joints such as those during the initial phase of collapse (Davies and McSaveney, 2007, 2009; Davies et al., 2007). The clasts within the deposit essentially explode creating a void space which

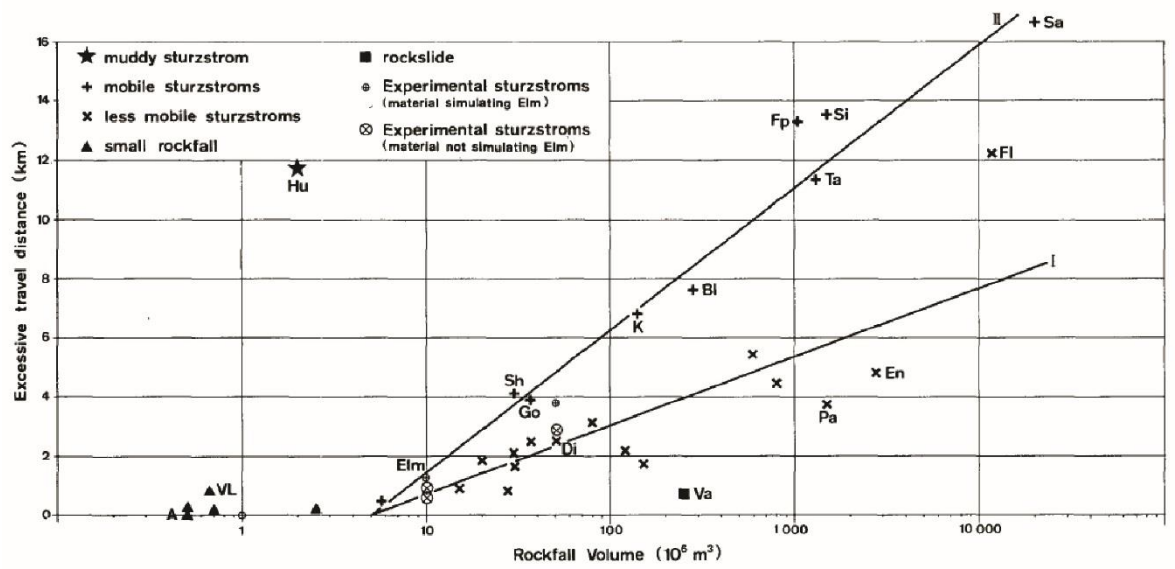

Fig. 1.2 Relationship of excessive travel distance to rockfall volume for RAs (sturzstrom) around the world from Hsu (1975). The excessive travel distance is the horizontal distance travelled by the tip of a RA beyond what would be expected for dry granular material under normal frictional conditions (without lubrication). Although all have excessive runout, there are two sub-groups, those that are more mobile and those less mobile. The steeper line represents more mobile RAs whilst the shallower line represents less mobile RAs. Abbreviations for rockfalls are as follows: A, Airolo; VL, Val Lagone; Hu, Huascaran; Sh, Sherman; Go, Goldau; Di, Diablerets; K, Kandertal; Bl, Blackhawk; Ta, Tamins; Si, Siders; Va, Vaiont; En, Engelberg; Fl, Flims; Fp, Fernpass; Pa, Palmira; Sa, Saidmarreh.

lowers the stress field around the clast. The void spaces created are rapidly closed and the stress fields continue the comminution of the material which drives the continual fining of the material within the flow (Davies and McSaveney, 2002). The continuing fragmentation of grains results in high pressure within the RA flow. This high pressure is hypothesised to support the overburdening material, reducing the force imparted on the shear layer at the base of the flow, effectively reducing the overall frictional resistance (Davies and McSaveney, 2009).

When the RA stalls there is usually a very high proportion of fine grained material within the internal structure of the deposit (McSaveney and Davies, 2006; Davies and McSaveney, 2009; Rait and Bowman, 2010). Comminution processes operate internally within the RA flow, therefore given the lower overburden pressure at the flow surface a carapace of less fragmented boulder material usually caps RADs (Deganutti, 2008). It should be noted however that not all RAs are hypermobile and that they can occur below the approximate 1 x 10^6 m^3 volume threshold (Davies and McSaveney, 1999; Allen et al., 2011); South Island examples include the Vampire Peak RADs and the Mount Beatrice RAD (Cox et al., 2008).

Recent research into the composition of the fine grained component of RADs has yielded insights into comminution processes at the microscopic level. It has been shown by Reznichenko et al., (2012) that the fine grained material produced through material comminution during RA motion contains microscopic grains which they term

‘agglomerates’. Agglomerates are coherent grains (<1mm) composed of microscopic (micron to sub-micron) particles that are diagnostic of RADs. These microscopic grains can only be identified using a scanning electron microscope (SEM) to identify the grains and on micrographs (images produced on a SEM). The work of Reznichenko et al., (2012) identified agglomerates within RAD material that had fallen onto glaciers, been supra-glacially transported and deposited as terminal moraines. This suggested that the RA diagnostic agglomerate grains were able to persist within passively rafted material for up to 10^4 years. Agglomerates could therefore be used to identify RADs that have been transported long distances from their source over thousands of years. The processes of agglomerate formation will be discussed in detail in Chapter 3.

1.3.1 RA impacts on mountain river systems

With high relief, narrow confined valley floors and river channels with resistant boundaries, mountain regions provide an ideal environment for RA generation (Korup and Tweed, 2007). Valley confined RADs are generally large enough to form cross-valley dams which instantaneously impact the equilibrium of the valley system (Fig. 1.3; Table 1.2). Flooding occurs upstream of the dam and lakes become impounded until either the dam fails or a stable overflow is established. Up to ~80% of landslide dams fail within the first year of formation (Ermini and Casagli, 2003); these dam failures can cause breach floods which drain the lakes (partially or fully) and rapidly remobilise large volumes of dam sediment downstream impacting the valley system far beyond the deposit (Cenderelli, 2000). The flooding itself can be a sizeable hazard if settlements and infrastructure reside downstream. The floods can undermine unconsolidated slopes downstream causing further slope instability away from the original RAD (Hancox et al., 2005). However over the longer term these floods can cause downstream aggradation in alluvial flats, on alluvial fans and braidplains (Hewitt, 1998; Korup et al., 2004). This rapid remobilisation of dam material can be followed by transient inputs of material from the remaining unstable dam over the long term (Hewitt, 2006; Davies and Korup, 2010). Continual reworking of these deposits can cause channel avulsion activity and the progradation of slow moving sediment pulses downstream which can disrupt habitat and infrastructure (Korup, 2004, 2005a; Hancox et al., 2005). This reworking of dam material by fluvial processes censors the deposit from the sedimentological record. Dam breaching and removal of material from the deposit obscures its original extent and can make it unrecognisable as a RAD. Over time only small remnants of the RAD may remain, of which the origin can only be deduced from detailed sedimentological study. Fluvial censoring is an important process to try to quantify as it can skew RAD magnitude-frequency relationships which has knock-on effects on hazard planning. The processes of fluvial censoring and their impacts will be discussed in detail in Section 1.4.1.

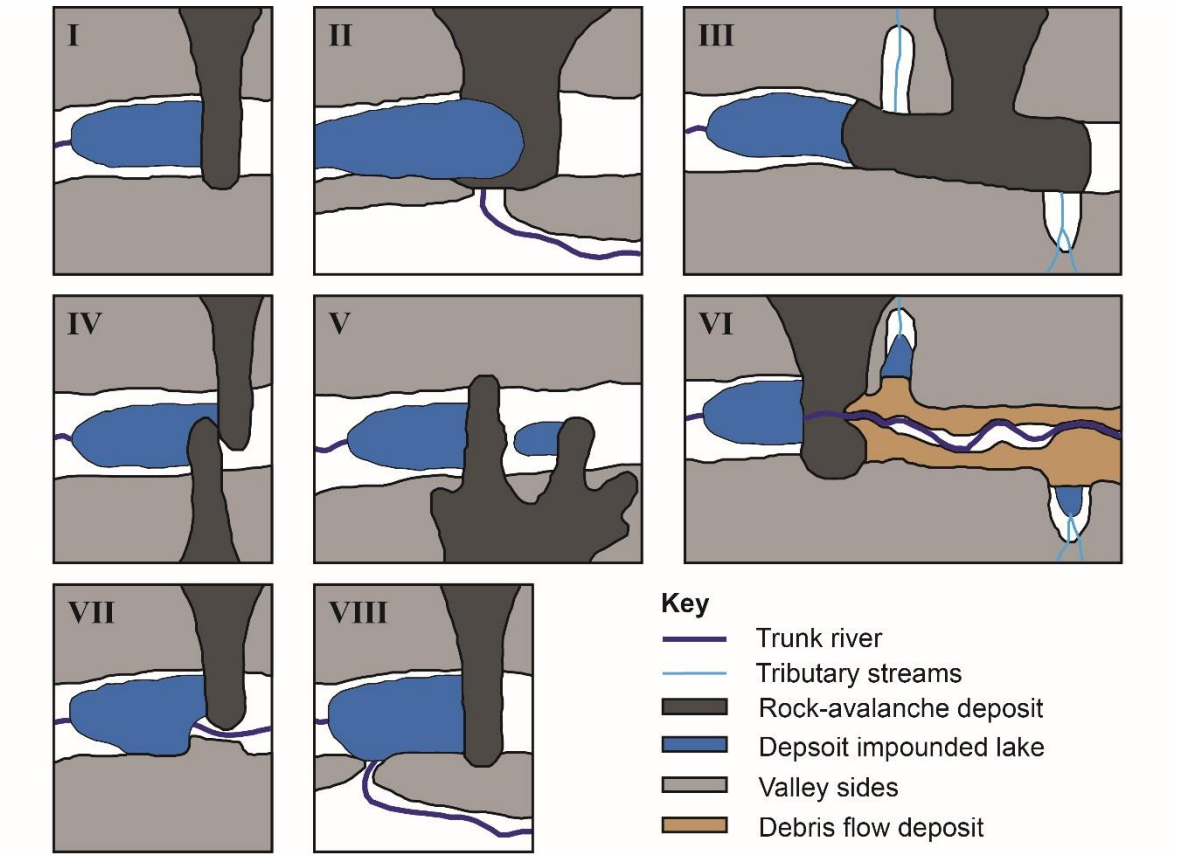

Fig. 1.3 Classification of landslide dam types within valley confined settings (after Costa and Schuster, 1988; Hermanns et al., 2011). See Table 1.2 for dam type descriptions.

Breached RA dams also drive the formation of knickpoints within river long profiles where rivers have been unable to incise back to pre-landslide bedrock (Korup, 2006b). Knickpoints in river long profiles are noticeable as overly steepened, convex river reaches separating a lower gradient upstream reach from an actively adjusting, steeper downstream reach (Korup, 2006b; Hewitt et al., 2008; Harrison et al., 2015; Bennett et al., 2016). Aggradation occurs behind breached dams when rivers are unable to mobilise sediment through the confined dam breach, this results in the development of lower gradient reaches upstream of dams. Overflow and breach channels through RADs are generally very steep compared to upstream and downstream reaches (Korup, 2006b); however breach floods can also cause rapid down valley aggradation and oversteepening of proximal downstream reaches (e.g. Harrison et al., 2015).

Alternatively, dams may remain stable and not fail catastrophically. Stable overflow channels can form over RADs and the deposit can persist in the landscape. In stable RAD dams, overflow channels are more likely to form rather than water siphoning through the deposit, as RADs have highly compacted interiors which are less permeable than other types of landslide deposit (Dunning and Armitage, 2011). Stable lake formation disrupts the sediment pathways through the valley system; fluvial material from upstream of the lake will be deposited when entering the lake and can eventually cause total infill of the lake. During this time the system downstream of the lake will be experiencing sediment

Table 1.2 Descriptions of landslide dam types based upon Costa and Schuster, (1988) and Hermanns et al., (2011). Landslide types likely to cause each dam formation are listed on the right. Conceptual models of each dam type are shown in Fig. 1.3.

Landslide dam type	Description of landslide dam and impacts	Landslide type
I	Large landslides than Type I, deposits spread across the valley width and have run-up deposits on opposite valley walls to the source area.	Avalanches, slumps, slides
II	A landslide dam formed at a drainage divide. Drainage is diverted to the lower valley however catastrophic flooding could occur in either valley if a breach was formed.	Avalanches, flows
III	Valleys are filled with landslide sediment both upstream and downstream of the source area. Very large volumes of landslide material.	Flows, avalanches
IV	Contemporaneous landslides of material from both sides of the valley. Deposits can adjoin head to head or be juxtaposed next to one another.	Falls, slumps, slides, avalanches
V	Multiple lobes of material from the same landslide fall into the valley and dam the river in multiple places. Some lobes can extend across the whole valley and some may not reach the opposite valley wall.	Falls, avalanches
VI	Chains of landslide dams causing trunk valley damming and tributary valley damming. In this example a landslide has blocked the trunk valley; dam breaching has developed into a down-valley debris flow which has subsequently blocked tributary valleys.	Avalanches, flows
VII	Similar to Type II landslide dam, however an overflow channel is formed through bedrock adjacent to the landslide dam. This means a very stable overflow is developed.	Avalanches, slumps, slides
VIII	Similar to Type II landslide dam, however drainage is shifted to a new stream course (in this example to the lower valley) and the old valley is abandoned.	Avalanches, slumps, slides

starvation due to the dam emplacement. Additionally, with the dam in place, downstream flow discharge may be lower than in pre-dam conditions; this may impact upon the ability of the river to entrain and transport larger calibre material. Formation of an overflow channel can eventually lead to the gradual excavation of the RA dam without a catastrophic breach and ensuing flood. In these cases dam crest height is reduced leading to lake drainage and remnant dam sections at the valley sides (Hewitt, 2006).

Ultimately, RADs can impact river long profiles and sedimentology thousands of years beyond the initial RAD event. In many cases it may be that the river system is

disturbed by additional RAD, hampering any recovery of the system to pre RA equilibrium (Hewitt et al., 2008; Harrison et al., 2015).

1.3.2 RA generated tsunami

RAs collapsing into water bodies may generate tsunamis which can have far reaching impacts; this extends the hazard posed by the RA beyond the initial deposit (Evans et al., 2006). Notable examples include (1) the 1934 Tafjord tsunami in Norway which reached a height of 62m and killed 41 people (Blikra et al., 2005) and (2) a cliff collapse of the flank of Mt. Campalla, Italy in 1783 which produced an 8.3m high tsunami wave killing 1500 (Bornhold and Thomson, 2012).

Unlike earthquake generated tsunamis, landslide generated tsunamis are most hazardous when formed in shallower waters (Bornhold and Thomson, 2012). The effectiveness of tsunami generation by any given landslide is governed by the volume, density and slope angle of material entering the water body. Increases in any of these factors increases the energy of tsunami waves (Bornhold and Thomson, 2012), this is why RAs (large volume, extremely fast, dense deposit) are capable of generating tsunamis. A large volume of water, usually the depth of the entire water column, must be instantaneously displaced by the RA; this displacement effect increases in likelihood when slopes next to water bodies become steeper (Pedersen et al., 2002; Berryman, 2005).

Quantification of the tsunami hazard posed from RAs is difficult as locating deposits does not intrinsically indicate that a tsunami was generated. Whilst evidence of historic RAs can be found it is difficult to discern if a tsunami was generated. It is necessary to find corresponding tsunamigenic deposits which can indicate that one was generated and the magnitude of that tsunami wave (Bornhold and Thomson, 2012). Recently many previously unknown sub-aqueously deposited landslides, including RADs, were discovered in Milford Sound, NZ (Dykstra, 2012) and in Storfjorden, Norway (Blikra et al., 2005). These were mostly pre-historic deposits and are thought to have generated tsunamis. It is currently unclear whether many more sub-aqueous deposits exist in fiords, lakes and oceans around the world, however it is a highly likely prospect given the results of the Blikra et al. (2005) and Dykstra, (2012) studies.

1.4 RAD censoring processes

In areas where RAs have occurred there are often questions as to whether the observed frequency and spatial distribution of deposits fully represents the occurrence of RAs over time. Censoring processes which remove or obscure RADs from the sedimentary record can drastically alter frequency distributions within a given area or deposit inventory (Davies and Korup, 2010). Censoring of RADs occurs through three

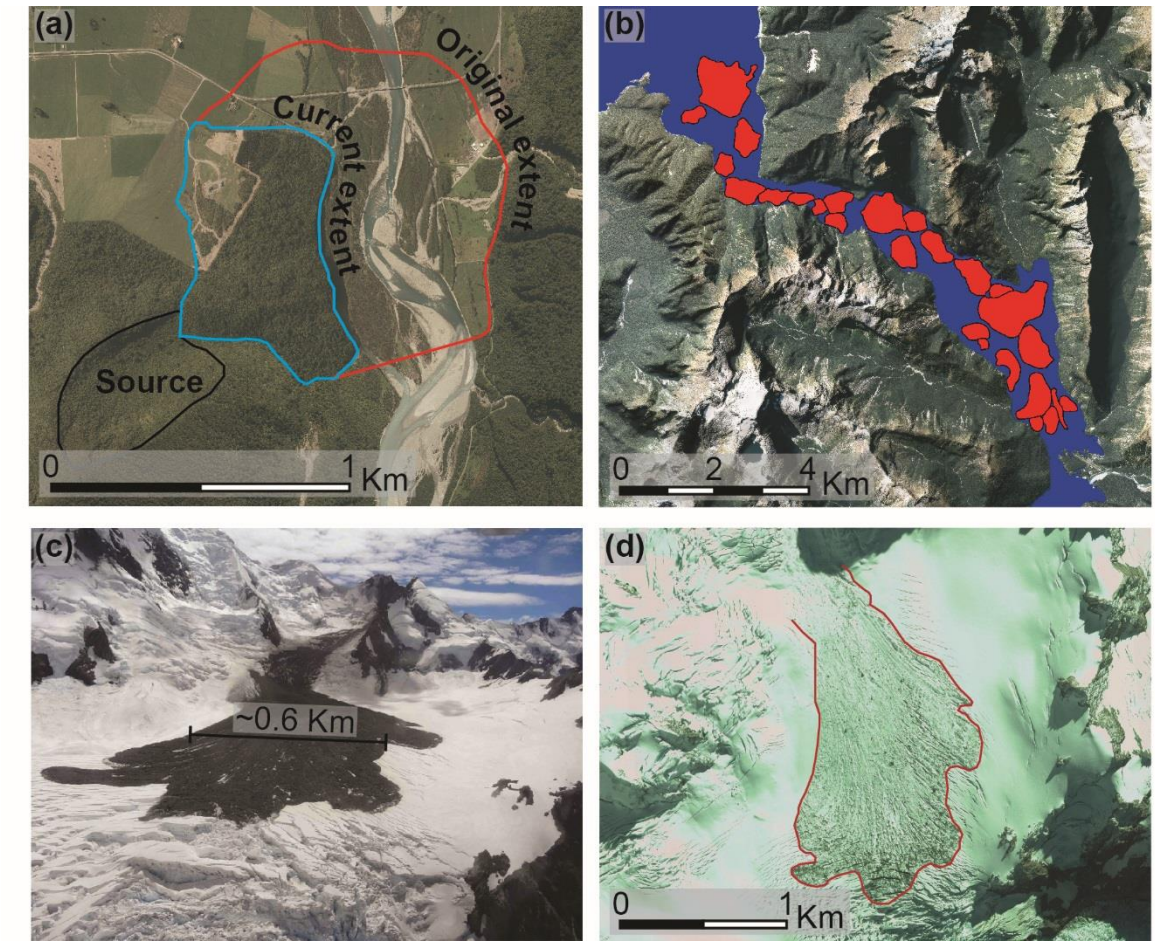

Fig. 1.4 Examples of landslide censoring mechanisms within the South Island, NZ; (a) Fluvial censoring of the ~1220CE Mt. Wilberg RA deposit by the Wanganui River (Chevalier et al., 2009). The majority of the deposit has now been removed by fluvial action. Thick vegetation also covers the remaining deposit making it relatively difficult to identify; (b) Shown in red are 26, previously undetected, large sub-aqueous landslides recently identified by Dykstra, (2012) within Milford Sound, NZ; (c) Image of the 2013 Mt. Dixon rock-avalanche, taken 25 days after failure (Dunning et al., 2015; © Charlie Hobbs); (d) Google Earth image of the 2013 Mt Dixon rock-avalanche taken on 13/04/2013 showing the rapid sequestration of the deposit into the glacier (Google Earth, 2013).

main mechanisms, (1) active landscape processes, (2) landscape features and (3) human error. Landscape processes and features which censor RADs include fluvial erosion (Fig. 1.4a; Korup, 2005b), sub-aqueous occlusion in large water bodies (Fig. 1.4b; Blikra et al., 2006; Dykstra, 2012; Taig and Mcsaveney, 2015) regrowth of vegetation on source scars (Fig. 1.4b; Chevalier et al., 2009) as well as englacial entrainment in accumulation zones and supraglacial transport and deposit deformation in ablation zones (Fig. 1.4c and d; Hewitt et al., 2008; Allen et al., 2011; Uhlmann et al., 2013; Dunning et al., 2015). In terms of human error, in-situ and reworked deposits can be misidentified in both desk based mapping activities and when examining deposits in the field; typically RADs have been misidentified as moraines or debris flows (Hewitt, 1999, 2001; Tovar et al., 2008a; Davies et al., 2013b; Reznichenko et al., 2015).

Different censoring processes are likely to have greater or lesser impacts depending upon their location. For example, in NZ's Southern Alps high rainfall in

catchment headwaters may have a significant impact on fluvial erosion processes (Barth, 2012), however in the Himalayas the semi-arid environment (Hewitt et al., 2008) may lessen the impact of rainfall and fluvial induced erosion. It is important that work continues in trying to quantify the extent to which RADs may be censored as incomplete inventories of deposits can severely impact the quantification of the magnitude and frequency of hazardous RA events. The next section will discuss and review the current state of knowledge of each of the aforementioned censoring processes in greater detail.

1.4.1 Fluvial

Fluvial erosion is thought to be one of the most pervasive censoring processes that remove RADs from the sedimentary record in mountain and valley confined environments. RAs which block valley cross-sections in narrow, high-relief valleys can be removed by trunk rivers in a relatively short time period (Korup, 2005c). Particularly in the case of RAs, as opposed to other landslide types, if a river can remove the coarse boulder carapace and erode the easily entrained fine-grained, pulverised interior then censoring of the deposit can be relatively rapid (Korup and Tweed, 2007; Davies and McSaveney, 2011; Korup, 2011). However in some cases the boulder carapace may armour an overflow channel and prevent further erosion into the deposit for the foreseeable future (Korup, 2005d), this does not however preclude further down cutting at a later date.

Given the propensity for large RADs within valley confined mountain environments to form dams, catastrophic failure is likely over the first year post-emplacement (Ermini and Casagli, 2003). Catastrophic failure of RA dams can remove large quantities of RA material within a very short space of time during the initial failure (Korup and Tweed, 2007). Subsequent to failure and lake drainage, a slower and more progressive phase of fluvial incision into the dam begins that will transiently erode material from the breached RA complex, typically during high-flows (Hewitt, 2006). Highly active landscapes, with high rainfall and rapid uplift, may increase the extent to which fluvial censoring of deposits occurs (Barth, 2012).

Whilst erosion of RADs within valley confined settings is progressive and ongoing the process of complete removal can take thousands of years leaving traces of the deposit visible in the landscape (Reznichenko et al., 2011). However, the remnant sections of deposits may be difficult to discern as having an RA origin. Over long 10^3-10^4 year timescales the progressive removal of RA material from river valleys is likely to censor deposits and make remnants difficult to visually identify (Fig. 1.4a). Where ancient deposits can be identified it is often difficult to quantify their extent and initial volume as deposit boundaries may have become modified or removed. Typically the study of RAD impacts on fluvial systems, over long 10^3-10^4 year timescales, needs to be conducted

using the channel morphology and river long profiles as indicators of ancient RADs (Ouimet et al., 2007).

1.4.2 Glacial

Two distinct processes may censor RADs in glacial environments; (1) rapid englacial entrainment of RA debris in the accumulation zone of a glacier, obscuring it from detection (Dunning et al., 2015) and (2) supraglacial transport of material away from the source area over time (Hewitt, 1999; Hewitt et al., 2008).

Dunning et al., (2015) recently showed that the 2 x 10^6 m^3 2013 Mt Haast RAD which fell onto the Grand Plateau glacial accumulation zone was undetectable to conventional remote sensing methods after just 3 months. Accumulation of snow and ice had covered the deposit removing the contrasting deposit/ice boundary as well as smoothing the deposit morphology so that surface texture did not indicate the presence of the RAD. Dunning et al., (2015) further suggest that there may be stacked sequences of large RADs within glacier accumulation zones around the world. These archives need further investigation to quantify their deposit censoring potential.

In terms of the censoring of RADs by supraglacial transport the difficulties lie in identifying deposits as RA derived rather than being other landslide and glacially derived debris. RA material may become supraglacial transported either by falling onto the surface of the glacier or being exposed from englacial ice through ice melting in the ablation zone of the glacier (Evans and Clague, 1999; Dunning et al., 2015). Exposure of englacial RA debris is usually irregular across the glacier surface complicating its identification as RA derived (Hewitt et al., 2011). For material that falls directly onto the ice in ablation zones, if not identified shortly after the occurrence of the RA the deposits can become difficult to identify. Over the short term the morphology of the deposit can become distorted by glacier movement at rates of tens to hundreds of metres per year (Hewitt et al., 2011). Supraglacial RA material can collapse into crevasses and moulins creating surface topography that is not distinctive to RADs; additionally over the longer term RA debris can become modified by weathering and transport processes on the glacier surface and take on characteristics that would not be diagnostic of RA material (Hewitt, 1999, 2009b).

Glacierised environments provide many problems with the identification of RADs in the past. RADs have commonly been misinterpreted as moraine complexes generated by climate driven glacier advance. Recently some moraines have been reinterpreted as RADs that have fallen onto glaciers, been rafted down valley on the glacier surface and formed terminal moraines. Examples of reinterpreted moraine complexes come from the Himalayan Karakoram and NZ Southern Alps (Hewitt et al., 2008; Evans, 2008; Dortch et al., 2009; Hewitt, 2009a; Reznichenko et al., 2010; McColl and Davies, 2011; Deline et al., 2015).

1.4.3 Vegetation

Censoring of large RA deposits and source scars due to the re-growth of vegetation does not appear to be a common occurrence within the global record as many of the mountain ranges where RADs are observed are high-altitude and do not sustain large areas of vegetation. However, particularly for the South Island, vegetation growth is a major problem when attempting to identify RADs (Fig. 1.4a; e.g. the Wanganui-Wilberg RAD; Chevalier et al., 2009; Malamud et al., 2004).

Vegetation cover can have two major consequences for RAD identification but can on occasion also provide valuable insights into deposit extent. The first consequence is that densely vegetated areas, such as the west coast of NZ's South Island, RADs and source scars can become completely occluded under thick forest cover. In monsoon regions of the globe, vegetation cover on large landslide deposits can establish and occlude the deposit within a few years to a decade (Barnard et al., 2001). Whilst modern events may be recorded with ease the potential for rapid vegetation colonisation and cover may make ancient deposits very difficult to identify and reliably date (Korup, 2005c).

The second consequence of vegetation cover is that when potential RADs are identified it can often be difficult to examine any surface morphology which indicates a RA origin for the material. This may lead to mis-identification of deposits if sediment sections cannot be located to confirm a RAD origin. As an example, Chevalier (2008) notes that vegetation cover on the Round Top RAD in NZ has concealed the hummocky surface topography of the deposit.

However, vegetation can also aid in the aerial delineation of RADs. Often RAs destroy large swathes of vegetation in the initial event. In some cases when vegetation regrows over the deposit there are marked differences in the surviving pre-RA and the regrown flora. These can be used to delineate the boundaries of individual deposits or multiple deposits on the same site (Nash, 2003).

1.4.4 Sub-aqueous occlusion

Another method of censoring RADs from observation is by occlusion in water bodies such as lakes and fiords. As previously mentioned RAs falling into lakes can generate large tsunamis which can have significant impacts on a given region. Given their potential impact on life and infrastructure, historical tsunami generating RADs that affect populations are often recorded. However, globally these events are sparse (Plafker and Eyzaguirre, 1979; Evans, 1989; Pedersen et al., 2002; Hermanns et al., 2006; Hilbe and Anselmetti, 2014). Few records exist to globally quantify the number of prehistoric RAs within lakes, fiords and oceans even though it is highly likely that a significant archive of RADs that may or may not have generated tsunamis is stored there.

Individual prehistoric large RAs have been recorded by lake bathymetry studies in Alaska and Norway (Bornhold et al., 2007; Lysså et al., 2010); however little work has been done to quantify the number of RADs that have been censored from the record by sub-aqueous occlusion. Recently some studies by Blikra et al., 2006 and Dykstra, 2012 have started to uncover the extent to which large RADs have impacted regional areas. Blikra et al., (2006, 2005) identified 59 previously unknown >0.5 x 10^6 m^3 RADs within the Storfjorden area in Norway which are thought to post-date the last glaciation. Similarly, work by Dykstra, (2012) and Taig and Mcsaveney, (2015) show the presence of ~26 previously unrecorded, large RADs which will almost certainly have generated tsunami waves (Fig. 1.4b). The Blikra et al., (2006) and Dykstra, (2012) studies show that within these small regions there have been large numbers of potentially hazardous RA events and that there is the potential for many more censored RAs to exist in water bodies. It is important to fully quantify the censoring via this process as without it our ability to quantify magnitude and frequency relationships of RAs as well as reliably calculate hazards is severely limited.

1.5 Research gaps

A number of research gaps have been identified from the literature review above and are detailed below;

1. RAs are known to have occurred within differing mountain regions of the South Island of New Zealand. However, no study to date has examined the distribution of all known rock-avalanching events on spatial and temporal scales across the entire island.
2. Furthermore, as a study including all known RADs on the island has not been previously carried out it is unclear to what extent censoring processes have obscured or eroded deposits within the South Island. Whilst the censoring processes documented above are known to occur, little work has currently tried to quantify their effects on magnitude frequency distributions of RADs.
3. Currently no methods exist to trace fluvially reworked RAD material and examine the extent to which deposits are fluvially censored. Fluvial censoring is the last censoring process to have not received research attention on how it affects RA inventories.
4. Sediment entrainment and transport processes in rivers are well understood but no studies have attempted to trace the redistribution of RA material through river systems to examine the censoring, transport and storage of that material.

1.6 Thesis aims and objectives

The overall aim of this thesis is to examine the processes acting to fluvially censor RADs within high-mountain environments on the South Island, NZ. As part of this the study wishes to establish whether reworked RAD material can be traced through river systems using a diagnostic micro-sedimentological signature. This diagnostic tracer could then be used to identify previously unknown, fluvially censored, RADs and recover 'lost' deposits in the sedimentological record. In order to achieve this overall aim the following research objectives have been established.

Aim 1

To examine controls on RA occurrence and censoring processes in the South Island, NZ over the Holocene period.

Specific objectives

- To develop a multi-event, multi-temporal literature based inventory of all known RADs on South Island, NZ in order to summarise the current extent of our knowledge on South Island RADs.
- To examine the spatial and temporal distribution of the inventory to determine where regional and chronologic data gaps exist or if a sampling bias exists within the literature.
- To compare the RAD distribution against spatially variable preconditioning, preparatory and triggering factors such as lithology, rock mass structure, rainfall, seismicity and tectonics; as well examining the spatial variability of censoring processes in order to determine whether gaps in the record reflect non-occurrence of RAs or censoring processes.

Aim 2

To examine the potential for the routing and storage of fluvially reworked RA material through South Island river catchments.

Specific objectives

- To map area and calculate volume attributes, using empirical area-volume relationships, for all RADs within the inventory produced in Aim 1.
- To delineate South Island river catchments and examine the potential routing and storage of fluvially reworked RA material within those catchments.

Aim 3

To ascertain whether agglomerates can be effectively utilised to trace fluvially reworked RA material through river systems as a diagnostic tool for detecting fluvially censored RADs.

Specific objectives

- To collect fine grained sediment samples from pre-selected NZ field sites.
- To conduct controlled laboratory based 'washing' experiments on RAD material and collect sediment samples at selected experimental time intervals. This allows the examination of the influence of turbulent water flow on agglomerate preservation. Turbulent fluvial transport processes are expected to modify the external morphology of agglomerate grains.
- To mount the 63µm – 1mm grain size fraction of collected sediment samples in resin for scanning electron microscope (SEM) analysis to determine agglomerate presence and morphology.
- To analyse SEM micrograph outputs from RAD, river profile and alluvial fan material to examine the strength of the agglomerate sedimentological signal away from known RAD point sources.

Aim 4

To examine the redistribution and storage of RA material in NZ river systems by modelling an idealised river system in a laboratory based micro-scale flume.

Specific objectives

- To develop a microscale flume model of an idealised river system based upon South Island prototype rivers.
- To use UV sand, as an analogue for a RAD, in order to trace the spatial and temporal patterns of sediment distribution and storage through the microscale model.
- To observe and catalogue the morphological and sedimentological response of the flume micro-scale model over time and identify reaches which store archives of fluvially censored, simulated RADs.
- To develop a conceptual model of the sedimentological impact of RADs on river systems which can be applicable to valley confined environments around the world.

1.7 Thesis structure

An introduction to the major literature defining RA occurrence in the global context has preceded the aims and objectives of the thesis. Much of the NZ specific literature concerning RA occurrence was purposefully excluded from this initial literature review as it forms much of the development of the inventory (Aim 1) and the context of Chapter 2.

Aims 1-4 above form the basis for three distinct results chapters within this thesis. Due to the differences of subject and methodological approaches within the results chapters they each contain a small literature review which is specifically relevant to the content of that chapter. A brief summary of each chapter is given below.

Chapter 2: South Island specific literature discussing the physical setting of New Zealand as well as RAD occurrence on the island will be summarised. The literature will be developed into an inventory of all known RADs on South Island over the Holocene period. The methods of inventory development, mapping and attribute calculation will be presented. Spatial and temporal distribution of RADs within the inventory will be discussed in terms of the potential for censoring of the sedimentological record of events. Using the inventory an analysis of the distribution of RAD with regard to potential landslide trigger mechanisms will be undertaken to examine whether gaps within the RAD record are controlled by trigger factors, deposit censoring or sampling bias. RAD volume and location information will then be used to determine potential sediment routing and storage areas of fluvially reworked RA material through South Island catchments.

Chapter 3: This chapter discusses field based collection and laboratory based analysis of South Island RAD sediment samples. Analysis of samples will allow an assessment whether agglomerates are an effective way of tracing fluvially reworked, RA derived material, through river systems. As a chapter specific topic, the formation and detection of agglomerate grains will be discussed at the outset of this chapter; this includes a short review of the mechanisms behind RA transport and depositional processes to which agglomerate formation is inherently linked. The rationale behind selected South Island fieldsites will be outlined as well as background to the RAD and rivers that were visited. The methodologies behind sample collection in the field, sieving and resin mounting preparation along with final sample analysis on the SEM will be outlined. Using the SEM data a discussion of the detectability of agglomerates downstream of RADs will be conducted.

Chapter 4: This chapter discusses the results of a laboratory based micro-scale flume model designed to investigate the fluvial redistribution of RAD material through South

Island river systems. The chapter will begin with a brief chapter-specific literature review of micro-scale flume modelling and structure-from-motion (SfM) photogrammetry which plays a major role in the methodology. A detailed outline of model design and setup, sand and water input quantification as well as the model workflow will be presented. The impact of RADs on the morphology and sedimentology of the flume model will be presented from the pre-RA system to long-term RAD censoring processes. UV sand will be used as an analogue for a RAD and traced through the flume model at multiple time-steps in order to examine the morphological changes in the fluvial system over time. Sub-surface stratigraphy of the model river will be examined at the end of the model runs to identify key storage areas within the idealised channel system. The morphological and sedimentological evolution of the flume will be presented as a summary model which can be used to identify potential areas of RA sediment storage and examine sediment redistribution within prototype river systems around the world.

Chapter 5: This final chapter will draw together the major findings of the three results chapters which will have used desk, field and laboratory based techniques to examine the potential for RAD censoring by fluvial processes in the South Island, NZ. Flume modelling and field studies will examine the processes by which RADs can be censored from the fluvial environment given the environmental conditions within the South Island. Processes of deposit censoring and shredding of the traceable reworked RAD material signal observed within the flume modelling will be discussed with relation to the observed field based signal of agglomerates. The potential for sedimentary archives of reworked RAD material, identified in all three results chapters, will be discussed with regard to areas which should be focussed on in future studies of identifying fluvially censored RADs. The wider significance of the research will be discussed with regard to our current knowledge of RA occurrence and the incompleteness of the sedimentary archive of these events.

Chapter 2

Distribution and controls on Holocene rock-avalanche occurrence on the South Island, New Zealand

2.1 Introduction

This chapter discusses the current body of knowledge concerning the occurrence of RAs on the South Island. To date no inventory has complied and analysed the distribution of RADs over the entire South Island. It is also apparent that major RA inventories do not cover all of the mountainous regions of the island. Therefore, in this chapter, a new multi-event, multi-temporal, literature based RA inventory is presented for the South Island. Fig. 2.1 shows an overview map of New Zealand as well as the tectonic settings of the islands and regions of interest which will be discussed in detail throughout this chapter.

Previous NZ RAD inventories show a predominance of deposits in the eastern Southern Alps (ESA) on western facing slopes (Whitehouse, 1983; Allen et al., 2011). In Fiordland and the western Southern Alps (WSA) the majority of landslides occur on slopes above modal hillslope angles of 32° (Clarke and Burbank, 2010). Clarke & Burbank (2010) hypothesise that threshold slopes, for RA generation, in Fiordland and the WSA are controlled by bedrock fracturing. In most South Island mountain ranges, large ≥M6 earthquakes are known to have triggered RAs (Hancox, 2010) and also precondition rock-masses for failure in future seismic events (Parker et al., 2015). Rainfall has been cited as both a preparatory or triggering factor for RAs in the South Island (Hancox and Thomson, 2013) and it has been suggested that heavy rainfall events before an earthquake can considerably increase the number of landslides produced co-seismically (Hancox, 2010). Some recent RAs, between 1969 and 2014, near the Southern Alps main-divide (SAMD) in the central region of the Southern Alps (SA), occurred without any apparent trigger and show an upward trend in the rate of RA generation (McSaveney, 2002) that has been linked to increasing seismic moment release (McSaveney et al., 2015). However, it is thought that RADs are underrepresented within archive landslide inventories for the South Island. Previous research has censoring by fluvial erosion (Korup, 2005b), sub-aqueous occlusion (Dykstra, 2012), regrowth of vegetation on source scars (Korup, 2002), glacial entrainment and removal (Allen et al., 2011; Dunning et al., 2015), as well as

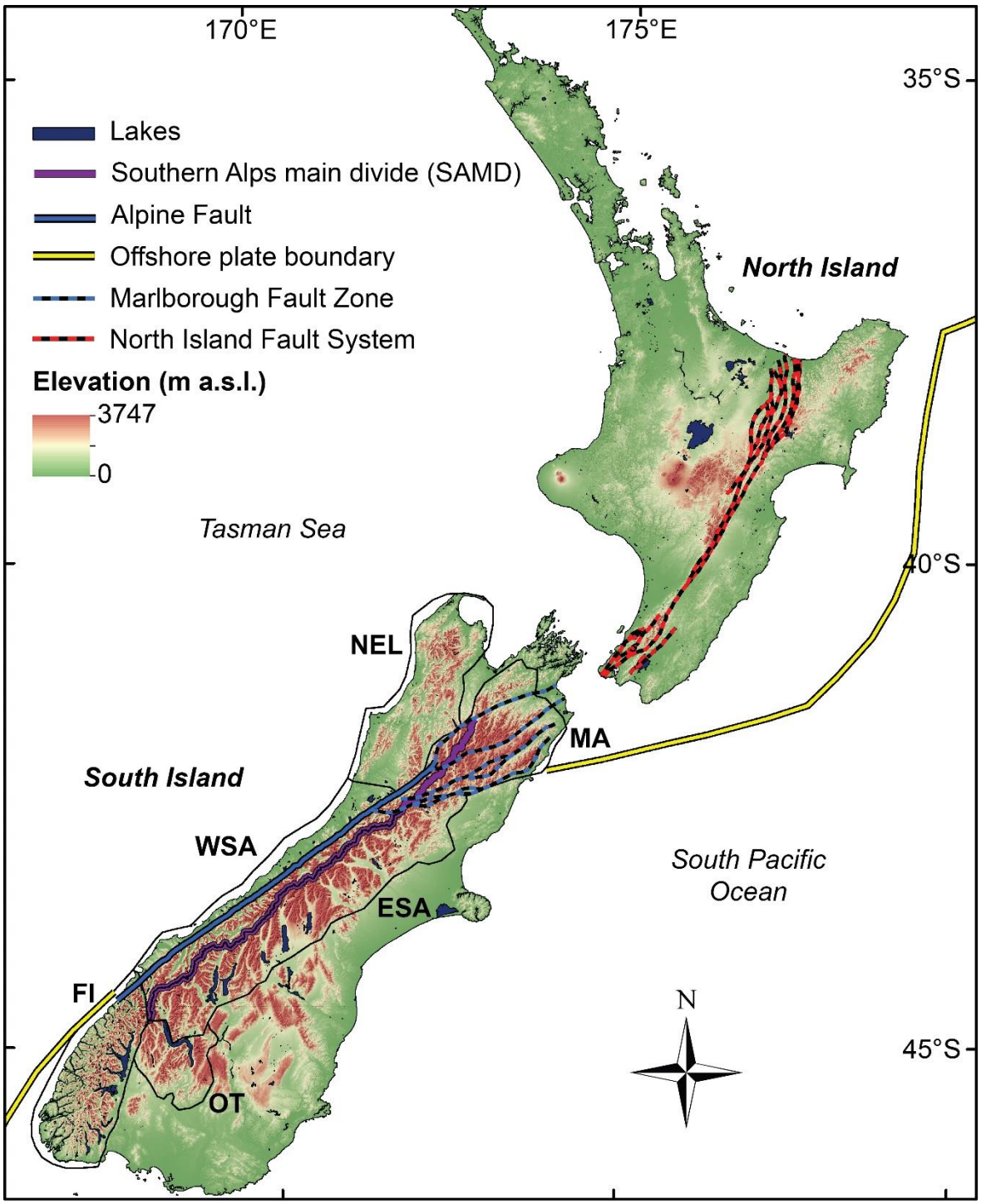

Fig. 2.1 Location map of New Zealand's South Island. Regions of interest in the South Island are highlighted, Nelson (NEL), Marlborough (MA), western Southern Alps (WSA), eastern Southern Alps (ESA), Fiordland (FI) and Otago (OT). Other features of interest are the extensive fault systems on both islands and the main divide of the Southern Alps mountain range.

misidentification of in-situ and reworked deposits (Tovar et al., 2008b; Reznichenko et al., 2015).

As stated in the thesis aims in Section 1.6, in order to examine potential processes controlling RA occurrence and the censoring of RADs within the South Island, this chapter will collate all known RA events into an inventory. The spatial and temporal distribution of

this inventory can then be analysed in relation to the presence of different triggering mechanisms and likely censoring processes. This will help to indicate likely areas where RADs may have been removed from the sedimentological record or simply not generated in the first place.

2.2 Methodology

2.2.1 Physical setting of the study

The South Island contains four major mountainous regions; the SA mountain range running from northern Fiordland up to southern Marlborough dominates by aerial extent and hosts the tallest peaks in NZ (up to 3,724 m a.s.l. – Mt. Cook). Other ranges in the South Island with differing topographic, geological and tectonic settings are the West Nelson Mountains in the Nelson region (up to 1875 m a.s.l. – Mt. Owen), the Inland (up to 2885 m a.s.l. – Tapuae-o-Uenuku) and Seaward Kaikoura (up to 2608 m a.s.l. Mt Manakau) ranges in Marlborough to the north east, and Fiordland (up to 2723 m a.s.l. – Mt Tutoko) in the south-west (Fig. 2.2).

The South Island sits astride the Australian-Pacific plate boundary which forms the dextral strike-slip Alpine Fault (AF; Sutherland et al., 2007). The fault can be traced for over ~850km from off-shore Fiordland, on to land in the SA where it follows the western edge of the range north before reaching the Marlborough Fault Zone (MFZ). Here the Hope, Clarence, Awatere and Wairau faults bifurcate from the main AF (Berryman et al., 2012). The AF is broken into segments and strike-slip deformation along the fault varies between segments. Deformation is 23 ± 2 mm/yr at the southernmost onshore segment just north of Fiordland (Sutherland et al., 2006), increasing to 22-29 mm/yr ± 6mm/yr for the central segment which runs the length of the SA. Displacement rates diminish to between 6.3-10 ± 2 mm/yr as the AF reaches the MFZ where the Hope fault bifurcates and reduces to 4 ± 1 mm/yr where the Awatere fault bifurcates (Sutherland et al., 2007).

Although there is rapid plate movement along the AF boundary there have been no major earthquakes since records began ~170 years ago (Berryman et al., 2012). Evidence suggests that AF ruptures are capable of producing large >M_w8 earthquakes (Robinson and Davies, 2013). The last major rupture of the AF was ~1717CE and with a ~329 year mean return interval a large M_w>8 earthquake has an ~30% likelihood of occurring within the next 50 years (Berryman et al., 2012; Biasi et al., 2015).

The transpressional plate movement associated with the AF has resulted in current uplift rates of ~7 mm/yr in the SA (Hovius et al., 1997; Norris and Cooper, 2000). This uplift is balanced by average regional denudation rates of ~9 ± 4 mm/yr based upon landslide mapping of west coast river systems (Hovius et al., 1997). However SA rivers are underloaded with sediment, implying that they are capable of transporting the majority

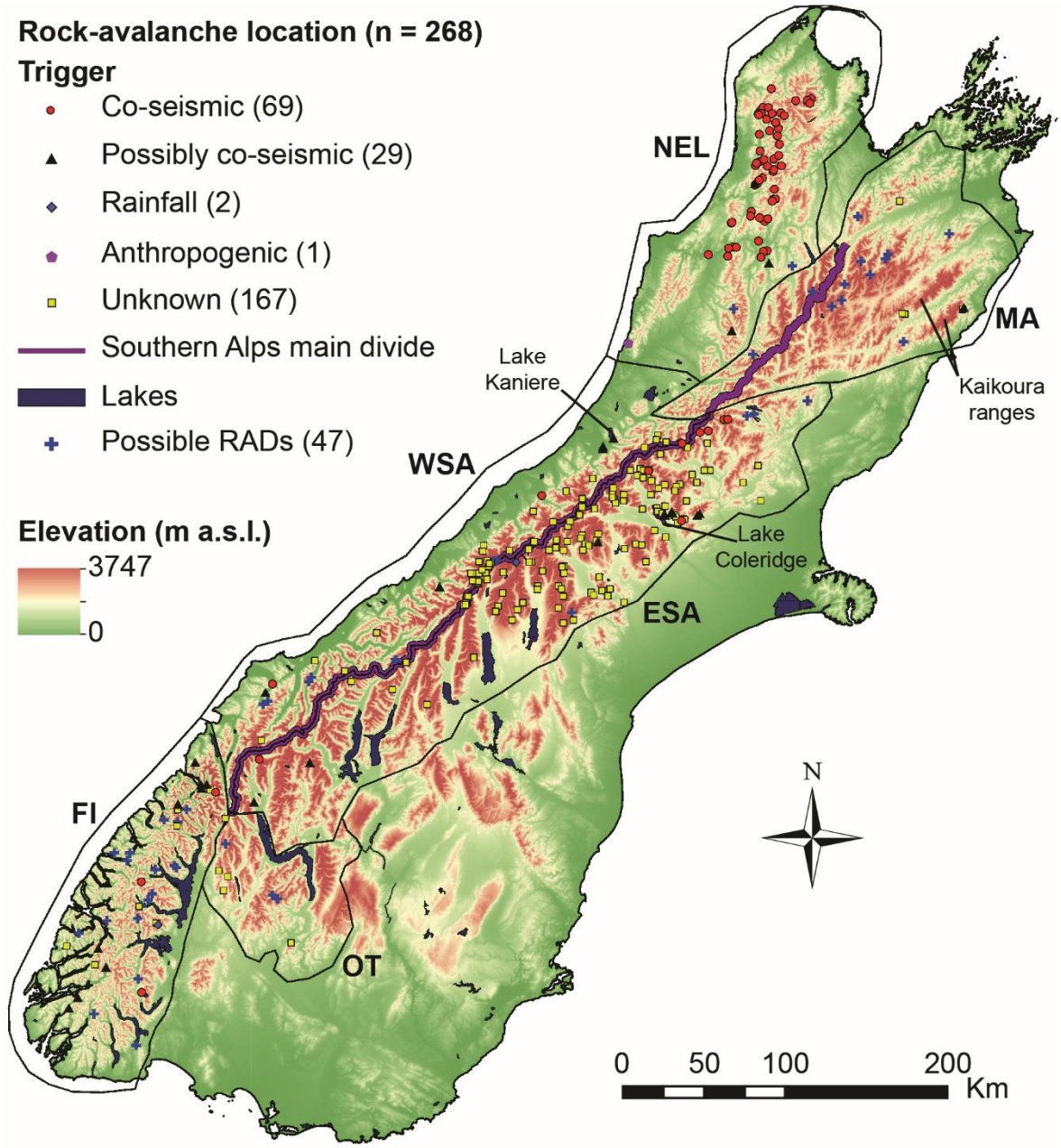

Fig. 2.2 Distribution of 268 RADs and 47 possible RADs within the South Island, NZ. Symbols show trigger mechanisms attributed to each RAD where known. Highlighted regions of interest are Nelson (NEL), Marlborough (MA), western Southern Alps (WSA), eastern Southern Alps (ESA), Fiordland (FI) and Otago (OT).

of sediment that they entrain out to the ocean, or into lakes (Burbank and Anderson, 2011).

2.2.2 Development of the inventory

RA inventories can be used to examine controls on deposit distribution, analyse triggering factors, temporal trends, and discuss short and long term impact of RADs on the landscape. However, typically in historic and pre-historic multi-temporal inventories many events remain with unknown trigger factors as the events surrounding RA generation are not known; e.g. seismicity, pre-failure slope conditions, antecedent rainfall.

Nine main inventories contain the majority of known RADs within the South Island. They cover different regions and temporal scales as well as recording variable levels of detail capturing attributes such as size, age, trigger and impacts on the landscape. Relatively complete landslide inventories, including deposit areas and volumes, are required in order to fully understand processes of landscape evolution in mountainous environments (Brardinoni and Church, 2004) as well as better determine landslide hazards and high-risk areas (Guzzetti et al., 2009), and, perhaps identify 'RA gaps', areas where the factors exist for RA generation, yet there is a paucity of deposits.

Records for 268 geo-located RADs on the South Island (Fig. 2.2) were collated from articles, technical reports, geological maps and PhD theses (Fig. 2.3; Table 2.1; inventory shapefile and complete reference list available in Digital Appendix 2.1). Where co-ordinates were unavailable for deposits they were located on topographic maps or aerial and satellite imagery. All location data are presented using WGS1984.

Multiple definitions of a 'rock-avalanche or rock-avalanche deposit' appear in the literature used to collate the new inventory, from simple volumetric constraints (e.g. $>10^6 m^3$; Cowan et al., 1996; Wood et al., 2011) to more comprehensive multi-criteria approaches (Whitehouse, 1983; Allen et al., 2011; Hungr et al., 2013). In this study an assemblage of features which is considered diagnostic and common to all RADs is used: these features include motion characteristics of the RA, deposit morphology, and deposit sedimentology (McSaveney and Davies, 2006; McColl and Davies, 2011; Hungr et al., 2013; Dufresne et al., 2016a). Descriptions of deposits and RA definitions within the literature were scrutinised against the diagnostic features to assess their suitability for inclusion in the inventory (Digital Appendix 2.2).

Many of the deposits satisfy multiple criteria, whilst some only satisfy individual criteria. Descriptions matching multiple criteria were included whilst deposits only satisfying single criteria were included at the author's discretion after examination of the deposits on aerial imagery. Where available additional attributes were recorded including age, area and volume (as stated in the literature), source area geology, trigger factors, river dam occurrence and runout onto glaciers (Digital Appendix 2.1). Where a single deposit has conflicting attribute information from multiple sources a decision was made by the authors on which attribute value to use; the decision was based upon the modernity of each source and methods they used to derive their data. Any attribute conflicts are noted within the inventory.

Of the 268 deposits in the inventory 177 have age data associated with them (Fig. 2.4) spanning 10,250BP (Wilberforce River valley – inventory number 88; Whitehouse & Griffiths 1983) to 2014 (Hillary Ridge, Cox et al. 2015), with a strong bias towards younger deposits. It is likely that many older RADs have been censored from the current inventory by erosional processes or concealment by vegetation, lakes or glaciers

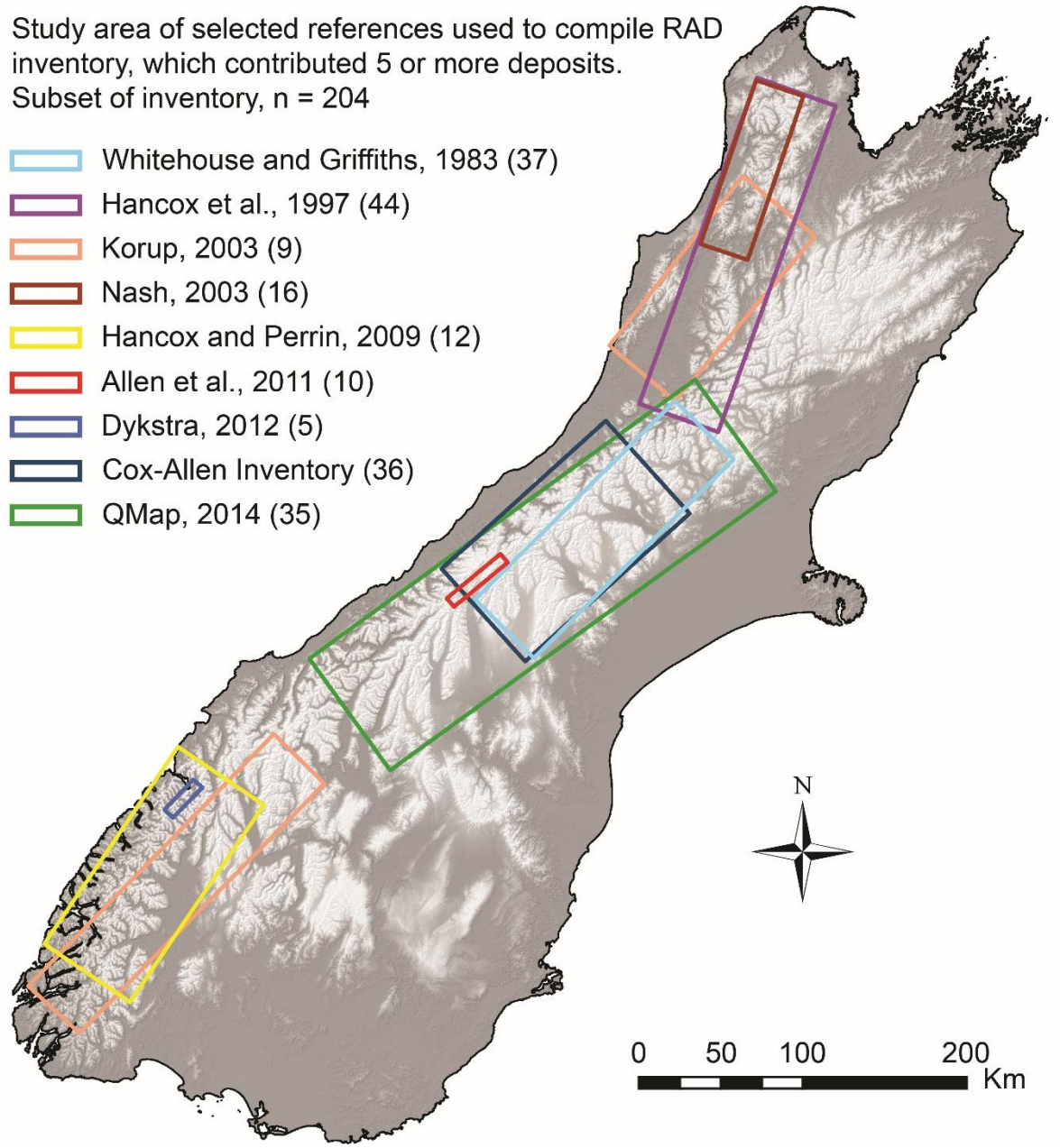

Fig. 2.3 Study area of previous RAD inventories in the South Island which have contributed 5 or more deposits to the inventory presented in this thesis. The number of deposits contributed is shown in brackets, this constitutes a subsection of the total inventory of 204 deposits. A breakdown of each inventory is shown in Table 2.1.

(Korup, 2005c; Blikra et al., 2006; Dunning et al., 2015). The inventory is assumed to be incomplete over the time period that it covers. The oldest RAD recorded in any NZ inventory is Green Lake at 12,000 BP (inventory number 266); however there are discrepancies within the literature about the landslide type (Whitehouse, 1983; Hancox and Perrin, 2009); equally the proposed ancient Mount Roon RAD (inventory number 154) has questions surrounding its source and extent. This has prompted the exclusion of both deposits from further statistical analysis.

It was noted that no major RAD inventory covered the Marlborough region and that Fiordland had less coverage than other areas (Fig. 2.3), suggesting that the inventory may be subject to a spatial bias. Using the deposit morphology descriptors compiled from the

Table 2.1 Selected inventories of landslides in the South Island New Zealand from which the new inventory was compiled. These inventories contributed five or more deposits to the inventory.

Inventory name	Inventory size	Number of deposits used in this study*	Region	Temporal scale
Whitehouse & Griffiths, 1983	46	37	CSA	-10,250 – 1929
Hancox et al., 1997	102	44	National	1848 – 1995
Korup, 2003	232	9	WSA/Fiordland	-2050 – 1980
Nash, 2003	26	16	Tasman	1929
Hancox and Perrin, 2009	40	12	Fiordland	-12500 – -6144
Allen et al., 2011	509	10	CSA	1893 – 2009
Dykstra, 2012	11	5	Milford Sound	-
Cox-Allen Inventory, pers. comm, 2015	-	42	CSA	1850 – 2013
Qmap, accessed 12/2014	-	35	National	-

* Some deposits exist in multiple inventories but have only been represented once here

rest of the inventory (Digital Appendix 2.2) aerial imagery of Marlborough and Fiordland was analysed (LINZ, 2014; Google-Earth, 2016), along with the GNS QMap data (Rattenbury and Isaac, 2012; Edbrooke et al., 2014), to identify any potential RADs. A total of 47 possible RADs (Fig. 2.2; Digital Appendix 2.1 – deposits 275-321), which satisfied a number of morphological descriptors, were identified in these regions. These deposits were mapped in order to show that there is potential for extensive deposit censoring in the South Island; However they are not ground-truthed and were therefore excluded from further statistical analysis. It is unclear in most cases whether deposits mapped in other inventories have been ground-truthed or not.

2.2.3 Deposit area and volume attributes

The extents of 234 RADs were mapped in a GIS using 1:5,000-1:10,000 orthorectified aerial images and 1:50,000 topographic maps (LINZ, 2014). Some inventories already contain 2D area attributes; however for consistency deposit extents were remapped and 3D area values were calculated for further analysis. To derive 3D area estimates a 25m DEM (LRIS-Portal, 2015) was used to derive a triangular irregular network (TIN) surface from which area values could be calculated from the mapped deposit extent polygons. Where it was not possible to remap a deposit, due to uncertainty

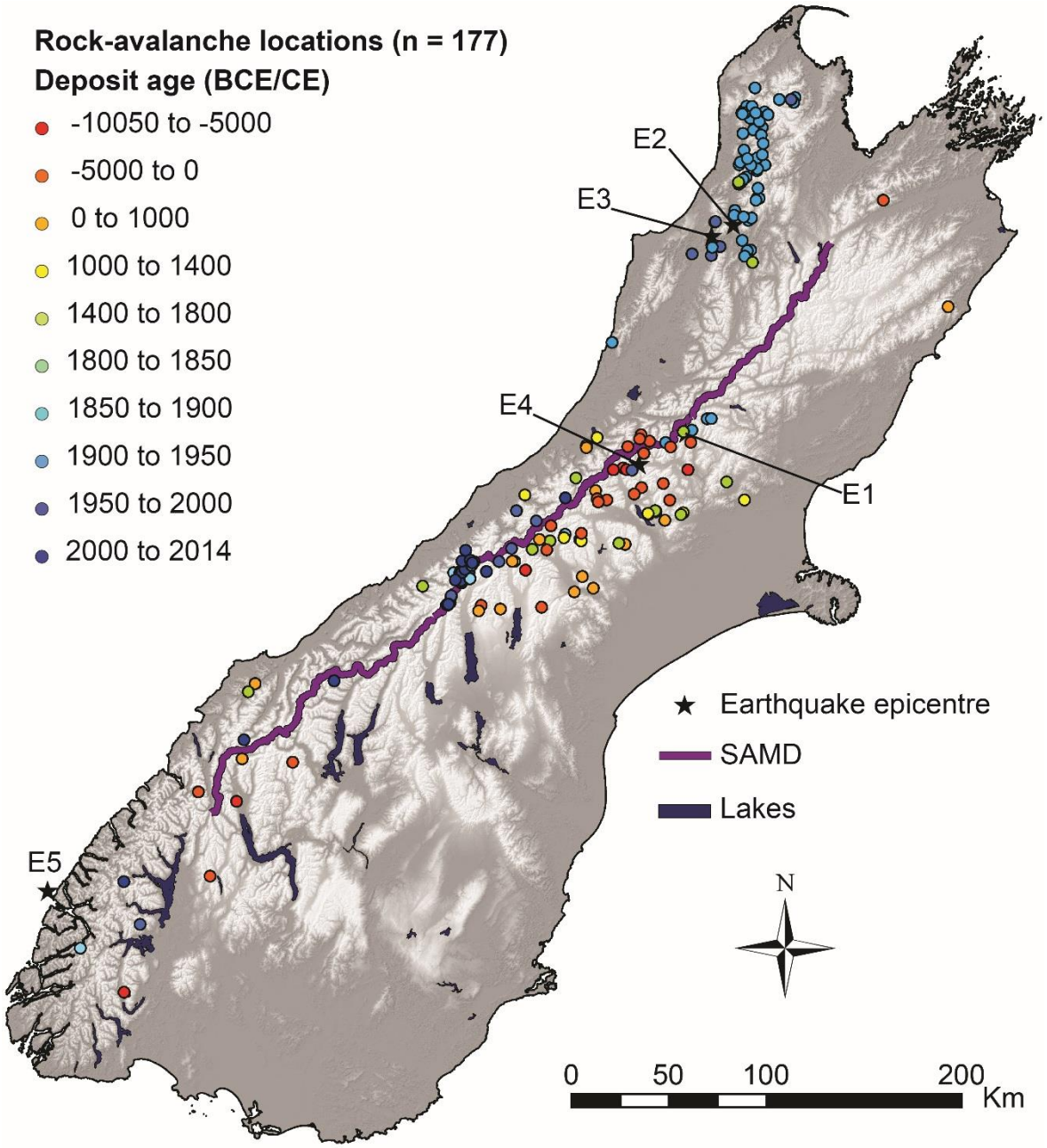

Fig. 2.4 Distribution of 177 RADs with age information from the inventory. Clustering of younger deposits occurs in the Southern Alps and Nelson regions whilst older deposits are scattered throughout the island.

in the location or extent in remotely-sensed data, but a value for area was quoted in the literature this value was used for analysis.

Using this combination of mapped and literature based areas a total of 241 deposits have area attribute information. Literature based areas may have more uncertainty as often it was unclear how these values were derived, and anecdotally some are field-based estimated without measurements.

Any mapping based upon aerial imagery or topographic maps has inherent operator error as minor misplacements of polygons during mapping can results in larger scale errors on the ground which alter the deposit values that are computed (Malamud et al., 2004). This error, whilst unavoidable can at least be recognised. Landslide polygons

have been plotted by the same operator for the entirety of the mapped inventory to minimise error, and a conservative error estimate of 5% was calculated for areas values based on mapping at a 1:10,000 scale (after Malamud et al. 2004).

Using deposit area and empirical relationships between area and volume from a landslide inventory in the SA, (Korup, 2005c; Guzzetti et al., 2009), landslide volumes were calculated using Equations 2.1 and 2.2. Equation 2.1 shows the scaling relationship between landslide area (A_L) and volume (V_L) (Korup, 2005c; Guzzetti et al., 2009). Input values for the x-intercept coefficient 'ε', and scaling exponent or slope 'b', in Equation 2.2 were taken from the Korup (2005) study derived from area data of landslide deposits >1km^2. Here this equation is used on deposits under this threshold as well and therefore is being extrapolated beyond its original range.

$$V_L = \varepsilon A_L^b \quad (\mathbf{2.1})$$

$$V_L = 0.02 \times A_L^{1.95} \quad (\mathbf{2.2})$$

In some cases due to a lack of an area estimate it was not possible to calculate deposit volumes in this manner. In these cases, where the information was available, values from the literature are used for analysis. This combination of calculated and literature based volume estimates mean that 254 deposits in the inventory have volume attribute information. In cases where volume information has been quoted from the literature the method associated with the calculation of the volume is unclear, again, anecdotally these may only be crude estimates in some cases.

Using deposit areas it is possible to derive a probability density function (PDF; Fig. 2.5) to characterise the magnitude-frequency relationships present in the inventory. Standard landslide inventories have their magnitude-frequencies best described by power-law functions with a rollover at small landslide areas where the power-law breaks down (Malamud et al., 2004; Brunetti et al., 2014). The source of the rollover has been attributed to different mechanisms. Firstly as a function of undersampling smaller deposits during inventory compilation due to censoring of landslides or the scale at which mapping was conducted (Stark and Hovius, 2001; Brunetti et al., 2009). Secondly the rollover can appear as a real distribution where there are fewer small deposits as a function of local surface morphological variations (Guzzetti et al., 2002). Most landslide inventories usually contain a wider range of volumes/areas, whereas this inventory is limited to the largest landslides above the magnitudes where the rollover is usually observed, but where most scatter around the power-law fit occurs. Area values were counted into logarithmic bins which increase in size with increasing area (Malamud et al., 2004). Using the binned data,

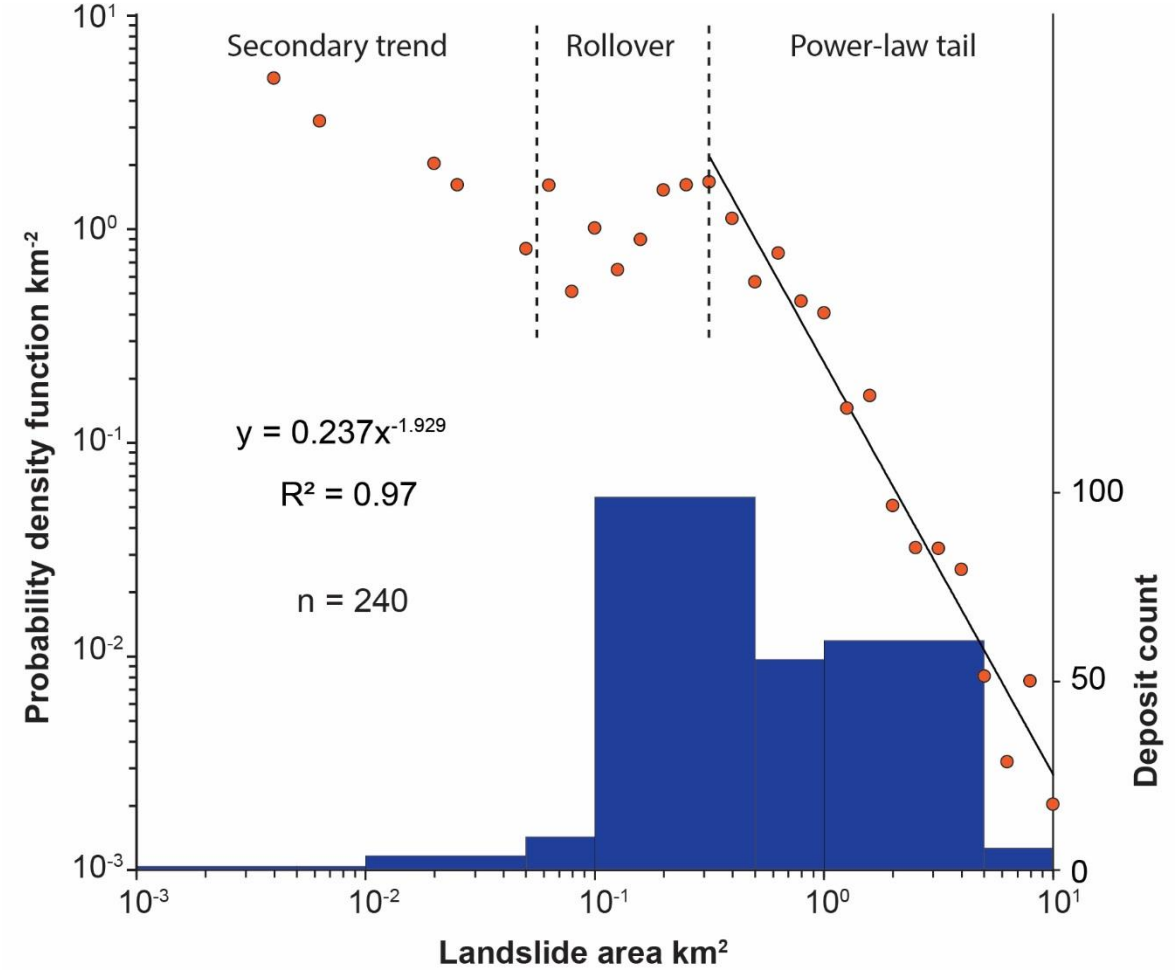

Fig. 2.5 Probability density function for RAD area (km^2); the histogram within the plot (right axis) shows the frequency of RADs within each landslide area size range.

Equation 2.3 (Malamud et al. 2004) was used to calculate the PDF for each bin (Fig. 2.5), where $p(A_L)$ is the probability density function for area, N_{LT} is the total number of landslides with area information and δN_L is the number of landslides contained within a particular bin, '$A_L + \delta A_L$'.

$$p(A_L) = \frac{1}{N_{LT}} \frac{\delta N_L}{\delta A_L} \quad \textbf{(2.3)}$$

RAD locations and volume calculations can be used to examine how deposits are spatially distributed within river catchments, how much RA sediment is in a catchment system and where that material could theoretically be redistributed and stored downstream. This can indicate which catchments are most affected and which may hold archives of previous events. Drainage basin areas were delineated using a flow accumulation and flow direction raster for the South Island, generated in a GIS using a 25m DEM (LRIS-Portal, 2015). Total RAD counts and their cumulative volumes were calculated per catchment. Using 2D catchment area and area of Quaternary sedimentation within catchments from the GNS QMap database (Rattenbury and Isaac,

2012; Edbrooke et al., 2014) it was possible to calculate a ratio of RAD volume per catchment as a proxy for potential concentration of RA material.

2.2.4 South Island tectonics and seismicity

Earthquake epicentres ≥M6 with depths of less than 45km (GeoNet, 2015) and where possible associated shaking intensity isoseismals of ≥MM9 (Modified Mercalli), were plotted for the South Island (Fig. 2.6; Downes 1995). These values were chosen as this is the likely lower limit of earthquake magnitude and depth above which RAs can be generated co-seismically (Cox and Barrell, 2007). The measured earthquake database for ≥M6 earthquakes only extends as far back as 1817 - it does not cover the time range of the RA inventory and is useful for comparison with the most recent events. In order to address this pre-historic gap in the record a peak ground acceleration (PGA) model from the New Zealand National Seismic Hazard Model (Stirling et al., 2012) was used examine the long term likelihood of high PGA over a 2,500 year return period. PGA has an approximate relationship to MM which allows the use of it as a proxy for high magnitude earthquakes in the past (Hancox et al. 2002; Fig. 2.7). The model shown in Fig. 2.7 is PGA over a 2,500 year return period, essentially modelling the likelihood of high-magnitude earthquakes (associated with AF rupture primarily). A PGA value has been assigned to each deposit;

Fig. 2.7 plots A-F show the frequency distribution of PGA values for the regions of the South Island shown. Hancox et al. (2002) correlate PGA, approximate Modified Mercalli (MM) intensity shaking and earthquake induced landsliding (EIL) opportunity. PGA values of ≥0.5 are likely to have ≥MM9 intensity shaking and have high to very high EIL opportunities.

The transpressional movement of the AF (Norris and Cooper, 2000) generates deformation along the plate boundary and across the island which can be measured as shear strain. Maximum shear strain rate (ppm/yr; Beavan et al. 2007) for the South Island is shown in Fig. 2.8 plotted along with the main active fault systems, the AF and Marlborough Fault Zone (MFZ; Berryman et al. 2012). Maximum shear strain rates for each RAD location were interpolated using a surrounding cell-based average and plotted as a frequency density for each region (Fig. 2.8 plots A-H).

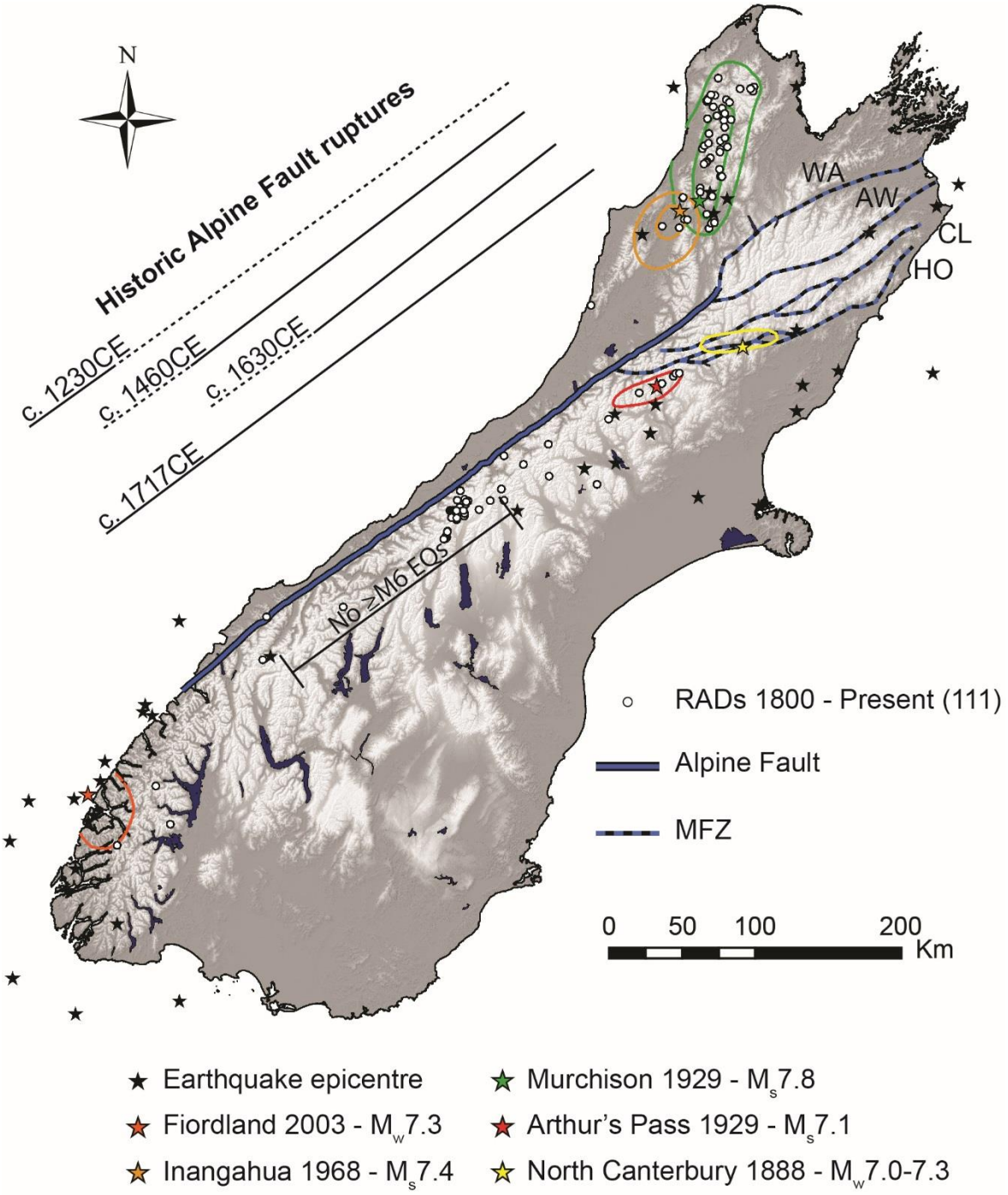

Fig. 2.6 Map of South Island ≥M6 earthquake epicentres from 1817 and isoseismals with ≥MM9 intensity shaking where data is available (Downes, 1995; GeoNet, 2015). Isoseismals are colour coded to the associated epicentre. Black lines indicate the rupture length and approximate date of prehistoric **AF** earthquakes (solid = known, dashed = inferred; after Robinson and Davies, 2013). Faults in the MFZ are the Wairau Fault (WA), Awatere Fault (AW), Clarence Fault (CF) and Hope Fault (HF).

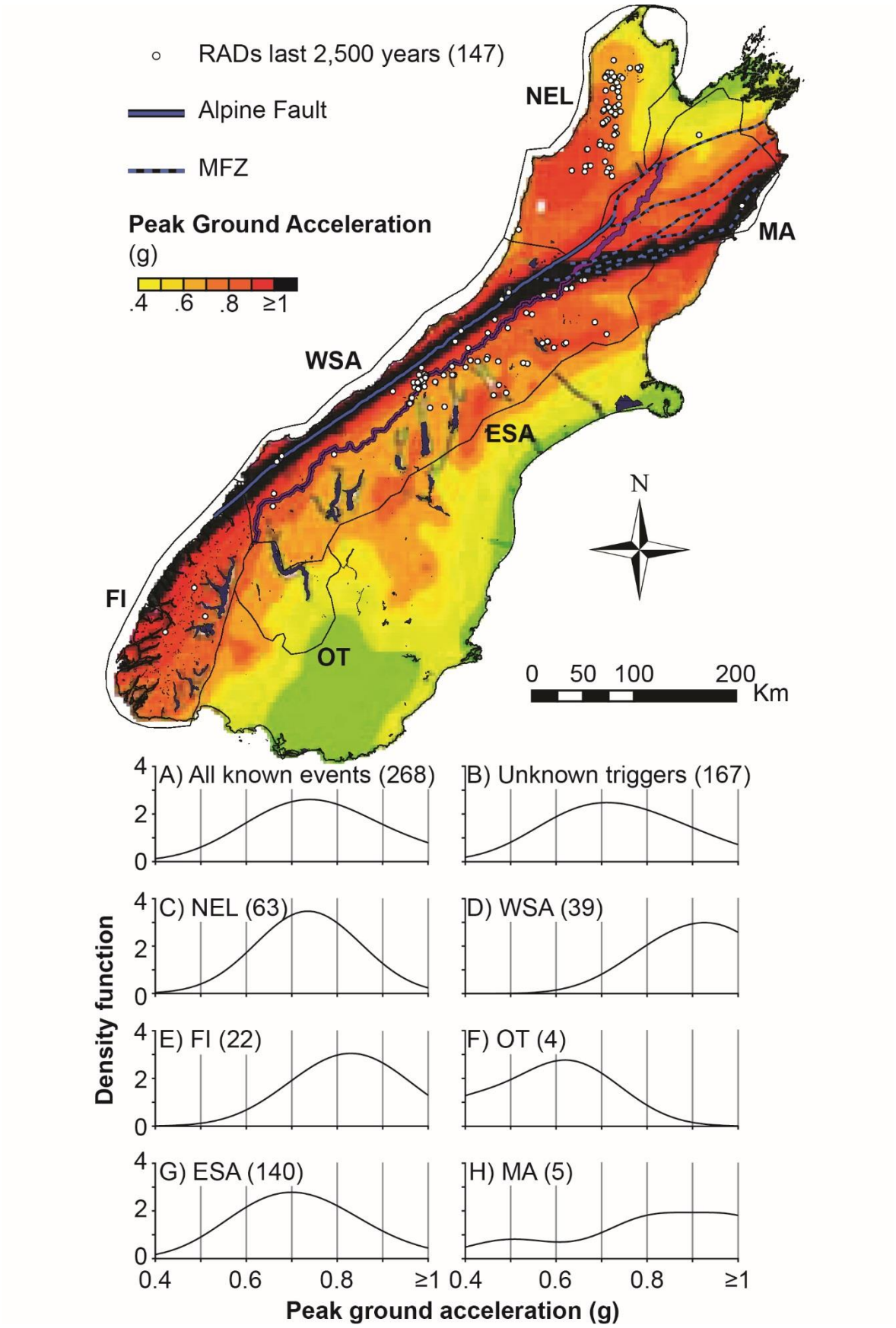

Fig. 2.7 2,500 year peak ground acceleration (PGA; Stirling et al., 2012) map for the South Island with RADs recorded over the last 2,500 years (n = 147). PGA is measured in 'g' (9.81m/s). Plots A-H show the frequency distribution of PGA values at RAD locations for the entire inventory and by region.

2.2.5 South Island geology and hillslope characterisation

Geological data (Fig. 2.9) were classified from the GNS QMap series (Rattenbury and Isaac, 2012; Edbrooke et al., 2014); the adopted classification groups rock types based on assumptions of relative strength and genesis; igneous rocks are classified as plutonic and volcanic; The plutonic rocks in Nelson are predominantly Granite whilst Fiordland are composed of Granite, Diorite and Gabbro. Volcanic basalts and tuffs are mostly confined to small areas of the east coast. Metamorphic rocks are classified as schists and semi-schists and are the most prevalent metamorphic rock-types in the island. A separate category 'other metamorphic rocks' was used for the multiple sub-classes that cover small area at the South Island scale. Sedimentary rocks were differentiated into sandstones, limestones, mudstones and conglomerates.

Hillslope gradient frequency distributions for mountainous regions of the South Island were calculated using a series of sampling zones. Twenty-four sampling locations were placed in mountain regions of the South Island (Fig 2.9 A-X). Slope values contained within each sampling polygon were used to construct kernel density curves for slope frequency (Fig. 2.10 A-X). A regional slope frequency curve was also generated for the outlined South Island regions (Fig. 2.9 and Fig. 2.10). Slope frequency curves for zones A-X (Fig. 2.10) were used to examine if distributions varied between rock-types. Average slope angles for zones immediately adjacent to RA source areas were used as a proxy for pre-RA slope angles; these angles were plotted on the regional kernel density curve in order to examine the distribution of slope failure angles (Fig. 2.10 – NEL, WSA, FI, OT, ESA, MA).

The structural geology of slopes can control the occurrence of landslides, and the mechanisms of failure (Grelle et al., 2011). Regional bedding dip angles were generated from point data spread over the South Island using a nearest neighbour interpolation algorithm (Fig. 2.11). This does not display the dip of discrete bedding planes, their relation to slope aspect and other major discontinuities; all of which have an impact of the stability of individual slopes. However, the dip frequency plots on (Fig. 2.11 plots A-H) give an indication of the predominant structural environment at RAD locations.

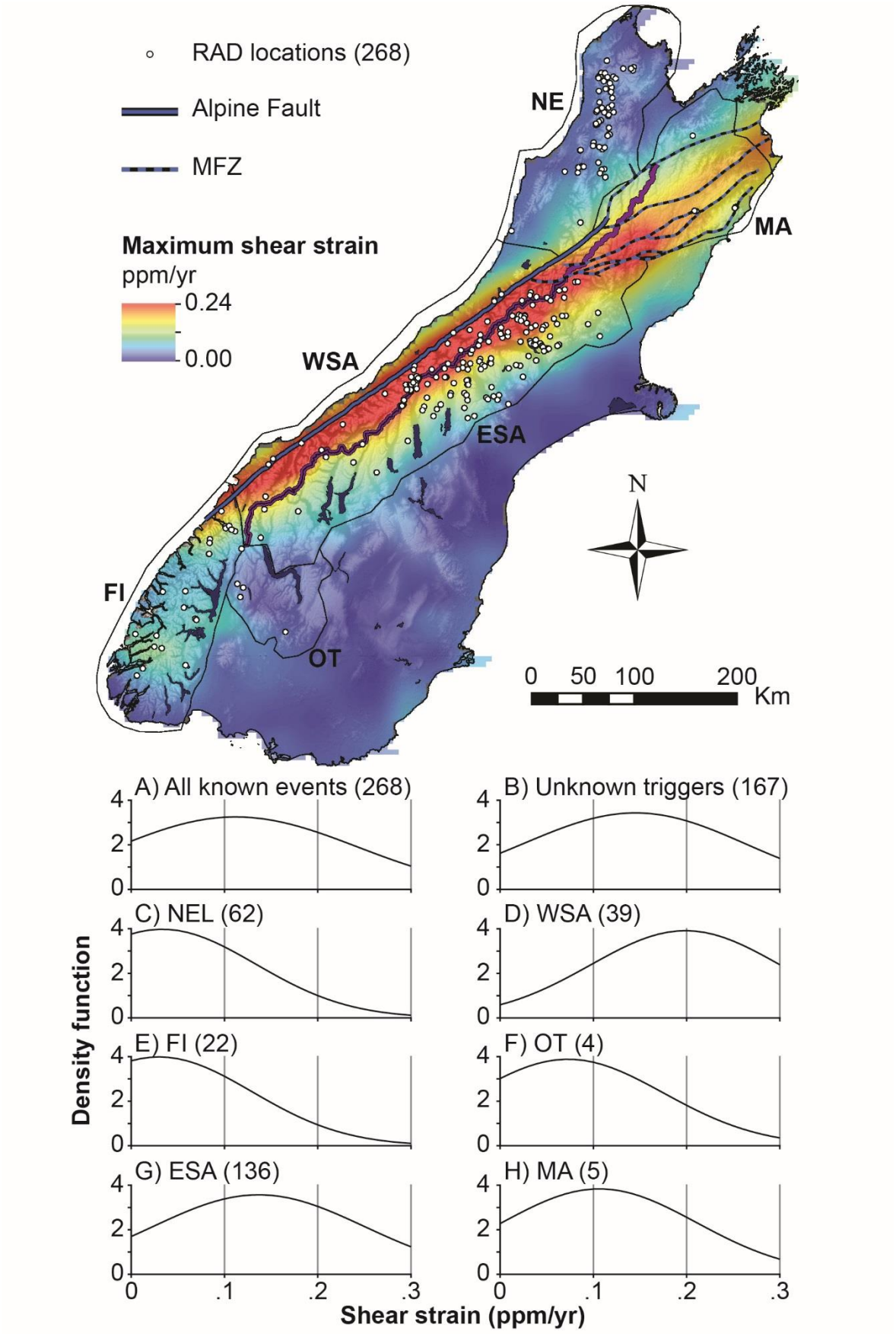

Fig. 2.8 Map of maximum shear strain experienced in the South Island (Beavan et al., 2007). Plots A-H show the frequency distribution of shear strain values at RAD locations for the entire inventory and broken down by region.

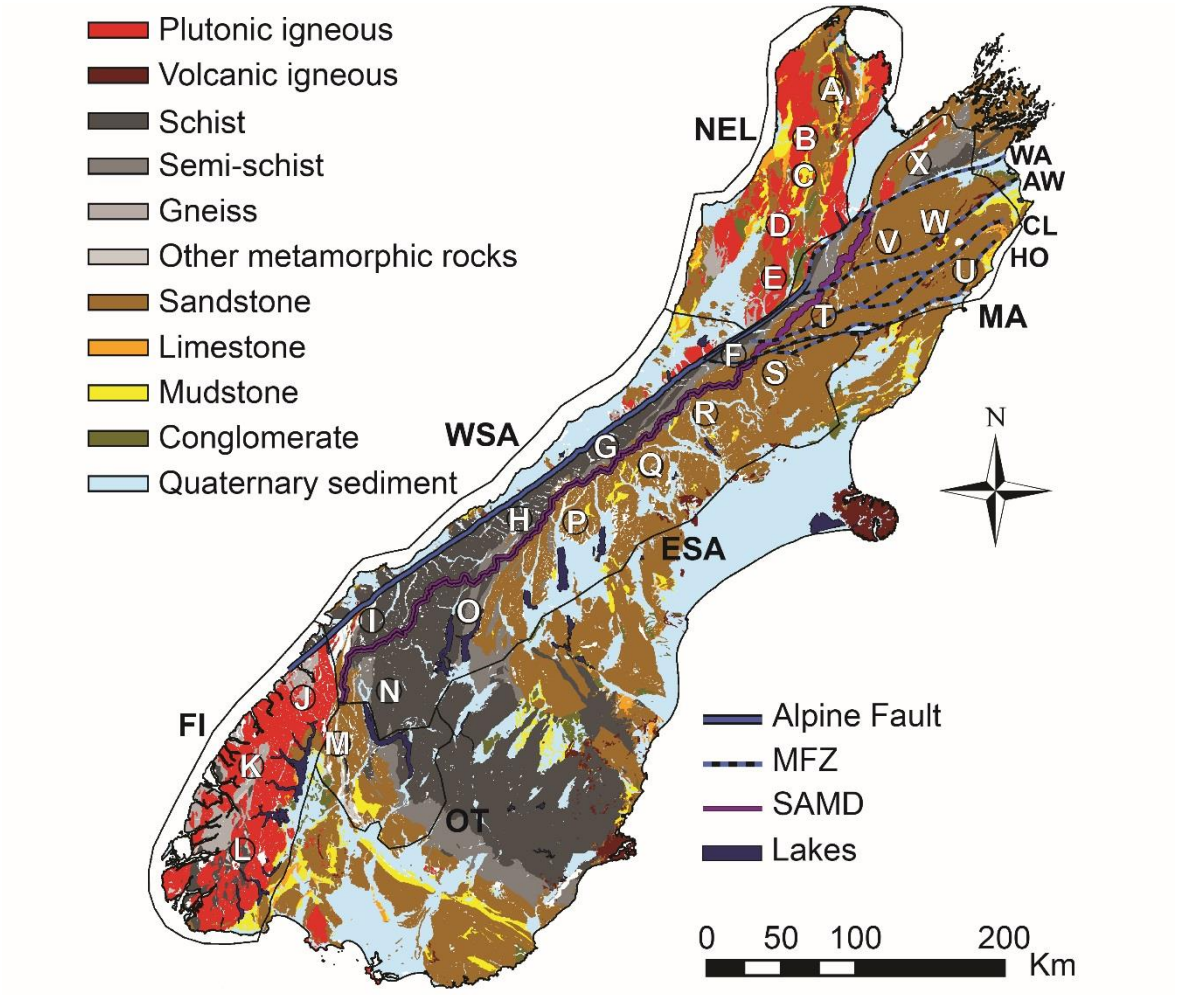

Fig. 2.9 Geological map of the major rock types composing the South Island (Rattenbury and Isaac, 2012; Edbrooke et al., 2014). The Alpine Fault and the Marlborough Fault Zone (MFZ) are depicted. Regions of interest are outlined, Nelson (NEL), western Southern Alps (WSA), Fiordland (FI), Otago (OT), eastern Southern Alps (ESA) and Marlborough (MA). Circles A-X locate sampling zones for kernel density plots of slope frequency, which are shown in Fig. 2.10.

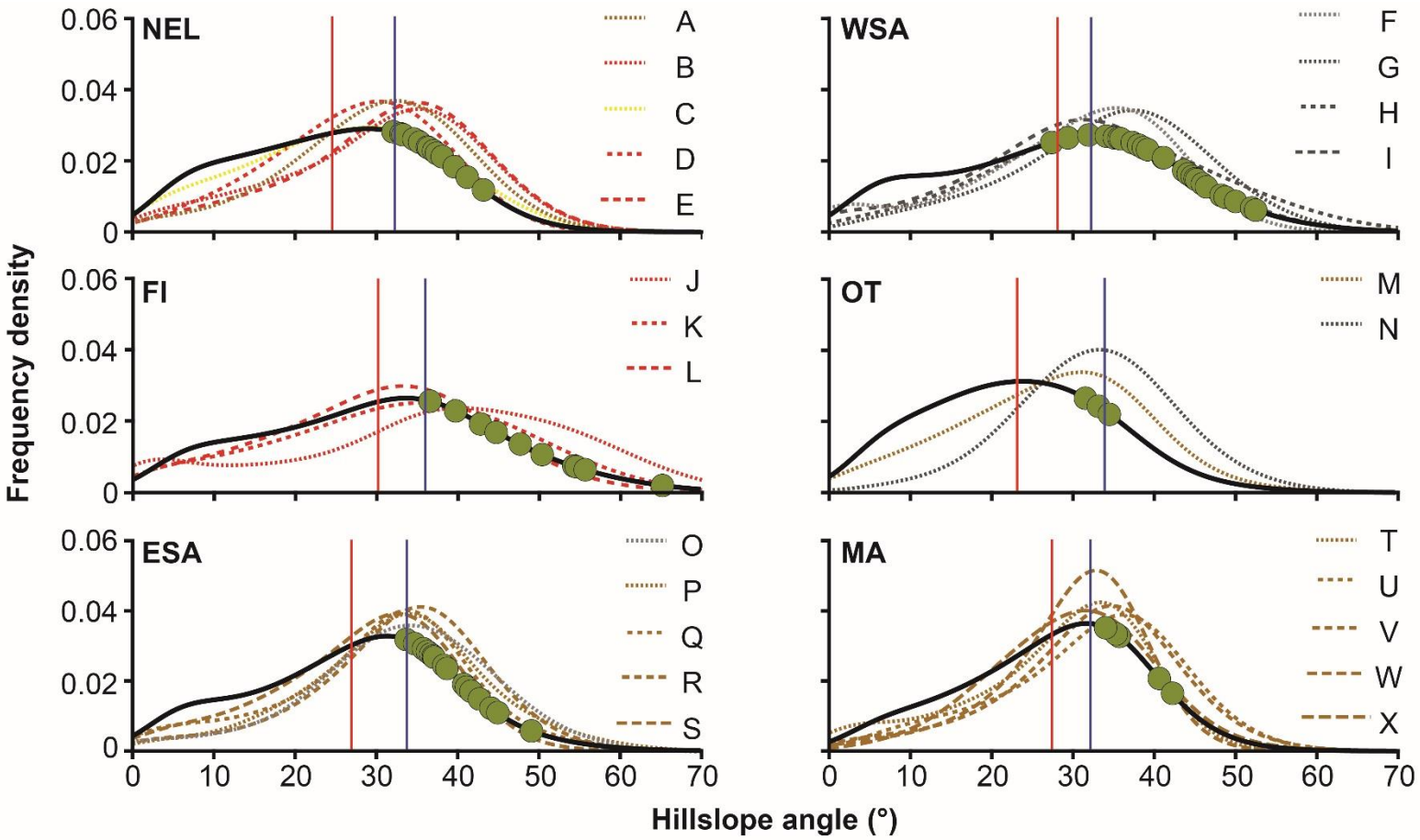

Fig. 2.10 Slope frequency distribution plots over the regions of interest: NEL, WSA, FI, OT, ESA and MA (black line). The regional slope distribution plot was constructed using slope values extracted from a 25m DEM of the South Island. Red vertical lines indicate regional mean and blue vertical lines indicate regional modal values of slope. Coloured dashed lines indicate slope frequency distributions in areas A-X depicted in Fig. 2.9. Plots A-X are coloured corresponding to the main rock type in the sample area. Plots A-X are given in order to indicate whether the regional slope distribution (black line) is similar to smaller samples taken from each region. Green dots indicate the estimated pre-failure slope angle of RA source areas, which are located within each region. Pre-failure slope was estimated by sampling slope angles adjacent to source areas.

Table 2.2 Mean (Me) and modal (Mo) values of hillslope angles within regions and labelled circular polygons in Fig. 2.9. Regional Me and Mo values are shown in Fig. 2.10. Rock types are names after Fig. 2.9.

Region	Regional Hillslope angles (°)	Pre-failure slopes steeper than Me and Mo (%)	No. of RADs	Sample name	Me	Mo	Main rock type
NEL	Me – 24.59 Mo – 32.28	Me – 100 Mo – 92	62	A	30.35	34.87	Sandstone
				B	30.92	36.57	Plutonic
				C	26.71	27.65	Mudstone
				D	27.55	29.02	Plutonic
				E	31.70	34.96	Plutonic
WSA	Me – 28.12 Mo – 32.23	Me – 96 Mo – 88	39	F	31.31	37.72	Semi-schist
				G	34.30	38.15	Schist
				H	33.78	28.17	Schist
				I	30.88	32.96	Schist
FI	Me – 30.23 Mo – 36.02	Me – 100 Mo – 100	22	J	39.07	39.90	Plutonic
				K	33.30	36.19	Plutonic
				L	30.71	33.44	Plutonic
OT	Me – 23.10 Mo – 33.85	Me – 100 Mo – 33	4	M	27.57	31.61	Sandstone
				N	32.68	34.37	Semi-schist
ESA	Me – 26.95 Mo – 33.75	Me – 100 Mo – 83	136	O	33.46	32.80	Schist
				P	32.68	34.08	Sandstone
				Q	30.62	33.79	Sandstone
				R	33.14	36.83	Sandstone
				S	28.50	33.17	Sandstone
MA	Mean – 27.41 Mode – 32.12	Mean – 100 Mode – 100	5	T	28.97	33.71	Sandstone
				U	32.26	36.72	Sandstone
				V	32.50	33.87	Sandstone
				W	30.16	33.09	Sandstone
				X	29.81	30.71	Sandstone

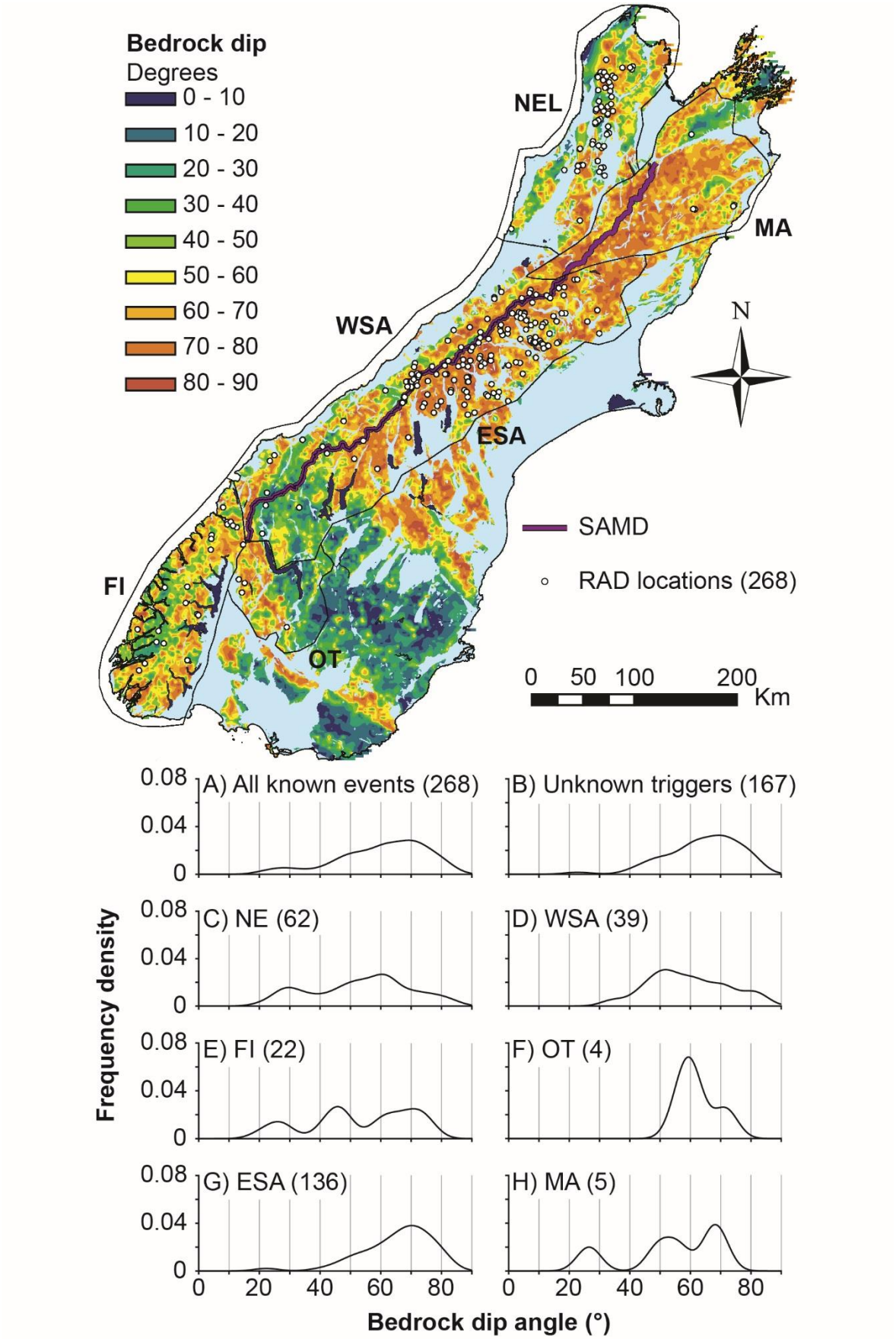

Fig. 2.11 Grid of bedrock bedding dip angle for the South Island (after Cox and Barrell, 2007). Plots A-H show the frequency distribution of bedrock dip values surrounding RADs for the entire inventory and by region.

2.2.6 South Island Rainfall

Interpolated average annual rainfall (AAR) data for the South Island during the period 1981-2010 are shown in Fig. 2.12 (Wratt et al., 2006; NIWA, 2015). Swath profiles of AAR and coincident average elevation were generated across the South Island (Fig. 2.12 A-J). Swath profiles were generated by averaging the values for each parameter (AAR or elevation) transverse to the direction of the profile. Once values were averaged across the swath, a profile of maximum, average and minimum values parallel to the swath was extracted and plotted.

Analysis of pollen records for Southland in the South Island by Vandergoes et al. (1997), show that the climate was probably drier than present between 10,000 to 4,000BP with the modern climatic regime being established by ~4000BP. This indicates that the rainfall data is appropriate for comparison with RAD distribution for the last ~4000 years.

AAR for RAD over the last 4000 years was exported from these data using a surrounding cell-based average; i.e. nine cells were used including the central cell which contained the RAD. Frequency density plots of AAR for RAD locations in South Island regions were derived to highlight regional patterns (Fig. 2.12 plots NEL, MA, WSA, ESA, FI).

2.3 Results

2.3.1 Spatial and temporal distribution of rock-avalanches in the South Island

RADs have not been mapped in their entirety within the South Island, evidenced by the growing literature identifying new deposits in the landscape (Reznichenko et al., 2012; Barth, 2014). Much of the literature used in the compilation of the inventory were carried out with a discrete regional focus to create event based (e.g. earthquake) as well as historical inventories. Despite these limitations, the inventory does allow for consideration of the spatial and temporal patterns of rock-avalanching in the South Island and to identify regions and settings that still require further in-depth investigation.

At the broadest scale 88.3% of deposits in the inventory are clustered in three areas, the WSA (14.5%), ESA (50.7%), and NEL (23.1%) regions (Fig. 2.2). Deposits in Fiordland, coincide with areas that have received more attention in the literature such as Milford Sound. Marlborough has only six known deposits; however the region is not covered by any detailed inventory/investigation, a notable anomaly for the mountainous terrain of the South Island (Fig. 2.3). The RAD record for the period from 1979 to present is considered complete due to improved monitoring of RA occurrence; 73% of events during this period have fallen onto glaciers where deposit preservation potential is low (Dunning et al., 2015). With the exception of Lake Coleridge (Fig. 2.2) there appear to be very few RADs located around the large lakes and fiords of the South Island.

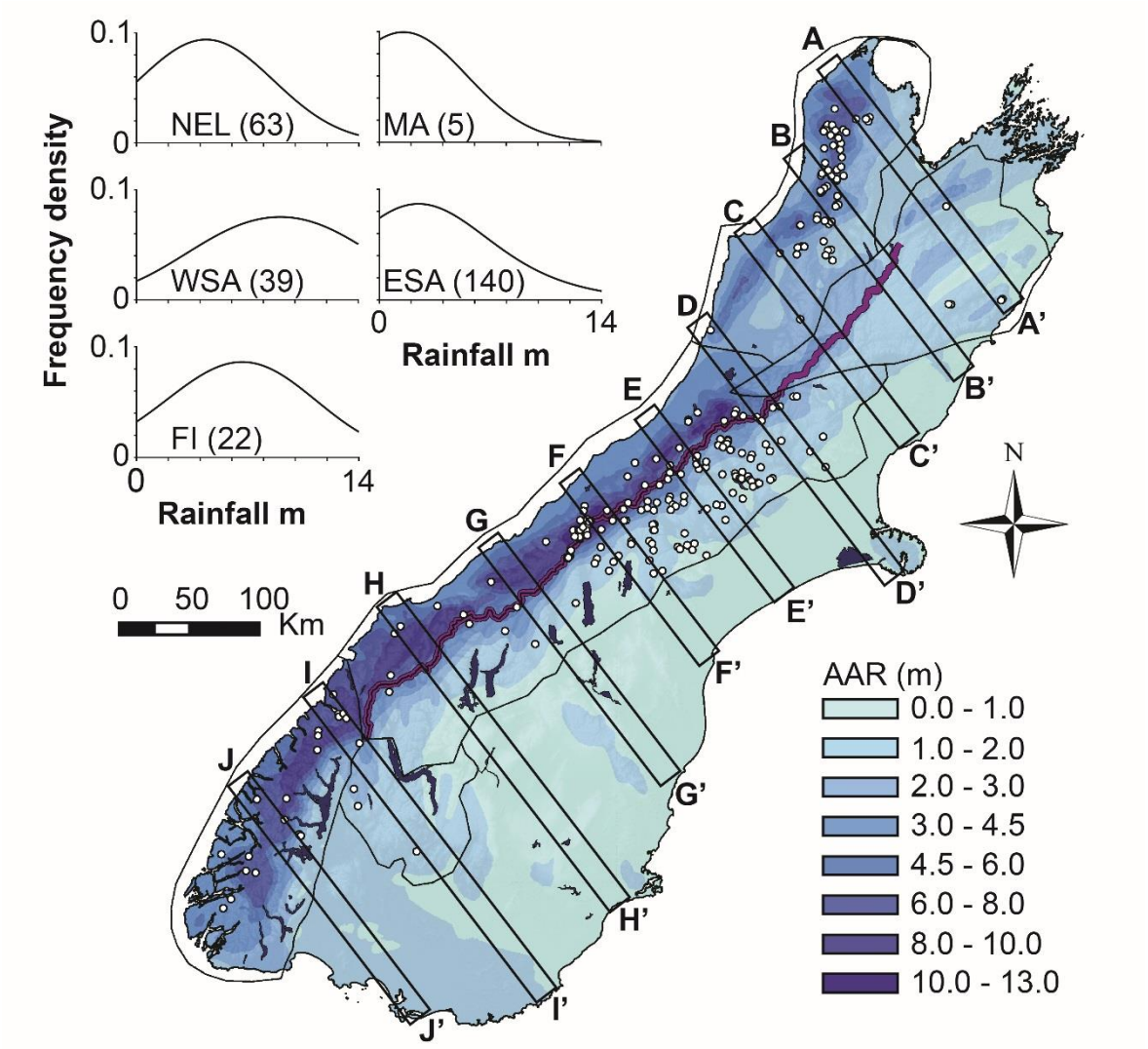

Fig. 2.12 Average annual rainfall (AAR) for the South Island (1980-2010; Wratt et al., 2006; NIWA, 2015) and RADs for the last 4000 years. Lettered boxes indicate the location of swath profiles of both elevation and rainfall across the South Island which are displayed in Fig. 2.12 Cont.; Plots NE = Nelson, WSA = Western Southern Alps, FI = Fiordland, MA = Marlborough and ESA = Eastern Southern Alps show frequency density plots of AAR at RAD locations by region.

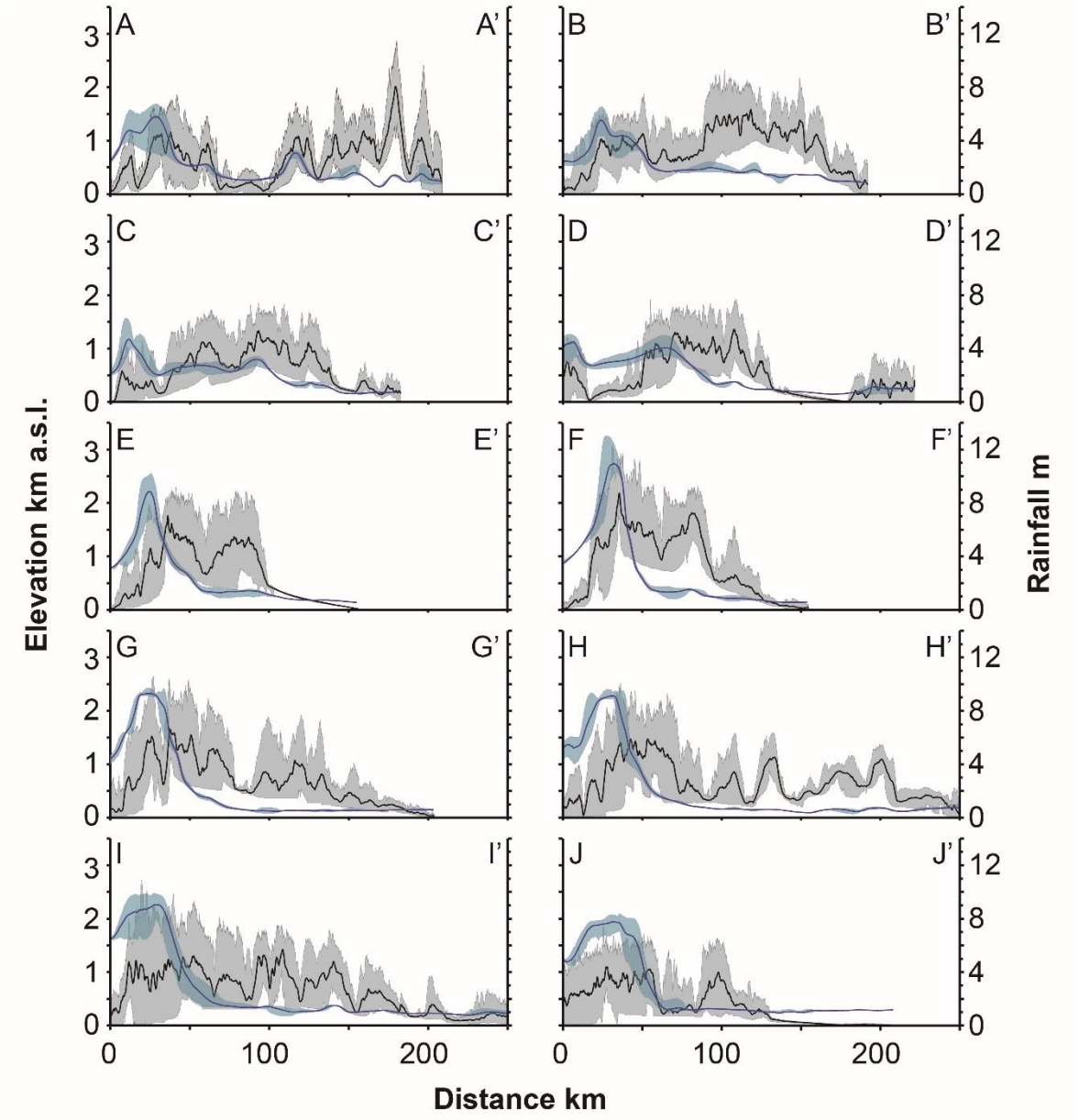

Fig. 2.12 Cont. Plots A-J show swath elevation profiles (black line = mean; grey shade = min-max) and rainfall profiles (blue line = mean; blue shade = min-max) for the areas highlighted in Fig. 2.12.

Of the 268 deposits recorded in the inventory 177 have either absolute or approximate ages (Fig. 2.4). Of those 177, 93 have occurred within the last 100 years (66%), and over the last 1000 years 131 deposits are recorded (74%; Fig. 2.13). Large gaps in the record of >500 years (Fig. 2.13a G1-G7) are confined to the early to mid-Holocene with better temporal coverage in the late Holocene period. Within the last 1000 years (74% of events) gaps in the data reduce to a maximum of ~150 years, with >50 year gaps persistent up until 1800 (Fig. 2.13b G8-G14). RAs since ~1850 can be grouped upon their age and location (Fig. 2.4). Deposits from 1850-1900 are clustered close to the SAMD in the central SA. Deposits from the period 1900-1950 are predominantly centred on Arthur's Pass and Murchison. Deposits from 1950-2000 are typically close to the SAMD or in Nelson. The 23 modern deposits from 2000-2014 are spread down the SAMD from the central SA through to Fiordland.

The inventory indicates phases of apparent increased RA occurrence and quiescence over the last 100 years (Fig. 2.13c). The 1929 Arthur's Pass and Murchison earthquakes collectively generated 55 RADs, a rapid increase in the temporal distribution. However, following this there is a phase of quiescence over the period 1929-1991, where few RAs appear to be generated. Only 11 RADs are recorded between 1929-1991, indicating an average recurrence interval 5.6 years. Subsequently between 1991 and 2004 10 RAs occurred, 8 of which have no known triggers, an increase in average recurrence to every 1.2 years. A sharp increase in the rate of RA occurrence to 0.5 years on average is visible between 2004 -2010 (Fig. 2.13c) before a reduction in recurrence intervals to every 1 year between 2010-2014. These phases could reflect some relatively short term controls on the generation of RADs. Previous estimates of recurrence intervals for smaller areas of the SA also recognise this recorded increase in activity (Allen et al., 2011; McSaveney et al., 2015).

Over the last 1000 years, recurrence intervals are 6.7 years on average and 46.5 years on average for the entire database; however, the latter calculation assumes the oldest event is Green Lake 12,500 BP and that all RADs without ages are intermediate. Given that the interglacial started at ~11,500 BP (Barrell, 2011) it is likely that the majority of deposits with unknown dates, which are not included on Fig. 2.4, post-date Green Lake, however it is possible that some may precede 12,500 BP.

Whilst the temporal data associated with each deposit is assumed to be correct the time series as a whole needs to be treated with some caution. It is likely that the gaps in the record noted in Fig. 2.13 are at least partially driven by a lack of information from historical sources and censoring of the deposits over the entire time period of the inventory. As previously mentioned, there are many deposits without any age data associated with them, as no sustained research has sought to date all of the identified RADs. Additionally it is likely that not all historic deposits have been reported if they were

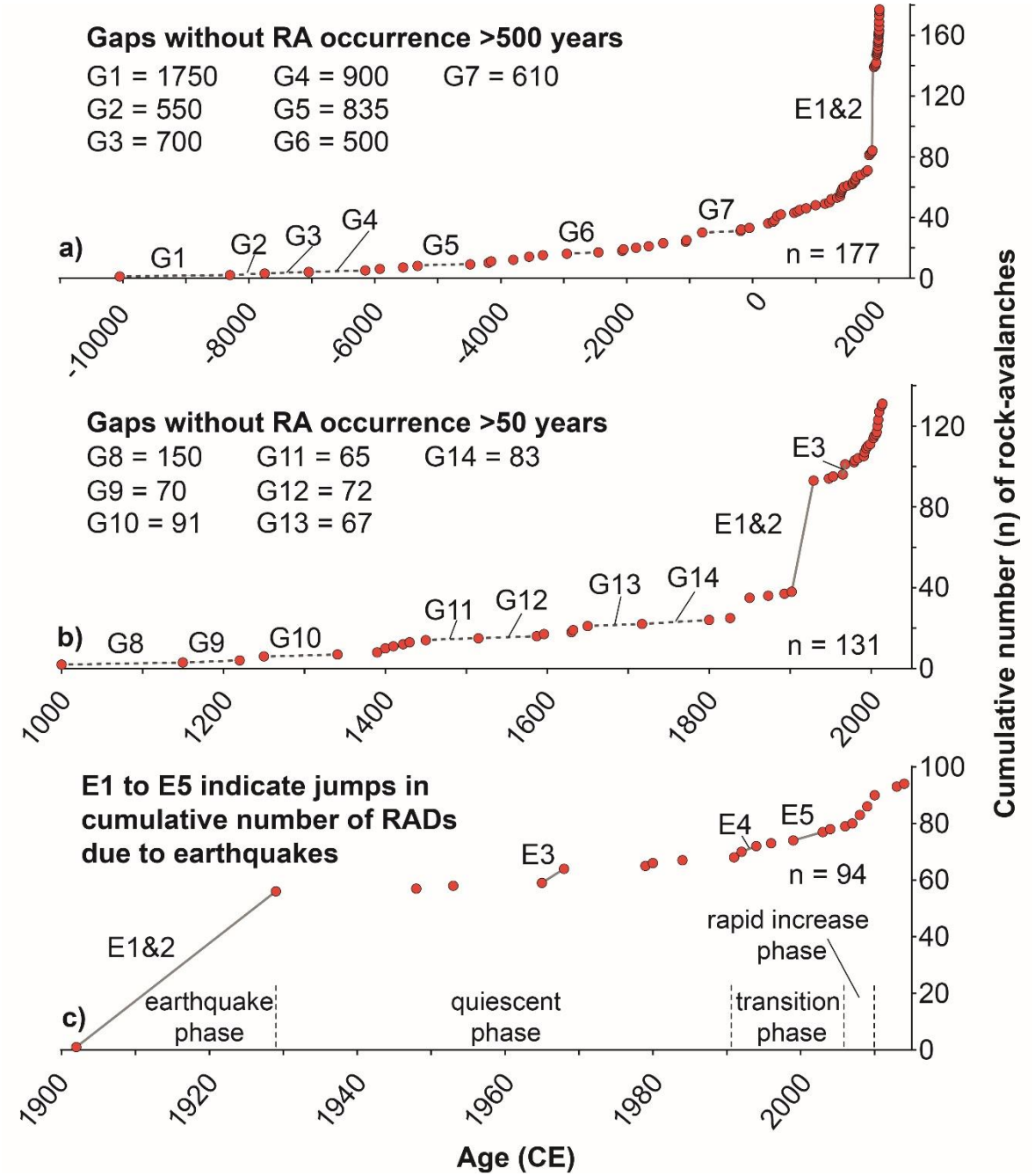

Fig. 2.13 (a) Cumulative RA occurrence for the Holocene epoch, G1-G7 represent >500 year gaps within the record; (b) Cumulative RA occurrence for the last ~1000 years, G8-G14 highlight ≥50 year gaps in the record; (c) Cumulative RA occurrence for the last ~100 years, E1-E5 show earthquakes known to have generated RADs, their epicentres are marked in Fig. 2.4

not witnessed or did not cause some form of reportable disruption. This is a source of bias identified by Ibsen and Brunsden (1996) when compiling an inventory for landslides on the Isle of Wight, UK. In terms of pre-historic RADs there will have been extensive censoring of deposits and obviously no written records in order to fill in gaps within the temporal record. Some deposits will have been lost from the record forever.

However, treating the database as a historical inventory, that is, as the best record of RADs surviving in the landscape, relations for RAD area can be calculated (Fig. 2.5). Landslides in the inventory range in area from $>10^{-3}$ – A_L – $<10^{1}$ km^2. The probability

density for area (Fig. 2.5) $p(A_L)$ shows a tail >10-0.7km^2 best fitted by a power-law distribution with a scaling exponent α = -1.93. Area PDF shows a rollover at deposits with a <0.2km^2 aerial extent. This is reminiscent of magnitude-frequency relationships seen in other databases covering all landslide types (Frattini and Crosta, 2013; Brunetti et al., 2014). The smallest RAD in the inventory is comparatively large when compared to other landslide inventories that incorporate all landslide types. In part the >0.04-0.2km^2 rollover reflects the sampling strategy, as a number of non-RA mass movements would overlap at these spatial extents. The deposits within the rollover (0.04-0.2km^2) are predominantly small valley based RADs in Nelson and the northern ESA. The rollover continues into a secondary trend at smaller aerial extents (0.04-0.004km^2), which is unusual for a landslide PDF. The RADs in the secondary trend are predominantly composed of deposits in the Cox-Allen inventory (Fig. 2.3; Simon Cox, Pers. Comm, 2015). These RAs have occurred at high elevations in the SA, adjacent to the SAMD and have fallen onto glaciers between 2008 and 2010.

2.3.2 Triggering of rock-avalanches in the South Island

Of the 268 RADs presented, only 101 (38%) have a known trigger, or a high probability of a known trigger (Fig. 2.2); 98 are co-seismic, 2 are rainfall triggered and 1 is anthropogenically triggered. The vast majority of events (62%) cannot easily be described with a simple trigger suited to identifying similar causative events in the future, therefore a range of possible drivers of RA occurrence and their spatial and temporal implications is analysed.

Advances in landslide monitoring imply that ascribing triggering factors to an event should potentially be improved for more recent events. However, since ~1850, after which historical records of landslide occurrence have improved, triggers can only be ascribed to 61% of the 106 events; 52 of these RADs are accounted for by a single event, the 1929 Murchison earthquake. Of the 30 RAs that have occurred since 1979, 26 have no apparent trigger. These modern deposits are all located close to the SAMD and are particularly centred on the highest region of the range near Mount Cook. Given that the majority of events in the inventory cannot be attributed a trigger mechanism, a range of possible drivers for RA occurrence and their spatial and temporal implications are analysed.

2.3.3 Tectonics

Where a trigger mechanism has been ascribed to South Island RADs, the trigger is overwhelmingly earthquake shaking. However, extensive landslide mapping often only follows seismic events generating a bias (Fig. 2.3). Co-seismic RAs account for 83% of events (Fig. 2.2) between 1900-present (Fig. 2.13c E1-E5). Known earthquakes are

associated with strong spatial (Fig. 2.2, and Fig. 2.4) and temporal RAD clusters (labelled E on Fig. 2.13a-c), particularly in Nelson with the majority of deposits associated with the 1929 Murchison (Fig. 2.13c E2) and 1968 Inangahua (Fig. 2.13c E3) earthquakes. Another small co-seismic cluster is the 1929 Arthur's Pass earthquake (E1) whilst the 1994 Arthur's Pass (E4) and 2003 Fiordland (E5) earthquakes only produced one RA.

Fig. 2.6 shows the epicentres of earthquakes that were ≥M6 and located at depths ≤45km between 1817-present; ≥M6 and shallow (≤45km) events were used as these thresholds are likely to generate co-seismic RAs (Hancox et al., 1997). Clusters of co-seismically triggered deposits are associated with the M_S7.8 1929 Arthur's Pass earthquake in the ESA, as well as the M_S7.8 1929 Murchison and M_S7.4 1968 Inangahua earthquakes that affected Nelson. NEL has the majority (95%) of co-seismically triggered RADs and they are associated with these two earthquakes. Other RAs within the NEL cluster have probable co-seismic origins indicated in source inventories. The 1929 Arthur's Pass earthquake is known to have triggered four RAs in the northern ESA (Fig. 2.6). Other clusters of co-seismic and possibly co-seismically triggered RADs are located in northern Fiordland, in the WSA at Lake Kaniere and in the ESA surrounding Lake Coleridge (Fig. 2.2). Where the triggers are known, Fiordland events are mostly attributed to co-seismic or possibly co-seismic triggers. The M_w7.3 2003 Fiordland earthquake was only responsible for generating one RA, and the more recent M_w7.8 2016 Kaikoura earthquake off the coast of Marlborough has only generated one deposit which is possibly a RA. Clearly these earthquakes are a contrast to the generation of RAs in other regions of the island.

A seismic gap in the 1817-present epicentre data is apparent in the lower WSA/ESA regions and is coincident with a gap in recorded RADs over the same time period (Fig. 2.6). This region has no ≥M6 shallow depth earthquakes and no earthquake epicentres are located along the AF during the 1817-present time period either. However AF ruptures plotted on Fig. 2.6 (after Robinson & Davies 2013) show that major prehistoric earthquakes have occurred across this region in the relatively recent past.

As the NZ seismic record is comparatively short, a modelled 2,500yr return period PGA map (Fig. 2.7), which incorporates fault sources and estimated ground motions of historical earthquakes, is used to predict seismic hazard over a 2,500 year time period (Stirling et al., 2012). Of the RADs for the last 2,500 years, overlain on the map (Fig. 2.7), 99.6% have PGA values above the threshold 0.5g likely needed for RA initiation; the majority are within 0.7-0.8g (39%) and 0.8-0.9g (27%). Examining the PGA relationship of the entire inventory, frequency density plots (Fig. 2.7 A) show the majority of RADs occurring in high modelled PGA regions of ~0.7->1g. However all mountainous regions of the South Island have high PGA, therefore this relationship would be expected. However regional differences are present with the WSA and Fiordland having the majority of

deposits in high-PGA zones (Fig. 2.7 D and E). Similarly, Marlborough has a skewed distribution towards high-PGA, however there are a lack of deposits in this region. Given the similarities in the PGA map between these three regions it would be expected that Marlborough would have more deposits than are currently known.

Earthquakes are an efficient trigger, however, between rupture events the accumulation of strain/seismic energy has been tentatively linked to the cumulative, and increasing temporal pattern of non-seismic rock-avalanching in South Island (Fig. 2.13c; McSaveney et al., 2015). Fig. 2.8 shows the maximum shear strain generated by the relative plate motions of the Pacific and Australian plates. The highest strain rates of ~0.24 ppm/yr, can be seen thorough the SA, coincident with the trace of the AF. Where the AF bifurcates into other faults in the MFZ, shear strain rate is attenuated from ~0.19ppm/yr proximal to the SA down to ~0.13ppm/yr to the north-west. In NEL where a number of co-seismically triggered RADs are clustered the strain rate is low in comparison to that of the SA with an average value of 0.03 ppm/yr. Likewise the Fiordland region, which has few (known) active fault systems, exhibits relatively low shear strain with a regional average of 0.06 ppm/yr. Frequency density plots of the occurrence of RADs against regional maximum shear rates (Fig. 2.8) show that rock-avalanching has occurred across the whole range of values in the South Island. Although the lack of RADs in Fiordland correlates well to shear rate (Fig 2.8 E), Nelson is a notable anomaly, with exceptionally low shear strain, but a dense population of deposits known to have mostly been generated by the 1929 Murchison and 1968 Inangahua earthquakes. In Nelson three RADs pre-date and two post-date these earthquake generated clusters; of those five, one is anthropogenically generated, two are listed as possibly co-seismic and two are re-activations of a 1929 source area. This suggests that earthquakes are required to generate RAs in Nelson and that accumulation of strain between events is not enough to trigger spontaneous events. Potentially shear strain accumulation has prepared slopes for failure by the next large earthquake in a region, however this cannot be shown here.

2.3.4 Hillslope distributions

On a regional scale there is surprising similarity between modal slope values (Table 2.2) with Nelson, WSA, ESA, Otago and Marlborough having modal hillslope angles of 32-33°. Modal hillslope values calculated for each region are all above 32° and estimated pre-failure hillslope angles for RA source areas show 86.7% of deposits failed from slopes steeper than the modal hillslope angle for their region (Table 2.2). Additionally 99.5% of RAs failed above the mean hillslope value for each region (Table 2.2), only one deposit, located in the WSA (Fig. 2.10 F-I), falls below the regional mean angle of ~28°. Distributions of hillslopes are skewed further towards steeper slopes (Fig. 2.10) and modal hillslope angles exceed those at which it would be expected large landsliding could occur.

Broadly it appears that for the majority of examples (Fig. 2.10 A-X; Table 2.2 A-X) rock type is not a significant factor in the mean and modal hillslope values. For example, plutonic rocks in Nelson and Fiordland produce the highest and almost lowest mean hillslope values. Similarly sandstones have a large range of mean and modal hillslope values across the South Island.

Hillslope gradient frequency distributions vary between the different mountain regions of the South Island. Nelson hillslopes (Fig. 2.10 A-E) show similarities in the distribution regardless of the rock-type except for areas of predominantly mudstone lithology which appear to have a larger proportion of low angled slopes between 3°-30°. WSA has on average, steeper slopes than the Nelson region with mean values of 31°-34° for areas F-G (Fig. 2.10; Table 2.2). The Fiordland region is predominantly Plutonic rocks and whilst the distributions in plot J (Fig. 2.10) shows hillslopes are skewed to steeper gradients between 35°-60°, the regional average mimics sub-samples K and L (Fig. 2.10). This indicates that the same rock-type can produce a large range of hillslope conditions and that possibly it is not a good indicator of RA occurrence.

ESA Sampling locations have comparable mean and modal hillslope angle values to those of Marlborough with a range of means of ~28° to ~33° and modal values between ~32° to ~36° (Fig. 2.10 O-S). Both of these regions are predominantly composed of sandstones and other sedimentary rocks, however the distribution of RADs within the regions differ dramatically. This again indicates that lithology may not be a good indicator of where RADs will occur.

2.3.5 Geology

RAs occur across all major rock-types in the South Island. The majority occur in sedimentary rocks and in particular greywacke east of the SAMD in the central SA. RAs in sedimentary rocks account for 66.4% of the inventory as a whole with sandstones making up 94% of those deposits (Table 2.3). Sandstone deposits are mostly identified in the CSA and Marlborough with some additional occurrences in Nelson. RAs in Metamorphic rock account for 15.3% of the RADs within the database and are mostly confined to the West Coast region, east of the SAMD with some located in Otago where the semi-schist rocks turn and run across the island.

Rock-avalanching within igneous rocks occurs within Nelson and Fiordland where plutonic igneous rocks are more prevalent and account for 18.3% of the RADs. Very few of the RAs within the inventory occur within volcanic igneous rocks, potentially due to the minimal representation of this rock type within the island and particularly within mountainous terrain.

Regional bedding dip data (Fig. 2.11) indicates general patterns of steep and low

Table 2.3 Number of RADs occurring within differing rock-types in the South Island. Rock-types are split into geological sub-divisions.

Rock type	Total number of RADs	Geological sub-divisions
Sedimentary	n = 178 (66.4%)	Sandstone (n=167) Mudstone (n=6) Limestone (n=5)
Metamorphic	n = 41 (15.3%)	Schist (n=25) Semi-schist (n=11) Gneiss (n=3) Granulite (n=2)
Igneous (Volcanic, V; Plutonic, P)	n = 49 (18.3%)	Basalt (n=3) V Diorite (n=1) P Gabbro (n=6) P Granite (n=39) P

angle dipping in certain rock-types. Bedding dip in SA sandstone and schists both east and west of the SAMD appear coincident with steep bedrock dipping planes between 50°-90°. Marlborough, which sees the continuation of sandstone geology from the ESA, shows similar dipping plane characteristics to the ESA. A shift to lower angled 50°-70° dipping planes is seen in the eastern Marlborough region towards the coast. Nelson has some steep dipping planes up to 90° associated with sandstones and igneous intrusions; however, there is a dominance of 30°-50° degree dipping planes in eastern areas of Nelson. Rock-type in the Fiordland region correlates well with the dipping characteristics of the bedrock; the plutonic volcanic rocks show higher dipping characteristics than the metamorphic rocks in the south-west of the region (Fig. 2.9, Fig. 2.10 and Fig. 2.11). A band of low angled dipping planes, predominantly between 0°-30°, is noticeable in the schists that align down the southern WSA and turn across northern and central Otago to the east coast.

The frequency density plots show that the majority of RAs occur on steeply dipping bedrock between 40°-90° (Fig. 2.11 A). Every region sampled shows high bedding dip values corresponding, for the most part, with the occurrence of rock-avalanching regardless of the rock-types shown in Fig. 2.9.

2.3.6 Rainfall

Average annual rainfall (AAR) is highly variable across the South Island and is dominated by westerly low pressure systems from the Tasman Sea (Fig. 2.12; Henderson

and Thompson, 1999). AAR is orographically enhanced on the west of South Island and therefore shows a dominance of high rainfall over the Nelson, West Coast and Fiordland regions with up to ~13m. In comparison, some areas east of the SAMD receive as little as ~0.3m. There is rapid attenuation of rainfall from west to east across the majority of the South Island (Fig. 2.12 cont. E-J). Peak rainfall does not usually coincide with the highest elevation on the SAMD; rather it lies to the west of peak elevation as the western range front reaches ~1000m in elevation. In every profile the variability in rainfall within the swath sharply decreases as rainfall attenuates across the mountain ranges (Fig. 2.12 cont.).

Only two of the RADs listed within the inventory have a rainfall trigger associated with them. These RADs have both occurred in areas of rainfall attenuation and are on the eastern side of their respective mountain ranges. AAR at the Iris Burn RAD (inventory number 260) is 2.6m whilst the Murchison Glacier RAD (inventory number 171) in the ESA has an AAR value of 8.8m.

Frequency density plots of the rainfall values at each RAD shows that the majority of deposits occur in relatively low rainfall environments (Fig. 2.12 NEL, MA, ESA). Marlborough and the ESA show the majority of RADs occurring with 0-4m of annual rainfall, however this does not account for the intensity and duration of the delivery of that rainfall. The WSA and Fiordland have the majority of RADs occurring within high-rainfall zones; however, no WSA RAs and only the Iris Burn in Fiordland have a rainfall trigger.

2.3.7 Routing of rock-avalanche sediment through South Island catchments

Modelled suspended sediment yields (SSY) for the South Island vary dramatically between different regions. Fig. 2.14 shows SSYs for the South Island (Hicks et al., 2011; NIWA, 2015) Nelson and Marlborough show similar and relatively low SSYs between 10-500 $t.km^{-2}yr^{-1}$, whilst Fiordland shows very low yields of between 0-200 $t.km^{-2}yr^{-1}$.

The SSY model does not explicitly weight hillslope erosion processes, delivery processes to river channels or in-channel bank erosion processes. Instead, the model uses a driving factor and a supply factor. The driving factor determines the rate at which erosion and delivery processes operate within the landscape based upon rainfall and runoff. The supply factor determines the availability of sediment and the proportional delivery of that sediment to the river channel network, i.e. geological factors (lithology, induration, weathering and deformation), erosion processes, soils and slope morphology (Hicks et al., 2011). Hicks et al. (2011) adjusted supply factor values for four South Island regions (Northwest Nelson, Fiordland, central/axial Southern Alps and Mackenzie Country) based upon the presence of different factors affecting sediment yields in these regions. For example regional tectonic settings, glacial history and uplift rates vary

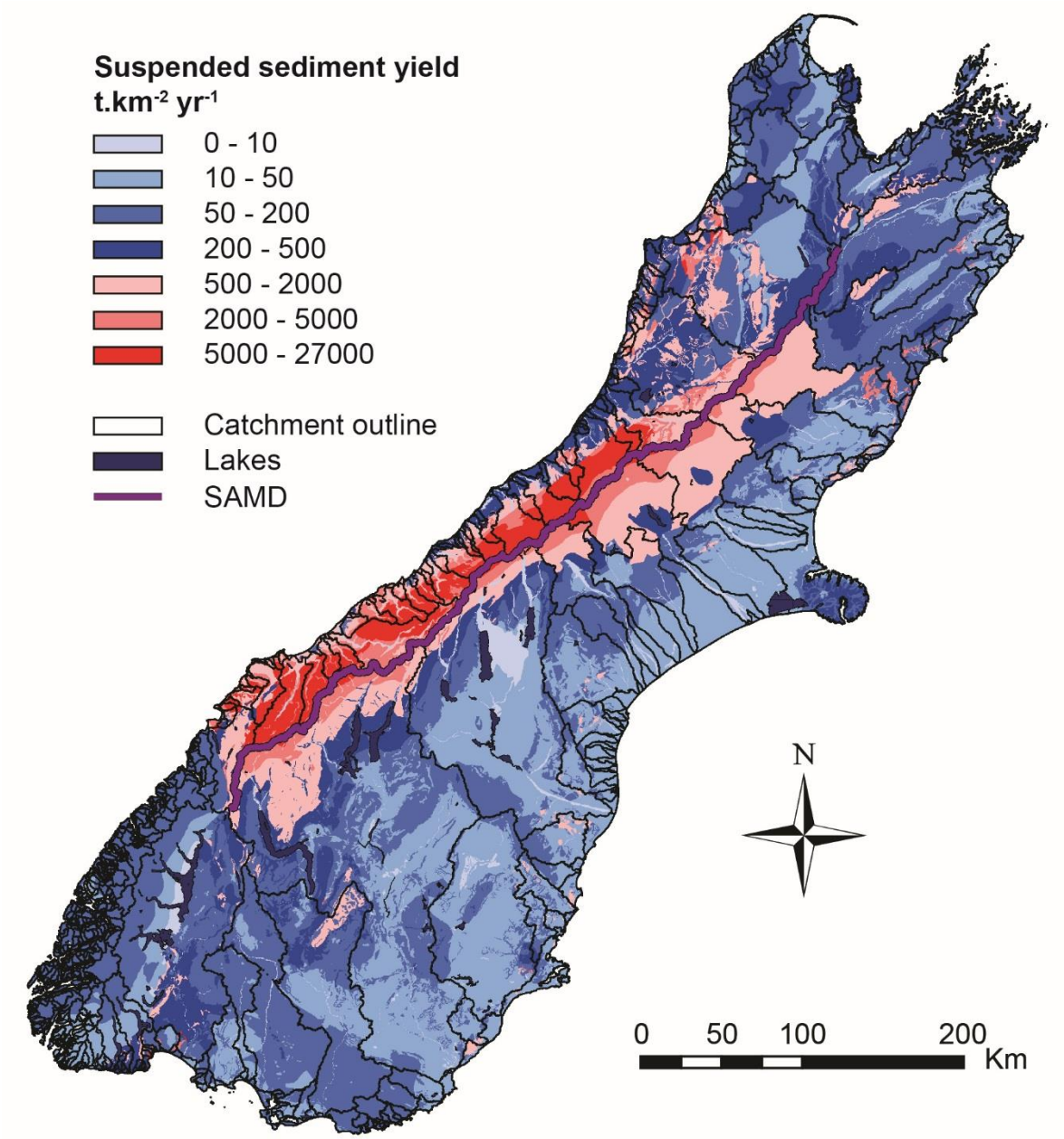

Fig. 2.14 Map of suspended sediment yields (SSY; Hicks et al., 1996; NIWA, 2015) for the South Island, showing large areas of sediment production within the Southern Alps mountain range and relatively low sediment production in all other mountain regions.

between South Island regions, therefore the supply factors were altered until modelled SSYs were in line with recorded data for selected rivers.

The Hicks et al. (2011) SSY model does account for some input of sediment from glacial sources. Previous work has shown that in glacierised catchments, glacier sediment may not be the largest contributor of sediment to a catchment; Hicks et al. (1990) examining the sedimentation of Ivory Lake in the Southern Alps determined that 60% of sediment entering the lake was derived from the rock walls surrounding the lake and those upstream above the glacier. Some of the sediment was directly inputted into the lake by runoff whilst some rockfall material onto the glacier surface was remobilised by

runoff and sluiced into the lake. This indicates that landslide material may be more significant to SSYs in glacierised catchments than glacially eroded material.

The WSA has the highest SSYs for the Island with a range of 500-27,200 $t.km^{-2}yr^{-1}$ extending from the SAMD to the western range front along the whole length of the mountain range. The WSA sediment production is dominated by landslide material from high-magnitude, low-frequency landsliding events (Hovius et al., 1997) indicating the glacial signal is probably less important in these river systems. These high-magnitude, low frequency landsliding events will include RAs. In the ESA, whilst sediment production is high in the glacierised headwaters this signature is rapidly curtailed by large lakes present at the range front of the lower and central SA as well as glacial lake systems in the Mt Cook region. Lakes are assumed to sequester all sediment that is delivered into them. If landslides, including RAs, are larger contributors to suspended sediment in glacierised catchments than glacially eroded sediment then RA material should be present in the suspended sediment of both WSA and ESA catchments but may be held in sinks such as lakes. This SSY model is primarily used in this thesis to indicate that WSA catchments have relatively higher levels of suspended-sediment than other regions of the South Island and that lakes in the ESA could be efficient traps for fine-grained, fluvially reworked RAD material.

Fig. 2.15 shows the cumulative volume of RA material contained within major South Island catchments (Digital Appendix 2.3). Most notable are the higher volumes of material within large east draining catchments with values up to $1.5km^3$. This is expected considering that they cover a larger spatial area of mountainous terrain within the SA and that these catchments contain large numbers of RADs which amass to large sediment volumes. Smaller catchments draining the WSA have fewer RADs per catchment which in some cases means that there is very limited RA material. However, some of the catchments, such as the Cascade River in the south (Fig. 2.15), display similar cumulative RAD volumes to those of the ESA catchments despite the considerably smaller area. Nelson and Marlborough show moderate cumulative volumes compared to the SA of between $0.0008\text{-}0.08km^3$. However, given the similar cumulative RAD volumes the Marlborough catchments have few deposits whereas Nelson catchments have high deposit counts within each catchment. There are many catchments with headwaters in mountainous terrain that have no recorded RADs; these catchments occur in the Nelson, Marlborough, WSA and Fiordland regions.

Fig. 2.16 shows the cumulative volume of RADs as a ratio to catchment area. Smaller western draining catchments have fewer deposits however the material is more concentrated within these smaller areas leading to comparable concentrations of material to ESA catchments which have larger RAD populations but larger catchment areas. In some cases, such as the largest South Island catchment, the Clutha, it can be seen that

even though the headwaters are in mountainous terrain there are very few RADs and that the volume of material is relatively small in comparison with the catchment area. Conversely catchments such as the Cascade River on the west coast have very high-volumes of RA material given the catchment size. This pattern is repeated in many Fiordland river systems where the catchment area is very small but the RADs have high volumes.

In terms of the storage of material within river catchments, Quaternary sedimentation is going to be the main sub-aerial sink for reworked material. Therefore a ratio of RAD volume to area of Quaternary sediment within each catchment was calculated (Fig. 2.17). It can be seen that scattered west coast catchments, the north of Fiordland and one catchment in Nelson have high ratios of RAD volume (m^3) to Quaternary sediment area (m^2). Some of these catchments have comparable ratios of between 1-6:1 RAD volume (m^3) to available Quaternary sediment area (m^2); with the John O'Groats catchment in Fiordland having a 697:1 ratio. This indicates that RAD material stored in these Quaternary deposits is likely to be higher in concentration than the eastern draining catchments even though the ESA has denser populations of RADs.

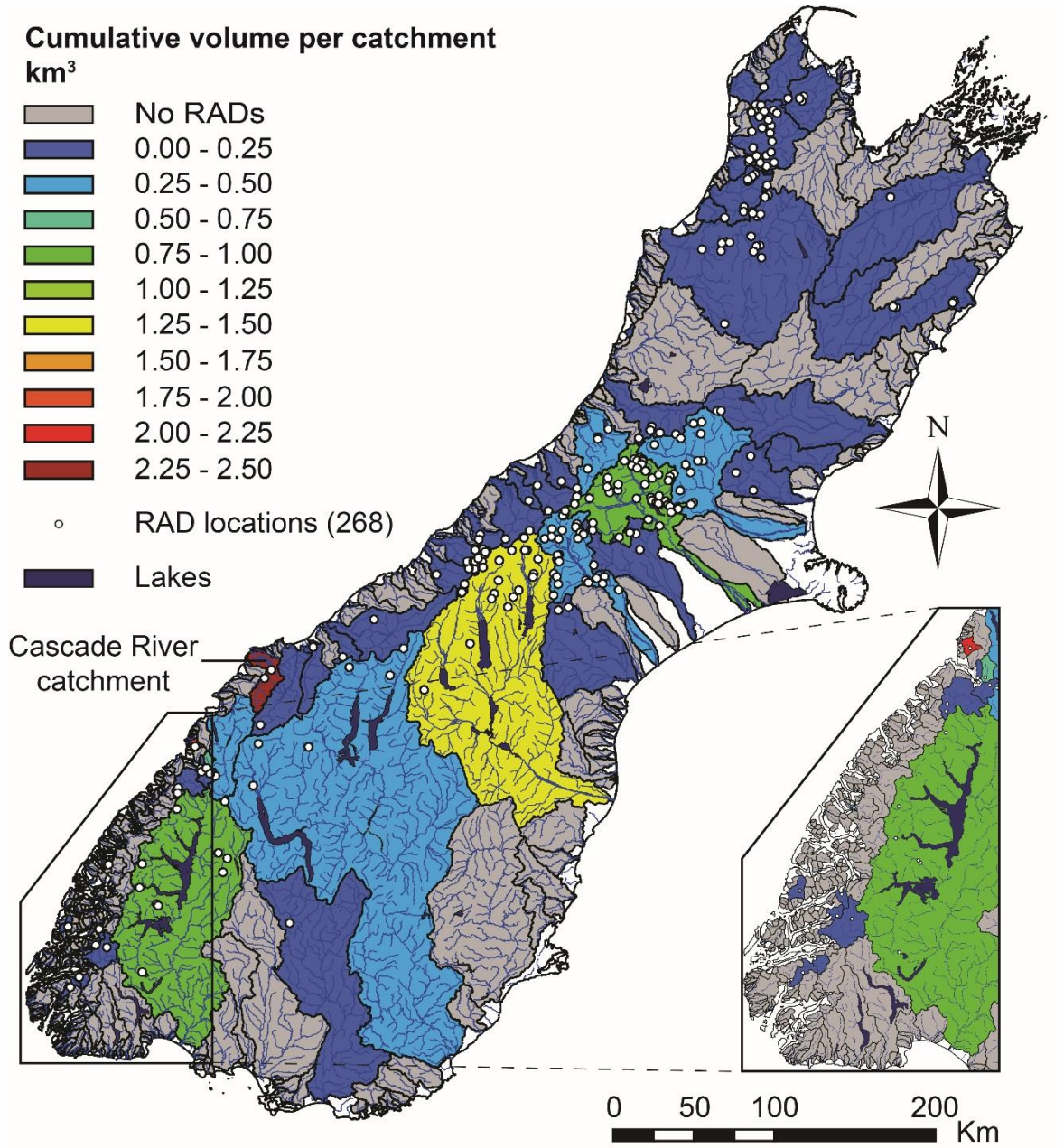

Fig. 2.15 Cumulative RAD volume (km^3) within South Island catchments. The Cascade River on the west coast is indicated. The inset figure is a zoomed view of Fiordland showing smaller densely packed catchments.

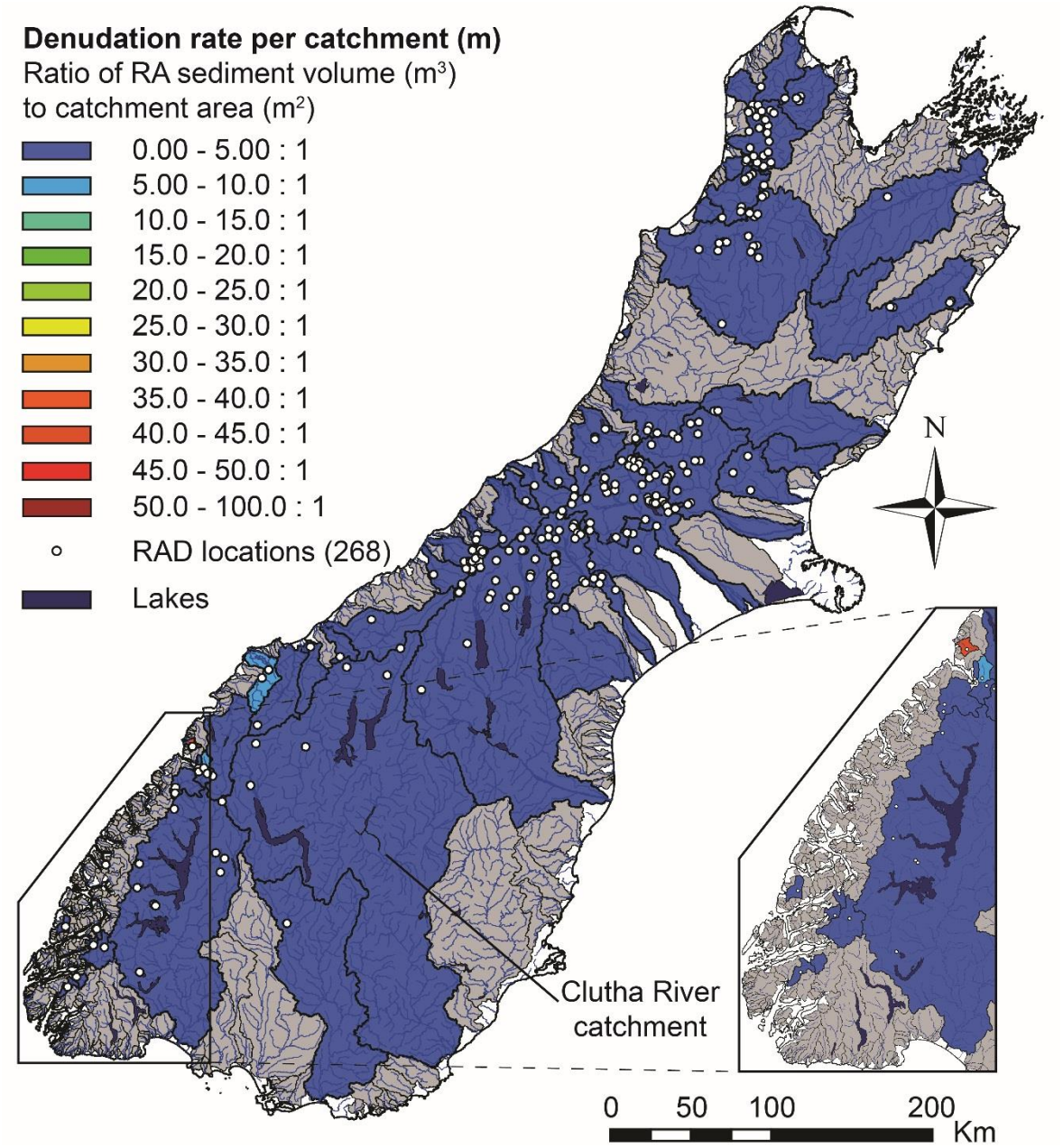

Fig. 2.16 Map of South Island showing the denudation rate per catchment due to RAs over the time period of the inventory; i.e. the ratio of RAD sediment per catchment (m^3) to catchment area (m^2). The inset figure is a zoomed view of Fiordland.

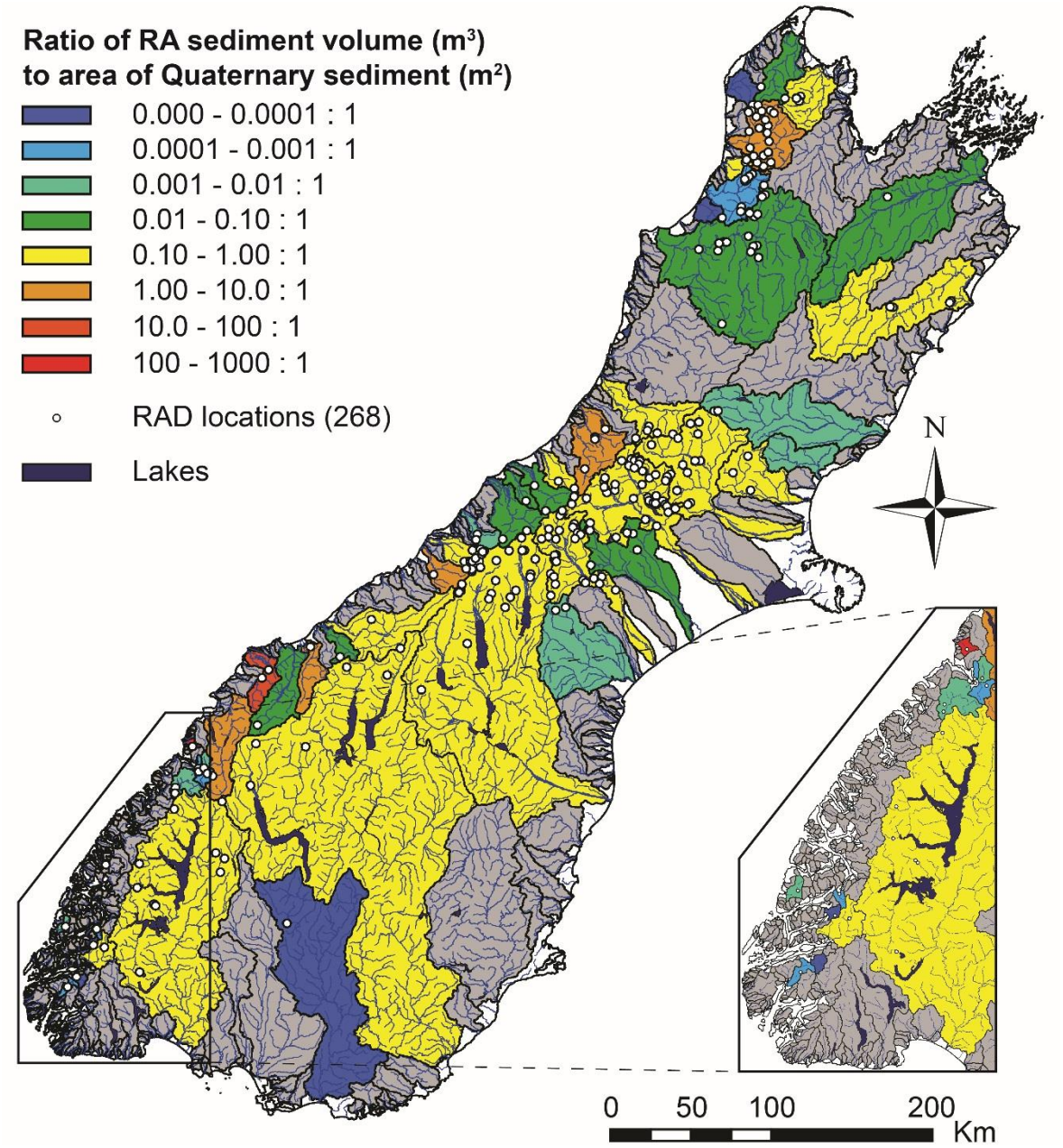

Fig. 2.17 Catchments with ratio of RAD volume per catchment (m^3) to the area of Quaternary sediment deposition within the catchment (m^2). The inset figure is a zoomed view of Fiordland.

Fig. 2.18 shows the potential storage and routing of RAD material within South Island catchments. Recent RAs in the central SA, near the SAMD, have often fallen glaciers meaning they may either reside on the surface of the ice (Evans, 2008) or material will be sequestered into englacial ice (Dunning et al., 2015). Eventually these deposits will be worked down the glacial system to become moraine material. Beyond ice bound deposits the majority of RADs occur close to rivers and lakes. Many of these rivers have the capability to rework RAD material downstream.

Green markers in Fig. 2.18 indicate RADs that may be reworked by rivers into lakes; lakes which may act as potential sinks for RAD material are marked in orange. The majority of RADs are connected to fluvial systems which have a direct outflow to the ocean without obstruction by lakes (Fig. 2.18 red markers). This indicates that fluvially reworked RAD material in these catchments will likely be deposited in alluvial material or washed out into pelagic sediments. RADs above glaciers (Fig. 2.18 yellow markers) are buffered from the fluvial system and may only contribute sediment to glacial meltwater systems until they are glacially reworked into moraines.

In the Waitaki catchment (Fig. 2.19) fluvially reworked RAD material would travel down rivers and into the major lakes of the region indicating that these may be major stores for a large volume of RA or other landslide material. Additionally RAD material that is reworked by glacial meltwater may be stored within glacial lakes at the terminus of SA glaciers (Fig. 2.19). The Waitaki is indicative of other catchments to the south where the majority of reworked RAD material would be sequestered by lake systems. In total 59 RADs from the inventory are located upstream of lakes, 14 of those in the Waitaki catchment. If RADs have been censored by fluvial erosion, lakes may present an archive of their occurrence. However fluvial reworking processes do not take account of rock-avalanching directly into lakes and fiords which would accumulate more RADs into these sediment sinks.

2.4 Discussion

The compilation of the literature based inventory presented here has allowed the analysis of the spatial distribution of RADs within the South Island of NZ to be analysed in conjunction with a number of factors which could trigger or pre-condition slopes for failure. The inventory as it stands is considered incomplete on a number of accounts; firstly, it is highly likely that RADs are missing from the inventory, especially beyond the last ~100 years as seen in Fig. 2.13. The large gaps within the temporal record over the majority of the last 12,000 years suggest both missing data from undated deposits and deposit censoring.

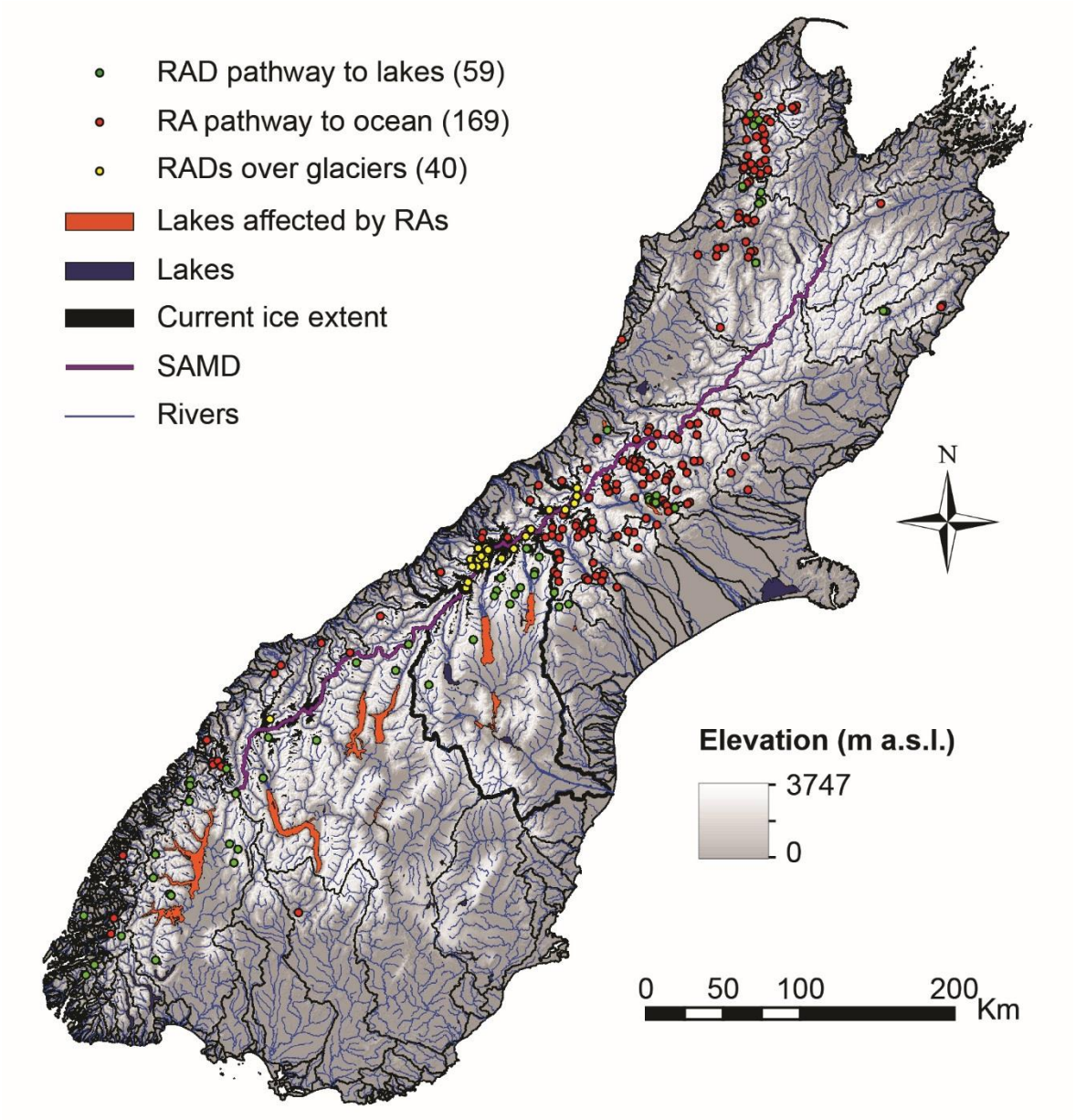

Fig. 2.18 Map of RADs with pathways to lakes, the ocean or glacial entrainment. Lakes in orange block fluvial pathways in catchments and could be significant sediment sinks; these lakes could potentially store reworked RAD sediment. The thicker catchment outline shows the zoomed section in Fig. 2.19.

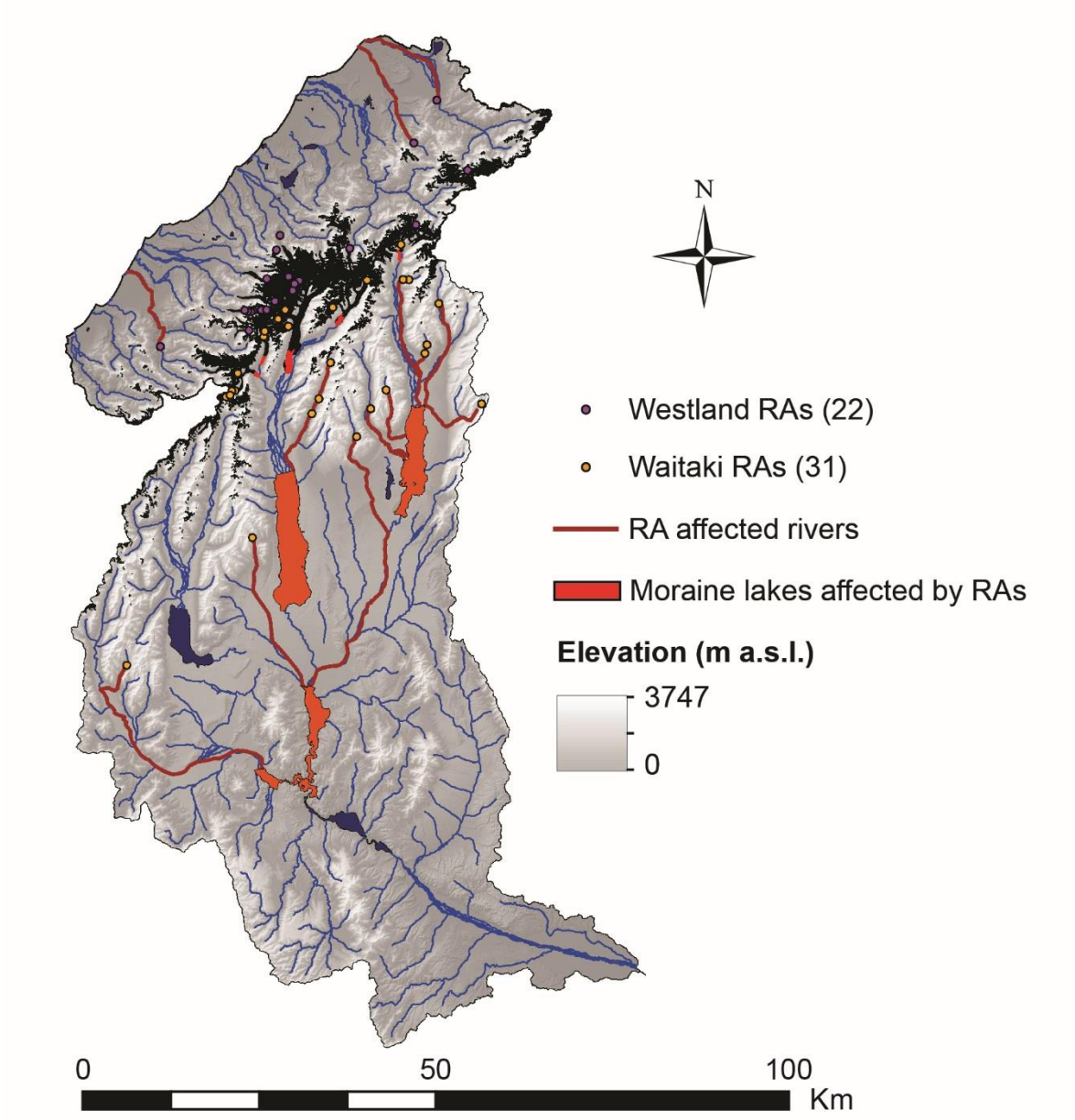

Fig. 2.19 Comparison of fluvial sediment routing characteristics in east and west draining catchments. Large east draining catchments in the south mostly drain into large lakes and reservoirs whereas small west draining river systems mostly have unobstructed channels to the ocean. Glacially entrained RAD material can be routed to moraine dammed lakes.

As research has progressed, views on return periods for RA occurrence in the SA have shifted; based on an inventory of 42 RADs, Whitehouse & Griffiths (1983) suggested a 92 year return period for $>10^6 m^3$ events over the last 1,700 years. McSaveney et al. (2015) show that occurrence rates for the 2004-2014 rise to every 0.5 years on average. However, in this study this has been further broken down to include the last 100 years (Fig. 2.13c) to explain phases of RA generation and quiescence. The temporal distribution of RADs over the last 100 years appears to show phases of RA occurrence which could be linked to changes in the accumulation, release and transference of strain throughout the South Island fault system. Initially the large 1929 Murchison and Arthur's Pass earthquakes dominate the temporal distribution; however, this is followed by a 62-year quiescent phase with limited RA generation where recurrence rates are only 5.6 years on average. The large 1929 earthquakes released accumulated shear strain with their rupture and Berryman (1980) hypothesised that this led to a period of relative earthquake inactivity in the region. With the occurrence of modern aseismic RAs linked to accumulating shear strain by (McSaveney et al., 2014, 2015), the quiescent phase between 1929 and 1991 (Fig. 2.13c) could therefore represent a period of strain accumulation after large earthquake events where few RAs are generated as (1) shear strain released after the 1929 earthquakes has no accumulated back to a threshold required for RA generation and (2) there is a period of relative earthquake inactivity after the 1929 events (Berryman, 1980); ~60% of the ≥M6 earthquakes from this period occur offshore of Fiordland (Fig. 2.6; GeoNet, 2015).

A further breakdown of the time periods used by McSaveney et al. (2015) show two distinct phases of the increase in average RA occurrence rates. The onset of a rise in RA occurrence to every 1.2 years on average is visible from 1991 to 2004; 10 RAs occurred in total in this time period, and of the 8 RAs with unknown triggers, 7 occurred in high shear strain environments (Fig. 2.8) mostly adjacent to the SAMD. The increase in occurrence rates in 1991 indicates that this could be a transitionary period where shear strain accumulation, due to crustal deformation, has crossed a threshold and is driving the detachment of fractured and weak bedrock in the SA generating RAs. The period of 2004-2010 sees RA occurrence rates increase to every 0.5 years on average (Fig. 2.13c), again all deposits are clustered around the SAMD and are in high shear strain environments. This indicates that after the transitionary phase there is a rapid acceleration of RA occurrence. After 2010 the rate of RA occurrence decreases to every 1 year; however, it is unclear where this trend will go in the future.

The PDF plot for landslide area (Fig. 2.5) has implications for both the generation of modern RAs and the censoring of deposits from the sedimentary record. Above $0.2 km^2$ the inventory represents a traditional negative power law trend for landslide area data (Brunetti et al., 2014). However, some log bins used for the analysis have no recorded

deposits, indicating that some may be missing from the inventory. The rollover, incorporating RADs with aerial extents between 0.04km^2 and 0.2km^2, further indicates that the inventory is not complete within this size range. A common problem for landslide inventory PDFs is the undersampling of smaller deposits due to the scale of images used for mapping or the censoring of those deposits from the record (Stark and Hovius, 2001; Davies and Korup, 2010). The rollover (Fig. 2.5) represents an incomplete inventory and the majority of RADs within the rollover are small, valley confined and restricted to Nelson and the ESA. It is therefore likely that deposits in this size range have been rapidly censored from other regions by fluvial erosion and vegetation cover. The WSA and Fiordland both have high rainfall which can increase the efficacy of fluvial erosional processes (Barth, 2014) and rapid vegetation growth (Malamud et al., 2004), obscuring deposits. As no deposits in the rollover exist within the WSA and Fiordland it is hypothesised that these censoring processes operate with greater efficacy in these regions of the South Island and that RADs may be more susceptible to these censoring processes within this size range. The secondary trend between 0.04km^2 and 0.004km^2 within the PDF for RAD area (Fig. 2.5) is not observed in typical landslide distributions. Six of the eight deposits within the secondary trend are those with unknown triggering factors between 2008 and 2010. They are located within the high SA above glaciers. The deposit ages, location near the SAMD, plus the deviation of the secondary trend from the rollover and inverse power law of the larger deposits indicates that this sub-population of the inventory is process driven and linked to shear strain accumulation (McSaveney et al., 2014, 2015). However the location of many of these RADs over glaciers indicates that these smaller deposits could be rapidly censored by glacial sequestration processes (Dunning et al., 2015) which could also have affected the distribution of the secondary trend.

The spatial distribution (Fig. 2.2) indicates that the Marlborough and Fiordland regions have fewer deposits than would be expected in these mountainous regions. Both regions have experienced earthquake shaking since 1800 that is capable of producing RAs (Fig. 2.6), yet only one deposit is recorded; the PGA for both regions suggests that high MM shaking is likely to have been experienced in these regions within the last 2,500 years (Fig. 2.7) and for Marlborough the geological conditions, similar to that of the ESA, suggest that RADs should be present in this region (Fig. 2.9). 12 deposits were identified in Marlborough and a further 18 in Fiordland, with good potential of being RADs based upon size and surface morphology; however field investigations would be needed to confirm this through sedimentological analysis. Current research is looking at addressing the sub-aqueous and glacial censoring using remote sensing techniques (Dykstra, 2012; Dunning et al., 2015). The inventory presented here shows a distinct lack of deposits surrounding lakes and fiords within the South Island; given the identification of 26 large landslide deposits within Milford Sound (Dykstra, 2012; Taig and Mcsaveney, 2015) it

appears likely that an archive of RADs exists in these environments but are currently censored from the record. Misidentification of deposits is also being addressed by sedimentological analysis techniques (Reznichenko et al., 2012), however these techniques are just beginning to make impacts in NZ and cannot yet trace deposits that have been buried or reworked by fluvial activity, limiting the amount of palaeo-reconstruction of RADs that can be done.

Whilst attempts have been made to systematically map the majority of deposits within the inventory there are still gaps in the data for landslide area, volume, age and trigger factors for known deposits. Area, volume and age have the potential to be addressed through intensive field and laboratory investigations. For pre-historic and ancient deposits without known trigger factors it is difficult to accurately attribute factors to them as it impossible to know the antecedent conditions leading to rock mass collapse.

Given the available information compiled in the database it appears that different regions of the South Island are controlled by differing preparatory, preconditioning and trigger factors. There is also the likelihood of censoring processes removing deposits from the sedimentary record. Here each of the defined study regions is examined with regards to the potential controls on RA occurrence.

2.4.1 Southern Alps

The SA mountain range hosts the majority of RADs within the inventory. The spatial distribution is split between the large cluster in the northern and central WSA/ESA and sparse distribution in the southern section of the mountain range. The vast majority of RAs within the SA have occurred above regional modal hillslope angles of ~32°, a threshold hypothesised by Clarke and Burbank, (2010) for RA generation. Slope gradient distributions indicate that hillslopes within the southern section of the ESA/WSA, where diminished RAD occurrence is observed are also above regional modal hillslope gradients. Furthermore, similar geology is maintained between the northern and southern ESA/WSA indicating that similar levels of RAD occurrence would be observed if this was a controlling factor in their generation within this region. Shear strain accumulation has already been discussed as a trigger for modern events with no known trigger mechanism within the highest mountain region of the SA (McSaveney et al., 2015); however the accumulation of shear strain does drop in the southern section of the ESA and could account for the paucity of deposits. With the exception of the 2007 Young River deposit, the deposits in the southern section of the ESA are all ancient or have no age data associated with them; they are also associated with a gap in the occurrence of >M6 earthquakes since 1800. These factors both suggest that RADs are scarce in the southern ESA as there haven't been any earthquakes large enough to trigger them and shear strain

accumulation is too low to generate them in between seismic events, unlike other zones of the SA.

In the southern WSA there are occurrences of modern RADs near the SAMD, however there is a scarcity of deposits when compared to the ESA. Many of the conditions necessary for RAD generation exist within the WSA region. Given the likelihood of RADs being generated in the WSA due to large AF earthquakes (Fig. 2.6) or through the accumulation of shear strain throughout the region in earthquake quiescent phases (Fig. 2.13c) there are fewer deposits than expected. This is further supported by the lack of smaller RADs located within the probability density distribution for deposit area. It is therefore suggested that deposits have been censored from the WSA; this is likely driven by the high rainfall causing higher fluvial erosion rates when compared to other South Island regions and temperate rainforest vegetation growth driven by the climate. Examples of pre-historic and aerially larger deposits are located within the WSA but are heavily eroded by fluvial processes (Chevalier et al., 2009; Barth, 2014) adding further evidence to support deposit censoring.

2.4.2 Nelson

Nelson is entirely dominated by earthquake generated RADs and almost exclusively by the 1929 Murchison earthquake (Fig. 2.2; Hancox et al. 1997). Given the difference in the Nelson region to the other South Island regions examined it is not unsurprising that rock-avalanching here is dominated by a single trigger. In this region many of the other factors affecting RA triggering that have been discussed would appear to limit their occurrence rather than encourage it.

Nelson has relatively low topography in comparison to the SA, Fiordland and Marlborough; as well as predominantly stronger igneous rocks throughout the region (Fig. 2.9; Table 2.2). Hillslope frequency distributions show comparatively shallower slopes than those of other regions, maximum shear strain rates are also consistently low and only comparable in magnitude to Fiordland. However ≥M6 earthquakes have been shown to have occurred frequently within the last ~200 years and moderately high shaking is probable over the 2,500 year recurrence period of the PGA map. This indicates that in order to generate rock-avalanching on the scale that is observed in Nelson then an earthquake trigger is needed and will be again if more rock-avalanching is to occur. Parker et al., (2015) whilst examining the 1929 and 1968 EILs from the Murchison and Inangahua earthquakes found that areas which experienced strong ground motion in the former earthquake were more likely to have slope failures in the latter earthquake. Given that only one RAD was recorded between 1929 and 1968 and that event was the re-activation of a previous RA source scar; plus only two recorded RADs occurred pre-1929,

both dating back to 1650 and thought to be co-seismic, it would appear that earthquakes are needed for widespread RA generation in Nelson.

2.4.3 Fiordland

Twenty-two RADs reside within the studied Fiordland region and age information shows a wide variety of deposit ages starting at ~6,144BP suggesting that RA occurrence has been ongoing in this region since the mid-Holocene. However deposits are sparsely located within the region given that RA generating preconditions and triggers are present within the region. Hillslopes are predominantly steeper than other areas of the island with regional modal values of 36°, above the threshold of 32° hypothesised for RAD generation. PGA maps suggest that there is a moderate likelihood that strong, RA generating ground shaking will have occurred within the last 2,500 years, however only three of the known deposits within the region are within this time period. Many of the deposits are either confirmed to be co-seismically triggered or probably co-seismically triggered indicating that earthquake shaking is required for the majority of RA generation in the region; however many of the earthquakes capable of generating RAs in Fiordland occur offshore, probably due to the offshore location of the continuation of the AF in this region.

In terms of rock-type and bedrock dipping factors the region is similar to that of Nelson, an area which is almost completely earthquake controlled, indicating that a similar limiting factor may be present in Fiordland. It is possible that RA generation is heavily linked to onshore earthquakes in Fiordland and few RADs are generated as a result of fewer onshore earthquakes. However 18 deposits were identified in Fiordland which have good potential to be RADs (Fig. 2.2) suggesting that a censoring and potentially sampling bias might be present. Given the coastal location of earthquakes capable of generating RAs there is potential for large scale occlusion of deposits within fiords; this has already shown to be the case within the populated Milford Sound (Dykstra, 2012) and could easily account for the sparsity of deposits within the region.

2.4.4 Marlborough

Although only the Miller stream deposit is attributed to possible co-seismic activity the proximity of the four other Marlborough deposits at Lake Chalice, Lake McRae and the Wharekiki River, to the Wairau, Clarence and Hope Faults respectively it is feasible that these events were co-seismically triggered.

There are some stark similarities between the Marlborough region, which is sparsely populated with RADs and the ESA which is densely populated with RADs. The geology remains consistent throughout the ESA and up into Marlborough with sandstone-

greywacke rocks dominating. Regional hillslope gradient distributions and regional bedrock dipping distributions are also comparable between the two regions.

PGA maps which are shown by Hancox et al. (2002) to be closely linked to EIL opportunity show high PGA values throughout the majority of the Marlborough region. Other examined regions of the island such as the WSA and Fiordland which have similar PGA values show higher rock-avalanching rates than that of Marlborough. Given that co-seismic landsliding events correlate relatively well with a 475 year return period of EIL opportunity (Hancox et al., 2002) and within that pattern of landsliding there have been co-seismically triggered RADs within Nelson, the SA and Fiordland it would be expected that there be many more RADs within the Marlborough region. The position of the active MFZ as well as historic earthquakes capable of generating RADs also indicates that more RADs would be expected within the region. Currently the only deposits that have been dated in the Marlborough region are ~1700-2000 years old, indicating that there is the potential for many ancient and modern RADs to have been censored. Again, analysis of aerial imagery of the region identified 12 deposits with good potential for being RADs based upon their surface morphology. Whilst these deposits cannot be explicitly identified as RADs they show that there is potential for excessive censoring of deposits within this region. However, notably two historic earthquakes, the 1848 M~7.4 Marlborough produced no known RADs and the 2016 M_w 7.8 Kaikoura earthquake produced only 1 possible deposit.

This leads to three possible outcomes, firstly there are many RADs within the Marlborough region and they have been censored by fluvial processes, vegetation cover, prevalent scree cover or non-identification of deposits. Secondly, as only 1 deposit was generated in the 2016 Kaikoura earthquake, hillslopes may be preconditioned by past earthquake activity and tectonic strain and large scale rock-avalanching may occur during a future large earthquake rupture. Linked to this it is possible that co-seismic RAs are not generated in Marlborough during earthquake inactivity, unlike the ESA/WSA regions. Thirdly there is an as yet unexamined control which is preventing the occurrence of RAs within the region.

2.5 Summary and conclusions

A large RAD inventory of 268 deposits and 47 potential deposits has been presented. The inventory had the aims to (1) Compile information on RADs into a single, user-friendly data source; (2) Use the spatial distribution of the RADs to hypothesise controls on their occurrence within differing regions of the island; (3) Use the spatial and temporal distribution of the inventory in order to examine whether deposits may have been censored within the South Island and (4) Examine the potential sedimentological legacy of RADs at the catchment scale.

Analysis of the inventory has shown that controls on RA occurrence appear to vary between mountainous regions of the South Island, with earthquake generation being a key trigger in the Fiordland and Nelson regions. Characteristics of the SA show that whilst earthquake shaking has had an impact on the generation of deposit clusters, such as near Arthur's Pass, modern RADs from 1979-present are well correlated with greater shear strain measurements along the SAMD. Many of the deposits remain with unknown trigger factors however 2,500 year PGA models indicate that seismic activity may have had a larger impact on RAD occurrence than can be shown here. The Marlborough region is topographically and geologically similar to the ESA, however shows the occurrence of very few rock-avalanching events. RADs that have been recorded are proximal to major faults indicating that seismic activity is a likely cause for those events. Given the similarities in bedrock structure, seismic activity and modelled PGA as a proxy for EIL opportunity there appears to be little difference in the examined controls between the SA and Marlborough but a large difference in the occurrence of RADs. This suggests either another as yet unexamined control, censoring of deposits on a massive scale, RAs only occurring during earthquake shaking or bias in the lack of detailed RA research in the region. Analysis of regional hillslope angle distributions and estimates of pre-failure slope angles for RA source areas show that the majority of RAs are initiated on slopes steeper than 32° indicating this as a threshold value for RA generation.

The spatial distribution of the inventory shows that rock-avalanching occurs in areas with very intense rainfall and very little rainfall. From the information available it appears that rainfall has little impact as an actual trigger mechanism within the South Island, although many events have unknown trigger factors. This does not exclude rainfall as a preparatory factor in RA initiation. Many of the events with known triggers in the database have little information on antecedent conditions and therefore rainfall as a preparatory factor cannot be ruled out.

The temporal inventory shows large gaps within the record, some of more than 1000 years. Whilst not every deposit within the inventory is included in the temporal analysis, due to missing data, they would not be sufficient to fill the gaps in the record. This again suggests that as would be expected deposits have been censored from the record and that this censoring does impact the older early Holocene record more so than the mid to late Holocene.

In terms of the redistribution of RA sediment through fluvial systems it is clear that much of the RAD volume lies in the SA, east of the SAMD. However, in terms of catchments which are most affected by large RADs it appears that a number of smaller West Coast catchments have high volumes of sediment in comparison to their size. Large east draining catchments in the central and lower SA have high-volumes but much of this sediment will end up entrained in lake deposits. Eastern draining catchments in the

northern SA show high-volumes of material and the ability to redistribute that material throughout the entire river length. Small west draining catchments also have clear pathways from RA source to the sea implying that much of this sediment will be carried straight through the system, however many alluvial fans have evolved on the western range front of the SA and therefore these areas may be an excellent sink for RA material.

Chapter 3

Tracing a micro-sedimentological signature of rock-avalanches through fluvial systems

3.1 Introduction

This chapter discusses field and laboratory analysis of rock-avalanche (RA) sediment, controls on fluvial reworking of RA material and detection of that material in NZ river systems. The work of Reznichenko et al., (2012) shows that agglomerates, coherent grains (<1mm) composed of microscopic (micron to sub-micron) particles that are diagnostic of RADs (Reznichenko et al., 2012), persist for up to 10^4 years in RA sediment that has fallen onto glaciers, been supra-glacially transported to the terminus and deposited as moraine material. This indicates that agglomerates are able to persist through glacial entrainment and passive water percolation processes. Due to the preservation potential of agglomerates in glacial systems, the presence of a large number of RADs within the South Island and the apparent censoring of those deposits (Chapter 2), it has been anecdotally suggested that RA material and therefore agglomerate grains may be ubiquitous within South Island fluvial material (Tim Davies, 2014 pers. comm.).

If fluvially reworked agglomerates are preserved in fluvial depositional environments, then they can be used to indicate the presence of censored or previously unidentified RADs upstream of any given sampling location. Given the preservation potential of agglomerates in passive glacial transport, the hypothesis tested in this chapter is that agglomerates will be preserved under turbulent fluvial transport and depositional processes.

To test the preservation potential of agglomerates within fluvial systems, sampling of RAD and fine-grained fluvial sediment was conducted in South Island river systems. Three sampling strategies were employed to test the traceability of agglomerates through river systems, (1) Systematic sampling of RADs and fluvial sediment downstream from the deposit, (2) Stratigraphic sampling through an alluvial fan known to have been affected by RA dam breach flooding and pluvially driven flooding (3) Systematic single point sampling of West Coast rivers. Sampling locations were selected to ensure that there should be agglomerate grains located in in-situ deposits, there is known and recorded reworking of RAD material in dam breach flooding and contemporary river processes have the potential to continue to rework the deposits.

3.1.1 Agglomerate formation and detection

Whilst the internal RA 'flow' processes driving the hypermobility of RAs, such as dynamic fragmentation, are still debated within the literature (Chapter 1) all agree that there is intense comminution of material during RA motion (Davies et al., 1999; Hungr, 2006; Rait et al., 2012; Pudasaini and Miller, 2013). The fragments of material resulting from comminution are within a high-pressure confined environment during RA motion; when grains are fractured they cannot disperse as void spaces generated by clast fragmentation rapidly collapse. Instead fractured grains 'agglomerate' through interparticulate forces, a characteristic occurrence in very fine-grained RA material (Reznichenko, 2012; Reznichenko et al., 2012). For dry, granular material interparticulate forces are predominantly electrostatic charges between particles and van de Waals forces between the molecules which compose particles (Castellanos, 2005), this is especially true of particles in the >40μm size range (Zhu, 2004). The fine-grained matrix is closely bonded and can therefore bond some of the larger grains observed within agglomerates. Whilst agglomerates are generated within this high-stress environment it also hypothesised that they may also be destroyed by the high shear stresses generated during RA motion (Mauri McSaveney, 2016 pers. comm.). Experiments conducted by McSaveney, (2016 pers. comm.) show that agglomerates can be generated in the lab using ring shear apparatus to comminute material in an intense pressure environment; these agglomerates were also be destroyed by ultrasounding the grains. It is possible that similar breakdown of agglomerates could occur during RA motion as grains are agglomerated and then comminuted again; in essence, agglomerates may be continually forming and being destroyed as the RA travels down-slope, they are not simply accumulating within the RA sediment. This indicates that agglomerates may not be ubiquitous within a RAD and we are only observing a fraction of the agglomerates that have been generated and persisted to this point.

Reznichenko et al., (2012) were the first to formally identify agglomerates and link them to being diagnostic of RAs. Agglomerates have previously been described within the 63μm-1mm GSF and are defined as being widely graded, sub-angular clasts, composed of finer material down to sub-micron size; they also remain intact after sieve preparation (Reznichenko et al., 2012). Under SEM analysis agglomerates, from ancient and modern in-situ RADs, have key identifiable criteria:

1. Agglomerates should be a coherent, individual grain (Fig. 3.1a),
2. Composition of poorly sorted sub-angular clasts held together by a matrix composed of large proportions of micron to sub-micron particles (Fig. 3.1c and d),
3. Contain few voids within the agglomerate grain,

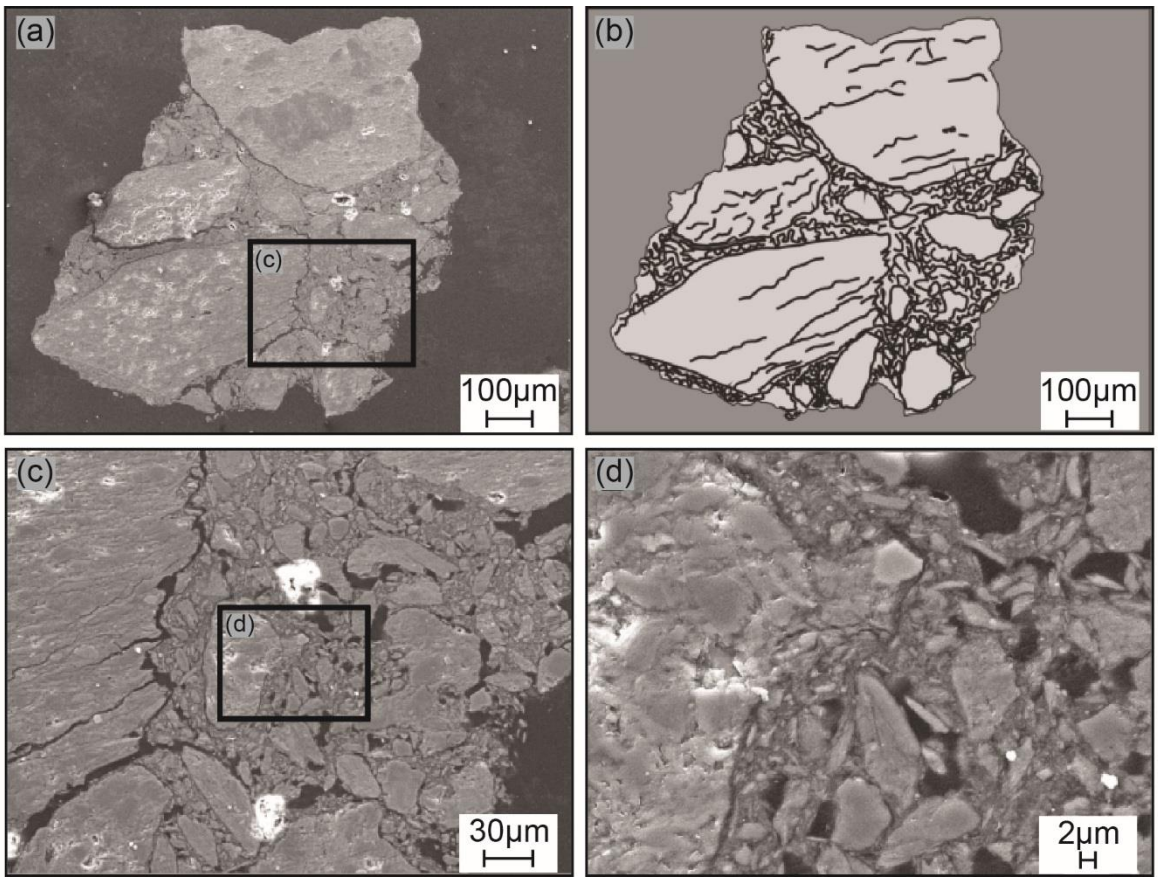

Fig. 3.1 Example of a RA agglomerate grain from Reznichenko (2012); (a) Internal structure of the agglomerate showing the poorly sorted, sub-angular clasts that compose the entire grain; (b) Sketch outline of the agglomerate in (a) highlighting the larger component clasts and the fine grained matrix in between; (c) Zoomed section of the agglomerate in (a) showing the fine grained matrix composed of many sub-angular and sub-rounded particles down to sub-micron size; (d) zoomed section from (c) showing the sub-micron grains that compose much of the fine-grained matrix.

4. In-situ agglomerates may have a coating of fine-grained material adhering to their exterior (Reznichenko, 2012; Reznichenko et al., 2012).
5. Agglomerates should also be free of organics as RAs occur in large rock masses which are largely free of organic material (Reznichenko, 2012).

Agglomerates have been shown to persist through gentle washing in laboratory conditions (Reznichenko, 2012). The above identification criteria were used to distinguish RA agglomerates from other grains within this project. Grains that are sedimentologically similar to agglomerates, in that they are agglomerations of fine grained material into coherent grains, are also found within fault gouge, this supports the theory that agglomerates are generated by high-stress comminution of material (Keulen et al., 2007; Reznichenko, 2012).

3.2 Field site review

Ram Creek and the Stanley River were selected as sites where RADs could be accessed directly as well as fluvial sediment profiles downstream (Fig. 3.2). Poerua River

was selected as a site where the RAD was not accessible, however samples could be taken from an alluvial fan downstream where the river has re-incised through the fan surface. Single spot samples of fine-grained fluvial sediment were collected at an additional 17 West Coast, South Island rivers.

3.2.1 Ram Creek

Ram Creek is a small 9.5km long tributary river of Dee Creek, itself a tributary of the Buller River. The river lies in the Brunner Range west of the AF (Fig. 3.2). The Lyell Fault bisects the Ram Creek catchment near the headwaters in a southwest-northeast direction (Fig. 3.3; Harrison et al., 2015). To the east of the Lyell Fault is Devonian-Early Carboniferous Granite whilst to the west there are Miocene Sandstones and Mudstones (Edbrooke et al., 2014).

In 1968 the M_s7.4 Inangahua Earthquake generated a 4.4 x 10^6 m^3 RA that dammed Ram Creek with 2.8 x 10^6 m^3 of sediment (Inventory number 115; Nash et al., 2008). A landslide-dammed lake with a volume of 1.1 x 10^6 m^3 formed upstream of the RAD (Nash et al., 2008). The RA occurred just east of the Lyell fault in the Granite rocks. This means that Granite sediment downstream is likely derived from the RAD and is easily distinguished from the sedimentary rocks west of the Lyell Fault (Harrison et al., 2015). The Ram Creek dam survived for 13 years before failure; high intensity and persistent rainfall in the week preceding dam failure and on the 29th April 1981 raised the impounded lake level causing overtopping of the RA dam. 95% of the impounded lake volume was released as a catastrophic flood (Nash et al., 2008). The dam-breach flood remobilised ~1 x 10^6 m^3 of RA sediment downstream and formed a breach channel. Sediment from the dam was re-distributed up ~5.5km downstream by the breach flood, however the majority of material was deposited proximally to the RAD (Nash et al., 2008). The contemporary RA breach has 40m high steep sided walls and a narrow armoured river channel at its base (Nash, 2003; Nash et al., 2008; Fig. 3.4a). Due to the large volume of material deposited in a small catchment, Ram Creek continues to be in disequilibrium. Harrison et al., (2015) show that the river has been unable to rework the dam derived material and re-incise to the pre-dam, bedrock base level. This indicates that fluvially reworked sediment that is proximal to the RAD is likely to have been sourced from the RA material.

3.2.2 Stanley River

The Stanley River is a large 13.5km long tributary catchment of the Waingaro River. The catchment is located in the Tasman Mountains in the north of South Island (Fig. 3.2). The local geology is basaltic and andesitic volcaniclastic sedimentary deposits from the Devil River Volcanic Group (Edbrooke et al., 2014). The contemporary Lake Stanley RA dam in fact consists of at least three separate RADs with varying geological

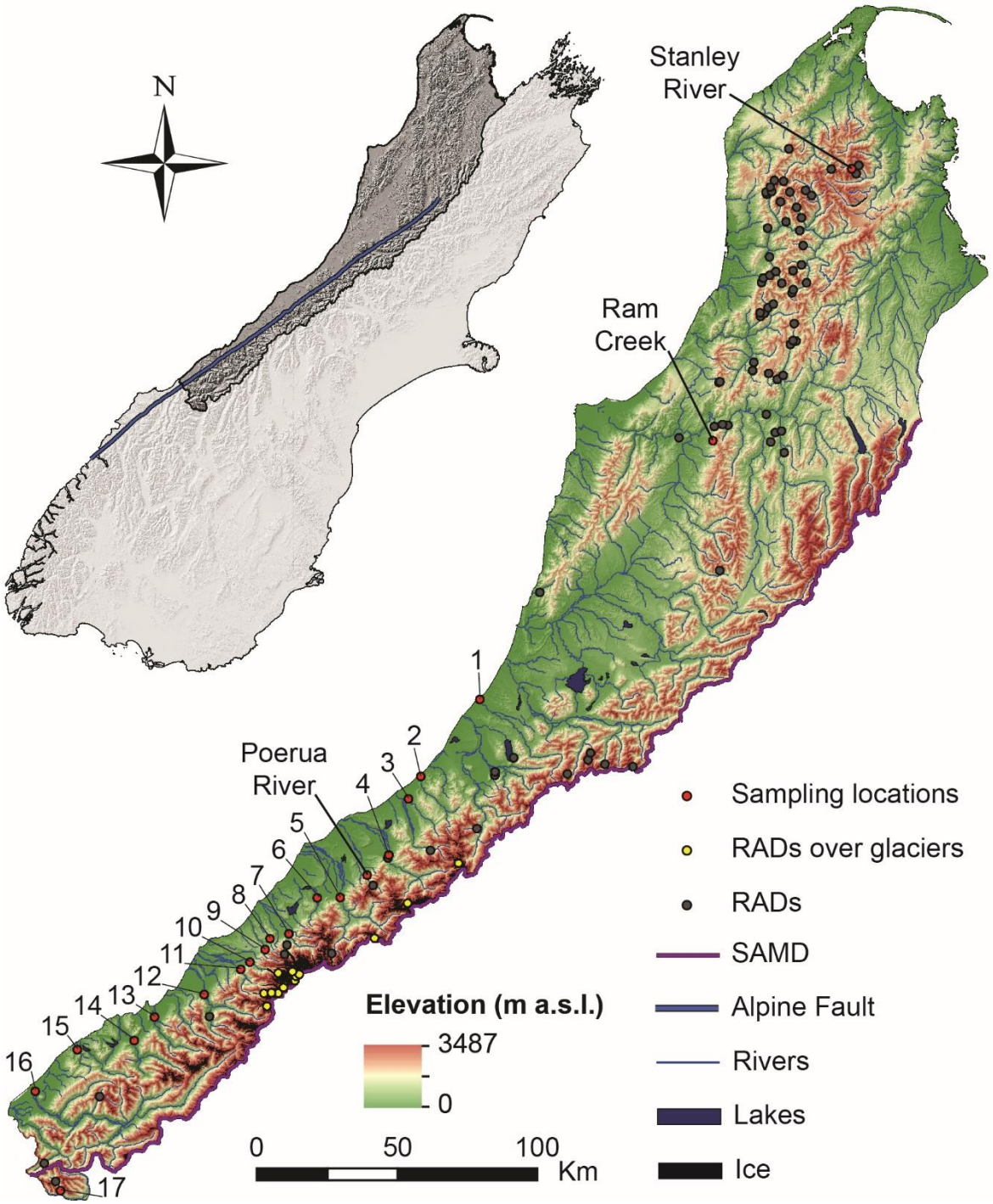

Fig. 3.2 River sediment sampling locations within the South Island. Stanley River, Ram Creek and the Poerua River sampling sites are indicated. Numbers indicate WSA river sampling locations where State Highway 6 crosses the river (Table 3.1).

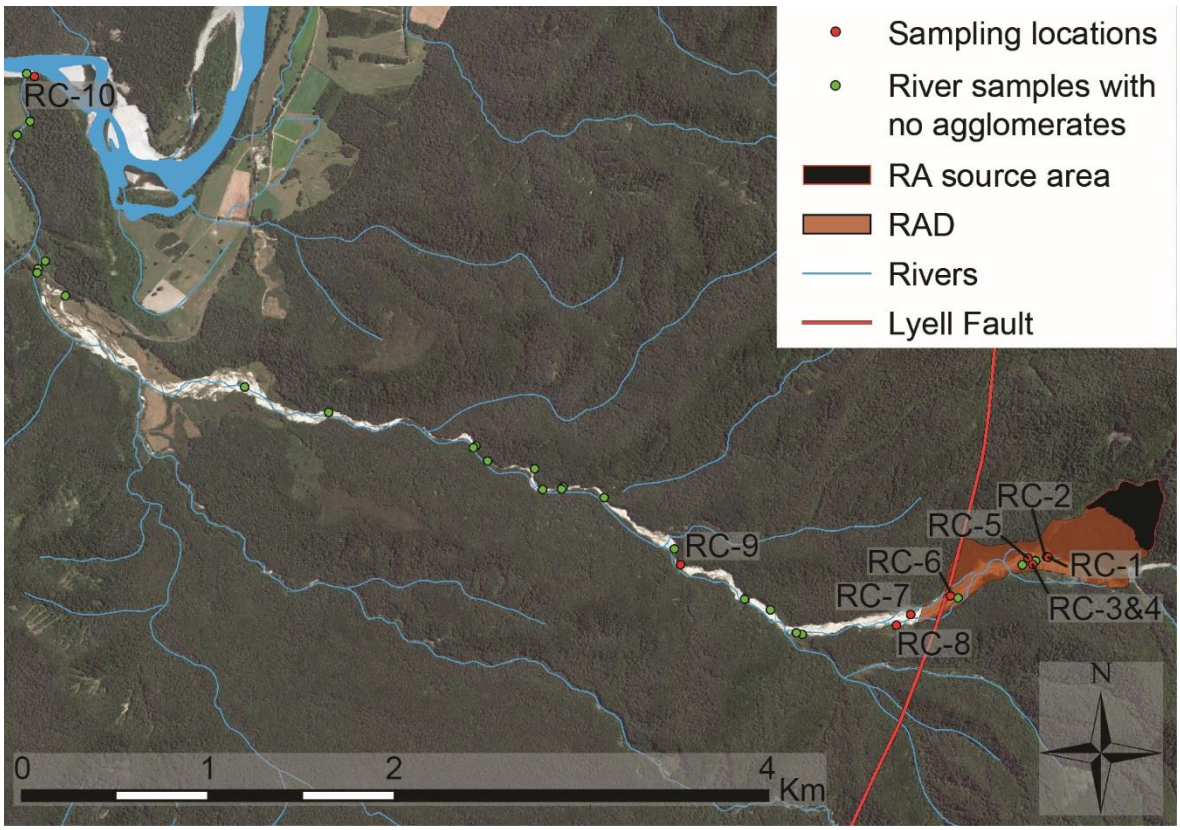

Fig. 3.3 Locations of sediment sampling sites in the Ram Creek valley. Further sample information is given in Table 3.2.

compositions and source areas (Inventory numbers 85, 207, 208; Nash, 2003). Nash, (2003) estimated that the RAD complex has a total volume of 18 x 10^6 m^3 but that the actual dam volume is 12 x 10^6 m^3 Analysis conducted from the data in Chapter 2 of this thesis suggests a lower total volume of 9 x 10^6 m^3.

The first and largest RAD was generated by the June 1929 M7.1 Murchison Earthquake and was sourced from thinly-bedded, fine-grained volcaniclastic sedimentary rocks (Fig. 3.5 I). This RAD fell ~800m from the source area and had a run-up onto the opposite valley wall of ~200m (Lowe and Green, 1992).

Regardless of total dam volume calculations, the 1929 RAD accounts for ~66% of the contemporary dam volume. Nothing is known of when this RAD was overtopped by the impounded Lake Stanley other than it formed a stabilised spillway channel.

The second RAD was deposited sometime between 1929 and 1968 and is inferred from vegetation growth on the deposit in aerial images taken in 1968. There is no known triggering mechanism for this RA. The deposit accounts for ~32% of the total dam volume and is sourced from an igneous intrusion located in the lower section of source area I (Fig. 3.5). Nothing is known of when this RAD was overtopped by Lake Stanley and incised to its present form.

The 1994 deposit was not witnessed and has no discernible trigger, however aerial surveys and unpublished reports suggest 1994 as its emplacement date (Nash, 2003). The deposit accounts for ~2% of the total dam volume and is sourced from an igneous

Fig. 3.4 (a) View of the Ram Creek breach channel showing numerous log jams and boulder armouring; (b) View looking up the breach channel from the downstream extent. G indicates areas where gullying is occurring, TrD indicates areas where gully fans have been truncated by fluvial erosion. The boulder armoured channel can be seen contrasted by the relatively fine material composing the RAD and gully deposits.

intrusion located in Fig. 3.5 II. The RAD blocked the Lake Stanley spillway channel, which had formed through previous deposits, to a depth of 10m. A small lake which formed behind the 1994 dam eventually overtopped the dam, breached and redeposited material up to 1km downstream (Nash, 2003).

Lake Stanley drains through a stable spillway through the RAD complex. The spillway can be broadly split into three sections with differing characteristics. From the lake over-flow the first 100m section of the channel is characterised by large sub-angular

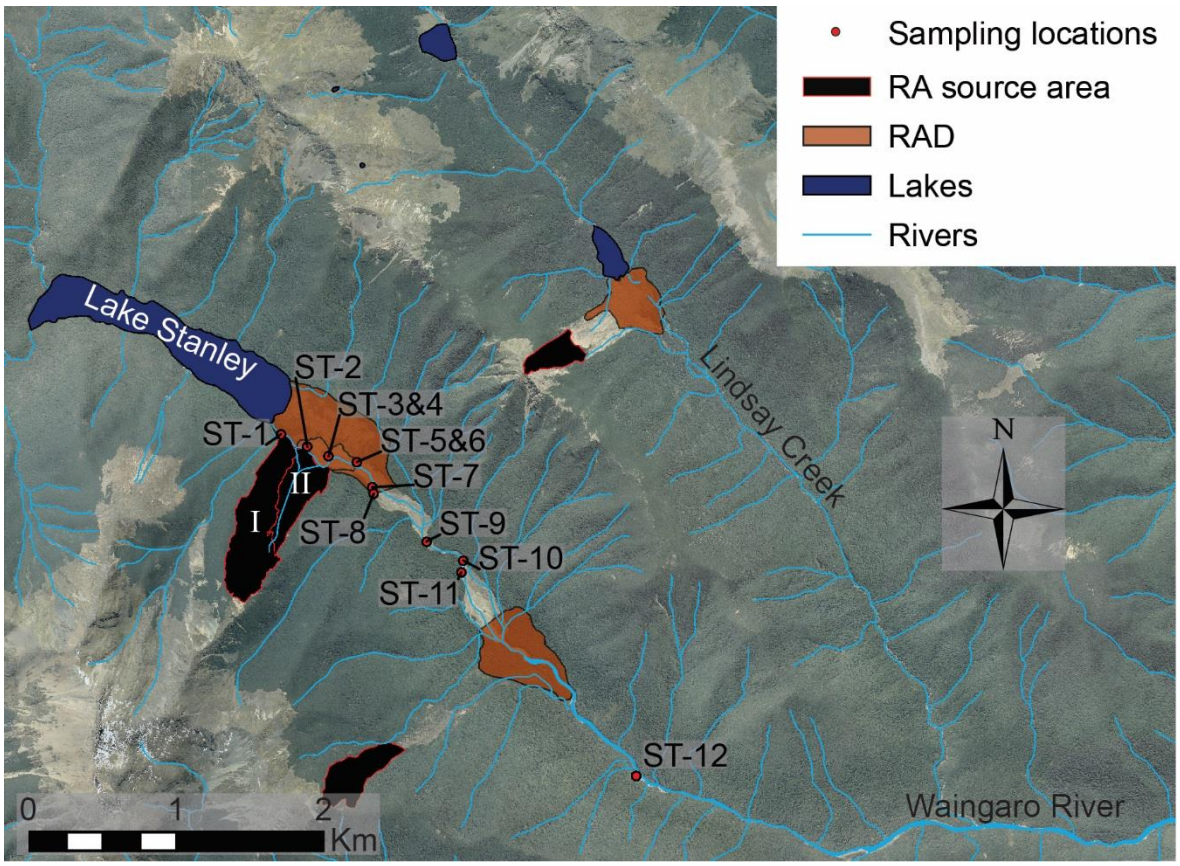

Fig. 3.5 Locations of sediment sampling sites in the Stanley River. Further sample information is given in Table 3.2. I indicates the 1929 and 1929-1968 source area; II indicated the 1994 source area.

to sub-rounded boulders, these clasts serve to armour the channel. There is very little influx of fine-grained material from the lake overflow. The channel boundary and RAD are heavily vegetated and no material reworking was visible during the 2015 field reconnaissance (Fig. 3.6a). The channel does not appear to have changed significantly between field reconnaissance by Nash, (2003) and during this study in 2015.

The second channel section is ~150m long. The contemporary river channel follows the true-left of the spillway and is similar to the first section. However a tributary stream enters the spillway at the top of this second channel section. This tributary stream has aggraded the true-right of the spillway channel with sub-angular to sub-rounded boulders, rounded cobbles and coarse-fine grained sands (Fig. 3.6 a and b). Some armouring of this tributary river bar appears to have occurred on its true-left flank, however fine grained material on the top surface of the bar may be available for fluvial transport during high discharge conditions.

From the bottom of the second channel section to the downstream extent of the RAD is a further 750m. The spillway through this lower channel section is characterised by boulder armouring from large 2-4m diameter boulders (Fig. 3.7a). The channel flow observed during sample collection is assumed to not be high flow given that there was evidence of out-of-channel fluvial working of gravel and cobble material. At the base of the

Fig. 3.6 Photographs of Stanley River RAD spillway channel sections. (a) Channel section 1 with large boulders. The tributary stream (Tr) can be seen entering the spillway at the top of Channel section 2. Sand to boulder sized material is present; (b) The boulder armoured bar in Channel section 2 of the spillway. Also shown is the sampling location for ST-01.

spillway walls, particularly the true-left valley side deposit, there are colluvial fans where material has either been washed downslope or has collapsed from the upper portion of the RAD (Fig. 3.7b). Colluvial material is composed of sand-cobble sized material with occasional large boulders.

In order to examine the channel stability a comparison of photographs taken in 1997, 2003 (Nash, 2003) and in 2015 was conducted. Nash, (2003) uses three features within the lower section of spillway channel in 1997 and 2003 photographs to examine channel stability over this six year time period, (1) A large boulder on the true –right of the

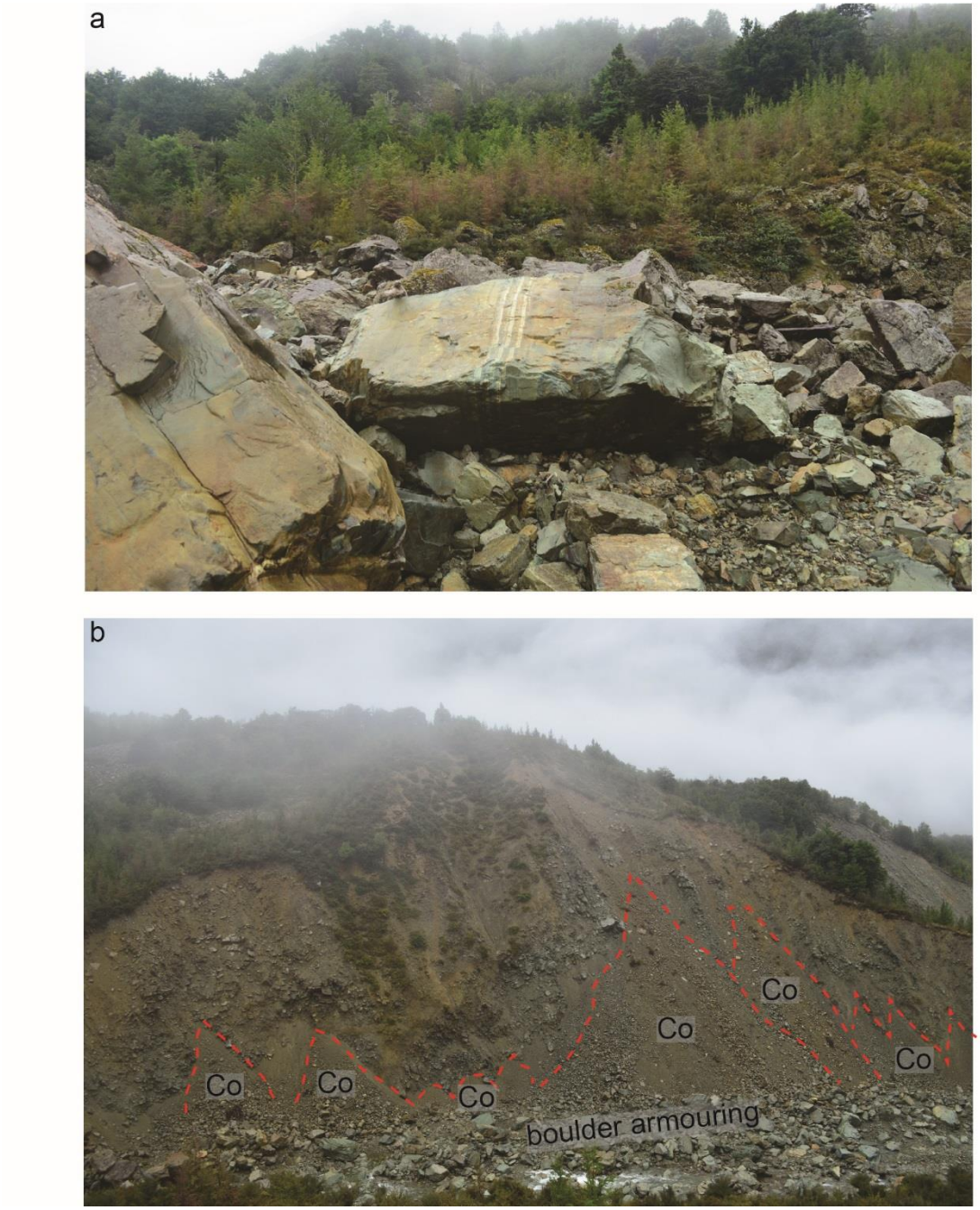

Fig. 3.7 Photographs of the Stanley River RAD spillway channel sections. (a) An example of the 2-4m wide boulder armour in the spillway channel; (b) Channel section 3 showing cones of colluvium (Co) at the base of the spillway wall. Note the area of out-of-channel boulder armour that buffers the colluvial material.

spillway (Fig. 3.8 P1), (2) A steep section of truncated RAD on the true-right of the spillway (Fig. 3.8 P2) and (3) A group of boulders on the true-left of the spillway raised up on a terrace level. Analysis of these same positions in 2015 (Fig. 3.8) reveals that the first two comparative elements are still in place on the true-right of the spillway. This indicates that little erosion has occurred on the RAD remnant on the true-right of the valley and of the boulders in the spillway channel. However the terrace level shown in photographs in 1997 and 2003 is not present in photographs taken during fieldwork in 2015. The terrace appears to have been removed allowing collapse of material from the RAD into the

spillway channel (Fig. 3.8 T). The 1997 and 2003 photographs do not show the same level of erosion occurring on the flanks of the RAD that are seen in 2015, indicating that the terrace was acting as a buffer between the deposit and channel. This could signify that increased mobilisation of RAD material into the fluvial system could be expected. Further examination of the photographs shows that there has been extensive vegetation growth on the flanks of the RAD on the true-right of the spillway which has stabilised these areas. Based upon the aerial extent of the 1929-1968 and the 1994 deposits the spillway channel cuts through both of these deposits implying that material from both of these deposits could be reworked by the Stanley River.

Fig. 3.8 View looking downstream in the Stanley River RA dam spillway channel in April 2015. The features highlighted P1 and P2 refer to preserved features which were identified in photographs of the spillway by Nash (2003) to assess channel stability between 1997 and 2003 (Nash, 2003). These features were identified in the photograph above, taken during fieldwork in 2015, in order to assess the stability of the channel between 2003 and 2015. P1 is a large boulder in the spillway channel; Photo comparison between 2003 (Nash, 2003) and 2015 shows that the boulder shown at P1 has been preserved in position. P2 is a steep section of truncated RAD that shows little evidence of erosion or collapse between 2003 and 2015, indicating channel stability in this area; P2 and the adjacent slope is much more vegetated than on 1997 and 2003 photographs. The area labelled T is the estimated extent of a boulder lagged terrace which is evident in 1997 and 2003 but not in 2015, this indicates fluvial erosion of this flank of the RAD.

3.2.3 Poerua River

The Poerua River is a 34km long river on the west coast of South Island (Fig. 3.2). The river flows from headwaters in the Southern Alps mountain range. The Poerua River is partly fed from the Poerua Glacier in its very upper reaches; whist the North Poerua Glacier partially feeds the Willberg River, a tributary of the Poerua.

The following description of the RA events and impacts is condensed from Hancox et al., (2005). The Mt. Adams RA occurred on the 6th October 1999 (Inventory number 52; Fig. 3.9) and has no known trigger mechanism. The RA was composed of schist and colluvial debris; it fell ~1800m and dammed the Poerua River with 10-15 x 10^6 m^3 of sediment. A main landslide dam was formed, however a split in the RA runout path enabled a smaller secondary dam to form downstream (Fig. 3.9); lakes developed behind both dams. The main dam was overtopped on the 7th October and a boulder armoured spillway channel formed rather than a full dam breach. However heavy rainfall in the Poerua Valley catchment on the 11th/12th of October caused a rise in river levels, this generated a breach channel through the RA dam which failed catastrophically early on the 12th October. The ensuing dam breach flood inundated valley confined alluvial flats, gorges and farmland downstream and deposited large amounts of gravel, sand and silt eroded from the dam breach. It was estimated that ~5.5 x 10^6 m^3 of sediment was deposited within the gorges and flats during the flood (Korup, 2004). With the exception of the farmland at the range front the flood remained within the main channel. Due to flood induced aggradation on the alluvial fan at the gorge exit of the range front, a large scale avulsion channel formed across the farmland there. Between 1999 and 2002 this avulsion channel continued to grow and rerouted much of the river flow. Observation by Hancox et al., (2005) and analysis of a series of aerial images (Fig. 3.10**;** Google-Earth, 2011; Digital-Globe, 2013; LINZ, 2014) show that the avulsion channel was transiently occupied at least throughout the period up to 2005 and has had re-activations as recently as 2013. Levees have been intermittently constructed to attempt to reclaim the land which the avulsion channel occupies (Fig. 3.10). Recent fieldwork in 2015 observed the most comprehensive levee construction to date which could be why little re-occupation of the avulsion channel has been observed recently. Hancox et al., (2005) show >4m of aggradation between 1999 and 2002 ~1km downstream of the gorge exit associated with the RAD and flooding. Observations during fieldwork in 2015 show that the river has begun to incise back into this deposited sediment on the alluvial fan at the gorge exit. This has exposed the uppermost ~3.5m of the interior stratified sediment of the alluvial fan. This leaves the possibility that aggradational material associated with the initial dam-breach flood is still buried below this level. It was from this sediment archive that samples were collected at this fieldsite. Between 1999-2003 the river has also incised back through

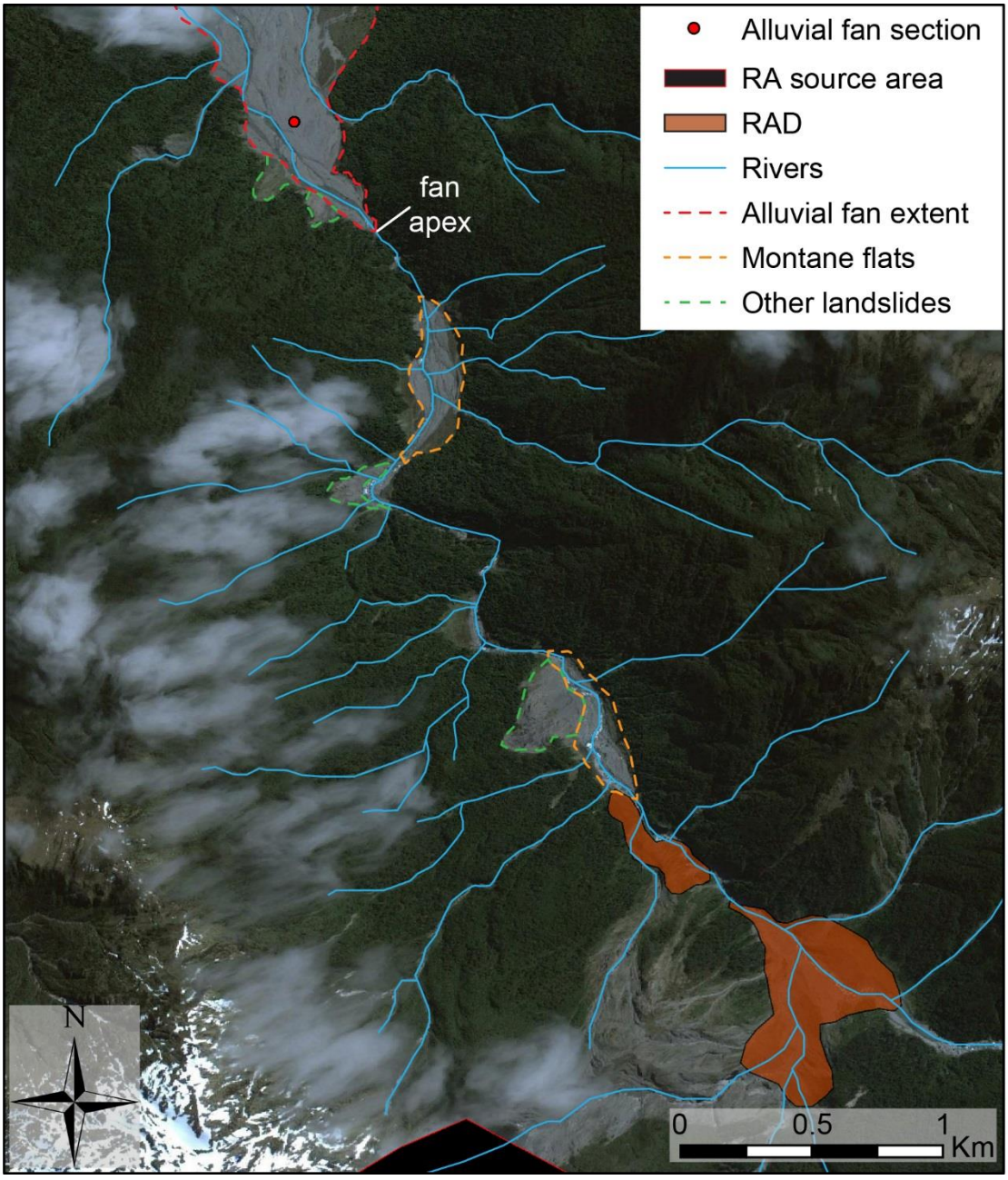

Fig. 3.9 Location of the Poerua River alluvial fan sediment section within the context of the RAD dam and montane flats. The sampling location is 4.6 Km downstream of the lower section of the RAD.

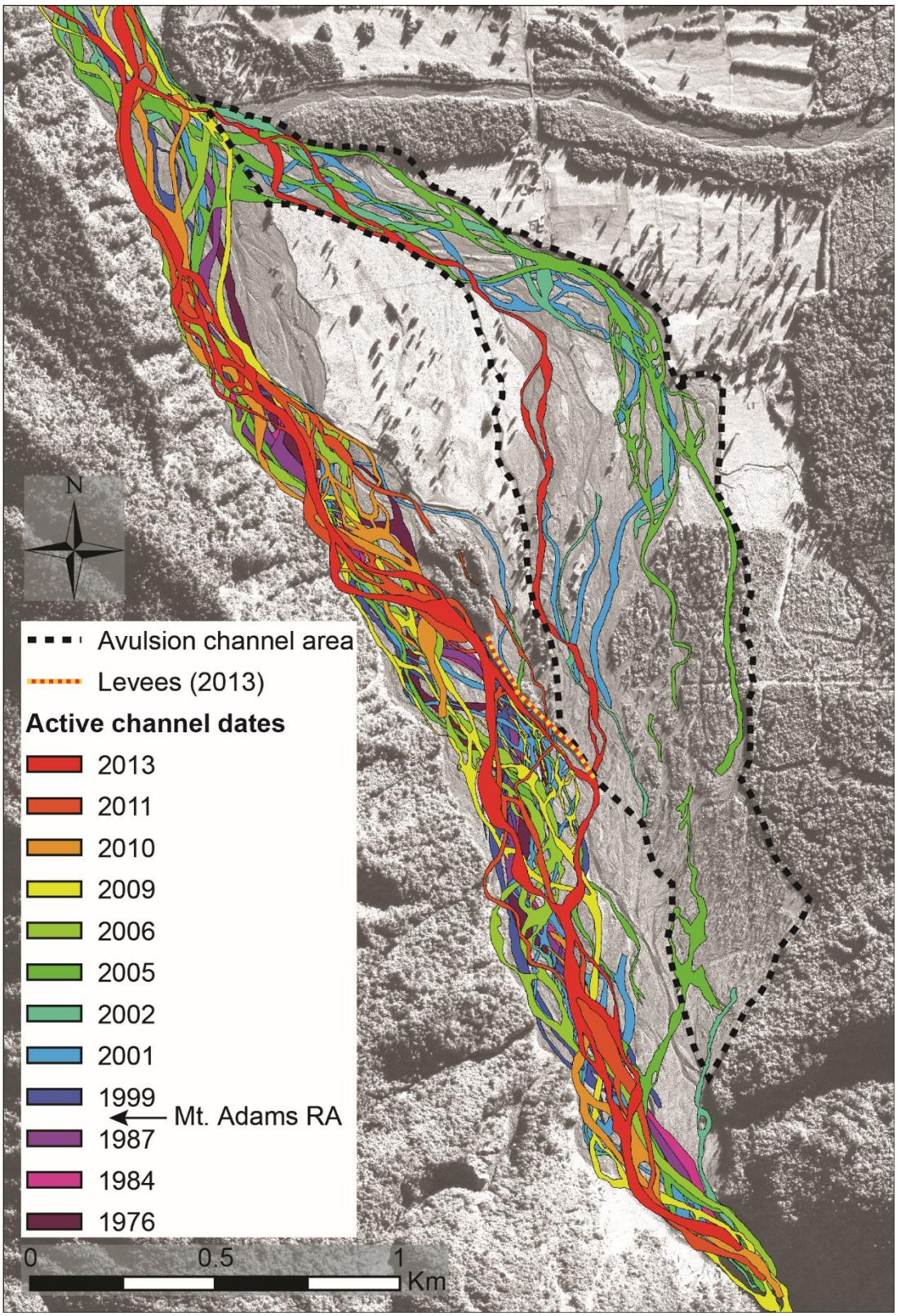

Fig. 3.10 Map of active channels in the wider Poerua River valley, downstream of the gorge. 1976-1987 channel locations precede the rock-avalanche. 1999-2013 channel locations post-date the RA dam. Imagery from Digital-Globe (2013).

the material deposited in the alluvial flats upstream on the alluvial fan (Hancox et al., 2005).This indicates that some of the material composing the alluvial fan may have come from the alluvial flats; However much of the material deposited by the dam break flood in the alluvial flats remains stored in those locations.

3.2.4 West Coast

The West Coast region of the South Island encompasses the high mountain regions of the SA west of the SAMD (Fig. 3.2). As seen in Chapter 2 the WSA geology is dominated by schist and semi-schist rocks. Many of the river systems draining the WSA have RADs in their catchments (Fig. 3.2; Chapter 2, Fig. 2.13); some are above ice and could be reworked by glacial entrainment and glacio-fluvial processes to deliver the sediment to the valley fluvial system. This indicates that in some of the WSA catchments there is going to be glacial sediment entrained in rivers. Many RADs are deposited in river valleys where they can be reworked by fluvial processes. However some of the catchments of the WSA which have headwaters in the high SA do not have any RADs present upstream. Table 3.1 shows the WSA rivers that were sampled for this project and specifies whether RADs, either in valleys or over glaciers, are present upstream of sampling locations. This indicates whether agglomerates would be expected to be present within fluvial sediment in WSA river systems or not. Additionally if agglomerates were located in rivers without RAs known to exist in the inventory then the presence of a fluvially censored RAD could be inferred.

The analysis of sediment routing within WSA catchments from Chapter 2 suggests that fluvially reworked RAD material would not be trapped in lakes and instead has clear pathways to the ocean. Hovius et al., (1997) also suggest that high-magnitude, low-frequency landslides, such as RAs, contribute the majority of material which is transported by NZ West Coast rivers. At the WSA range front, demarcated by the AF (Fig. 3.2), rivers cross a coastal plain. The transition from mountain valleys to the coastal plain is characterised by alluvial fans at the range front and wider braided channel patterns. As with the Poerua River, large floods can mobilise material within mountain valleys and deposit it on alluvial fans at the range front, whilst incision of rivers into fans allows the stratigraphic preservation of deposited material. The braided river system observed in many rivers on the west coast also allows the transient storage and remobilisation of material from river bars.

Table 3.1 West coast river sediment sampling locations for agglomerate analysis. Samples were taken where State Highway 6 crosses each of the river systems.

Sample number	River	Known RADs	Sample distance from RAD (km)	Average gradient upstream of sample (°)	Comments
1	Arahura	N	n/a	0.5	Long river system, upper reaches go back to the Southern Alps main divide (SAMD)
2	Mikonui	N	n/a	1.6	River source close to range front
3	Kakapotahi	N	n/a	5.4	River source close to range front
4	Wanganui	Y	0.6	1.3	x3 (x2 modern deposits in upper reaches above glaciers; x1 historic deposit from ~1220 at the range front, dam developed which has now breached).
5	Whataroa	Y	24.7	7.5	x2 (x1 down-valley of Whymper Glacier, x1 up-valley of Scone Glacier)
6	Waitangitaona	N	n/a	1.3	River source close to range front
7	Waiho	Y	6.7	2.4	x6 (x1 prehistoric Mt Roon is still debated; x5 small, modern, RADs from mountain peaks onto the top of the Franz Josef Glacier)
8	Omoeroa	N	n/a	2.4	River source close to range front
9	Waikukupa	N	n/a	11.4	River source close to range front
10	Fox	Y	5.6	2.6	x4 (x3 small modern RADs from 2009-2010; x1 small historic RAD from ~1850. All deposits are above glacier ice)
11	Cook	Y	12.7	14.0	x7 (x6 historic RADs from ~1850; x1 modern RAD from 2010. All deposits are above glacier ice)

12	Karangarua	Y	8.76	1.3	x1 historic cross valley RAD from ~1630. Developed landslide dam, which has since been breached.
13	Mahitahi	N	n/a	1.0	System extends back to near the SAMD and has high-mountain reaches.
14	Paringa	N	n/a	0.7	System extends back to near the SAMD and has high-mountain reaches.
15	Whakapohi	N	n/a	1.1	River source close to range front
16	Haast	Y	33.4	1.7	x1 modern deposit from 1992; River system is large and contains high-mountain reaches on the SAMD
17	Young	Y	3.23	4.7	x1 in upper reaches of catchment, near SAMD

3.3 Methodology

3.3.1 New Zealand South Island sample collection

Sediment samples to be used for agglomerate identification were systematically collected from (1) in-situ RADs, (2) fluvial material downstream of RADs, (3) alluvial fan deposits at the mountain range front and (4) fluvial material from west coast rivers where they cross the coastal plain. The following section outlines the collection of these different samples.

3.3.1.1 Downstream sediment profiles – Ram Creek and Stanley River

Downstream sediment profiles refer to the sampling strategy for the Stanley River and Ram Creek sites. Both of the RA dams were accessible as was much of the river channel downstream. This meant that the RADs could be sampled in order to confirm the presence of agglomerates; these RADs could then be indicated as the source for any agglomerates found in fluvial material downstream. Samples were then collected from fluvial aggradation deposits in downstream proximal and distal locations to the RADs. These deposits included (1) abandoned terrace sequences, particularly at the downstream end of RA spillway/breach channels; (2) Ram Creek dam breach flood/debris flow deposits; (3) material from abandoned channels in aggraded alluvial flats; (4) Palaeo

terrace sequences and (5) Fluvial material from the contemporary active channel. Ten samples from Ram Creek (Table 3.2; Fig. 3.3) and twelve samples from the Stanley River (Table 3.3; Fig. 3.5) are presented in this thesis. Additional samples were collected at Ram Creek, the locations of which are indicated on Fig. 3.3; however they do not show the presence of agglomerates or other interesting relevant grains and are therefore excluded from detailed analysis. Samples from RADs were collected from sediment sections that have been naturally eroded into the deposits by breaching or spillway incision; samples were collected from holes dug ~0.5m into the deposit as advocated by (Reznichenko, 2012) This is done in order to avoid soil/colluvium contamination and alteration of material by weathering processes that may have impacted sediment on the deposit surface.

3.3.1.2 Alluvial fan deposition – Poerua River

As fluvially reworked RAD material may be deposited within alluvial fans at the range front it was necessary to sample an alluvial fan deposit which is known to have been impacted and aggraded by a RA dam breach flood. The Poerua River alluvial fan saw ~4m of aggradation between 1999 and 2003. This aggradation was initially triggered by the dam breach flood in 1999, but continued up to 2003 with pluvially driven floods. The contemporary phase of river incision back through the alluvial fan material has exposed the upper 3.5m of the depositional sequence allowing access to the material that has been reworked into this deposit from upstream. The fieldsite review indicates that much of this material may have come from the alluvial flats. The alluvial fan sediment section was located ~0.5km downstream of the Poerua Gorge exit and alluvial fan apex (Fig. 3.9). The sequence can be broadly classified into four layers (Fig. 3.11). Layer 1 was ~1.75m deep and consisted of clast supported boulders and cobbles with interstitial pebbles and coarse sand; Layer 2 was ~0.25m deep and consisted of clast supported cobbles with interstitial pebble material; Layer 3 was ~0.4m deep and consisted of matrix supported cobbles and small boulders; the matrix was composed of coarse sand. Layer 4 was the ~1.1m deep basal unit of the exposed deposit and was composed of clast supported boulders up to 0.5m in diameter. Spaces between boulders were filled with interstitial coarse sand.

In total 11 samples were collected, which included all layers; Layers 2, 3 and 4 had higher resolution sampling with collection locations spaced every 0.25m through the deposit (Fig. 3.11). The upper Layer 1 had fewer samples due to its relative inaccessibility; however samples were collected from the lower and upper portions.

Table 3.2 Summary of Ram Creek sampling locations outlined in Fig. 3.3 with sample type and descriptions of sediment collected.

Sample number	Distance from RAD (km)	Sample type	Sample description
RC-1	0.00	RAD	Poorly sorted, angular basalt boulders with coarse grained sand/pebble matrix.
RC-2	0.00	Reworked RAD material	Small outwash fan of gully material from upper section of RAD. Still located within the RA breach channel. Material composed of angular cobbles with coarse grained pebble/sand matrix.
RC-3	0.00	Dam breach flood outwash terrace	Small angular basalt blocks in medium grained sand matrix. Same section as sample 4, middle sedimentary unit.
RC-4	0.00	Dam breach flood outwash terrace	Crushed granite blocks in a medium/coarse sand matrix. Same section as sample 3, lower sedimentary unit.
RC-5	0.00	RAD	Lower section of RAD within the dam breach channel. Small boulders and cobbles in a coarse grained sand matrix.
RC-6	0.48	Lower end of RAD or debris-flow deposit	Sub-rounded/sub-angular boulders and cobbles in sandy matrix. Terrace has young surface vegetation relative to surrounding bush.
RC-7	0.69	Fluvial or debris-flow terrace	Basal sedimentary unit of fluvial terrace. Poorly sorted boulders, cobbles and pebbles in coarse sand matrix. Terrace has young surface vegetation relative to surrounding bush.
RC-8	0.77	Debris-flow terrace	Poorly sorted granite boulders/cobbles in a coarse sand matrix. Trees have been buried in upright position, trunks are now dead. Larger boulders appear to be on up-valley side of tree trunks. Terrace has young surface vegetation relative to surrounding bush.
RC-9	2.00	Contemporary channel sediment	Sample taken from the in-channel sandy sediment.
RC-10	7.18	Buller River, upstream of Ram Creek confluence	Fine-coarsely graded river sand.

Table 3.3 Summary of Stanley River sampling locations outlined in Fig. 3.5 with sample type and descriptions of sediment collected.

Sample number	Distance from RAD (km)	Sample type	Sample description
ST-1	Breach channel	Fluvial sediment, in-channel bar	Bar surface in Stanley RAD breach channel which drains Lake Stanley. Tributary stream from hillside next to sample location. Poorly sorted boulders, cobbles, pebbles and sand. Sample taken from sandy material.
ST-2	Breach channel	RAD	Clast supported unit with interstitial fine grained sand. Evidence of ephemeral streams exiting the deposit indicating some porosity.
ST-3	Breach channel	RAD	Matrix supported sub-angular boulders and cobbles. Matrix is composed of light coloured sands/gravels. Some woody debris present in material. From same section as sample 4, lower stratigraphic unit.
ST-4	Breach channel	RAD	Highly pulverised rock unit directly above the unit from sample 3. Unit is dark in colour and only contains sand-pebble sized material. Another unit is overlying which contains large fractured clasts which are undisaggregated.
ST-5	Breach channel	RAD	Basal unit from section which contains sample number 6. Clast supported unit composed of angular boulders and cobbles with interstitial fine grained sand/gravel. Boulders are highly fractured but undisaggregated and some evidence of source stratigraphy is evident.
ST-6	Breach channel	Fluvial sediment, outwash terrace	Fluvial outwash overlying RAD in base of section. Stratified units of fine sand, angular boulders and cobbles. Units are relatively well sorted.
ST-7	0.05	Fluvial sediment, outwash terrace	Fluvial outwash terrace, clast supported deposit with interstitial medium/coarse sand. Poorly sorted deposit with large boulders, cobbles and pebble sized clast supported material. Young surface vegetation relative to surrounding bush.
ST-8	0.09	Fluvial sediment, abandoned river channel	Abandoned river channel, probably active during flooding. Winnowing of surface fines, sample taken in 10cm hole dug into channel base. Poorly sorted clast supported material with interstitial coarse sand and gravel fines.

Table 3.3 Cont. Summary of Stanley River sampling locations outlined in Fig. 4.5 with sample type and descriptions of sediment collected.

Sample number	Distance from RAD (km)	Sample type	Sample description
ST-9	0.75	Fluvial sediment, mid-channel bar	Recently active channel at distal end of alluvial flat immediately downstream of the RAD. Alluvial sands sampled.
ST-10	1.08	Fluvial sediment, abandoned river channel	Upstream end of the second alluvial flat downstream of the RAD. Likely to be recently reworked material in a flood overflow channel. Fine-grained material sampled in the channel.
ST-11	1.11	Fluvial sediment, Palaeo-terrace	Palaeo-terrace deposit with extensive ancient bush cover. Stratified units; basal unit is poorly sorted sub-rounded boulders to cobbles with interstitial sand; middle unit comprises well sorted, rounded cobbles with interstitial sands, upper unit is poorly sorted sub-rounded boulders to cobbles with interstitial sands. Upper unit has extensive, mature surface vegetation implying an pre-historic origin for the deposit.
ST-12	3.41	Fluvial sediment, abandoned river channel	Flood overflow channel with recent fluvial work. Sample taken from area of fines which has settled in a slackwater area behind boulder.

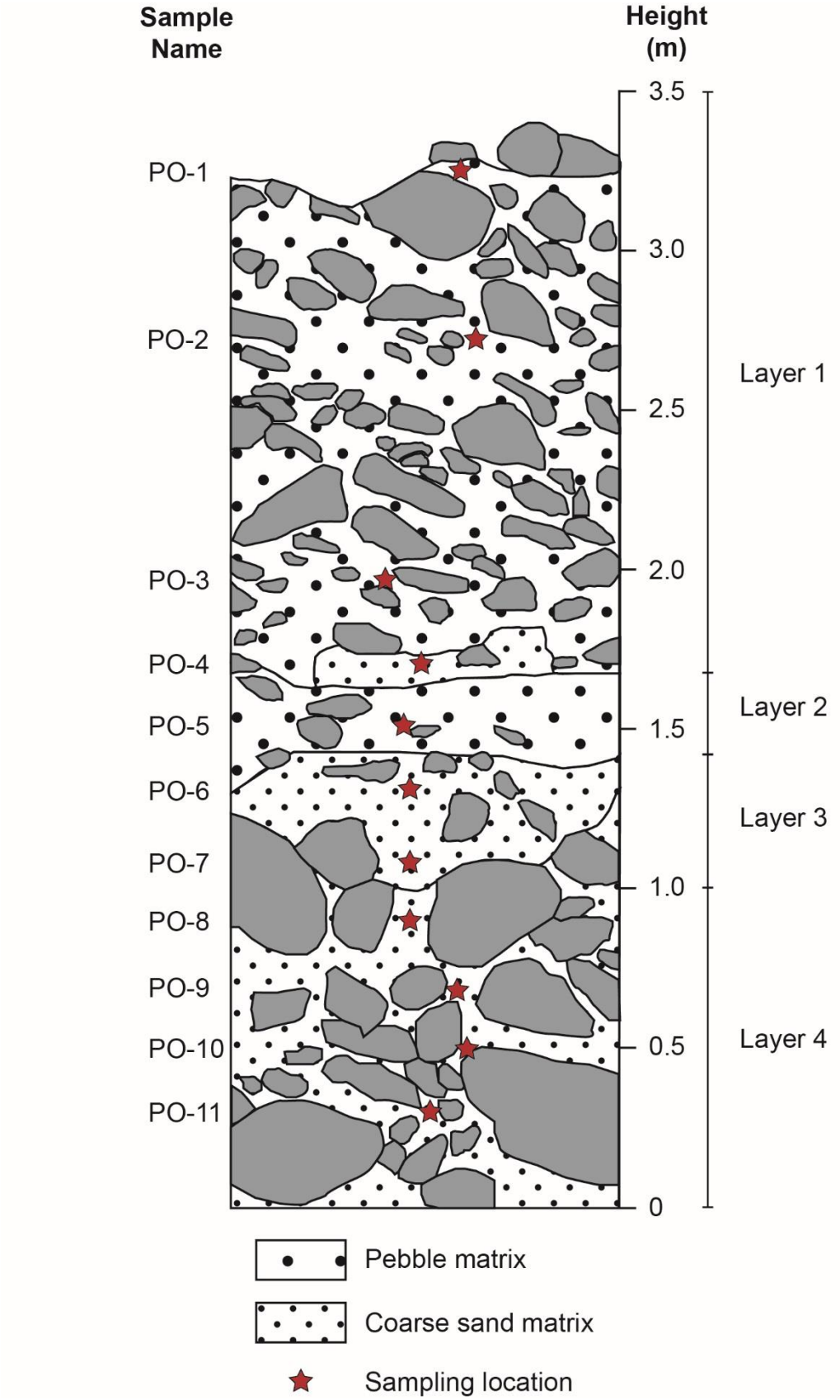

Fig. 3.11 Stratigraphic log of the Poerua River alluvial fan river cut section.

3.3.1.3 Spot sampling – West Coast, South Island rivers

West Coast catchments with and without known RADs were identified as part of the deposit inventory analysis in Chapter 2 (Fig. 2.13). Systematic spot sampling of sediment in 17 WSA rivers was conducted in order to examine if known and unknown RADs could be identified through agglomerate presence in fluvial material (Fig. 3.2; Table 3.1). It had been anecdotally suggested that agglomerate grains would be ubiquitous within the sediment of WSA fluvial systems (Tim Davies, 2014 pers. comm.). All of the sampled rivers crossed State Highway 6 (SH6), this allowed easy access for sampling. A single sample of fine-grained fluvial sediment was taken from each accessible river system at the point at which SH6 crosses the river. Samples were always collected from contemporary active channel margins where SH6 crossed the river.

3.3.2 Laboratory washing experiments

Agglomerate grains produced by ring shear experiments in the laboratory have been shown to be broken down by ultrasound (McSaveney, 2016 pers. comm.). Whilst ultrasound conditions are not present during fluvial transport, there are other mechanical processes which could lead to particle breakdown. For example, the collapse of vapour bubbles within river flow results in a pressure shockwave (Carling et al., 2017) which may be capable of breaking agglomerate grains apart. Alternatively, mechanical abrasion and breakdown of agglomerate grains could also occur during fluvial transport through particle collisions in the flow or via impacts with the channel bed if particles are saltating.

It is possible that turbulent river transport of agglomerates would produce similar ultrasound conditions through the collapse of vapour bubbles in the river flow. In order to test the preservation potential of agglomerate grains within turbulent fluvial environments a laboratory based sediment washing experiment was devised. The aim of the experiment was to subject an unmodified bulk sample of RA material to turbulent water flow and examine if agglomerates are readily affected by fluvial transport. The examination of the effect of fluvial transport on agglomerate grains could not be made at the experiment stage; instead, samples of material from the experiment were collected at specific time intervals for preparation and further analysis on a SEM.

A sediment sample that had been collected from a RAD in Kyrgyzstan was used to conduct the experiment. The Kyrgyzstan RAD material was a bulk sample, which was readily available to examine the effect of material washing. New Zealand South Island material was not used as those samples were small and much of the material was required for other analyses. It should be noted that the country of origin of the material used for this experiment should not change the outcome, as agglomerate grains are produced in RA deposits regardless of the rock type (Reznichenko et al., 2012). Therefore

material from Kyrgyzstan RADs are applicable to examining the general breakdown of agglomerate particles.

The RAD sample was placed in a 63μm sieve; this sieve size was chosen as agglomerates identified under SEM examination in previous literature have been located within the 63 μm to 1mm GSF (Reznichenko, 2012). The sieve and sample were placed at an angle under a high-power laboratory tap and water was run through the sample for 12 hours. The purpose of the sieve being placed at an angle was to ensure that the sediment was consistently under the water flow rather than distributed over the sieve and that a turbulent fluvial environment was created.

With the water running over the RA sample, small quantities of material (~4g) were subsampled from the sieve at pre-selected time-steps of 0.5, 1, 2, 3, 4, 5, 6 and 12 hours. A further sample of unwashed RA material was also taken to determine the presence of agglomerates before washing. Once subsampled from the sieve, the samples were dried and mounted in resin blocks for SEM analysis. SEM analysis of the resin mounted sample from each time-step was conducted to ascertain if agglomerates were present after sample washing. It is possible that agglomerates were broken down to finer GSFs during the experiment and washed through the sieve, therefore if agglomerates are detected in the collected samples they are a fraction of the grains surviving the 'washing' process.

3.3.3 SEM Sample preparation

Once samples had been collected they were prepared for SEM analysis. This preparation procedure applied to all of the samples taken, which includes laboratory washing experiments and NZ field samples. Samples were dried in an oven at 50°C; this provides a low temperature environment for slow drying of the sediment so that agglomerate grains are not damaged. Dried samples were sieved into specific GSFs using a sieve stack and shaking table. Reznichenko, (2012) used the 63μm to 1mm GSF to examine the presence of agglomerates within glacial samples. Therefore, samples were sieved into <63 μm, 63μm-1mm, and >1mm GSFs for analysis (Fig. 3.12). The 63μm-1mm GSF was taken on for further processing before examination under the SEM.

Sieved 63μm-1mm samples were homogenised and ~2g of material was scattered over the base of a resin mould. Struers EpoFix cold-mounting epoxy resin and FixiForm mounting moulds were used to prepare all of the samples. A cold mounting resin was used as hot resins may have damaged agglomerates during the curing process. Resin was syringed over the sample in the mould; syringing reduced the amount of air bubbles that were incorporated into the cured block. The resin was left for 24 hours to cure into a solid transparent block with the sediment in the base. The base of the moulds could be removed in order to extract the cured block (Fig. 3.12 and Fig. 3.13a)

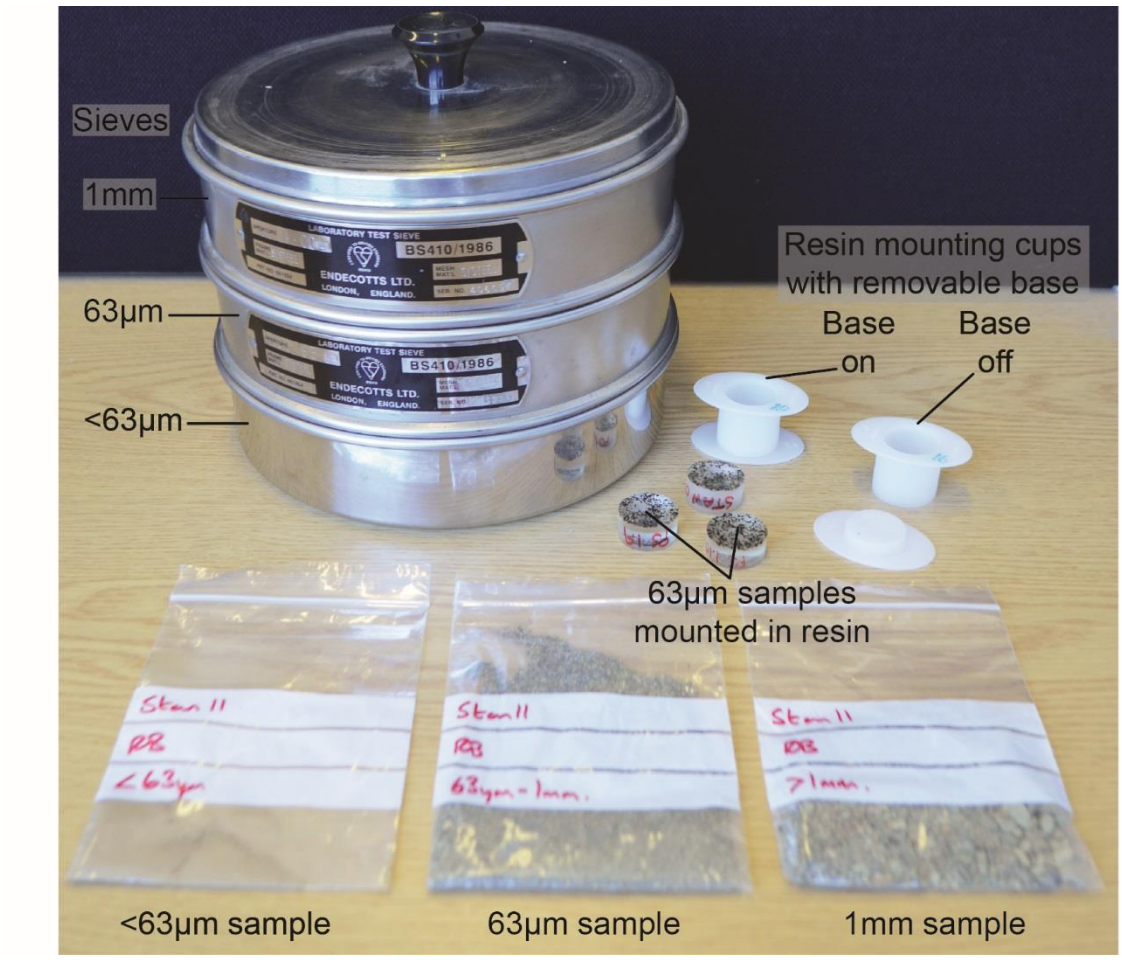

Fig. 3.12 Sample preparation equipment and grain-size fractionated samples required for the analysis of fluvial material under the Scanning Electron Microscope (SEM). Samples are initially fractioned using sieves before being mounted into resin blocks in the moulds.

In order determine agglomerate presence within the samples it was necessary to be able to examine the internal structure of the grains. This was achieved by polishing away the base of the resin blocks containing the sediment sample. The polishing process ground away the resin and parts of the enclosed grains leaving a polished surface with the internal structure of grains exposed for SEM analysis (Fig. 3.12; Fig. 3.13a and b). A series of polishing disks of progressively finer grade were used to coarsely remove the base of the block then finely polish. Grit grades used were 120 (115µm), 240 (53µm), 600 (16µm), 1000 (10.3µm). Polishing the resin blocks is not thought to damage or fragment agglomerates as the resin penetrates through any gaps within the grains. This provides a structural support to maintain grain structure during the polishing process. Once the resin blocks were polished they were ready for SEM analysis.

3.3.4 Scanning Electron Microscopy (SEM)

The resin blocks were mounted onto metal stubs with carbon tape and placed within the imaging chamber of an FEI Quanta 400 SEM below an electron beam. The imaging chamber is pumped to vacuum which removes dust and particulate matter which

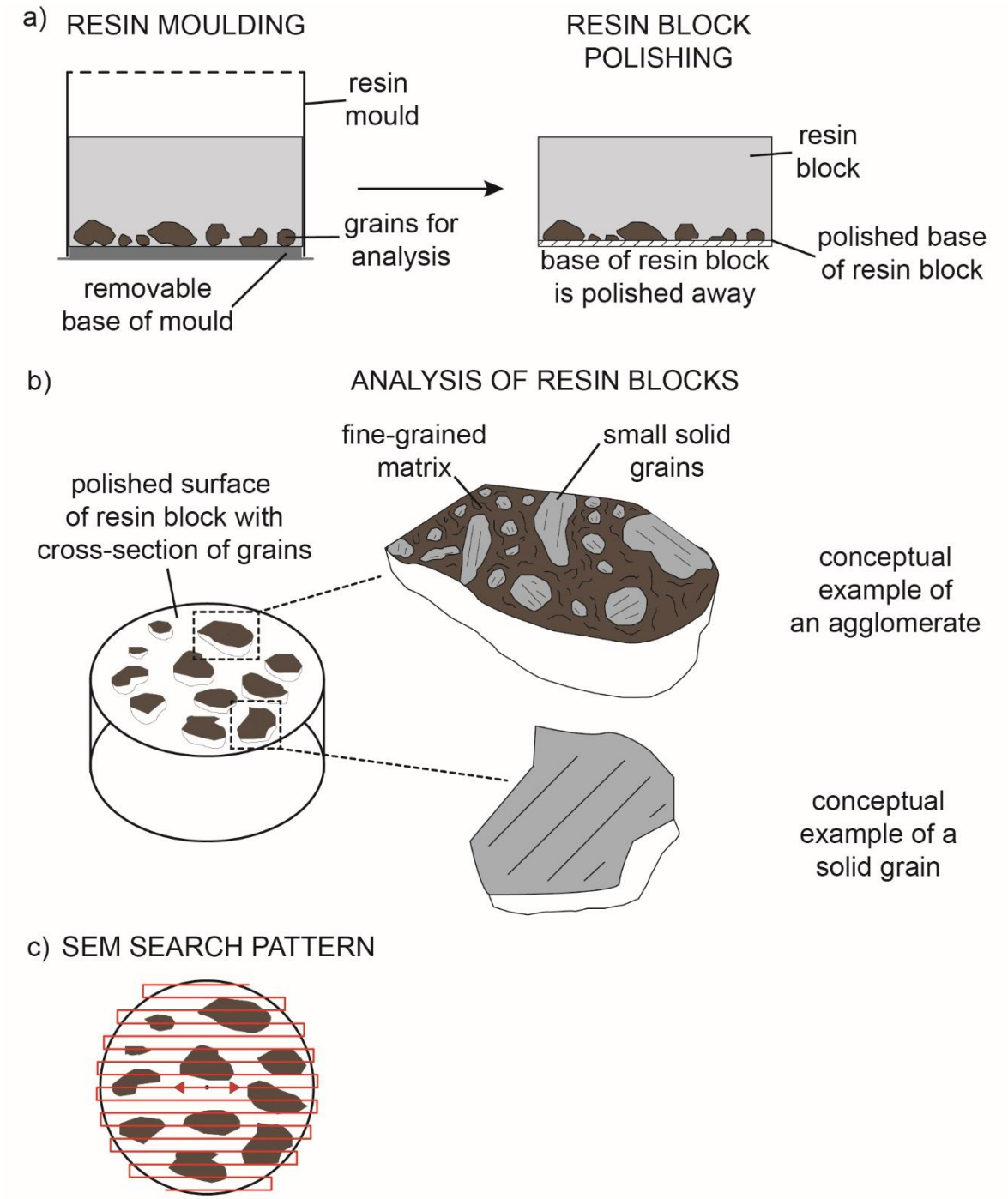

Fig. 3.13 Conceptual diagram of the preparation and analysis of NZ sediment samples; (a) Grains of material are dispersed at the base of a resin mould and covered with an epoxy resin. Once cured the base of the mould is removed and the hardened block can be extracted. Using a mechanical disk the base of the block is polished to a smooth surface finish which reveals the interior of the grains; (b) The block is ready for analysis on the SEM. Conceptual examples of what each grain type is expected to look like are given on the right; (c) A diagrammatical representation of the 'creeping line' search pattern that was used to examine resin blocks and identify agglomerate grains.

may interfere with the sample as well as protects the integrity of the electron beam source (Reed, 2005).

SEM imaging for the resin blocks can take two forms, either secondary electron (SE) or backscatter analysis. A simple breakdown of SEM operation is that a Tungsten

cathode produces a primary electron beam which can be targeted and focussed at different areas of a sample. The electron beam scans the focussed area sequentially from top to bottom in horizontal raster lines. The scanning speeds can be adjusted, however quicker scans result in lower resolution images; there resolution of images is a trade-off between scanning speed and time. In SE imaging electrons in the sample are displaced by electrons from the beam; the displaced electrons leave the sample, hit a detector and produce an image. Ejected SEs have very low energy, differentiating them from the primary electrons; given their low energy state they can only have come from the surface of the sample (Reed, 2005). In backscatter imaging the primary electrons from the beam impact the sample and are reflected back to a detector. Primary electrons that do not initiate secondary electron ejection penetrate the sample further and therefore the image developed from the backscatter technique is of material just below the immediate surface of the sample (Reed, 2005).

The resin used for sample mounting does not effectively conduct the charge generated from the electron beam; this charge can accumulate in the sample in SE imaging methods and hamper analysis. Therefore the backscatter imaging technique was used to examine the fine-grained material within the resin blocks as less charge accumulated. In order to examine the samples the SEM was set to 400x magnification, enough to be able to examine the composition of individual sample grains. From the centre of the sample (a point which could be reliably returned to automatically via the instrument software) the sample was examined by moving a single contiguous frame across the resin block in a 'creeping line' search pattern (Fig. 3.13c). This ensured that no grains were missed in the data collection. When a grain of interest was identified in the search pattern it could be zoomed in on and imaged at a higher magnification.

High resolution images of whole grains and particles down to ~2μm can be resolved easily on the SEM (Reed, 2005). However the electron beam width limits the resolution of SEM images; this means that clear images of individual sub-micron particles composing the agglomerate grains could not be resolved due to them being below the resolvable size range.

3.4 Results

3.4.1 Known sediment point sources

Fig. 3.3 shows the locations of sample sites in relation to the aerial extent of the original Ram Creek RAD. Much of the original RAD dam material downstream of RC-5 has been removed by fluvial erosion prior to this study. Samples with identifiable agglomerates in Ram Creek all come from within 1km of the RAD. Samples RC-1, RC-5 and RC-6 are in-situ RAD material (Table 3.2), with RC-6 interpreted to be the distal end of the RAD approximately 0.5km downstream of the breach channel. RC-1 and RC-5 do

not have agglomerates present; however aggregate type grains were found where larger grains are bound together by clays and organic material (Appendix 3.1a and e). Agglomerate grains were observed within RC-6 (Fig. 3.14b). The agglomerate grain shown in Fig. 3.14c is sub-rounded and is composed of larger grains in a fine-grained matrix; fine-grained material can also be seen adhering to the exterior of some of the larger grains. Coherent agglomerates were observed in sample RC-3, taken from flood outwash terraces immediately below the dam-breach channel of the RAD (Fig. 3.14a).

Further agglomerate grains were located in sample RC-8 which is ~0.8km downstream of the RAD breach channel. The RC-8 deposit is interpreted to be the debris-flow from the 1981 dam-breach flood as clasts are sub-rounded and there is no visible stratification; dead tree trunks are buried in upright positions indicating that deposition occurred in less extreme conditions that would be expected if this was RA deposition. RC-8 agglomerates (Fig. 3.14d and e) are coherent clasts composed of widely graded sub-angular material. Samples RC-9 and RC-10 (Appendix 3.1) have small clumps of material <100um in size which are similar in composition to agglomerate matrix material. These small clumps of sub-angular to sub-rounded material could potentially be dis-agglomerated remnants of agglomerate grains, however this is unclear.

Fig. 3.5 shows the sample sites for the Stanley River. Agglomerate grains were found within samples ST-2 and ST-4, but were not present in samples ST-3 and ST-5; all collected from the in-situ RAD (Fig. 3.15a and b). Agglomerates are therefore available for reworking by fluvial activity only from some sections of the RAD. Agglomerates in ST-2 and ST-4 are composed of widely graded clasts, have a fine-grained matrix and are coherent grains with a-axis measurements in the order of 600-700μm (Fig. 3.15a and b). ST-6 taken from the fluvial outwash terrace just below the RAD contained a smaller agglomerate grain (Fig. 3.15c) with an a-axis of ~140μm. The ST-6 agglomerate (Fig. 3.15c) was widely graded, with a fine-grained matrix composed of sub-angular to sub-rounded clasts. Beyond the identification of agglomerates within the outwash terrace in sample ST-6 no further agglomerates were identified in fluvial material.

Downstream sampling included other outwash terraces ~0.5km from the RAD breach channel (ST-7), surface material deposited in downstream alluvial flats (ST-9), temporarily abandoned overflow channels in flats and gorges (ST8, ST-10, ST-12) as well as ancient terrace material (ST-11). All downstream samples were located within 4km of the RAD. Different aggregate type grains were found in the fluvial material near the RAD and downstream with finer material grading, not the wide grading associated with agglomerates (Appendix 3.2a, e and f).

Samples collected from Ram Creek and Stanley River that contained agglomerates came from two domains (1) In-situ RAD material and (2) fluvial deposits associated with RAD dam breaches. A qualitative observation is that the identified

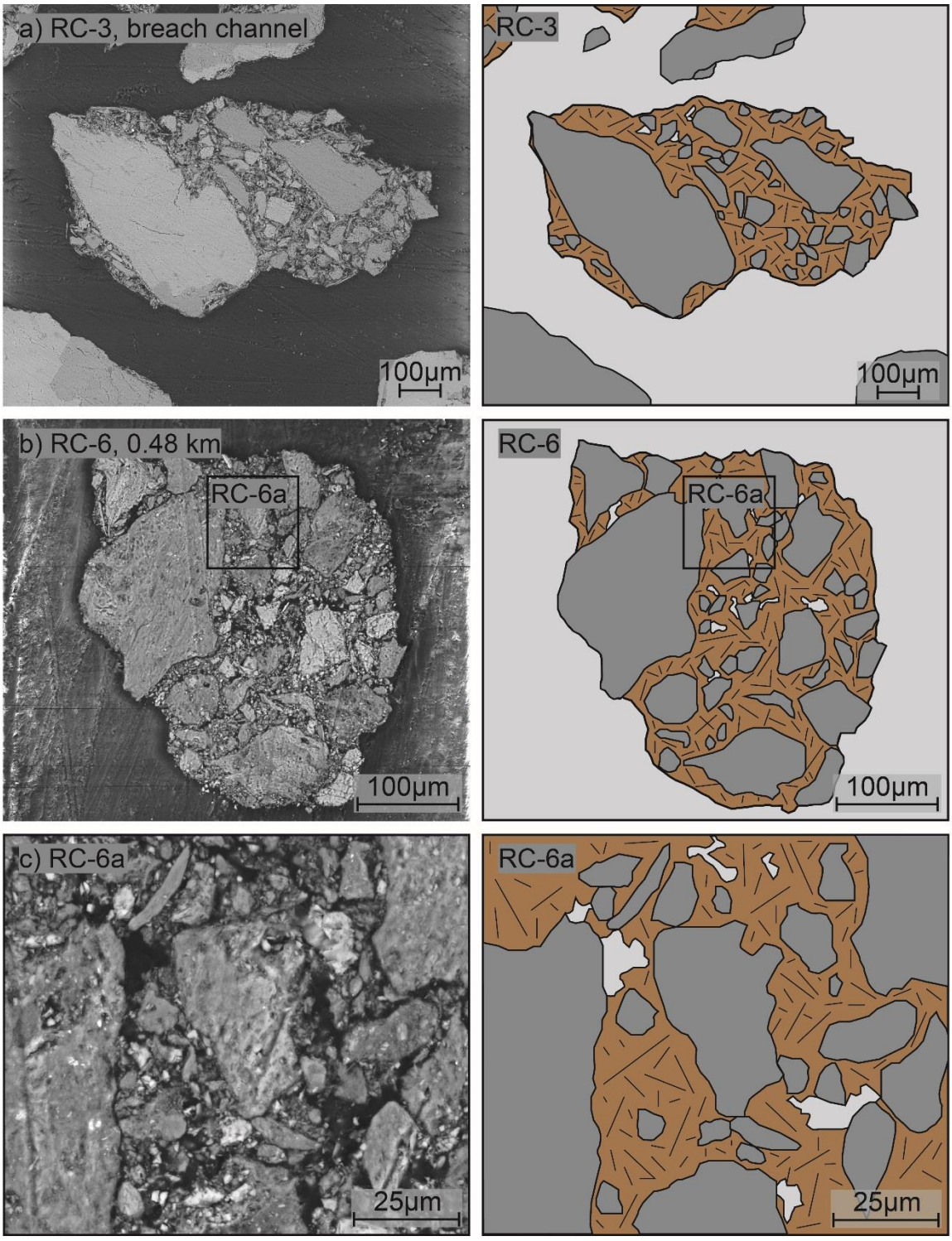

Fig. 3.14 Ram Creek river system RA agglomerates. On the left are SEM micrographs of agglomerate grains found within Ram Creek samples, sample names and their distance downstream of the RAD are indicated in the top left. On the right are interpretations of each of the SEM micrographs; solid grains (dark grey) are bonded together with a fine grained matrix (dashed brown) into a solid grain with only a few small gaps in the grain filled with resin (light grey).

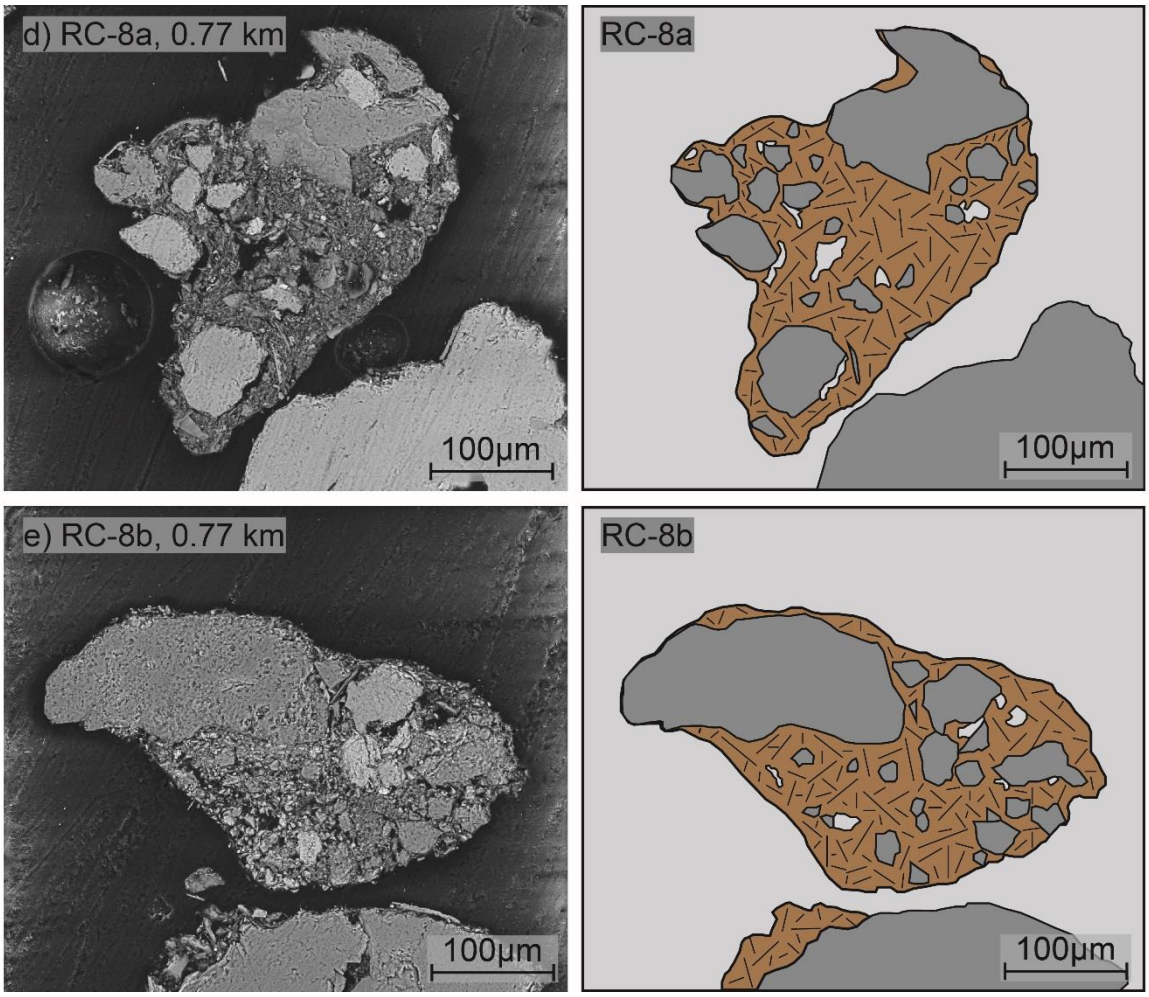

Fig. 3.14 Cont. Ram Creek river system RA agglomerates. On the left are SEM micrographs of agglomerate grains found within Ram Creek samples, sample names and their distance downstream of the RAD are indicated in the top left. On the right are interpretations of each of the SEM micrographs; solid grains (dark grey) are bonded together with a fine grained matrix (dashed brown) into a solid grain with only a few small gaps in the grain filled with resin (light grey).

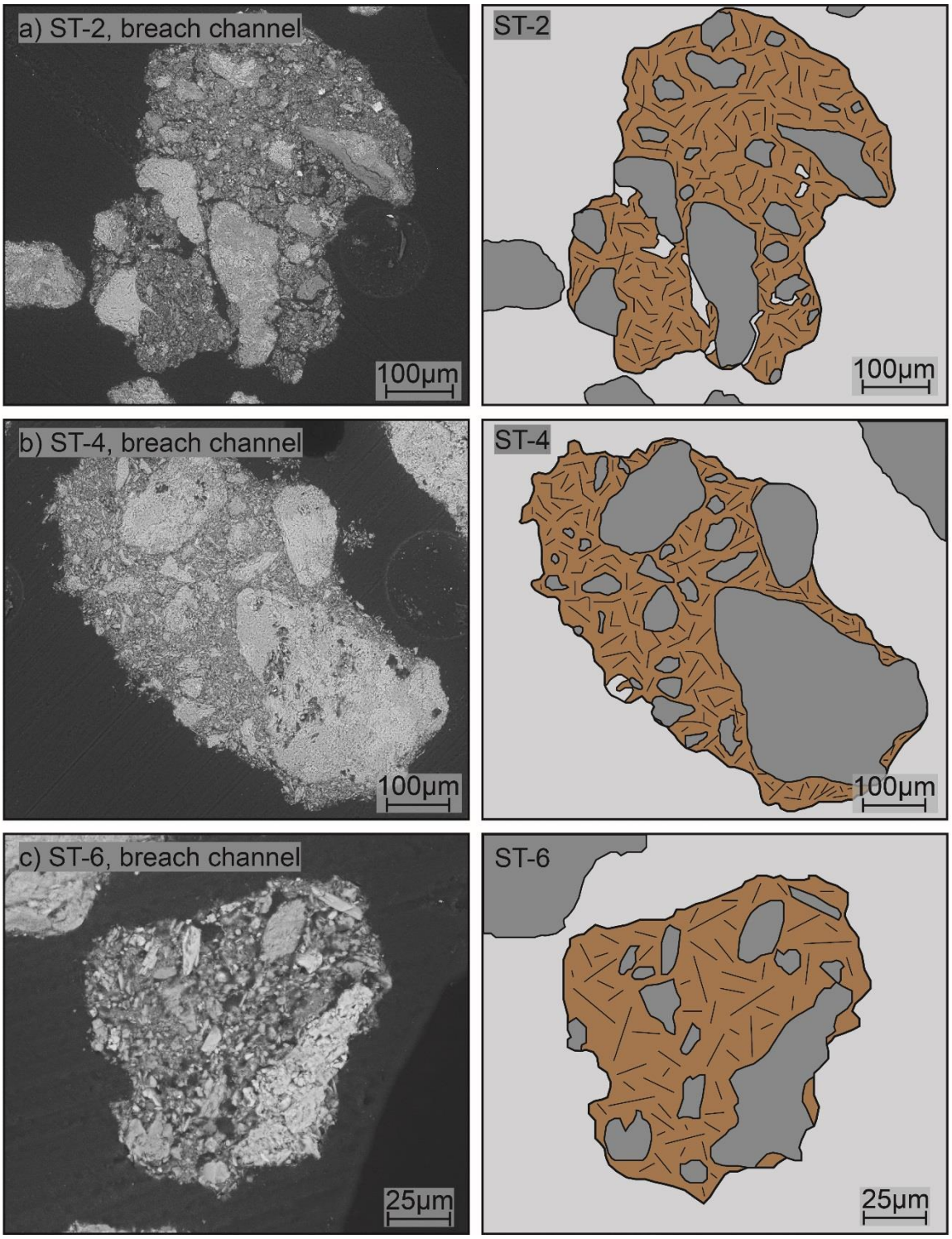

Fig. 3.15 SEM micrographs and interpretations of RA agglomerates from the Stanley River system. On the left are SEM micrographs of agglomerate grains found within Stanley River samples, sample names and their distance downstream of the RAD are indicated in the top left. On the right are interpretations of each of the SEM micrographs; solid grains (dark grey) are bonded together with a fine grained matrix (dashed brown) into a solid grain with only a few small gaps in the grain filled with resin (light grey).

agglomerate from the Ram Creek RAD (RC-6) has a large amount of coarser material with a lower proportion of fine-grained matrix than is observed in Stanley River RAD agglomerates (ST-2 and ST-4). Samples taken from contemporary fluvial material that are not associated with dam breaching did not appear to contain agglomerate grains, however many of the samples in these two systems came from modern surfaces. It was hypothesised that burial of agglomerate rich material may provide an explanation for the apparent scarcity of agglomerates in these fluvial systems. To address this hypothesised issue samples were taken from an alluvial fan in the Poerua River.

3.4.2 Poerua River

All eleven samples collected through the 3.5m section showed no sign of agglomerate inclusions, regardless of being in any of the identified four stratigraphic layers (Fig. 3.11). The vast majority of grains observed within the samples were clean, solid grains as evidenced by the SEM micrographs in Fig. 3.16. As no agglomerate grains were identified in these fluvial deposits a context image was taken for each sample which represented the type of material observed. Clasts are sub-rounded to angular and often display a high degree of fracturing (Fig. 3.16a, d, e, f). In sample PO-2 (Fig. 3.16b) an aggregate grain was located, however it is not thought to be an agglomerate. Close examination of the PO-2 grain shows that much of the material holding larger grains together is a matrix with no clearly definable micron sized material which would be expected of an agglomerate. The un-resolvable matrix material of the PO-2 grain is interpreted to be organic material bonding the grain together, a feature that excludes this grain from being an agglomerate based on the definition criteria.

3.4.3 West Coast rivers

Locations of sampled West Coast rivers are shown in Fig. 3.1. Table 3.1 indicates whether known RADs are present upstream of the sampling sites giving an indication as to whether it would be expected that agglomerates are present in fluvial material.

Of the rivers that have RADs upstream, in valleys rather than over glaciers, it is likely that deposits in the Whataroa River and Young River are being actively reworked by fluvial processes as they are modern and remain unvegetated. The RAD in the Wanganui River has a large vegetated terrace buffering the river from the deposit; however there is evidence of transient channel occupation directly adjacent to the RAD indicating that occasional fluvial reworking could take place. The RADs in the Karangarua and Haast Rivers are heavily vegetated, however the rivers do flow through breach channels, indicating that material could still be reworked from these deposits. Fig. 3.17 shows SEM micrographs from six selected rivers, which are representative of the 17 rivers that were

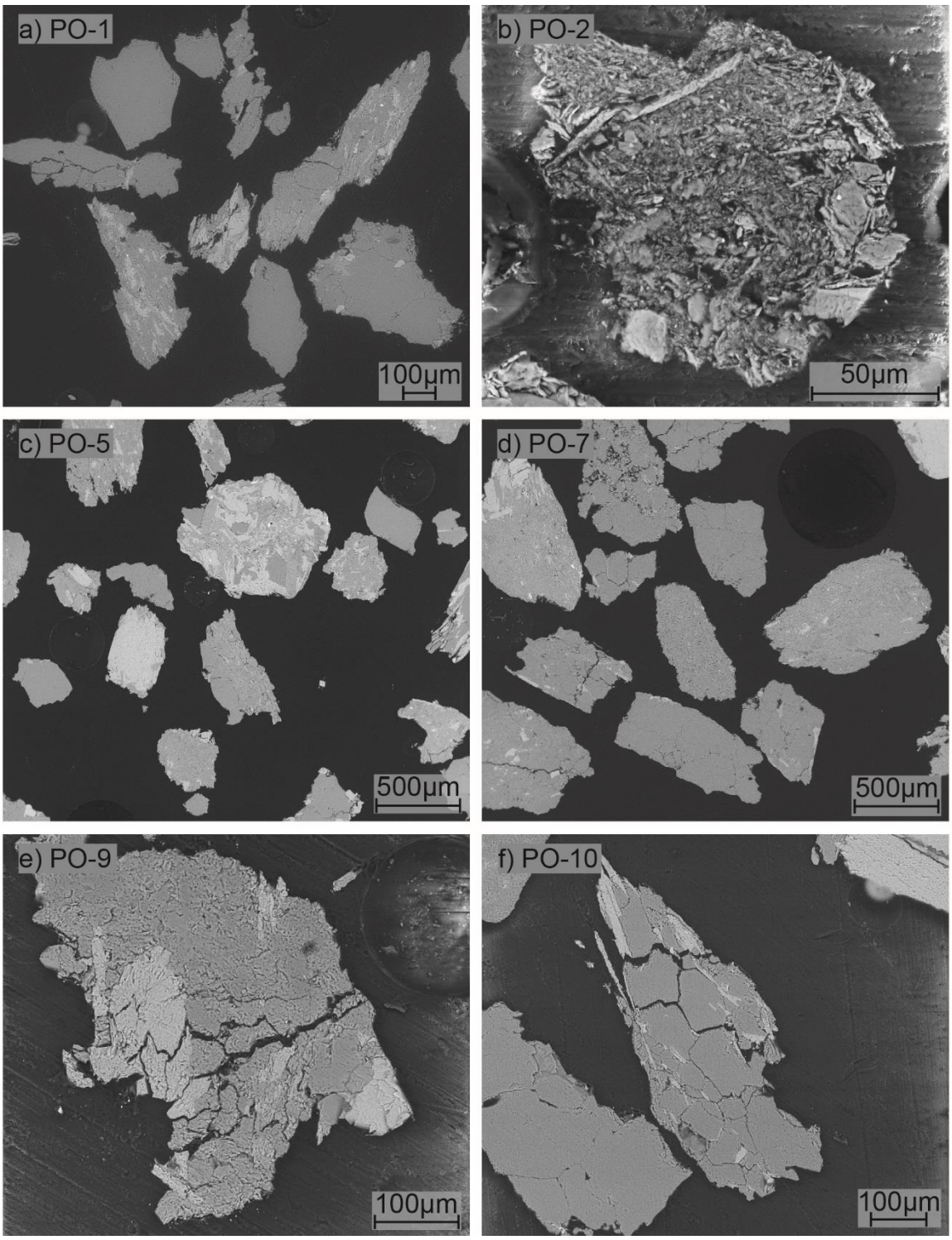

Fig. 3.16 SEM micrographs of fluvial material from the Poerua River alluvial fan river cut.

sampled; a full selection of micrographs is available in Appendix 3.3.

All of the samples collected show whole, clean clasts free of any adhering material. Clasts are rounded to sub-angular in appearance in all samples. Samples from the Mikonui, Whataroa, Waitangitaona, Omoeroa, Waikukupa and Young Rivers (Appendix 3.3b, d, e, g, i, o respectively) show a higher degree of grain fracture within the clasts. The degree of grain fracturing observed does not appear to have a relationship to the presence of known

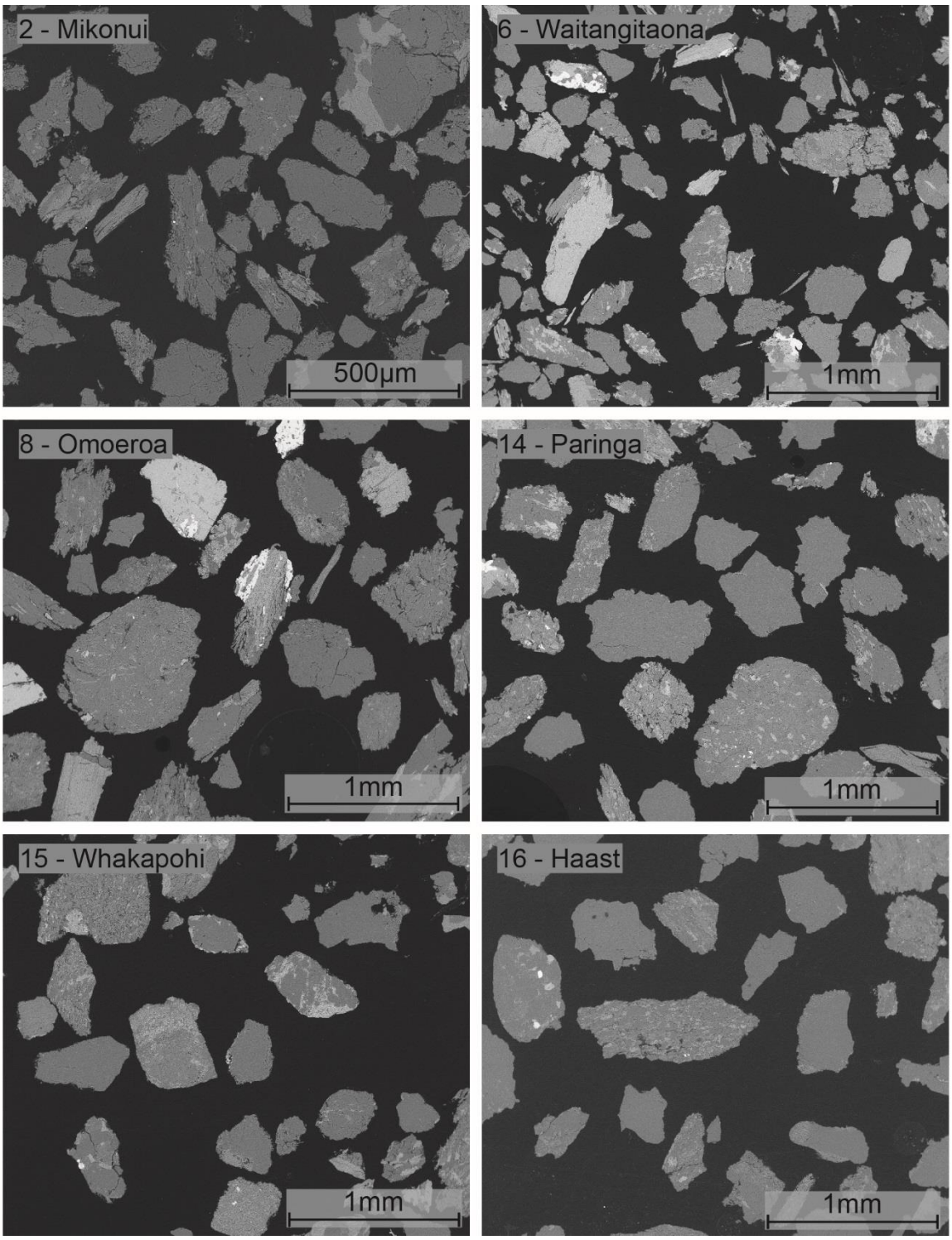

Fig. 3.17 Selected SEM micrographs of fluvial material from the spot sampling of West Coast river systems.

RAD in the river systems upstream of the sampling sites. However large, non-RA landslides could have occurred upstream of these sites generating fractured clasts.

3.4.4 Kyrgyzstan washing experiments

Laboratory based washing experiments of RA derived material show that agglomerates are present in unwashed and short washing time samples but disappear in long washing time samples. Examination of a sample of unwashed material contains multiple agglomerates. They are coherent grains composed of finer grained material (Fig. 3.18a). Larger sub-angular to sub-rounded clasts are clearly visible within the agglomerate grains, whilst a fine-grained micron to sub-micron matrix bonds the larger grains together. Fine grained material can be seen coating the agglomerate grains as well as being present in small quantities in the surrounding resin. Larger, solid, non-agglomerate grains were observed to also have a fine-grained coating of material around their edges (Appendix 3.4b).

Analysis of washed RA material from 1 hour into the experiment shows that fine-grained material adhering to the exterior of the grains has been removed and no fine grained material is 'free-floating' in the resin (Fig. 3.18b). Agglomerates are still present within the material, however those detected are smaller than observed within the unwashed sample; the agglomerate presented in Fig. 3.18b is ~220 μm in its long axis as opposed to the ~700 μm example in the unwashed material (Fig. 3.18a).

Beyond the initial 1 hour of washing agglomerates become uncommon within the samples. Small clumps of material that could once have been sections of agglomerate are present but they fail to satisfy the common agglomerate identification criteria. These small clumps of material have a fine grained matrix but are generally only holding together one or two <30 μm larger grains together (Appendix 3.4e). Whilst evidence suggests agglomerates are breaking down within the turbulent fluvial conditions an agglomerate grain was identified ~4 hours after the start of the experiment (Fig. 3.18c). Given the scarcity of agglomerate grains between 1-4 hours, the presence of a relatively large agglomerate within the 4 hour sample suggests two possibilities; (1) There may be a time variation in preservation potential between agglomerate grains, (2) Agglomerate concentration within the source material varies locally and samples will have varying quantities of agglomerates. Beyond the 4 hour sampling point no agglomerate grains were identified within the samples (Appendix 3.4), this suggests that breakdown of the grains within turbulent fluvial conditions is the more likely explanation for the lack of agglomerate detection. There may therefore be agglomerate fragments within <63μm material which was not sampled.

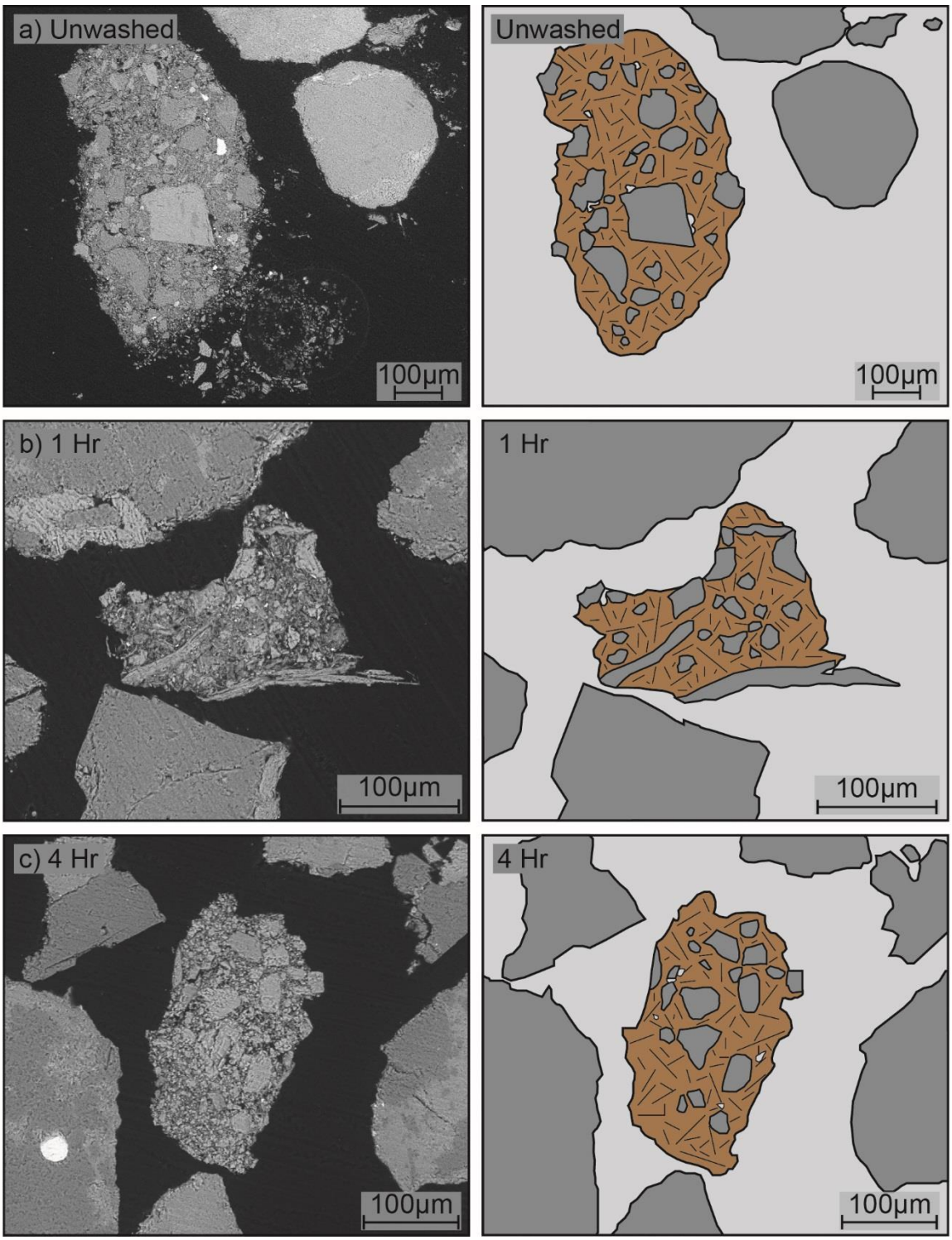

Fig. 3.18 SEM micrographs and interpretations of rock-avalanche agglomerates from the laboratory washing experiments.

3.5 Discussion

Reznichenko et al., (2015, 2012) have shown agglomerates to be preserved for at least 10^4 years within passive supra-glacial transport and moraine depositional environments. Given this preservation potential and the persistence of agglomerates after gentle washing (Reznichenko, 2012) the hypothesis was that detectable, albeit modified, agglomerates would survive through fluvial transport and deposition. Many RADs are in

inaccessible valley systems. Therefore detecting agglomerates in river sediment in accessible reaches downstream of RADs would allow the inference of there being fluvially censored deposits upstream. This would allow rapid identification of catchments affected by previously unknown, fluvially censored RADs; helping to fill gaps in RAD inventories around the world.

This section will first discuss localities where preserved agglomerates were detected and hypothesise as to why they are detectable there. In contrast, factors controlling the lack of agglomerates observed within the rest of the fluvial system will be examined. Based upon the sediment samples, laboratory washing experiments and analysis of fieldsite morphological processes there are five main factors that appear to influence the obscuration of the agglomerate signal in South Island rivers, (1) Agglomerate source material; (2) Supply limitation, (3) Dis-agglomeration of grains, (4) Dilution of RA material and (5) Burial of agglomerate rich material.

3.5.1 Sources of agglomerates

Contrary to the initial hypothesis that agglomerates will be preserved under fluvial transport and depositional processes, agglomerates are not preserved within the majority of fluvial material sampled in this project. However the locations where agglomerates were preserved give some indications as to why this might be the case. Both the Ram Creek and Stanley River RADs showed the presence of agglomerates in the deposits. However this sedimentary signal appears to be localised as some RAD samples did not show agglomerate presence.

At Ram Creek, a sample from the distal end of the RAD had agglomerates present but other in-situ RAD samples did not. Additionally, at the Stanley River only two of the four in-situ RAD samples contained agglomerate grains. Agglomerates are not ubiquitous throughout the deposits; this localised change in agglomerate presence may be linked to the formation and destruction of agglomerates by high shear stresses during RA transport (Mauri McSaveney, 2016, Pers. comm). Localised differences in material comminution would leave stratigraphic layers within the deposit with differing GSDs (Dunning, 2006) and agglomerate content.

Additionally, SEM examination of RAD samples show that when agglomerates are identified in the RAD material not all of the grains in the resin blocks are agglomerates. There are other solid grains within the samples and a qualitative visual analysis of the samples indicates that agglomerates are not in the majority. This shows that the majority of fine-grained material that is being entrained in rivers from RADs is not composed of agglomerate grains but other solid, pulverised fine-grained material. This localised disparity in agglomerate concentrations would make it more difficult to locate these diagnostic grains within fluvial material.

Fluvially aggraded dam-breach flood terraces downstream of the Ram Creek RAD show the presence of agglomerates. Similarly raised flood-aggraded terraces below the dam spillway of the Stanley River RAD contain agglomerate grains. However no other samples downstream of either deposit contained recognisable agglomerate grains. Given their detection in fluvial material at both sites agglomerates appear to be able to survive some reworking, however they are only found in higher magnitude flood samples. The proximity of the flood deposits to the RADs indicates that rapid erosion, transport and deposition allow the preservation of agglomerates. Flood deposits from further downstream could not be located and sampled so the dam-break signal cannot be traced further.

3.5.2 Sediment supply limitation

3.5.2.1 Ram Creek

Within Ram Creek there are limitations on the supply of RAD sediment to the river as well as limited transport of that material away from the deposit; this would hamper the transport and detection of agglomerates further down this system. Field reconnaissance shows that the active Ram Creek river is small and contained within an armoured channel at the base of the breach channel. During the reconnaissance period there was very little material being transported by the river. Harrison et al., (2015) note that the Ram Creek stream is unlikely to be able to transport the larger calibre dam-derived sediment that has been deposited there from the dam-break flood. Field reconnaissance pictures show that the contemporary Ram Creek river is too small to be able to reach and remove in-situ RAD material which may contain agglomerate grains.

Gullying of the breach channel wall has reworked material from the surface of the deposit and the weathered side walls to the river edges. Fans at the base of the gullies have been partially truncated by the Ram Creek stream indicating limited fluvial reworking. However remnant fan sections buffer the base of the side walls from the stream, similar to the development of terraces which defend deposits from further reworking (Hewitt, 2006). This means that the stream is currently not reworking any in-situ RAD material, only reworked gully material. Flooding within the catchment may be able to remove RAD material from the base of the deposit where gully material is not buffering the deposit. However this would be limited reworking during high-magnitude, low-frequency events.

This may explain why downstream sediment samples from the contemporary active stream channel do not contain any agglomerates. Agglomerates form in the high-pressure, deeper layers of the moving RA (Deganutti, 2008), not surface material; as shown before their presence is also localised. The gully material likely contains RAD surface material and some of the body facies. This indicates that agglomerate concentrations within gully material would be low. Further research is required on the

effects of weathering on the preservation of agglomerates; their preservation in glacial environments suggests they may survive prolonged weathering effects. Ultimately there is an agglomerate supply limitation problem within Ram Creek which reduces the likelihood of material being entrained within the contemporary river.

3.5.2.2 Stanley River

The Stanley River has a considerably higher discharge than Ram Creek but suffers from similar sediment supply limitation problems. Samples from the Stanley River RAD show the presence of agglomerates (ST-2 and ST-4). Therefore the supply limiting of sediment could be a major factor in why agglomerates are not located in contemporary fluvial sediment.

The armoured spillway channel and vegetated upper sections of the spillway imply that no reworking of RAD material is occurring in the upper two sections of the spillway channel. This channel morphology limits the river from entraining and transporting fine-grained RAD material which may contain agglomerates. However the removal of the terrace on the true left of the lower spillway channel between 2003 and 2015 shows that high discharge flows, capable of entraining large quantities of material have occurred in Stanley River. Now that this defended terrace (Hewitt, 2006) has been removed this has reconnected the sediment pathways linking the RAD spillway wall and the river. Cones of colluvium have brought RAD material to the base of the spillway walls but do not explicitly reach the river. The cones of material are different to that of Ram Creek in that they are not formed from 'washed' gully material, but collapse of the RAD spillway wall. It would require low-frequency, high-magnitude flows to mobilise this material; indicating only transient entrainment of RAD material into the fluvial system.

3.5.2.3 Summary

The geomorphology of the Stanley River spillway and Ram Creek breach channel suggest that the entrainment of RAD material which may contain agglomerates is transient in nature and may only provide pulses of material. Large pulses include dam breach floods or annual floods that might rework RAD, gully or colluvial material. Unlike the large Ram Creek breach only one small dam breach flood has occurred in the Stanley River system. This may be reflective of why no agglomerate material was found at any distance downstream of the Stanley RAD in flood deposits; there has yet to be a large enough flood to simultaneously mobilise a lot of RAD material downstream.

RAD deposition and the armouring of spillways inhibits the incision of rivers into bedrock (Hewitt, 2006; Ouimet et al., 2007); river incision on the West Coast is primarily driven by high uplift rates generated by the collision of the Australian and Pacific Plates

(Hovius et al., 1997). Therefore it is likely that rivers will incise through RADs and form terraces which can buffer the river from entraining RAD material unless there are high-magnitude floods to remobilise material. As an example the Wanganui-Wilberg RAD on the Wanganui River is on the Southern Alps range front (Table 3.1, Deposit 4). Whilst past fluvial reworking of this deposit is evident from analysis by Chevalier et al., (2009) the deposit displays very little evidence for contemporary fluvial reworking. The deposit is buffered from the river by a vegetated floodplain along most of the riverward flank. As the Wanganui River sample contains no agglomerates, despite its proximity to the RAD, it contributes to the hypothesis that sediment reworking from RADs is transient. Ultimately the morphology of spillways and breach channels has a significant impact on the ability of rivers to entrain RAD material into the flow.

3.5.3 Dis-agglomeration of grains

Fluvial reworking of material into the terraces near dam breaches (RC-3, ST-6) and to the reaches downstream (RC-8) preserve agglomerate grains from the RAD. The Ram Creek dam-breach flood (Harrison et al., 2015), redistributed ~1 x 10^6 m^3 of material 5km downstream and the 1994 Stanley RAD breach (Nash, 2003) remobilised dam material 1km downstream. This indicates that during the deposition of breach flood deposits, sediment supply limitation was not a factor.

SEM micrographs of material from the Poerua River show no presence of agglomerate, however there are many angular to sub-rounded clasts with a high degree of internal fracturing. The degree of internal fracture indicates a landslide or other mass-wasting process for the source of these deposited clasts. Mahaney, (2002) shows that mass-wasting derived grains have multiple fracture faces which can penetrate through the entire grain and micro-fracturing of grains is considered diagnostic of gravitational transport processes (Mahaney, 2002). The level of internal fracture of the fluvial reworked grains within the Poerua River samples points to a strong input from mass-wasting processes, most likely the RAD upstream. Given the preservation of solid fractured grains within the Poerua samples, but not agglomerates within the same material, it supports the hypothesis that dis-agglomeration has occurred. If dis-agglomerated the fine material would likely be removed as suspended load.

None of the West Coast river samples displayed agglomerate presence. The samples were usually taken kilometres away from the mountain range front, which would be the closest possible location where RAD material could have been entrained into a river. Many of the sampled West Coast rivers do have RADs present, however the majority are above glaciers close to the SAMD (Chapter 2) and others are valley confined, kilometres upstream of the range-front (e.g. Poerua River RAD). Alternatively, if agglomerate grains were able to be entrained in rivers as suspended sediment it may be

that they would not be deposited in channel sediment where samples for this study were collected; instead they may be transported and deposited in low energy environments such as backwaters, lakes and pelagic sediment.

The laboratory washing experiment provides an additional explanation as to why RAD material cannot be located within contemporary fluvial material. The results of the washing experiments support the preservation of agglomerates for short periods of time under fluvial transport conditions. The experiments suggest that agglomerates are broken down relatively quickly. Agglomerates were present in the unwashed laboratory sample; however, analysis of 'washed' samples show that agglomerates are undetectable after 4 hours. This suggests that agglomerates are susceptible to dis-agglomeration or breakdown due to mechanical abrasion under turbulent flow conditions, making them undetectable in distal parts of river systems due to these processes. Dis-agglomeration and mechanical abrasion will have significant impacts on the attainable transport distances of agglomerate grains, indicating that they may only be detectable within a short downstream range of any given deposit.

3.5.4 Dilution of RAD derived material in fluvial systems

Additionally to the issues of sediment supply limitation and dis-agglomeration it is expected that RAD material entrained by rivers will be diluted. Sediment fluxes from upstream, load from tributary rivers as well as non-RA landslides all contribute to the downstream sediment flux. Examination of the concentration of ultramafic rocks in river bedload composition in Westland (Cox and Nibourel, 2015) as well as rock-type counts within Ram Creek (Harrison et al., 2015) suggests that tributary rivers can rapidly change bedload compositions. This implies that each time a tributary stream joins downstream of the RAD the percentage composition of the transported material will change and the proportion of RA material will be diluted.

Stanley River and Ram Creek each have a number of tributary streams join them bringing in material of differing calibre and geology. It is likely that the sedimentary signal from RADs will be diluted and shredded (Coulthard and Van de Wiel, 2013) by material from other catchments as the majority of agglomerate rich material remains in storage in the deposit and is only released in pulses. Between the RAD and the mountain range front in the Poerua River valley there are at least four large landslides (Fig. 4.9) which have likely contributed large quantities of material to alluvial flats and alluvial fan material.

Tributary sediment dilution along with dis-agglomeration and supply limitation could also explain the lack of agglomerates within West Coast river samples, all of which were taken beyond the mountain range front. Many tributary streams have joined the main trunk rivers by this point and ordinarily RADs are located kilometres upstream.

3.5.5 Burial of agglomerate rich material

Agglomerate preservation is strongest in deposits that were rapidly reworked and deposited such as dam-breach flood terraces, however little evidence of distal flood material is available in the field. This could indicate material burial processes which are known to operate within RAD affected river systems (Hancox et al., 2005). Other deposits such as alluvial fans which have rapidly aggraded as a result of RAD breach floods, such as the Poerua River, could hold preserved agglomerates in buried material. The uppermost 3.5m of the Poerua River alluvial fan was sampled at a high-resolution of ~0.25m increments and yet no agglomerate grains were found within the deposit.

Based upon accounts of the alluvial fan, >4m of aggradation occurred on some parts of the fan surface between 1999 and 2002 (Hancox et al., 2005). This could mean that the 1999 dam-break flood material could be buried under subsequent aggradational material from 1999-2003. As shown before, the dam breach flood deposits are more likely to contain agglomerates. The uppermost aggradational material on the alluvial fan is sourced from dam-break flood material which had been stored in valley confined alluvial flats upstream (Hancox et al., 2005). The alluvial flat material is likely to have preserved agglomerates considering it was deposited during the dam-break flood. Given the provenance of the material that composes the upper alluvial fan it may be expected that the agglomerates would be present. However the alluvial fan will have been fluvially reworked and deposited twice and two tributary streams join the river upstream. This increases the time for fluvial dis-agglomeration to occur as well as allowing dilution of the bed and suspended load from tributaries.

3.6 Summary and conclusions

Agglomerates were detected within some sections of the Stanley River and Ram Creek RADs but not all RAD samples (See Appendix 3.5 for summary of agglomerate measurements). This indicates that agglomerates are available for fluvial reworking but only if localised sections of material are eroded from the RAD. Dam-break flood outwash terraces were shown to contain agglomerates, however no contemporary fluvial material was shown to have agglomerates present. Analysis of deposit sedimentology, sample composition under SEM, deposit erosional processes, washing experiment samples and the likely bedload material contributions shows a number of factors that affect the detection of agglomerates within contemporary fluvial material. These factors can be summarised as (1) localised agglomerate concentrations within RADs, (2) transient sediment supply limitation to fluvial systems from RADs, (3) dis-agglomeration of grains during fluvial transport (4) dilution of RA material by other sedimentary inputs into the system and (5) burial of dam-breach flood deposits by fluvial aggradation. These issues are briefly summarised below.

Analysis of sediment samples from the Stanley and Ram Creek RADs shows that agglomerate grains are relatively rare within the samples taken from the deposits. This suggests that either agglomerate presence may be localised or that they do not compose the majority of sediment within the deposit. Either way this leads to potentially not many agglomerate grains being reworked into the river system from the source and impacts upon agglomerate concentration within downstream fluvial material.

The morphology of the Stanley River and Ram Creek deposits both showed that very little fresh RAD material is being entrained in the river flow at any one time. Either gullying is washing weathered surface material from the breach channel walls in Ram Creek or cones of colluvium material are resting at the base of the spillway walls in Stanley River. This material is not reworked by the river on a day to day basis and is likely only partly removed in episodic high-discharge flows. This leads to RAD material supply limitation to the rivers.

Leading on from the issue of agglomerate concentration within the source deposit and material supply limitation to rivers; recent literature from the South Island has highlighted that changes in bedload composition of material can happen rapidly within fluvial systems. The impact of the addition of tributary stream material into the main channel significantly alters the bedload composition downstream. This indicates that RA material reworked into contemporary river systems will be significantly diluted by material from tributary streams. The exception to this appears to be from dam-break floods which rework large quantities of material from the RADs and deposits them in aggradational terraces. Here the quantity of RA material outweighs that coming from other sources and therefore preserves the concentrated agglomerate sedimentary signal.

Whilst agglomerates may be preserved proximally to the RAD after fluvial transport the preservation of agglomerates over the long term under fluvial transport is poor. The washing experiments show that agglomerate grains only survive fluvial transport processes for a short period of time; within the laboratory agglomerates were undetectable after 4 hours of turbulent flow. The presence of smaller agglomerate grains after the start of the washing experiments suggests that dis-agglomeration is occurring. This has significant implications for attempting to detect agglomerates distally from RADs. Likely this impacted the detection of agglomerates within the West Coast river samples which were located kilometres downstream of any known RADs.

Agglomerates have the potential to be preserved within RAD dam-breach flood material however as shown at the Poerua fieldsite it may be difficult to access this material for sampling if burial has occurred. This is similarly a problem within dam proximal locations such as alluvial flats if large scale aggradational events linked to dam breaching has occurred and much of the agglomerate rich material has been buried. This is true for the Poerua River and Ram Creek.

Ultimately it can be concluded that agglomerates are preserved in small quantities in dam proximal deposits associated with dam-breach floods. Contemporary river material does not appear to contain preserved agglomerates and they can therefore not be effectively used as a sedimentological tracer of censored RADs in river systems. Given the compounding factors of supply limitation, dis-agglomeration, dilution and burial associated with agglomerate detection the method was unable to examine the dispersion of RA material throughout West Coast river systems. The preservation potential of agglomerates in fluvial environments appears to be poor. In order to use this method to detect fluvially censored RADs, aggradational terraces associated with dam-breach floods within valley confined environments as well as lake sediment cores should be targeted for analysis.

As this method of tracing fine grained RAD material was met with limited success, Chapter 4 will examine the re-distribution of coarse grained RAD material within an idealised South Island river micro-scale flume model. The expectation is that examining the redistribution of RAD material on a catchment scale within the model may give a better indication as to where sediment from these deposits is stored within a river catchment. It could therefore help to inform future sampling campaigns within New Zealand fluvial systems to locate better agglomerate samples.

Chapter 4

Micro-scale flume modelling of the redistribution of rock-avalanche sediment through an idealised South Island river system

4.1 Introduction

This chapter presents laboratory based microscale flume experiments that examine the redistribution of RA dam material within South Island river systems. Many of the RADs within the South Island, particularly in the WSA, Fiordland and Nelson, are in narrow, steep, uplifting valleys with high AAR. As discussed in Chapter 2 and Chapter 3, it is therefore plausible that many deposits have been censored from the sedimentary record through fluvial erosion.

Chapter 3 determined the surprising lack of identifiable agglomerate particles within NZ river systems. A number of potential causes for the lack of agglomerates were identified, mostly dealing with the fine grained nature of the RAD source material. The flume experiment was designed to examine how coarse grained RAD material is reworked and stored within valley confined river systems. This could reveal if there are preferential target areas within river systems where agglomerates could be present.

A micro-scale flume model of an idealised South Island river system was developed. This idealised model contains a succession of differing fluvial environments based upon observations of South Island river systems, e.g. alluvial flats, gorges reaches and braidplains. Using ultra-violet (UV) sand as an analogue for a RA dam, the model was run six times with two possible RA dam conditions; either a fine-sand ‘un-armoured’ dam or a simulated boulder carapace ‘armoured’ dam. Here we examine where traces of the UV sand deposits were deposited within the differing reaches of the microscale flume model in order to inform where fluvially censored RAD material may be stored in NZ prototype rivers. This information is used to develop a summary diagram of the morphological and sedimentological impacts of a valley confined RA dam on the fluvial system and compare it to South Island prototype rivers.

Micro-scale flume modelling experiments in the past have focussed on determining the impact of engineering structures on prototype rivers (Davies et al., 2003, 2013a), modelling navigable channels in large rivers (Gaines and Maynord, 2001) and examining aggradation of deltas and alluvial fans (Davies and Korup, 2007; Wild, 2013). These models aim to present a comparable morphological response to the prototype rivers they

are modelling without having to maintain dynamic similarity (Davies et al., 2003). Standard, non-microscale flume models are usually large and expensive in order to maintain so many variables (Young and Warburton, 1996). Dynamic similarity of the model to prototype rivers is sacrificed for the convenience of being able to have smaller scale models in smaller laboratory spaces. Reynold's numbers (ratio between inertial and viscous forces) are not maintained within microscale modelling, therefore flow during model runs is laminar rather than turbulent (Davies et al., 2003). There is also no attempt to maintain Weber numbers within the model which would make surface tension effects in the model negligible. An attempt is made to maintain Froude numbers, relative depth and relative density of material within microscale models (Davies, 2007).

Froude numbers in microscale models have been observed to be similar to their prototype counterparts, i.e. approximately 0.6-0.7 for gravel bed rivers (Davies et al., 2003); therefore within this range when modelling gravel bed rivers, Froude numbers will have been approximately maintained from the prototype. The relative depth of flow to sediment grain size is approximately maintained in microscale models if fine sand and flow depths of 1-2mm are used (Davies et al., 2003). Additionally the relative density of material is maintained if water and fine sand are used as inputs (Davies et al., 2003).

Whilst micro-scale models do not recreate dynamic similarity, they have been shown in a number of cases to reliably model morphological characteristics of prototype river systems (Gaines and Maynord, 2001; Max et al., 2002; Davies et al., 2003, 2013a; Wild, 2013). Davies et al. (2013) recently modelled the impact of engineering structures on the aggradation of the Waiho River alluvial fan, NZ whilst Gaines and Maynord, (2001) cite numerous instances where the US Army Corps of Engineers have used microscale models to examine improvements in the navigability of rivers. In the experiment described in this chapter, rather than anthropogenic engineering structures, natural dam structures are modelled. The loss of dynamic model similarity generates laminar water flow conditions, in micro-scale flumes. However it has been shown that creating turbulent flow conditions, which would normally be observed in a river environment, is not always necessary to develop channel bed morphologies which may be expected to rely on turbulent flow, such as ripples, channels, braiding and meandering (Lajeunesse et al., 2010). This indicates that these models are effective at modelling fluvial morphological responses of landscape disturbances.

Micro-scale flume models have value in terms of examining the broad, relative, morphological response of fluvial systems to landscape disturbances (Davies et al., 2003; Wild, 2013) such as RA dam emplacement. Due to the lack of dynamic similarity of the model to prototype rivers, the timescale and aggradation/degradation variables within microscale flumes are typically treated qualitatively rather than attempting to be upscaled to real-world systems. Microscale flumes provide good qualitative indications of

morphological change driven by input disturbances such as landslides or engineering works (Davies et al., 2003; Maynord, 2006).

4.2 Methodology

Micro-scale flume models require a number of conditions to be met to ensure the reliable operation of the experiment. In this experiment the model is an idealised succession of fluvial environments and is scaled to represent gorges, alluvial flats and braidplains of South Island river systems. Input sediment properties (density and grain size distribution), input water and sediment flow rates, sediment and water delivery systems, model slope and channel boundary design also require careful consideration for model operation. The following sections detail the considerations made for the flume model experiment.

4.2.1 Flume model construction

An idealised model of a South Island river system was constructed in order to make the model results applicable to many different valley-confined fluvial systems. To achieve this, aerial images (LINZ, 2014) were investigated to identify common features within steep sided South Island river valleys. It was observed that many river systems have alternating successions of montane flats and confined gorge reaches. Many of these systems then expand onto a coastal braidplain at the edge of their respective mountain range fronts. Good examples of this succession are the Poerua River on the South Island west coast and Stanley River in Nelson, both of which were examined in Chapter 3.

The microscale flume model was setup on wooden base with an adjustable slope. For this experiment the model was run at an angle of 3° (Fig. 4.1a), this was the angle at which the input Silica sand could be moved by the chosen water input. Ordinarily in these model runs the slope of the model would need to be exaggerated relative to the prototype stream being modelled in order to initiate sediment motion (Davies et al., 2003). This model represents an idealised South Island river system and therefore does not have a direct prototype comparison. The average river slope from west coast rivers (Chapter 3 Table 3.1) ranged from 0.5° - 7.5° (excluding an outlier at 14°); this gives an average west coast river gradient of 2.4°. Given the flume gradient of 3° this means the flume model gradient is exaggerated by ~25% in order to initiate sediment motion. The model was constructed with rigid channel boundaries from large polystyrene sheets. Having drawn a grid onto the sheets the planform of the idealised river model design was drawn over the grid (Fig. 4.2a). The central sections of the design were cut out of the polystyrene using a hot-wire cutter. The channel boundary segments were then glued to another polystyrene sheet to form the channel base (Fig. 4.2b) and the gaps between the sheets were sealed

with caulk Waterproof outdoor masonry paint was then used to paint the inner channel to seal any holes in the model and prevent water leakage (Fig. 4.2c).

Froude numbers (*Fr*) that similar to those in prototype rivers needed to be maintained. Given that the micro-scale flume model here was not based upon a single prototype, more a succession of South Island river environments, there was not an absolute value that needed to be achieved. Previous studies of prototype west-coast river systems suggest *Fr* values of between 0.6-0.7 (Davies et al., 2003; Davies, 2007), whilst other authors suggest values of between 0.6-1 are acceptable for modelling gravel bed rivers (Malverti et al., 2008; Postma et al., 2008; Madej et al., 2009). For the micro-scale flume model estimates of *Fr* values were calculated for the different gorge, montane flat and braidplain environments using Equation 4.1. Where *v* is the flow velocity (estimated at 0.09 m s^{-1}), *g* is the acceleration due to gravity (9.81 m s^{-1}) and *d* is the average flow depth of a channel cross-section within a reach. Channel cross-sections were extracted from a base level DEM in order to estimate average channel depths.

$$Fr = \frac{v}{\sqrt{gd}} \quad (\mathbf{4.1})$$

Fr values were 1.0 for the Middle Gorge, 0.66 for the Lower Flat, 0.61 for the Lower Gorge and 0.8 for the Braidplain channels. These values are therefore consistent with scaled Froude-micromodels that have previously been used in the literature. Table 4.1 summarises the Froude, Reynolds (Equation 4.2) and Weber (Equation 4.3) numbers achieved in the microscale model for these four reaches, however as per the microscale flume methodology no attempt was made to match Reynolds and Weber numbers to prototype rivers.

$$Re = \frac{vR}{\nu} \quad (\mathbf{4.2})$$

Where Re is the dimensionless Reynolds number, v is the flow velocity (estimated at 0.09 m s^{-1}), R is the hydraulic radius of the channel (m) and ν (Greek letter Nu) is the kinematic viscosity (set at 1.307 x 10^{6} m^2 s^{-1}).

$$We = \frac{\rho\, v^2 l}{\sigma} \quad (\mathbf{4.3})$$

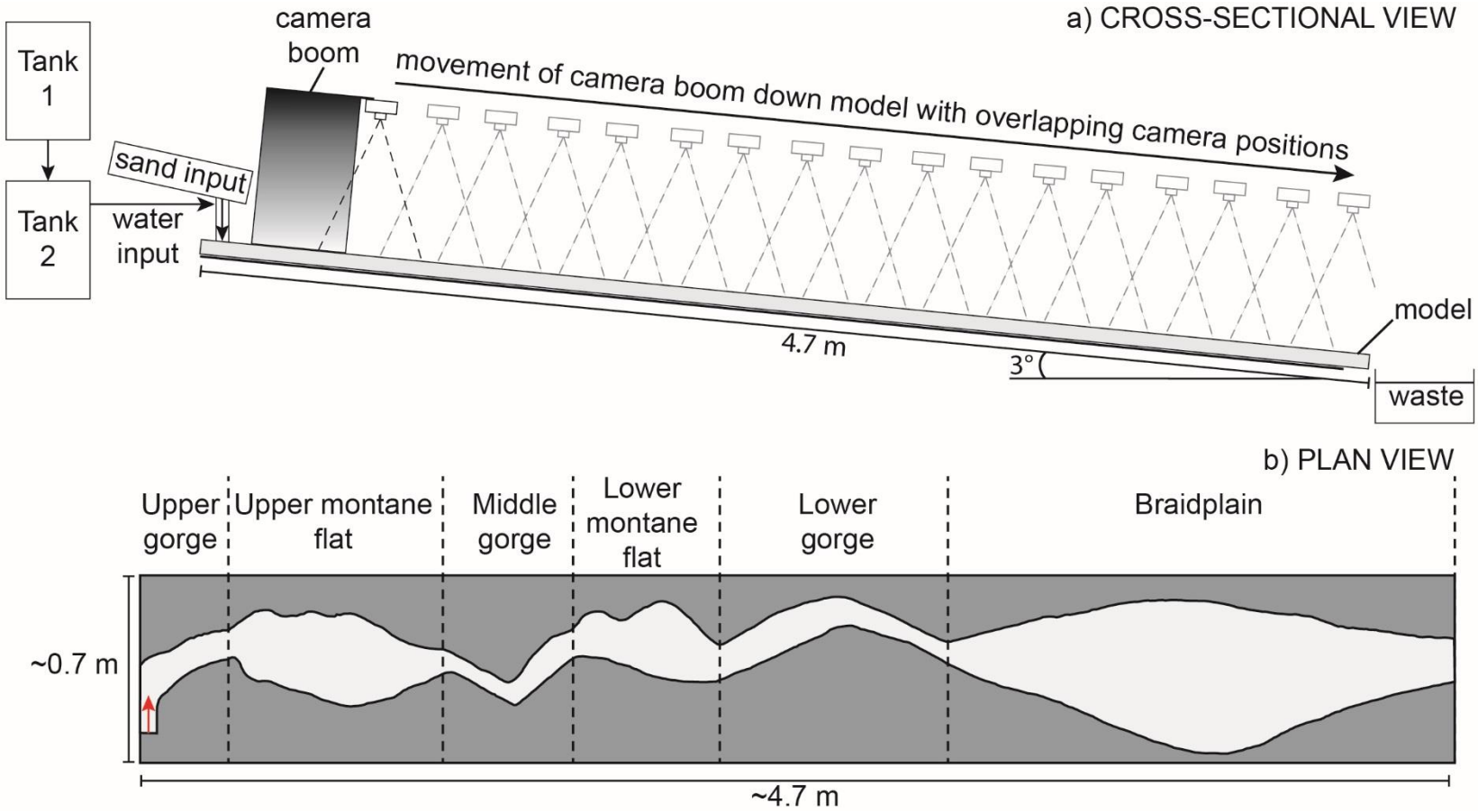

Fig. 4.1 Cross-sectional and plan view schematics of the flume model; (**a**) The cross-sectional schematic shows the model setup, sand and water input locations and the process of camera movement down the flume. Tank 2 and a sand input hopper feed into a tube where they are mixed before entering the model; (**b**) The plan view schematic shows the succession of fluvial environments, within the designed microscale flume model, based upon NZ prototype rivers. The red arrow indicates the water and sediment input location.

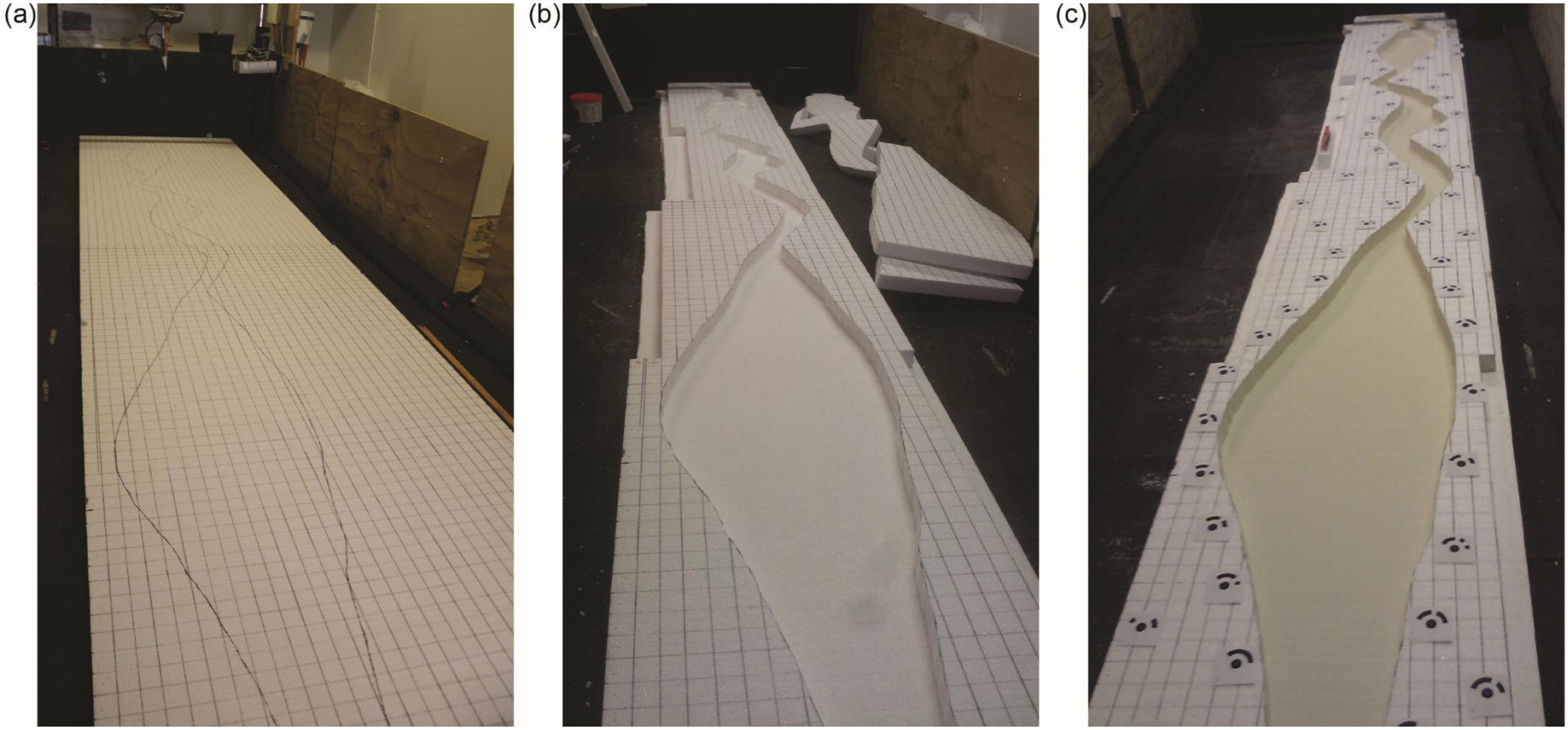

Fig. 4.2 Photographs showing the model construction procedure (a) The planform outline of the model is drawn onto the polystyrene sheets; (b) The large sheets are cut down to a more manageable size. Central sections of the model were cut out of the polystyrene using a hot wire cutter leaving the channel outline. Channel edges are glued onto a base polystyrene sheet which acts as the channel bed; (c) All gaps in the polystyrene sheets are sealed with caulk and the channel is painted with waterproof masonry paint. Ground control points (GCPs) were added onto the out-of-channel polystyrene surface.

Table 4.1 Summary of Froude, Reynolds and Weber numbers for channels in the Middle Gorge, Lower Flat, Lower Gorge and Braidplain reaches of the microscale flume model.

Flume model reach	Froude number	Reynolds number	Weber number
Middle Gorge	1.0	77	0.0005
Lower Flat	0.66	128	0.0011
Lower Gorge	0.61	131	0.0013
Braidplain	0.80	81	0.0008

Where We is the Weber number, ρ is the density of the fluid (taken as 1000 kg. m^{-3}), v is the flow velocity (estimated at 0.09 m s^{-1}), l is the average flow depth (m) and σ is the surface tension (set at 0.0728 N m).

The idealised South Island river flume model (Fig. 4.1b) begins in a short gorge reach where the sediment and water input feed enters the model. This upper gorge reach is also where a simulated RA dam was placed during the flume experiments. Following on from the upper gorge is an alternating montane flat and gorge sequence meant to represent some of the middle reaches of South Island rivers. At the end of the flume a braidplain reach was modelled to represent the river exiting the mountain range front onto the coastal plain. This reach has a free overfall into a waste trough as the downstream model boundary (Fig. 4.1a), providing the base level to which the rest of the model adjusts.

4.2.2 Model run conditions

The flume model was filled with a fine-grained Silica sand (D_{50} = ~295µm; Appendix 4.1) to a depth of 3cm for each experiment. The same sand was used as the sediment input into the top of the model which represented the base level flux of material into the system. In keeping with previous micro-scale flume model studies which have examined NZ gravel-bed rivers, fine-grained sand was used in conjunction with water as model inputs in order to maintain the ratio of flow depth to sediment grain size (Davies et al., 2003; Wild, 2013). Sand and water delivery into the model needed to be maintained at a constant rate for the experiment. To this end the water and sand inputs were quantified as part of the model setup.

A sand delivery system was devised using incrementally larger aperture holes drilled into test-tube caps. Holes were drilled at 0.1mm increments for sizes ranging between 2-2.5mm and 3-3.5mm. Sand was allowed to flow from a sonicated storage hopper through each aperture cap (Fig. 4.3a) onto a set of ADAM CBK logging scales.

The logger recorded the cumulative weight of sand on the scales every 10 seconds for 70 minutes; this was the time needed for the scales to reach their maximum weight capacity. Results of this input analysis are shown in Fig. 4.3b. Based upon Fig. 4.3b and observations of the flume model, the 2.5mm aperture cap was selected for use in experiments for three reasons; (1) Using this input allowed the model to equilibrate to base-line conditions without generating any naturally aggrading reaches; (2) Whilst minor variability is seen in the data for the 2.5mm delivery aperture larger apertures show increasing levels of instability, making them unreliable for maintaining a constant sediment supply; (3) The sediment inputs are similar to other micro-scale flume models of moving gravel-bed rivers in NZ (Davies et al., 2003; Davies, 2007).

Baseline water inputs were quantified using an Omega FTB334 logging flow meter. Gradations of 1.0mm width were added to a tap on the water input hose; this allowed the ability to repeatedly and accurately return to the same input value for the actual model experiment. The tap was opened to each gradation in turn and the outflow was recorded over a 4,200 s time period by the flow meter for each individual gradation. One litre of water passing through the flow meter produces 6646 pulses; this is known as the K-factor. The frequency of these pulses is proportional to the velocity of the flow within the meter and can therefore be used to calculate the rate of flow in L s^{-1} (*f*) using Equation 4.2; where *P* is the pulse count value from the flow meter and *K* is the K-factor.

$$f = \left(\frac{P}{K}\right) \qquad (\mathbf{4.2})$$

Results of water input quantification are shown in Fig. 4.4. Positions 1-5 on the graduated tap showed very little flow and so are excluded from the graph. Positions 6-8 show a gradual increase in flow as the tap is opened further. Similarly to the observations of the sand input quantification, once the tap is opened beyond Position 8 there appears to be increased instability in the water outflow for each graduation. In the case of positions 11, 16 and 17 the flow gradually reduces over the measurement period (Fig. 4.4). Given the information presented in Fig. 4.4 the models were run on Position 8, with an average flow of 0.02 L s^{-1}. This base level flow allowed the transportation of sediment in the model and showed little sign of flow instability throughout the quantification experiment. Again, this flow rate is similar to other micro-scale model inputs of NZ moving gravel-bed rivers. To compare to other microscale models of NZ river systems, Davies et al. (2003) use a input water flow of 0.025 L s^{-1} to model the alluvial fan at the Waiho River, whilst Hong and Davies, (1979), used an input flow of 0.02 L s^{-1} to model braiding in the Rakaia River.

The delivery rate of selected baseline sand and water inputs were not changed for

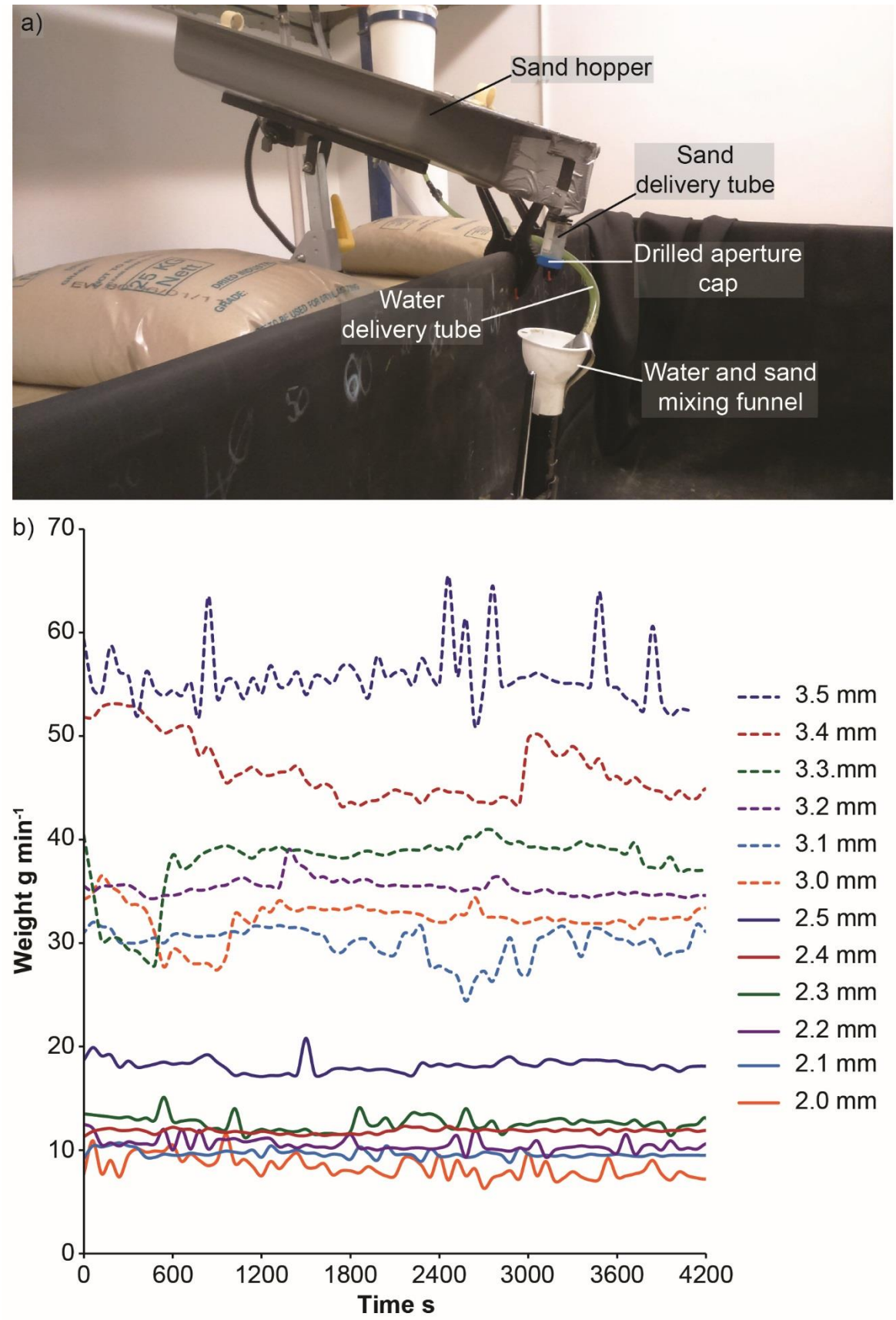

Fig. 4.3 a) Photos of the hopper and drilled aperture cap setup used to deliver sand to the flume model. Sand and water were mixed in the funnel before entering the model channel; b) Comparison of sand inputs into the model using caps with differing apertures to vary the sand flow.

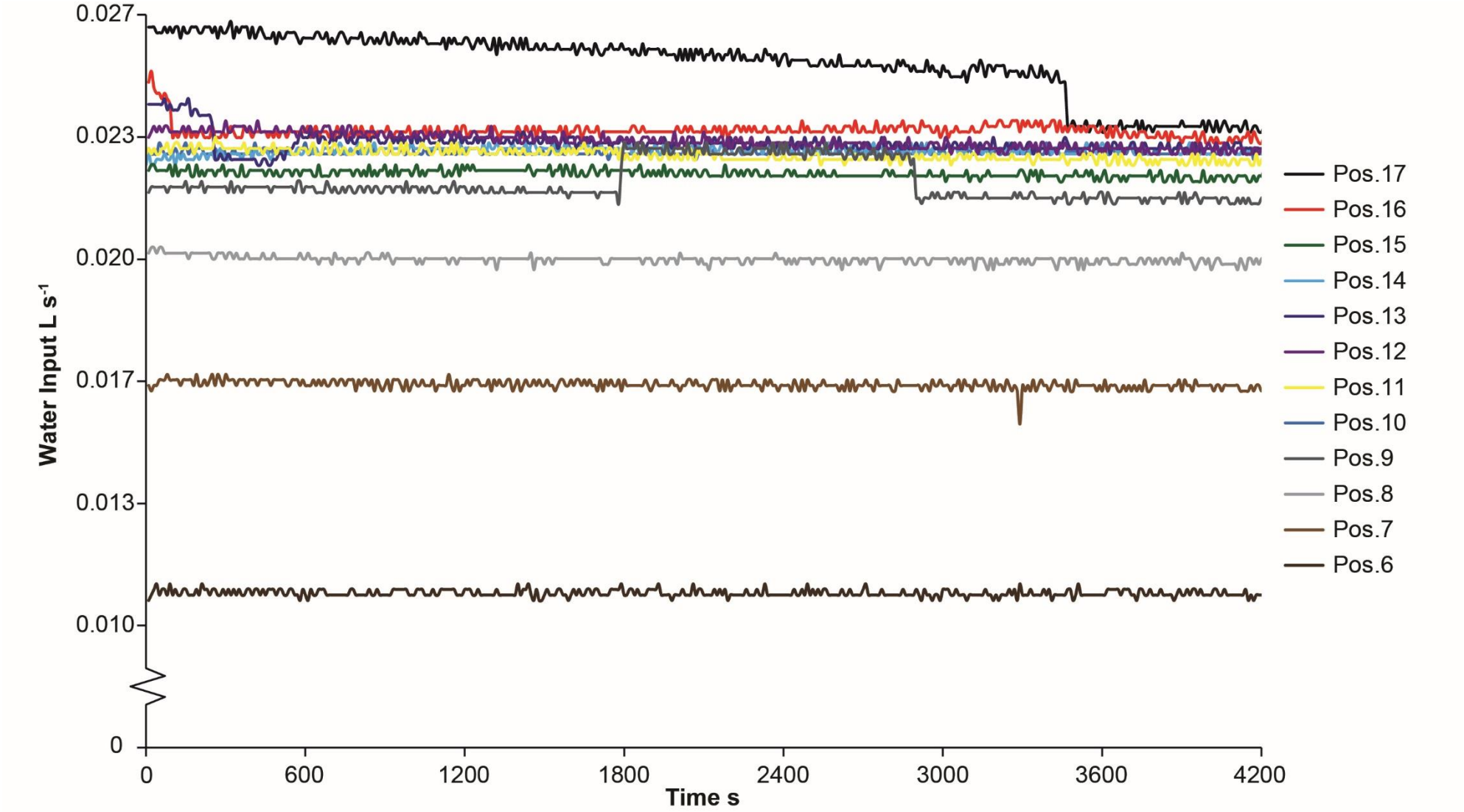

Fig. 4.4 Comparison of water inputs into the model using a graduated tap to vary the water flow.

any model run, ensuring that any morphological changes within the model are characteristic of channel disturbance from the simulated landslide dam rather than changes in baseline sediment and water delivery. These sand and water inputs were activated and run for ~6 hours to establish the baseline equilibrium conditions of the model channel.

4.2.3 Landslide design

After the baseline equilibrium conditions had been met, sand and water inputs were stopped in order to insert a landslide into the upper gorge. An analysis of cross-valley and down-valley topographical profiles of NZ, valley confined RA dams was conducted. This analysis provides an approximation of the cross-valley and down-valley topographical characteristics of RA dams in NZ. This analysis informed the morphological parameters for the micro-scale dam that was inserted into the flume model.

Sixteen landslide dams were selected from the RA inventory that was compiled in Chapter 2 (Table 4.2). The RADs used are all valley confined, some have been completely breached by rivers whilst others have overflow channels with lakes upstream. Topographic profiles over the length (down-valley) and width (cross-valley) of each deposit were taken from a 25m DEM (Barringer et al., 2002; LRIS-Portal, 2015). Profiles were taken within the limits of mapped deposits to avoid any bias from valley walls and other valley morphology.

With the x and y axis scaled equally, on the down-valley profile, it was possible to measure an average angle for the upstream and downstream slopes of each RA dam. These measurements were used see if there was a difference between the upstream and downstream morphology of these slopes (Table 4.2). The length (Fig. 4.5) and width (Fig. 4.6) scale (x-axis) of each RAD was normalised between 0-1. This allowed all cross-valley and all down-valley profiles to be plotted together regardless of scale for comparative purposes. Table 4.2 shows that all of the examined dams are breached or have well developed stable overflow channels. Eleven of the sixteen dams analysed have breaches or overflows located relatively centrally across valleys indicating a possible preferential failure location. Ten of the sixteen also either have a contemporary lake impounded or have evidence for infilled/drained lakes.

Down-valley length profiles (Fig. 4.5) show variation in morphology with undulating surface morphology, however most peak in the central range of the x-axis, equating to the approximate centre of each deposit in the field, regardless of the scale. Upstream and downstream slope angle measurements (Table 4.2) show that on average the downstream flank of deposits are steeper but only by a couple of degrees. Individually the deposits show variation in which slope is steeper.

Table 4.2 Table of South Island landslide dams of which downstream and cross-valley elevation profiles were derived to inform the design of the microscale flume model dam. Upstream and downstream angles refer to an average slope angle of the upstream and downstream dam slopes; BR = Breached, OV = overtopped, Ce = central, NVW = near-side to source valley wall, FVW = far-side to source valley wall

Deposit name	Upstream angle (°)	Downstream angle (°)	BR/OV	BR/OV location	Lake present
Taipo River (Hunts Creek)	-	8	BR/OV	Ce	Infilled
Lake Stanley	19	10	OV	NVW	Yes
South Opuha (Right Branch)	11	16	BR	Ce	No
Poulter River (Lake Minchin)	5	8	OV	Ce	Yes
Lake Marina	7	8	OV	Ce	Yes
The Roaring Billy	2	9	OV	Ce	Infilled
McTaggart Creek (Karangarua)	6	4	BR	Ce	Infilled
Lake Elmer	3	9	OV	Ce	Yes
Stanley Lower	2	6	BR	Ce	No
Dart River (Daleys Flat)	4	4	BR/OV	FVW	No
Poerua River	7	27	BR	Ce	Drained
Avoca River (Triangle Creek)	7	4	BR (large)	NVW	No
Lake Lindsay	-	6	OV (small)	FVW	Yes
Poulter River (Thompson Stream)	3	4	BR	Ce	No
Lawrence River (Hermitage Hut)	1	4	BR	NVW	No
Lake Phyllis	7	10	OV	Ce	Yes
Average slope	**6**	**8.5**	-	-	-

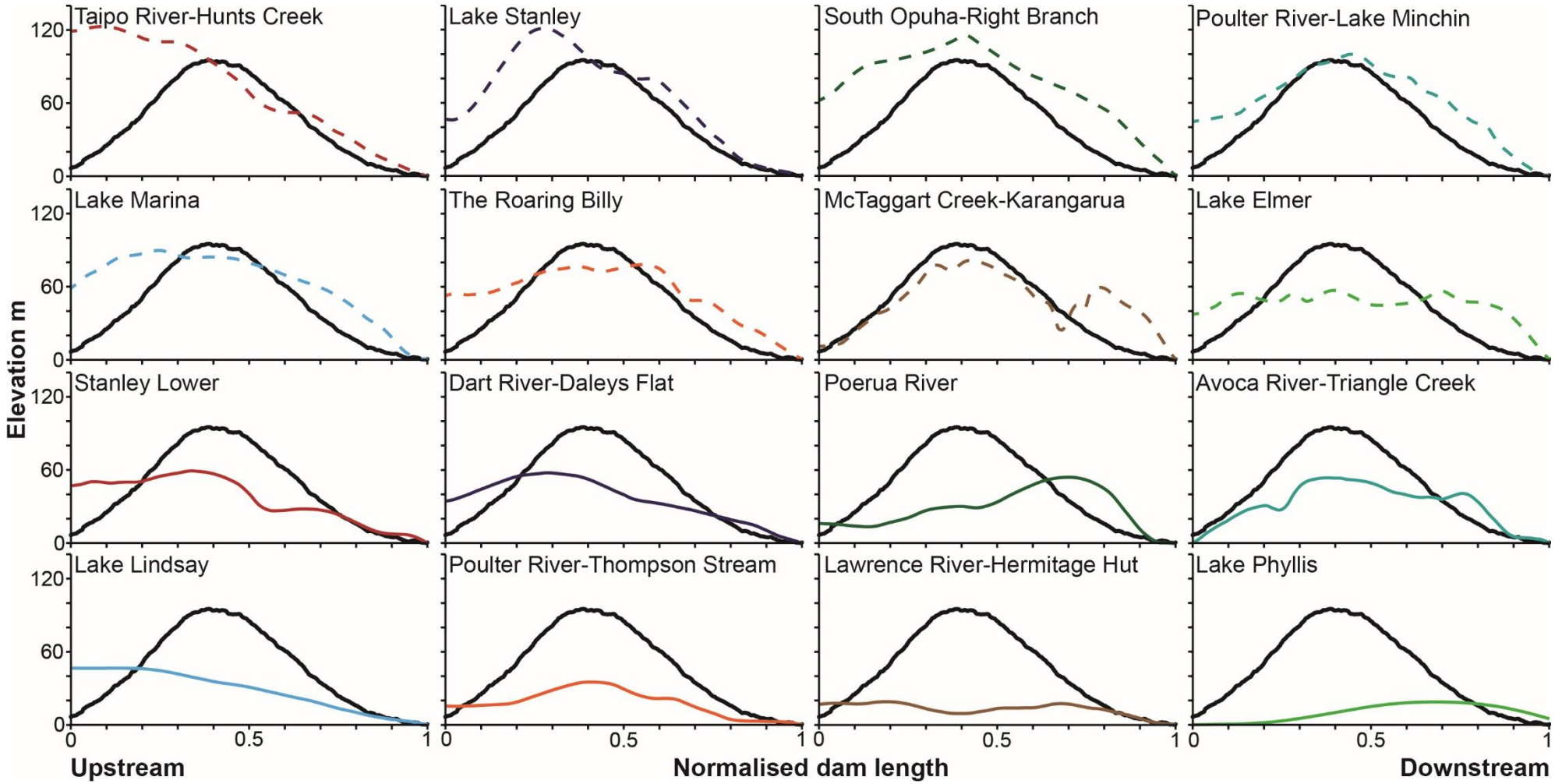

Fig. 4.5 Block diagram of down-valley RA dam profiles where the x-axis of each profile has been normalised. Profiles have been taken inside of boundaries of deposits depicted in the RA inventory in Chapter 3. Upstream and downstream slope angles from these dams were used to inform the flume model dam design. An average flume model dam cross-section is shown (black profile); the x-axis is normalised with the same method to other dams and the y-axis has been scaled to the average elevation of the NZ dam profiles.

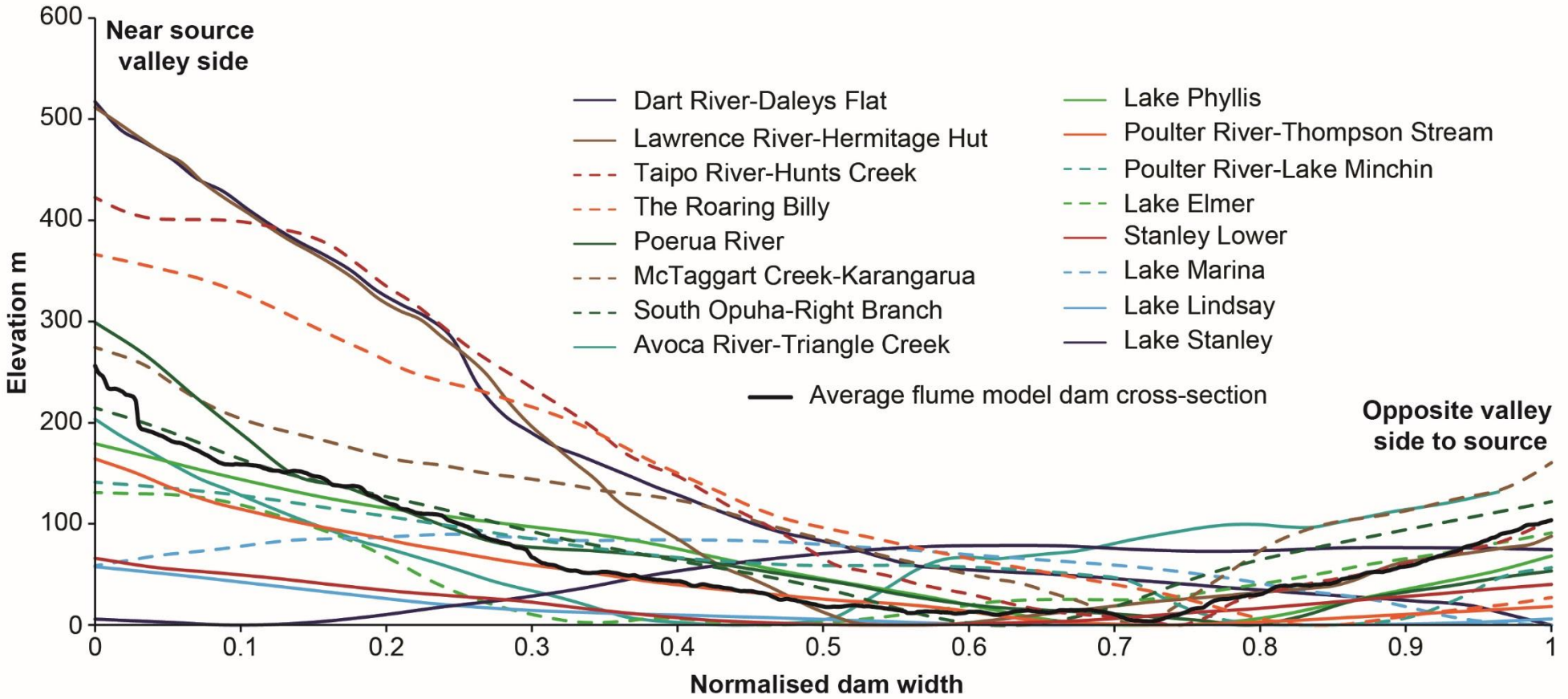

Fig. 4.6 Graph of cross-valley NZ RA dam profiles where the x-axis of each profile has been normalised. Profiles have been taken inside the boundaries of deposits depicted in the RA inventory in Chapter 2 and are all valley confined. In each case in the graph the source area is located off the left of the graph. Profiles indicate that in the majority of cases studied here the deposit is steeper and thicker closer to source and have a small run-up on opposite valley walls. An average flume model dam cross-section has been overlain; the x-axis is normalised with the same method to other dams and the y-axis has been scaled to the average elevation of the NZ dam profiles.

Cross-valley width profiles (Fig. 4.6) show a degree of similarity in surface morphology. Dam profiles are noticeably deeper towards the source area of each deposit, with the exception of Lake Stanley. Most deposits reach a minimum elevation towards the opposite valley wall from the source before rising back up as a small run-up. The morphology of the Lake Stanley deposit differs as a result of the surface being relatively flat and the overflow channel being incised on the source area side of the RAD.

Given the analysis of the morphology of these sixteen RADs the flume model dam was designed to be relatively symmetric in down-model profile and have similarly sloped upstream and downstream flanks (Fig. 4.5; Fig. 4.6). The cross-model dam profile mimicked a deep deposit on one side (source area side) with elevation decreasing across the dam before having a small run-up on the opposite model wall. The slope angles on the model dam were not exaggerated like the flume model slope as this made the dam construction less stable, especially when adding a carapace for the armoured model runs, before being able to continue the model water flow.

4.2.4 Tracing landslide material using UV sand

UV sand was used as a landslide dam analogue in the flume model. The UV sand allowed fluvially eroded landslide sediment to be traced via novel photographic techniques, in order to identify the patterns of fluvial redistribution and deposition of landslide material within the flume model. The UV sand used to construct the model landslide dams had a similar grain-size distribution (GSD) to that of the silica sand used as the base level sand. The Silica sand and UV sand have a similar GSD curve with D_{50} values of ~295µm and 230µm respectively (Appendix 4.1).

The size of the UV sand grains was appropriate to model RAD sediment given the small scale of the model. Fine Silica sand is an appropriate substitute for ordinary river sediment when modelling gravel bed rivers; with flow depths of ~1-2 mm in microscale models (Davies et al., 2003). The UV sand is slightly coarser than the fine Silica sand, however the internal material composing a RAD is often highly comminuted and can be similar in size to ordinary river sediment. This means that the UV sand is appropriate for use in modelling the body facies of the RAD as it is a similar calibre to the Silica sand, as would be expected for prototype river and RAD material.

The flume model runs were split into two experimental sets. The first set used an landslide dam composed of UV sand but with no form of coarse material carapace as might be expected of RADs in the field. The second experimental set had the same UV sand landslide but it was covered with a coarse grained carapace (D_{50} ~2.6mm; Appendix 4.1) which represented the boulder material often seen on the surface of prototype RADs. These different experimental sets were used to examine whether the course boulder carapace seen in field based RADs was an important factor in the fluvial erosion of the

relatively finer material composing the body facies of deposits. The coarse carapace material can collapse of the surface of RADs and provide protection to finer grained facies of deposits.

After inputting the UV dam the sand and water flow were re-started; in each case a landslide dammed lake was generated which eventually failed catastrophically generating a dam-break flood.

Six UV strip lights were used to illuminate the flume model to view the UV sand. Two lights were mounted on a custom made camera boom whilst the other four were positioned down the model on custom made brackets. During model operation cameras were setup to image the evolution of the landslide dam as well as monitor the montane flats and braidplain. Timers were set to capture images of each locale at 30 second intervals creating a timelapse of events which could then be used to monitor UV sand transport and deposition within the flume model.

Within each experimental set, two model running conditions were used, (1) Continuous running and (2) Start-stop running. In the continuous running conditions the flume was allowed to continue to run after the dam break for ~6 hours with the constant sand and water inputs (Table 4.3).

Table 4.3 Summary table of microscale flume model runs. For each run the landslide dam type, running conditions, sediment feed rate, water feed rate, run duration and the dam failure mechanism are shown.

Dam type	Model run	Running conditions	Sediment feed rate (g min^{-1})	Water feed rate (L s^{-1})	Duration of run (Hours)	Landslide failure mechanism
Un-armoured	1	Start-Stop	18.00	0.02	6	Overtopping
	2	Continuous	18.00	0.02	6	Syphoning
	3	Start-Stop	18.00	0.02	6	Overtopping
Armoured	4	Start-Stop	18.00	0.02	6	Overtopping
	5	Continuous	18.00	0.02	6	Overtopping
	6	Start-Stop: Long Run	18.00	0.02	22	Overtopping

In the start-stop models the sand and water inputs were turned off after dam failure had occurred and the subsequent lake drainage flood had subsided. This was done in

order to take sets of photographs, under both Halogen and UV lighting, for use in SfM reconstruction of the model morphology; 3D SfM models from this stage of each experiment are referred to as Dam Break time-step models from here on. From this point the start-stop type model had the sand and water inputs restarted and was run for a further ~6 hours, the same time period as for the continuously run models.

For both the start-stop and continuous model runs, after the ~6 hour running period the sand and water inputs were stopped and Halogen and UV image-sets were taken of the model. The SfM models reconstructed from these image sets are referred to as Post Dam Break time-step models from here on. In order to examine the running of the model for a prolonged length of time Model Run 7 has further Post Dam Break +8 hour and Post Dam Break +16 hour time-steps showing the morphological changes beyond the standard ~6 hour experiment duration.

4.2.5 Micro-scale model sediment coring

At the end of model runs it was necessary to examine the sub-surface stratigraphy within the model to see how landslide dam material had been incorporated into the baseline sediment flux of the model. It was also necessary to examine where in prototype NZ river systems it may be possible to find large quantities of landslide dam material based upon the flume model results.

A simple coring device was made from a standard 100ml laboratory syringe. The syringe plunger was removed and the nozzle of the main syringe chamber was sawn off. A bevelled edge was filed into the leading edge of the chamber, where the nozzle had been removed (Fig. 4.7a); this section of the syringe was the coring device. Another syringe chamber was sawn in half lengthways to make a channel in which cores could be logged after collection (Fig. 4.7b). The edge of the channel was coloured in UV reflective pen so that the core outline would show up well under UV light. Once cores were collected they were photographed under UV and Halogen lighting conditions and a simple core log was constructed based upon UV sand concentration within the stratigraphic layers (Fig. 4.8). Core sample locations were positioned so that a down-model profile could be constructed. Cores were also taken across the flats and braidplain so that 3D stratigraphy could be examined.

4.2.6 SfM model reconstructions in Agisoft Photoscan

Structure from Motion (SfM) is a photogrammetric method of creating low-cost, high-resolution DEMs using digital camera technology (Westoby et al., 2012). In the experiments presented in this thesis we use the Agisoft Photoscan software commonly used for image processing in SfM photogrammetry. SfM uses a series of overlapping

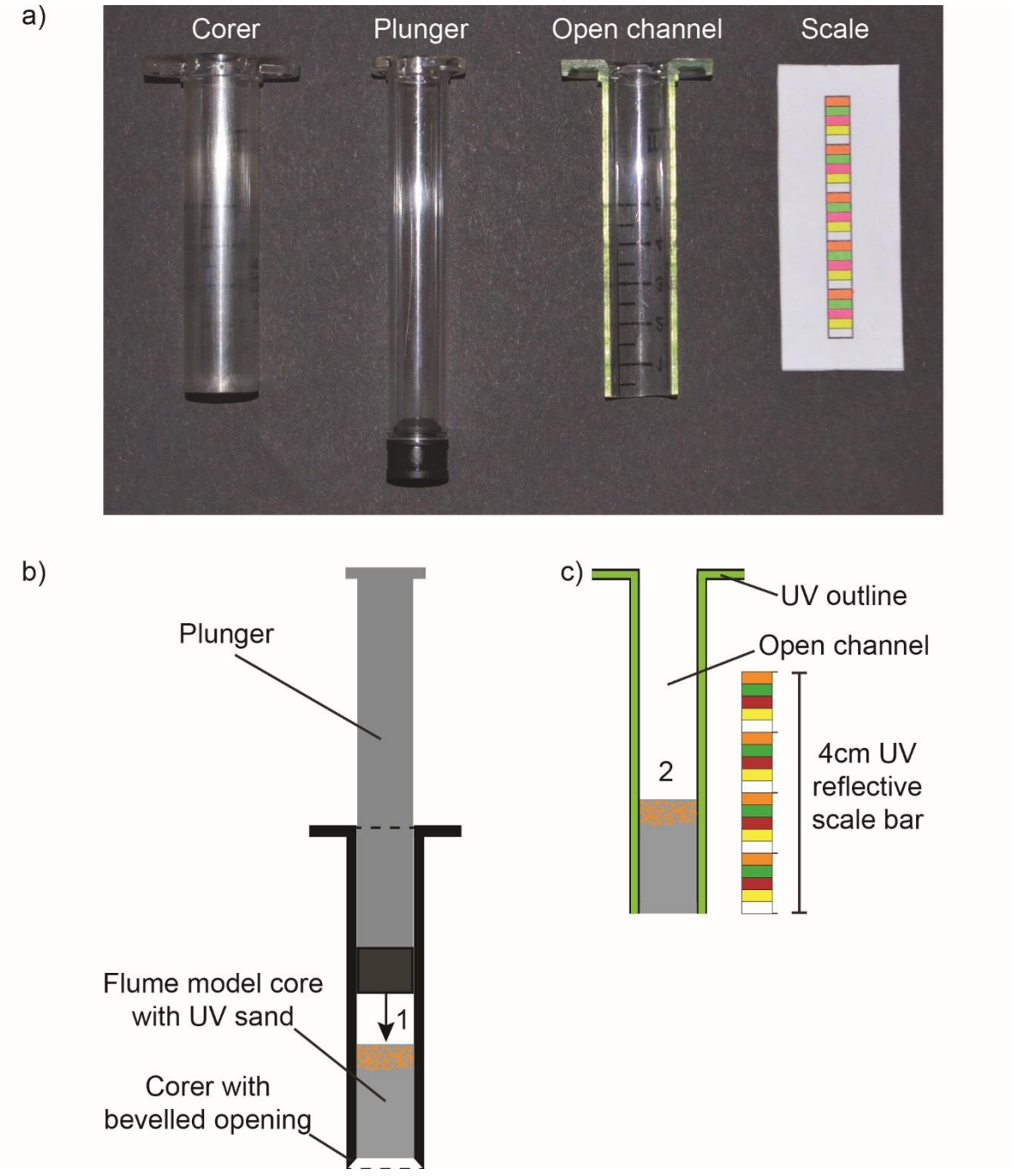

Fig. 4.7 (a) Equipment used to take cores from the model for sub-surface stratigraphy analysis; (b) Example operation of the equipment. The corer is used to collect a core, the plunger is then used to remove the core from the corer (1) and push it into (c), the open channel (2), for core imaging and logging. The open channel has a UV outline so that it is visible in photographs of the cores.

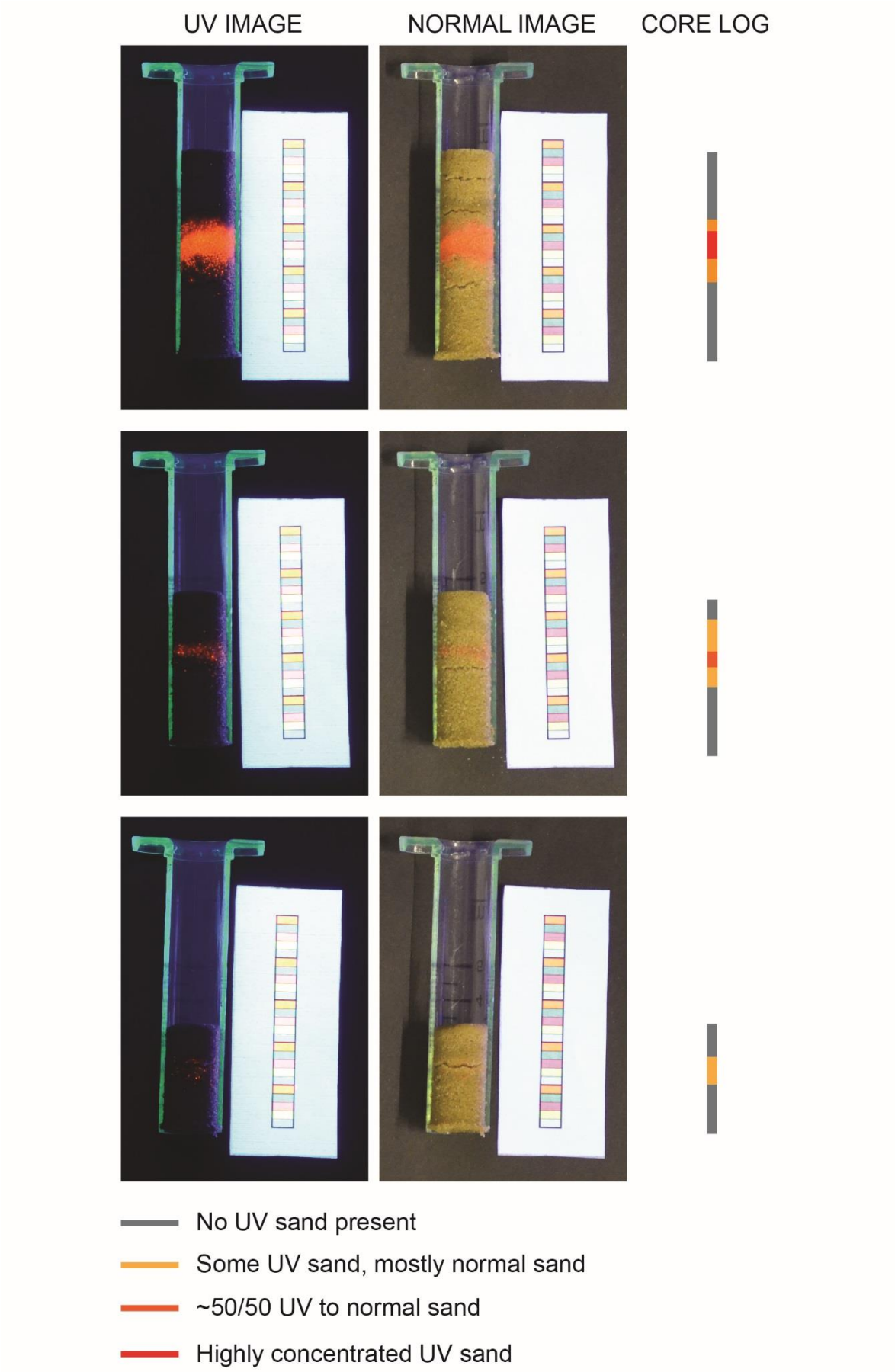

Fig. 4.8 Examples of the images taken of UV cores. Comparative images taken under Halogen lighting conditions are shown as well as the resulting core logs for each UV image which were used for analysis.

images to reconstruct the 3D geometry of a particular scene. Photoscan can pair overlapping images without pre-existing data on camera locations and pose, an improvement on traditional photogrammetry methods (Smith et al., 2015).

Model errors using SfM methods can be impacted by 1) the camera settings during image capture, 2) number and resolution of captured images, 3) percentage overlap of images, 4) presence of converging oblique images from multiple viewpoints, 4) scene lighting, 5) automated camera calibration within the software and 5) accuracy of measured GCPs including their placement within the model (James and Robson, 2012, 2014; Smith and Vericat, 2015; Smith et al., 2015; Micheletti et al., 2015). The range of the camera sensor from the scene being reconstructed is one of the most important factors in determining the model errors. Sub-mm errors are achievable with images captured in sub metre-ranges whilst km-range surveys are susceptible to metre-scale errors (Smith and Vericat, 2015).

Given the variety of errors that can be generated by camera, real-world scene conditions and software based parameters, care must be taken when setting up SfM surveys in order to minimise errors and develop DEMs with sufficient spatial resolution for analysis. The following section outlines how image data was collected and processed using SfM within Photoscan to produce high-resolution DEMs of the micro-scale flume model.

4.2.6.1 Image collection

Based upon previous literature (James and Robson, 2012, 2014; Smith and Vericat, 2015; Smith et al., 2015; Micheletti et al., 2015) the images collected for SfM reconstruction needed to fulfil a series of criteria:

1. Multiple images covering the same area of the model.
2. Convergent planar and oblique images, with a high degree of overlap.
3. Camera sensor to be within 1m of the model to enable sub-mm errors.
4. Well-lit, un-blurred, high-resolution images.

Image collection for SfM processing was standardised across all model runs. A Nikon D5100 dSLR, was used to take all images which were required for Photoscan. An arch shaped camera boom was designed (Fig. 4.9) allowing the collection of four images of the flume when located in any one position (Fig. 4.10a; Fig. 4.11b); Two planar images were captured looking directly down on the model and two oblique images set at 30° from horizontal (Fig. 4.9; James and Robson, 2014). The camera sensor was ~0.65m away from the target enabling the collection of high-resolution images of the model. In order to achieve the level of repeatability required a series of marks were made down the flume to indicate the location in which the boom should be placed for image collection. This constituted between 62 and 68 camera boom locations over the flume model (Fig. 4.10a).

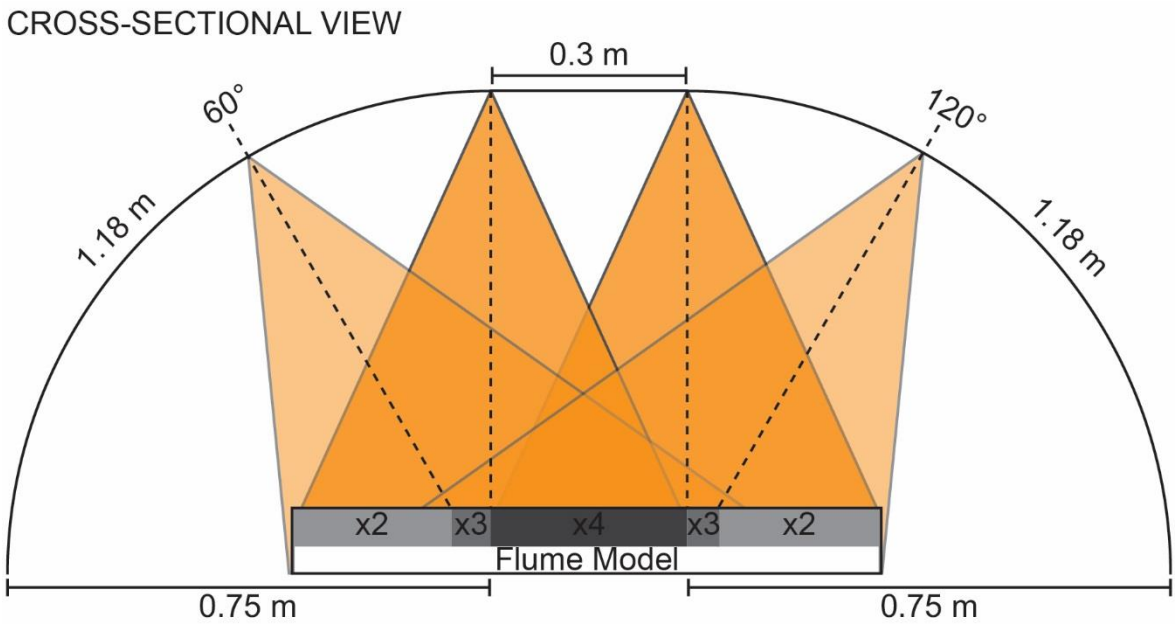

Fig. 4.9 Cross-sectional schematic of the camera boom which was designed for image capture of the flume model. Orange cones indicate the field of view of the four camera positions available on the boom. Four images of the model can be taken at any one time and then the boom can be incrementally moved down the flume for further image capture as shown in Fig. 4.10. Grey boxes indicate the number of photos that are overlapping in 2D at any given point on the model.

The boom allowed images to be taken with a degree of overlap (Fig. 4.10b). Cross-model images across the flume model only achieved 49% overlap this was balanced with an 80% overlap of down-model images. This overlap meant that between 8 and 16 images were covering any one area of the model channel (Fig. 4.10a). In total the number of images taken on each run varied from 248-272 (Appendix 4.2). Given the camera boom's design, it was straightforward to move down over the model to standard locations for all runs.

The use of the boom allowed each image to have uniform UV and Halogen lighting conditions regardless of its position over the model (Fig. 4.11). A bright 400 W Halogen lamp (Fig. 4.11a) and two 20 W UV lights (Fig. 4.11b) were mounted to the inner radius of the boom to provide consistent illumination over any model location.

Even with consistent lighting on the boom, camera settings needed to remain the same over model runs. Camera parameters were devised with differing settings used for Halogen and UV lit runs (Appendix 4.2). Images were taken under each lighting condition; ISO and exposure time settings were adjusted until images were not overexposed yet the detail, such as model morphology in halogen conditions and individual reflective grains in UV conditions were visible in images.

4.2.6.2 Model ground control points

Ground control points (GCPs) can introduce error into the model reconstruction workflow as they are used to scale the 3D reconstructed model in Photoscan. In order for

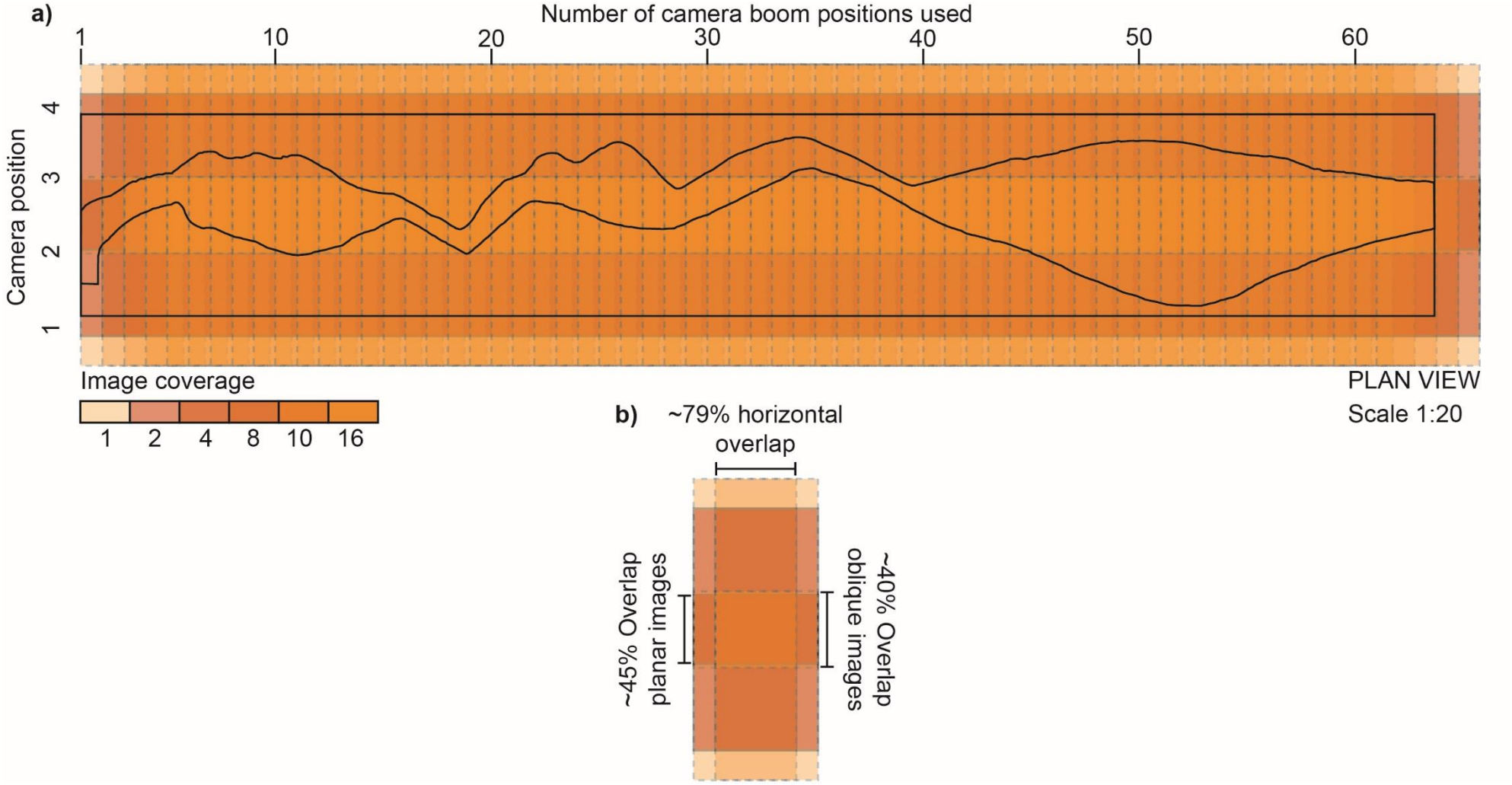

Fig. 4.10 (a) Scaled model plan view with idealised camera overlaps; deeper orange in the centre of the model indicates a higher amount of photograph overlap, the model design outline is overlain. Camera positions 1-4 indicate the camera locations on the boom in Fig. 4.11b; (b) Percentage of overlap of photos used in the construction of DEMs in Photoscan.

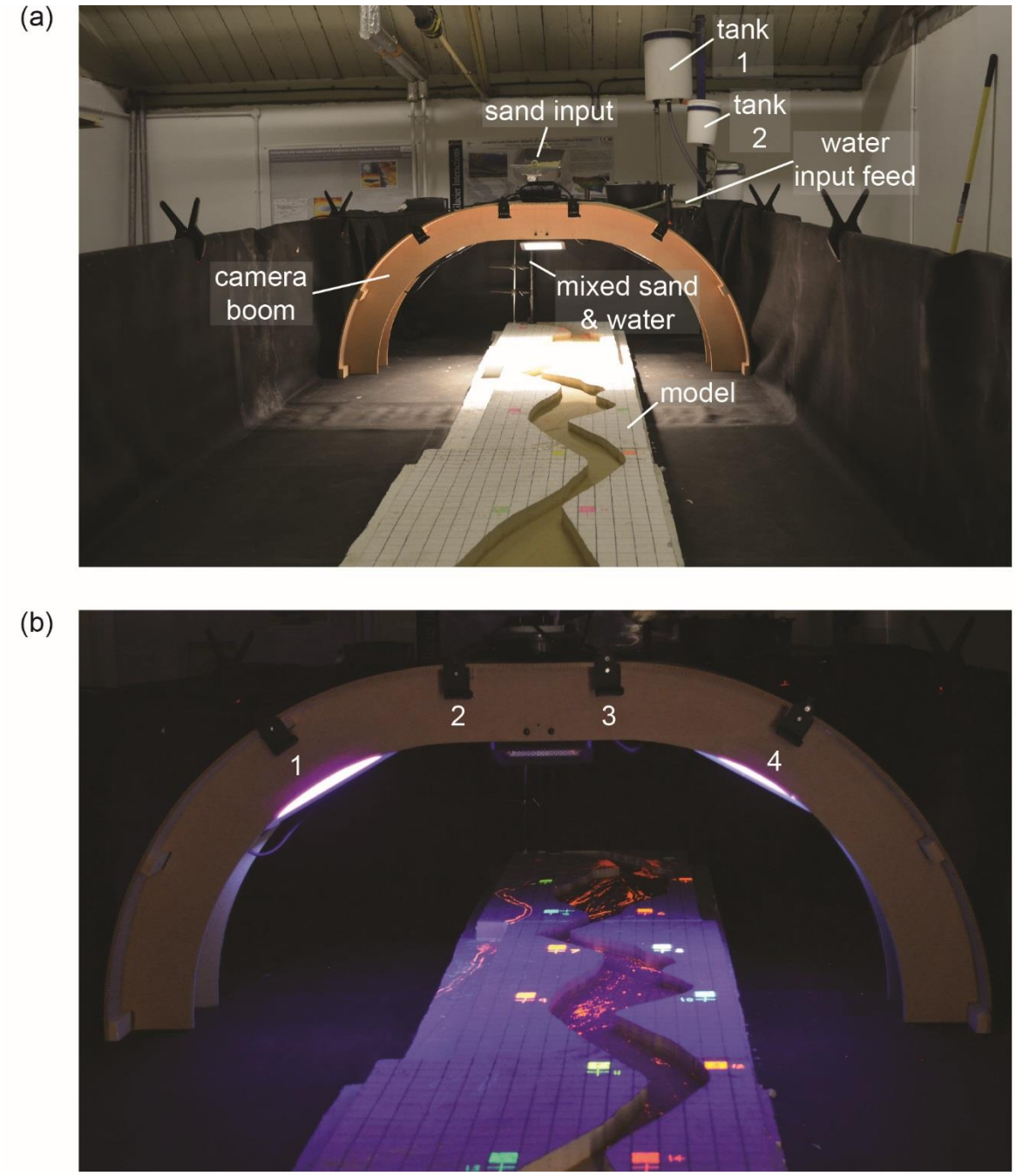

Fig. 4.11 Photos of camera boom usage (a) Halogen lighting conditions. A halogen light was fitted to the middle of the camera boom in order to illuminate the model evenly in each image. Annotations are consistent with the model schematic in Fig. 4.1; (b) Ultra-violet (UV) lighting conditions. Two strip UV lights were mounted to the sides of the camera boom in order to give sufficient illumination to the model under dark conditions; some illuminated UV sand is visible in the model channel. Numbers 1-4 indicate the camera mount positions from which images were collected.

SfM models to be mm accurate the real-world co-ordinates of the GCPs and the placement of those GCPs on images within the Photoscan software must also be mm accurate. A total of 104 UV and Halogen visible GCP markers were distributed across the flume model. GCP positions on the model were surveyed into a local coordinate system using a Leica Total Station. All GCPs were surveyed from a single station location next to the flume model using a reflector-less survey approach. This survey assigned X, Y and Z

coordinates to each GCP relative to the station location. These X, Y and Z coordinates were imported into Photoscan and markers corresponding to the GCPs were placed in each of the input images that was used to construct the 3D model.

The size of each GCP point on the real-world model was ~2mm in diameter. Marker flags were placed in the centre of each GCP point on each image in Photoscan. Given the size of the GCP points it was accepted that centrally placed marker flags could not be more than 1mm away from their intended position; therefore the GCP positional accuracy parameter was set to 0.001m in Photoscan.

The geo-referencing tool in Photoscan then linearly adjusts and scales the model to fit the GCPs. At this point some GCPs were removed if they significantly affected the RMS (root mean squared) error of the model; the points that were removed often came from the top and bottom of the model as these areas have less image coverage (Fig. 4.10a).

4.2.7 Flume model data processing

A workflow was developed for the processing of images taken of flume models. The workflow brings together image capture, Photoscan reconstruction parameters and post-reconstruction processing and analysis of the flume DEMs (Fig. 4.12). The 'Model Run' section of the workflow deals with the experimental runs and image collection. The Photoscan' section is all computer based and deals with the processing of the raw images into 3D model reconstructions, DEMs and orthophotos for different sections of analysis. Photoscan uses convergent and overlapping images taken from planar (nadir) and oblique (off-nadir) camera positions to estimate the real-world camera position within a digital 3D reconstruction space. The following description of the Photoscan algorithms and processing is summarised from Smith et al., (2015). First images are uploaded to Photoscan and 'keypoints' are identified in all of the images. Alignment of images is then achieved by matching keypoints visible in overlapping photos (Fig. 4.12 – Align photos). Once the images have been aligned the software uses a bundle adjustment algorithm to estimate the 3D scene geometry, the camera position in the digital space as well as internal camera parameters used to capture the image (e.g. sensor position and focal length).

The alignment of images results in the generation of a sparse point cloud as a result of the bundle adjustment connecting the simulated camera sensor positions to individual points in the 3D reconstruction space (Fig. 4.12). Once the sparse point cloud is generated the software uses multi-view stereo (MVS) image matching algorithms to increase the density of the point cloud.

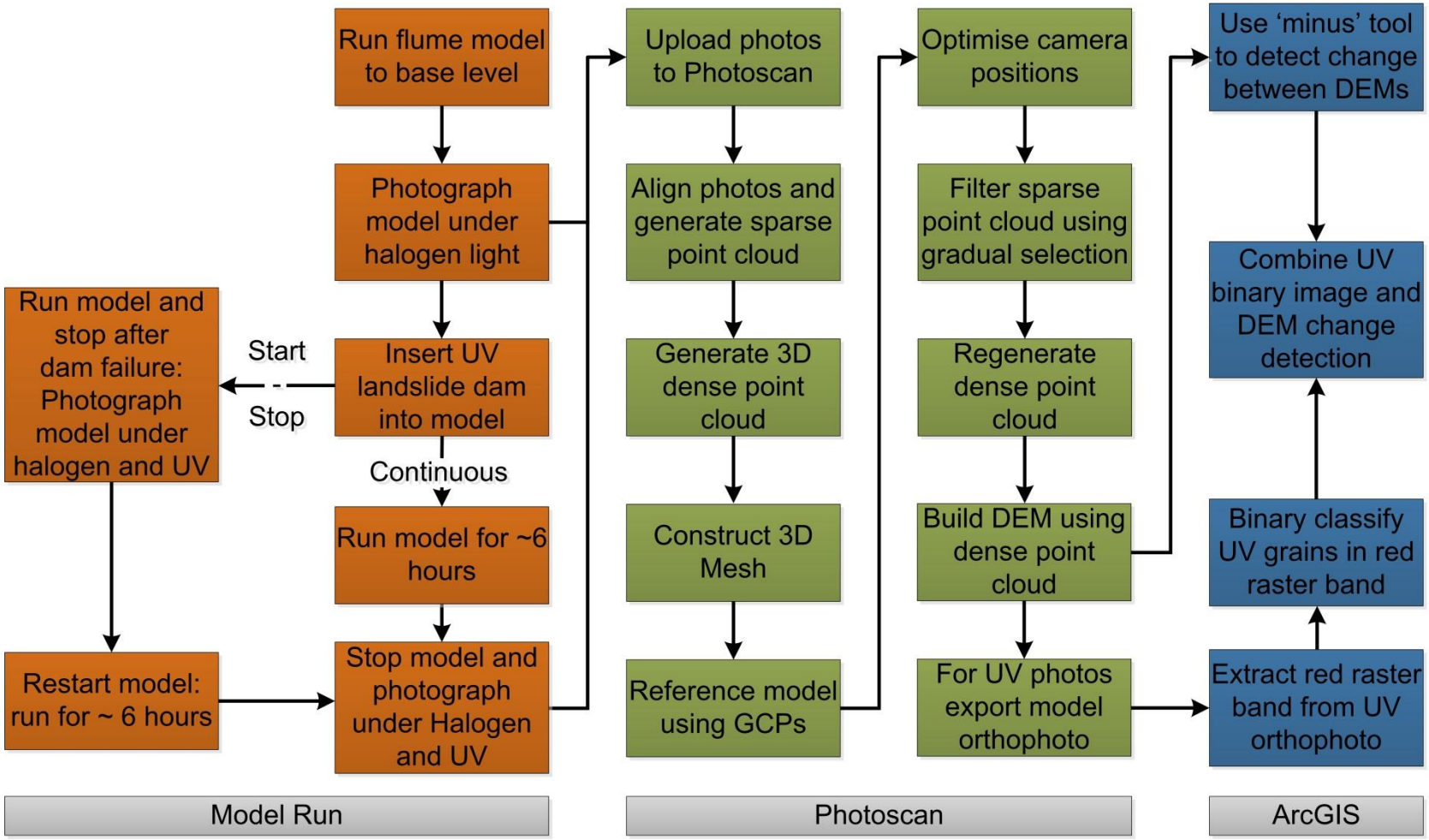

Fig. 4.12 Workflow for the collection of model data, construction of SfM models in Agisoft Photoscan and processing of DEMs and orthophotos in ArcGIS.

Once the scene geometry has been reconstructed, geo-referencing and optimisation algorithms can be used to improve model accuracy. Initially the point clouds will be in a local, unspecified co-ordinate system within Photoscan. Ground-control points with specific co-ordinate information are placed in each image and are used to reference and scale the model (Fig. 4.12; Smith et al., 2015). This GCP referencing of the model is a linear refinement and does not warp the model to fit the points. Well distributed GCPs with accurate positional information help with model accuracy and reduce the 'doming' effect which is seen by many SfM users (James and Robson, 2014; Smith et al., 2015). Once the model is referenced the software can non-linearly optimize the alignment of images (warping the model to fit the GCPs; Fig. 4.12). This optimization within Photoscan re-estimates the camera positions and the photo alignment from the first stage of the processing using the new GCP information available, improving the model accuracy. This stage deletes erroneous dense point cloud information and generates a new sparse point cloud. The new sparse could can be filtered to remove any points where the optimization has identified high re-projection errors based on the matching of image features. The dense point cloud is then regenerated and meshed in order to produce an accurate DEM of the flume model which can be exported and used for analysis in ArcGIS. Georeferenced orthophotos of the reconstructed scene can also be exported as all of the images are geo-located after point cloud generation. Halogen lit images were processed into DEMs for differencing analysis and long profile extraction; whilst UV images were processed into georeferenced orthophotos for the extraction of UV sand locations.

4.2.7.1 DEM differencing

In order to examine major morphological changes within the flume models the DEMs built in Photoscan were imported into ArcGIS for further processing (Fig. 4.12). All models were georeferenced in Photoscan using the same set of GCPs and therefore were coincidentally geo-located with each other when imported into ArcGIS. Each experimental run has at least two DEMs associated with it, Base Level and Post-dam Break. Experimental runs which are start-stop type have an additional intermediate Dam-break DEM. One of the experimental runs was also run for an extended running period and therefore has two additional Post Dam Break models, Post Dam Break +8 (+8 hours running time) and Post Dam Break +16 (+16 hours running time). The aim of DEM differencing was to produce a sequence of models which visualised the change between each time-step (Base Level, Dam Break, Post Dam) for each model run. To this end DEMs of difference were created for the following time-steps Base Level-Dam Break and Dam Break-Post Dam Break, these showed the morphological change across the model. A final Base Level-Post Dam Break difference model was created to show the gross-

change from the equilibrium state base level to the landscape disturbed end of the model run.

In ArcGIS the ‘minus’ tool can be used to show the difference between two coincidentally geo-located DEMs. Fig. 4.13 shows how the differenced DEM is created by subtracting one DEM from another. In this example a Dam Break model is used as the input DEM (Fig. 4.13a); the Base Level DEM (Fig. 4.13b) from the same experimental run is then subtracted from the Dam Break to produce a new DEM which shows the morphological change that occurred between the time-steps (Fig. 4.13c). As both input models have the same slope due to their coincidental georeferencing, the final differenced-model output has no slope and shows aggradation/degradation from the same planar baseline.

4.2.7.2 DEM Detrending

In order to examine the profiles of the Base Level DEMs the slope of the model was removed. Given the small scale of the model any channel elevation changes were dwarfed by the height difference between the top and bottom of the flume. Therefore the Base Level models were detrended to remove the slope. Fig. 4.14 shows a conceptual diagram of how the detrending of DEMs was achieved. Firstly the unchanged DEM was imported into ArcGIS and seven markers were placed on its surface (Fig. 4.14a). Secondly a trend surface was interpolated between those seven markers, essentially a surface which had the same slope as the model DEM was created (Fig. 4.14b). Using the raster calculator function in ArcGIS the trend surface was subtracted from the original DEM to produce a detrended flat DEM which could be used for analysis (Fig. 4.14c).

4.2.7.3 Extraction of UV sand locations

In order to extract UV sand locations, model orthophotos were imported into ArcGIS for processing (Fig. 4.15a). In ArcGIS the original colour orthophoto was separated into the individual RGB (Red, Green, Blue) bands (Fig. 4.15b). Given that the UV sand used was orange it was completely represented by the red band in the orthophoto. The red raster band was taken and reclassified into a binary image (Fig. 4.15c). This was achieved by using a mask to remove (clipping) the polystyrene edges of the model, leaving the in channel area. The majority of UV grains within the model have a pixel value in the red band of between 25 and 255. Values below this range are dark, meaning there is non-reflective Silica sand present. The values 25-255 were used in the ArcGIS Reclassify tool to assign any pixel within this range a value of 1 and any pixel below this range a value of 0. A value of 0 removes it from the image. With all of the non-reflective material removed from the image the newly extracted UV sand locations were overlain on top of the associated differenced DEMs to examine where the model landslide

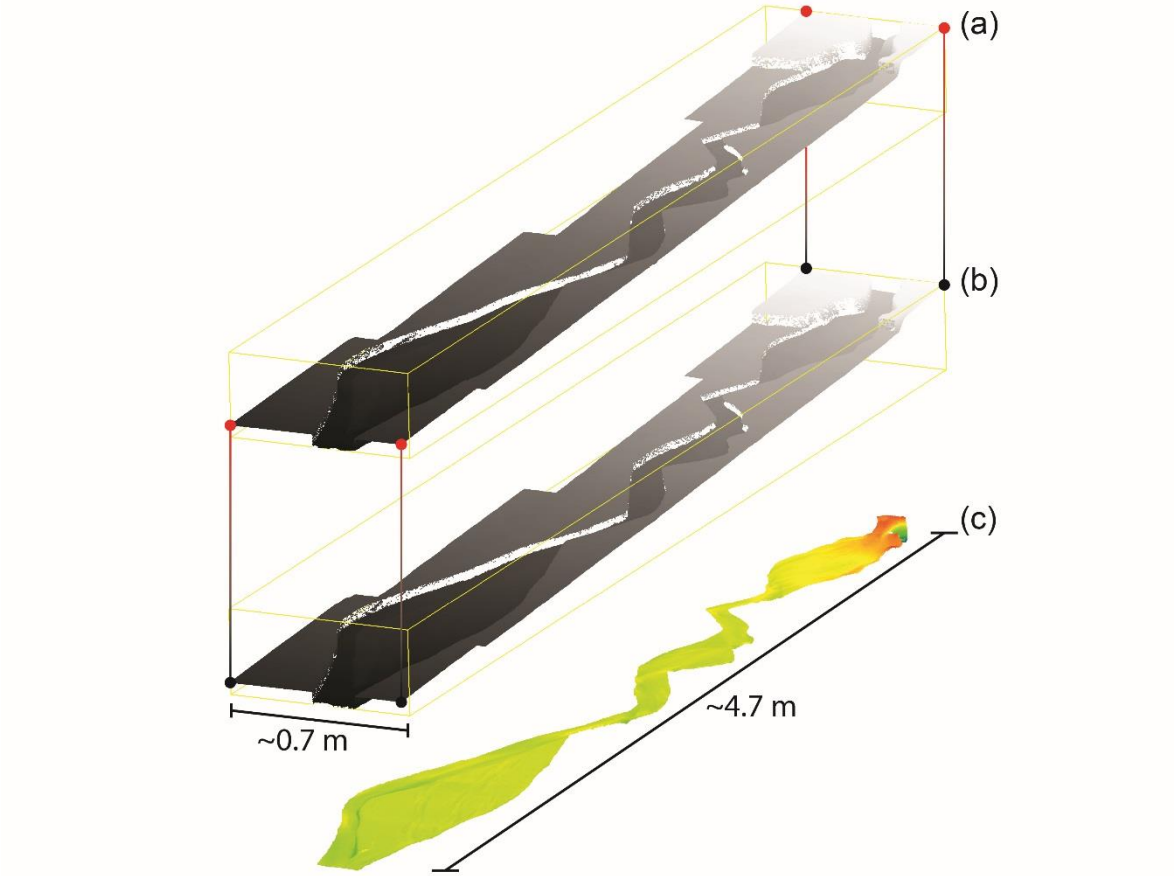

Fig. 4.13 Schematic diagram of the process of differencing two DEMs in ArcGIS; (a) DEM of the flume immediately after the Dam Break time-step (b) the Base Level DEM which will be subtracted from the Dam Break DEM; (c) The output differenced DEM which can be taken on for further analysis.

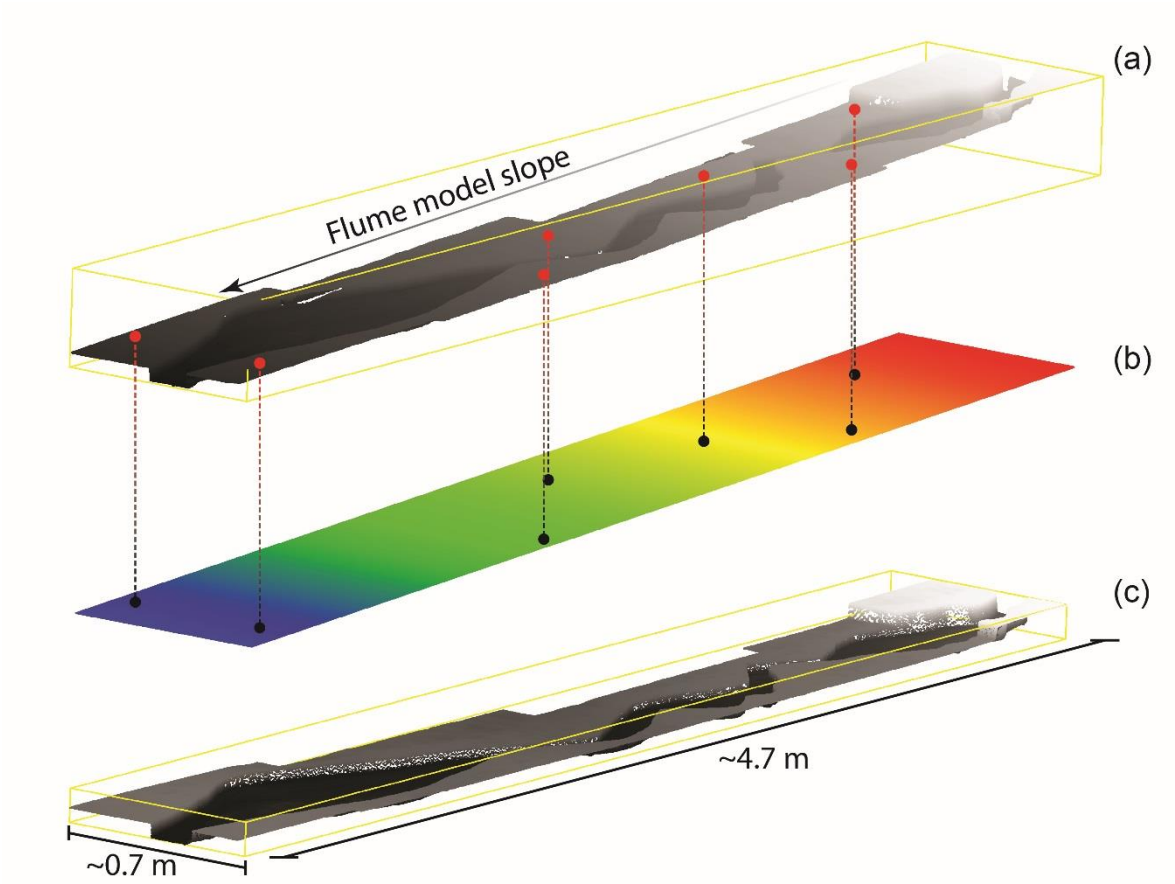

Fig. 4.14 Schematic diagram showing the process of detrending the base level DEMs from each of the flume runs. (a) Flume model DEM exported from Photoscan with the true model slope as it is in the laboratory; (b) Trend surface plane interpolated between the seven red markers on the DEM surface. The trend surface is subtracted from the original DEM to detrend the slope; (c) Detrended, flat model after the trend surface has been subtracted from the original DEM.

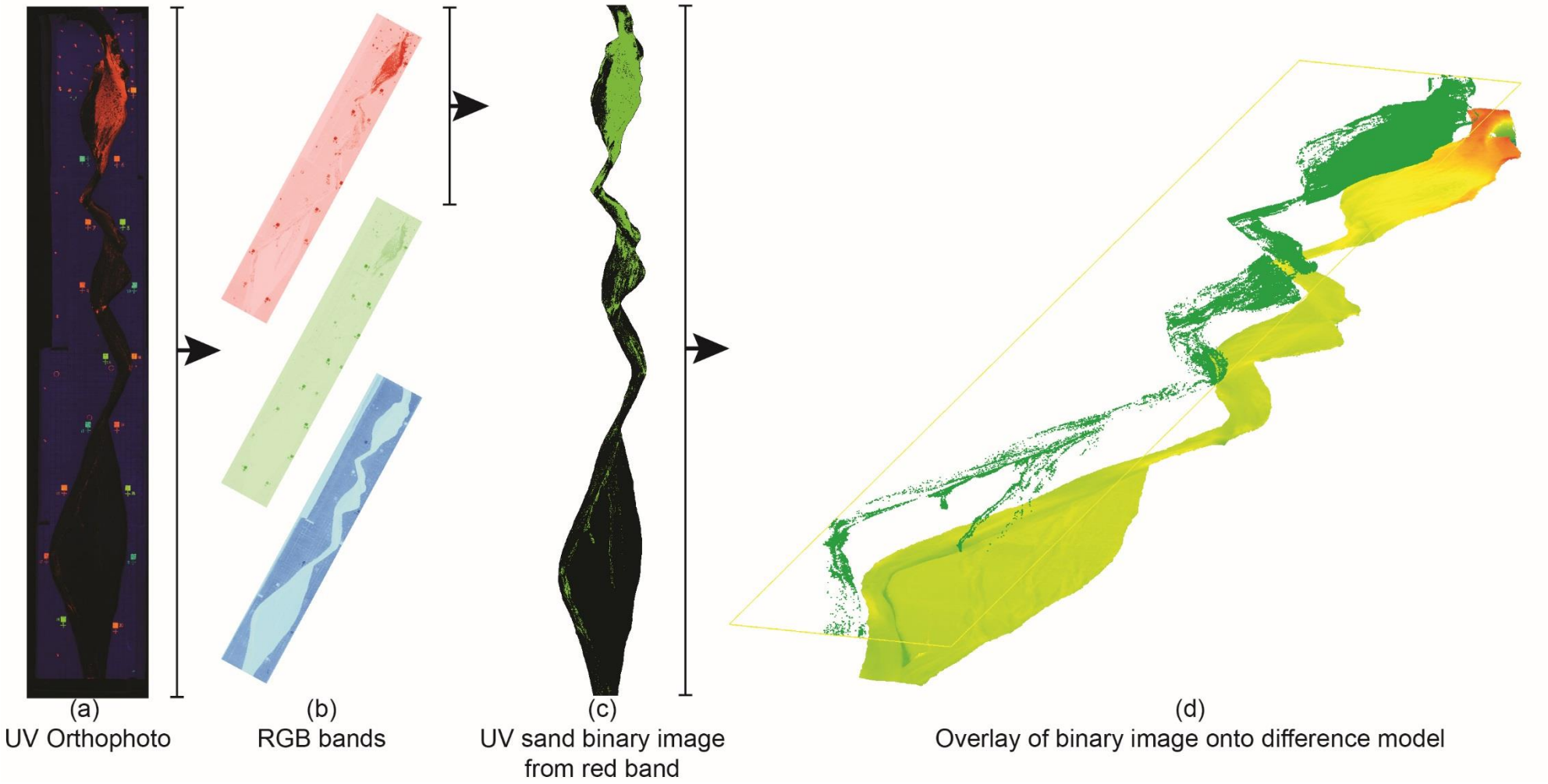

Fig. 4.15 Schematic of the UV sand location extraction method in ArcGIS (a) Output orthophoto from Photoscan; (b) RGB bands of the image are extracted in Arc. Orange UV sand is clearly visible in the red band; (c) Red band image is reclassified into a binary image based upon brightness intensity; (d) the non-UV data from the binary image is removed and the image is overlain onto the difference model for that run.

has impacted the fluvial system and where it may be possible to find landslide material in prototype rivers in NZ (Fig. 4.15d).

4.2.8 Model errors

Each of the model run time-steps was reconstructed as a DEM in Agisoft Photoscan. Within this software is an indication as to how well the reconstructed DEM fits the GCPs that were used. This is given as a root mean square (RMS) error for the entire model or by each individual GCP. The RMS errors for the reconstructed models are listed in Appendix 4.2. DEM RMS errors range between the model run time-steps from 0.005m to 0.008m. However, no one individual GCP has a location error of more than 0.015m. This gives confidence in the integrity of the model outputs.

For each DEM a profile line was taken down the polystyrene as the elevation of this should not change between model runs. This was done to ensure models were co-located for DEM differencing procedures. As can be seen in Appendix 4.3 the majority of model polystyrene profiles intersect for most of the length of the profile meaning they are coincident in the 3D digital space. However, a number of anomalies exist in the DEM profiles associated with the very upper section of the model and the lower end of the braidplain. In some DEM reconstructions the model elevations deviate from other DEMs. This could be in part due to the bowling effect that is often described in SfM literature (Smith and Vericat, 2015) where the ends of the models have less image and GCP coverage. Another explanation is that the survey location for GCPs was in a single location which had a poorer line of sight to the upper and lower reaches of the model which could have affected GCP accuracy.

The deviations in the lower reaches of some profiles suggests that erroneous aggradation or degradation signals could be produced in the lower Braidplain when models are subtracted in ArcGIS processing. These errors have therefore been examined and affected sections of models removed from analysis where they have been identified.

4.3 Results

4.3.1 Model run similarity

An examination of the base level models was undertaken in order to ascertain if each model run had similar starting conditions when the UV dam was inserted into the model. Using Run 2 as an example of a Base Level model (Fig. 4.16) it can be seen that there is an overall convex shape to the profile; this mimics an idealised, undisrupted, prototype river system with constant inputs (Harrison et al., 2015). The long profile shows steeper upper reaches in the upper gorge and upper alluvial flat. The profile shallows in the middle and lower reaches of the model in lower flats and braidplain. Small-scale

elevation changes are noticeable between each of the differing fluvial environments represented by the model; these reflect bedforms resulting from changes in flow regimes between the differing environments, such as a transition from an open alluvial flat to constriction of flow in a gorge. Base Level profiles for the other five model runs exhibit similar behaviour (Fig. 4.16). Vertical variations in the base line runs of the order of ~1cm exist in the upper reaches of the models, this is where sand and water inputs were located. However, after this initial variation the down-model profiles are coincident and have similar morphological changes between the fluvial environments represented in the model. The profiles show that base-level conditions for each model were similar before the insertion of the UV dam indicating subsequent morphological change was due to the landslide rather than initial conditions.

The model landslide dams also exhibited morphological similarity in both cross-model (Fig. 4.17) and down-model directions (Fig. 4.18), Upstream and downstream slope of model dams are of comparable angles; a trait which is reminiscent of the NZ prototype RA dams as shown in Figs. 4.5 and 4.6. Five out of the six models had dam failures by overtopping (Table 4.3). In these instances a lake was impounded behind the dam; once the lake level reached the lowest dam elevation an overflow channel was formed and the dam was breached. The dam in Run 2 was breached by syphoning under the true-left side of the dam. This is a less common occurrence in prototype dams; a process reflected in these experiments by only one dam failing through this mechanism. All breaches resulted in catastrophic failure of the dam and generated a dam break flood.

4.3.2 Model morphology

The micro-scale model allows the examination of the broad scale morphological changes that have occurred between each time-step in the model runs. Major morphological changes are examined for all models at the Dam Break (Fig. 4.19), Post Dam Break (Fig. 4.20) and gross change (Figs. 4.21 and 4.22) time-steps for the Upper and Lower alluvial flat reaches. These reaches were selected as they saw the most change over the model run time due to their proximity to the dam location. Table 4.4 provides a useful overview of the broad scale morphological changes that have occurred in all reaches across all model runs; however, it does not represent the finer morphological detail from each time-step as the classifications used are broad.

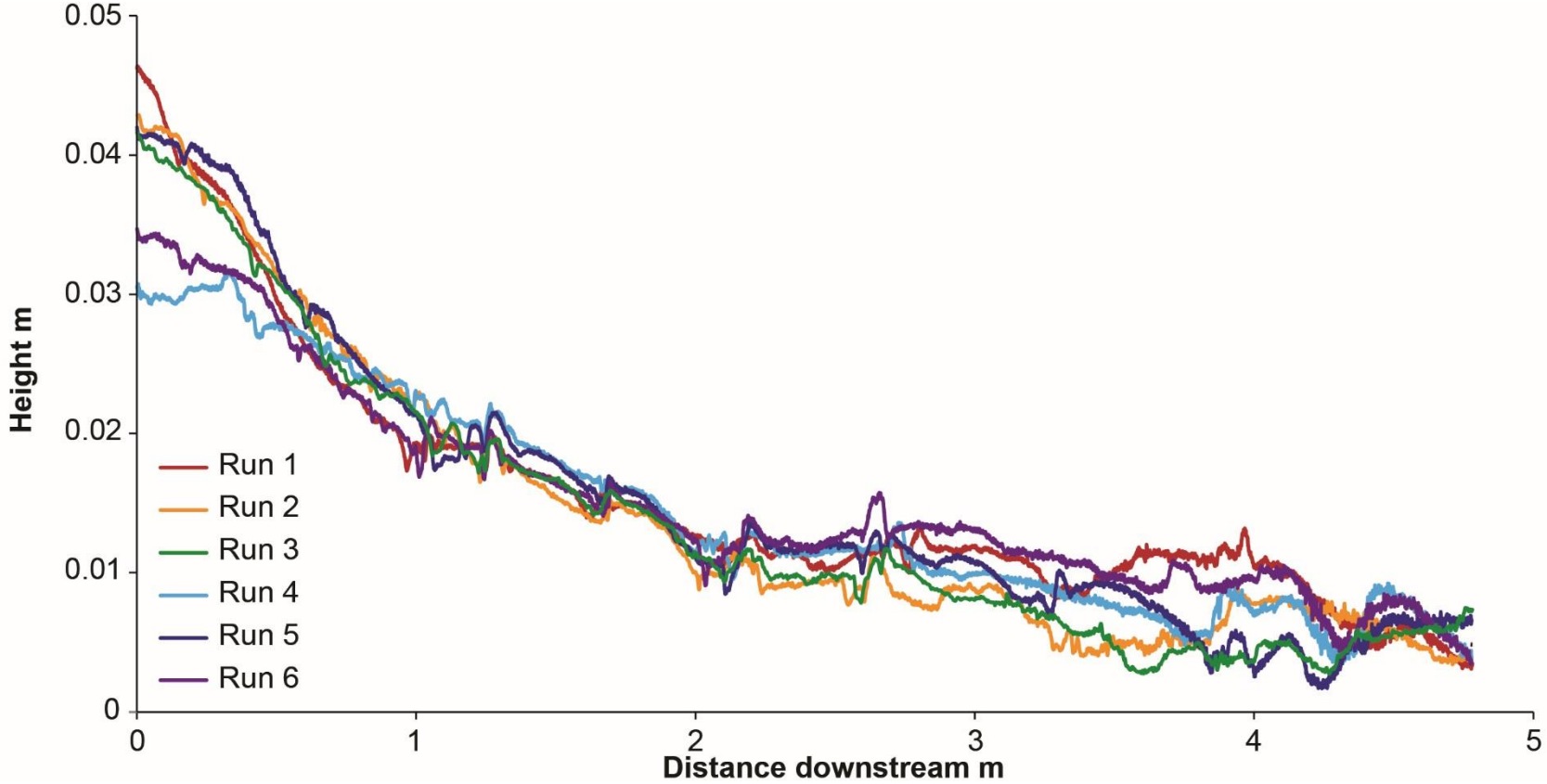

Fig. 4.16 Comparison of topographic profiles of Base Level flume models for all runs. The profiles are located in the same location and have been taken from detrended Base Level models.

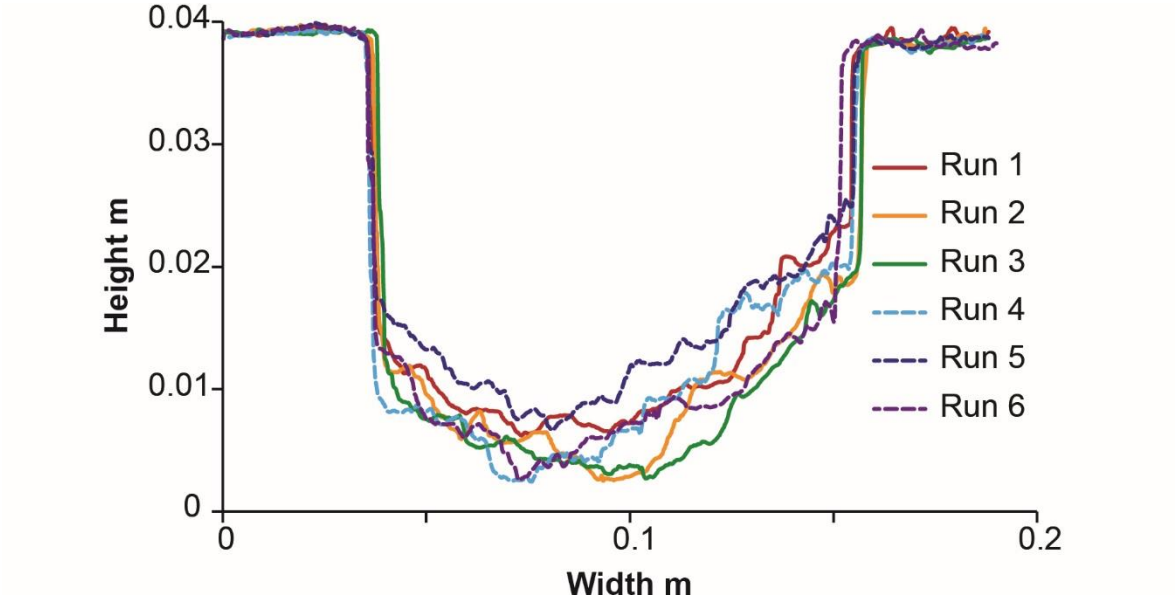

Fig. 4.17 Comparison of model landslide dam width profiles built for each model run. Dashed lines are armoured dam runs.

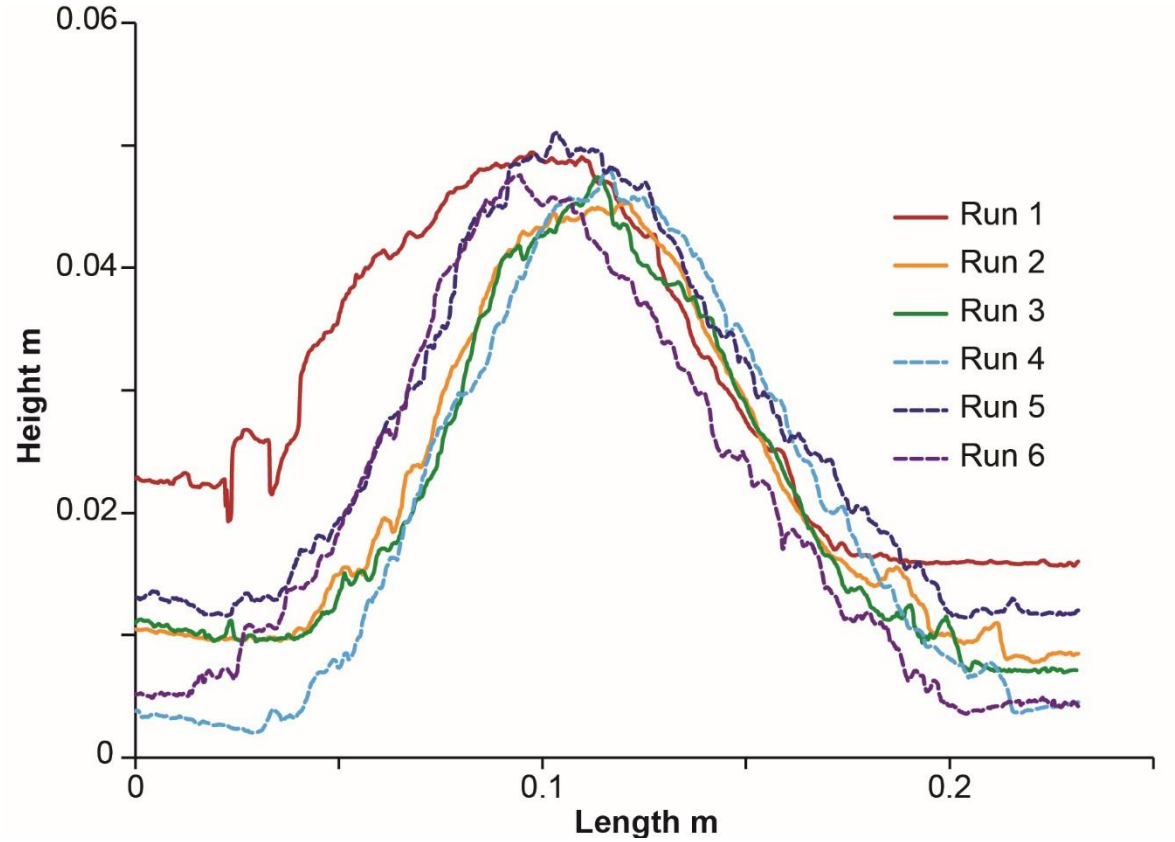

Fig. 4.18 Comparison of model landslide dam length profiles built for each model run. Dashed lines are armoured dam runs.

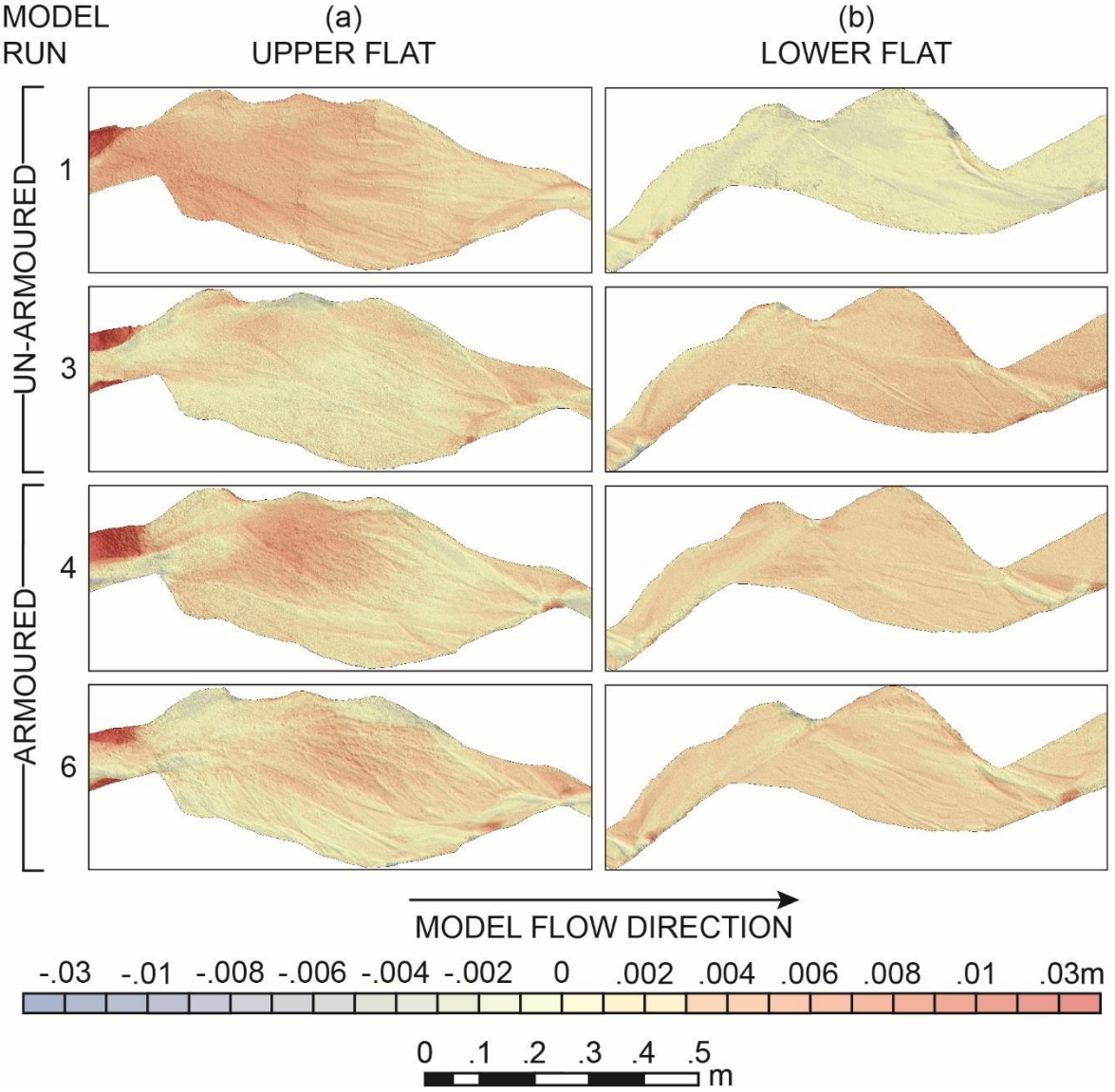

Fig. 4.19 Comparison of Dam Break differenced DEMs of the Upper and Lower Flats from all models. Dam Break difference DEMs result from the change between the Base Level and Dam Break time-steps. Runs 2 and 5 are excluded as they were continuously run and did not contain the Dam Break time-step.

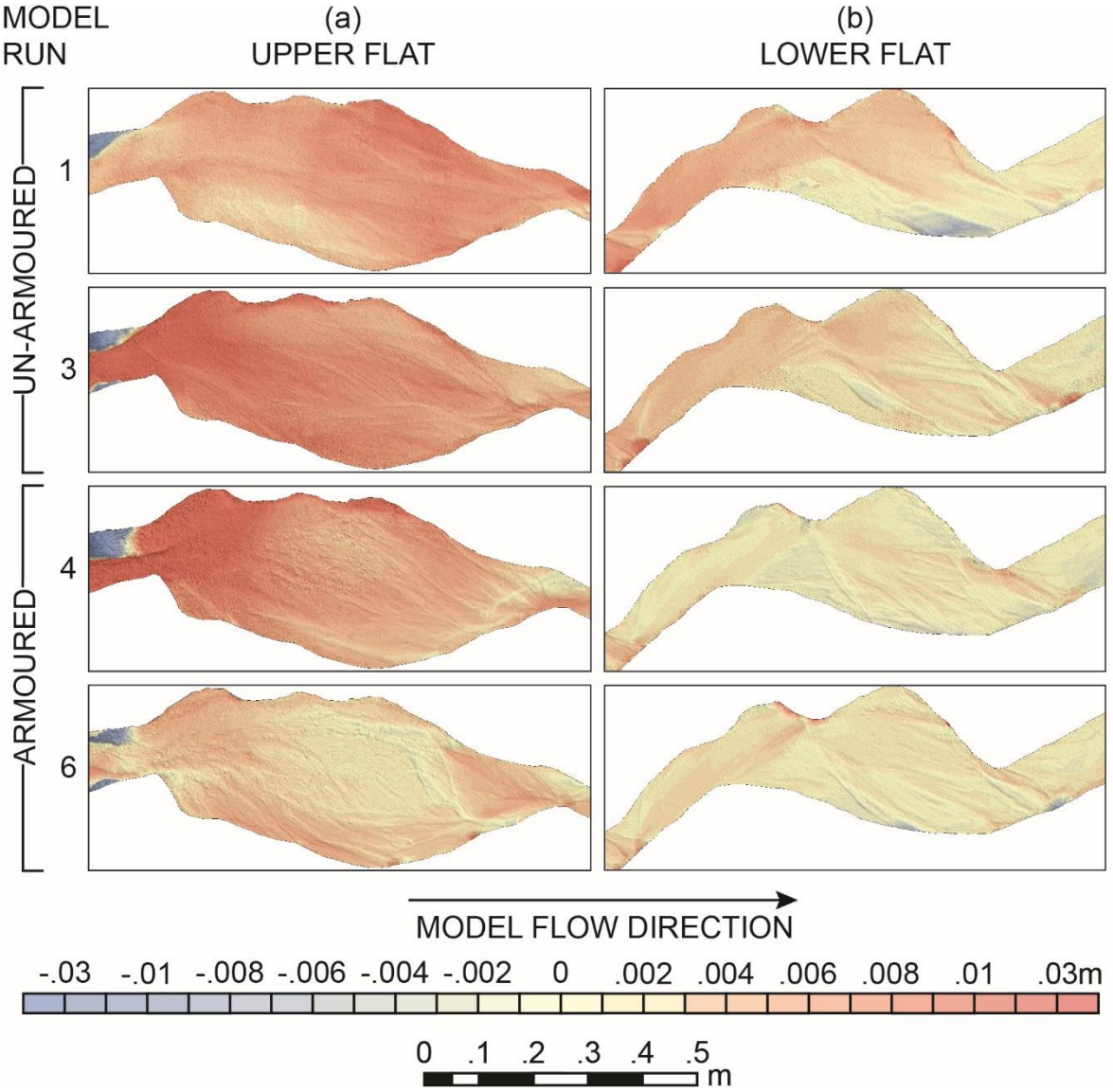

Fig. 4.20 Comparison of Post Dam Break differenced DEMs of the Upper and Lower Flats from all models. Post Dam Break difference DEMs result from the change between the Dam Break and Post Dam Break time-steps. Runs 2 and 5 are excluded as they were continuously run and did not contain the Dam Break time-step.

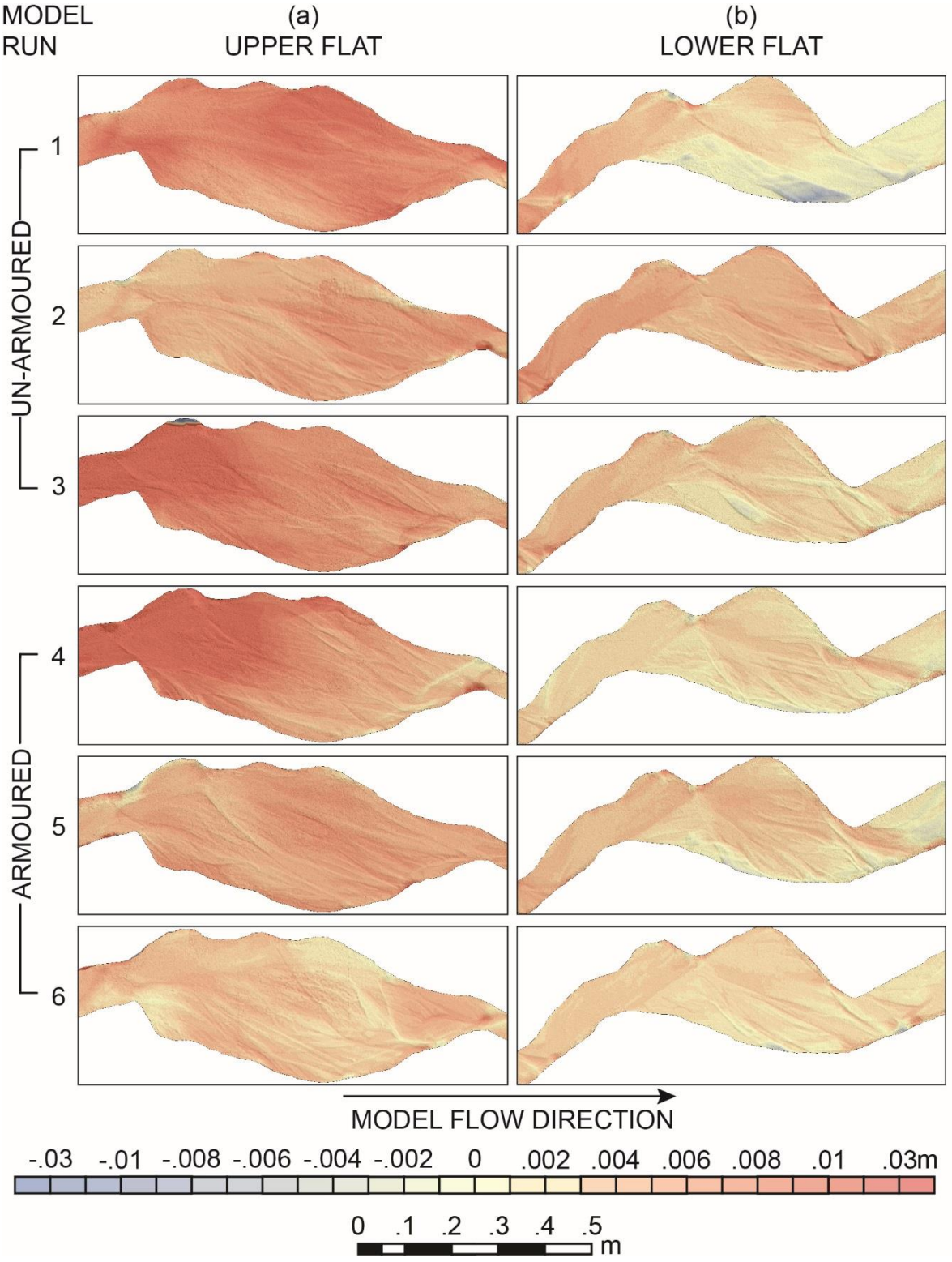

Fig. 4.21 Comparison of gross change difference DEMs of the Upper and Lower Flats from all models. Gross change DEMs result from the change between the Base Level and Post Dam Break models.

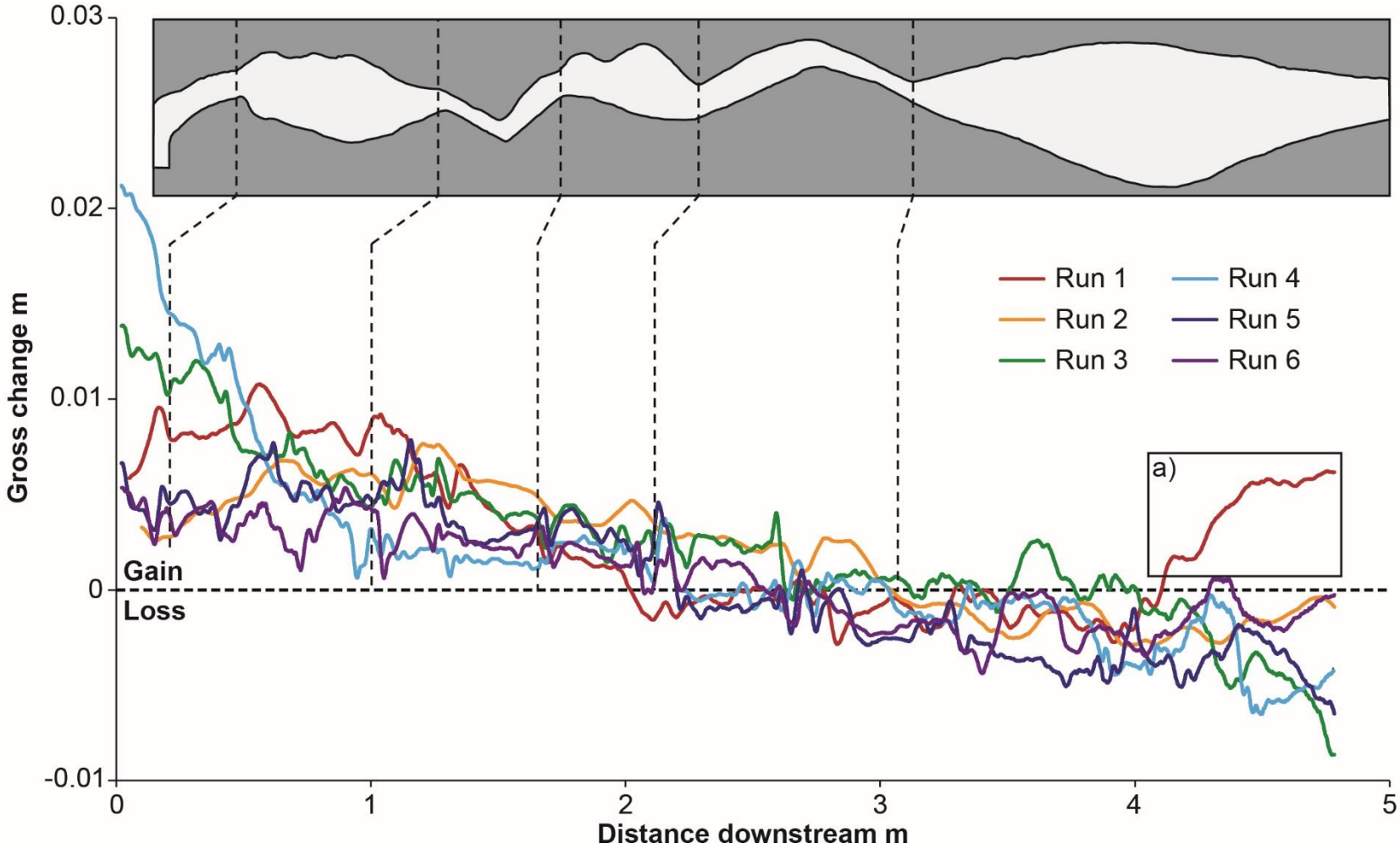

Fig. 4.22 Graph comparison of the gross change in models over the experimental time period. The dotted horizontal line indicates the level of no change. For Run 6 the gross change data was taken from the first Post Dam Break model in order to maintain synchronicity with other model runs. Box a indicates where the DEM for Run 1 has a 'bowl effect' an artefact from the SfM processing, this area was excluded from any analysis.

Table 4.4 Summary table for all flume models describing the morphological characteristics, the status of the landslide dam and the visibility of UV sand material after the stoppage of each section of the model runs. Key for the table is located below.

		UNARMOURED			ARMOURED		
		1	2	3	4	5	6
DAM BREAK MODEL							
Morphology	Dam status	PaRe		PaRe	PaRe		PaRe
	Upper flat	MAg		LAg	MAg		LAg
	Middle gorge	LAg		LAg	LAg		LAg
	Lower flat	NC/LDe		LAg	LAg		LAg
	Lower gorge	NC/LDe		LAg	LAg		LAg
	Braidplain			LAg	LAg/NC		LAg
UV sand	Upper flat	HCo		HCo	HCo		HCo
	Middlegorge	Di		HCo	HCo		HCo
	Lower flat	Di		Co	Co		Co
	Lower gorge	Di		Di	Di		Di
	Braidplain	HDi		Di	Di		Di
POST DAM MODEL							
Morphology	Dam status	CoRe	CoRe	CoRe	Rem	Rem	Rem
	Upper flat	MAg		HAg	HAg		MAg
	Middle gorge	MAg		MAg	HAg		MAg
	Lower flat	MAg		MAg/LAg	LAg		LAg
	Lower gorge	LAg		LAg	LAg/LDe		LAg
	Braidplain			NC	/LDe		LDe
UV sand	Upper flat- surface	NV	NV	NV	NV	HDi	NV/HCo
	Upper flat- sub-surface	CoBu	CoBu	CoBu	CoBu	CoBu	PaBu
	Middle gorge	NV	NV	NV	HDi	NV	NV
	Lower flat	NV	HDi	Di	Co	HDi	Di
	Lower gorge	HDi	HDi	Di	Co	Di	HDi
	Braidplain	Di	Di	HDi	Co	Di	HDi
GROSS CHANGE MODEL							
Morphology	Upper flat	HAg	MAg	HAg	HAg	MAg	HAg
	Middle gorge	HAg	MAg	MAg	MAg	MAg	HAg
	Lower flat	MAg	MAg	MAg	MAg	MAg	MAg
	Lower gorge	NC	LAg	LAg	LAg	NC	MAg
	Braidplain		LDe	LAg/LDe	LAg/LDe	LDe/MDe	MAg/MDe

Key for flume model features table					
Morphology	HAg	High aggradation	**UV Sand**	HCo	Highly concentrated
	MAg	Moderate aggradation		Co	Concentrated
	LAg	Low aggradation		Di	Dispersed
	LDe	Lowdegradation		HDi	Highly dispersed
	MDe	Moderate degradation		NV	Non visible
	HDe	High degradation		PaBu	Partial burial of discrete UV sand unit
	NC	No change		CoBu	Complete burial of discrete UV sand unit
	PaRe	Partial removal of dam			
	Rem	Remnant of dam visible			
	CoRe	Complete removal of dam			

4.3.3 Morphology of un-armoured dam models

Table 4.4 summarises the morphology of the flume runs from the difference models of each time-step; all of the models are available in Appendix 4.4. Runs 1-3 are the un-armoured dam experimental models which will be discussed in this section. Run 1 is first described as an example of an un-armoured dam model before being compared to the other models in the experimental set. Runs 1 and 3 are start-stop type models, whilst Run 2 is a continuously running model.

The landslide dam in Run 1 failed by overtopping at the lowest elevation of the crest and generated a dam break flood (Fig. 4.23a). At the Dam Break time-step, immediately after dam failure, there is partial removal of the UV dam (Table 4.4) where an overflow channel has been incised through the material and the edges of the breach channel have been eroded. Run 1 exhibits moderate aggradation within the Upper Flat and Middle Gorge, reaches that are proximal to the dam location (Fig. 4.19a; Table 4.4). The distribution of UV sand within the model (Fig. 4.24a) indicates that the majority of this aggradation is the deposition of UV material immediately downstream of the simulated landslide (Fig. 4.23d). The Lower Flat (Fig. 4.19b) difference models and Lower Gorge observations (Table 4.4) show low-level degradation occurring in these reaches as a result of the passage of the dam-break flood. Linked to this degradation is the relative absence of UV sand material (Fig. 4.24a). The pattern of UV sand distribution within the Middle Gorge and Lower Flat indicate deposition along the edges of the flood flow with little overbank or avulsion activity (Fig. 4.24a). Very little UV material is visible in the lower reaches of the model, reflecting the lack of transport of UV material down the system in the dam break flood.

The dam has been completely removed at the Post Dam Break time-step (Fig. 4.20 1a; Table 4.4) and there is no surface UV material present to indicate its past existence there. There are significant morphological changes occurring within model reaches when compared to the Dam Break time-step, with all model reaches exhibiting aggradation. Moderate level aggradation is observed throughout the Upper Flat, Middle Gorge and Lower Flat (Fig. 4.20 1a and 1b; Table 4.4). Aggradation in the Lower Flat is confined to the area occupied by the main channel, to the true-left of the reach, throughout the model runs (Fig. 4.20 2b). This aggradation is not reflected in the presence of high-concentrations of UV sand in the surface material of the model (Fig. 4.24b) indicating that this is generated by the deposition of Silica sand over the model reaches. The Lower Gorge has also undergone low-level aggradation, a change from the initial degradational signal observed in the Dam Break time-step difference model. There is no visible surface UV sand throughout the Upper Flat, Middle Gorge and Lower Flat of the model after the Post Dam Break time-step (Fig. 4.23f; Fig. 4.24b) indicating removal of the material from the model system or burial of UV sand within the sub-surface architecture by

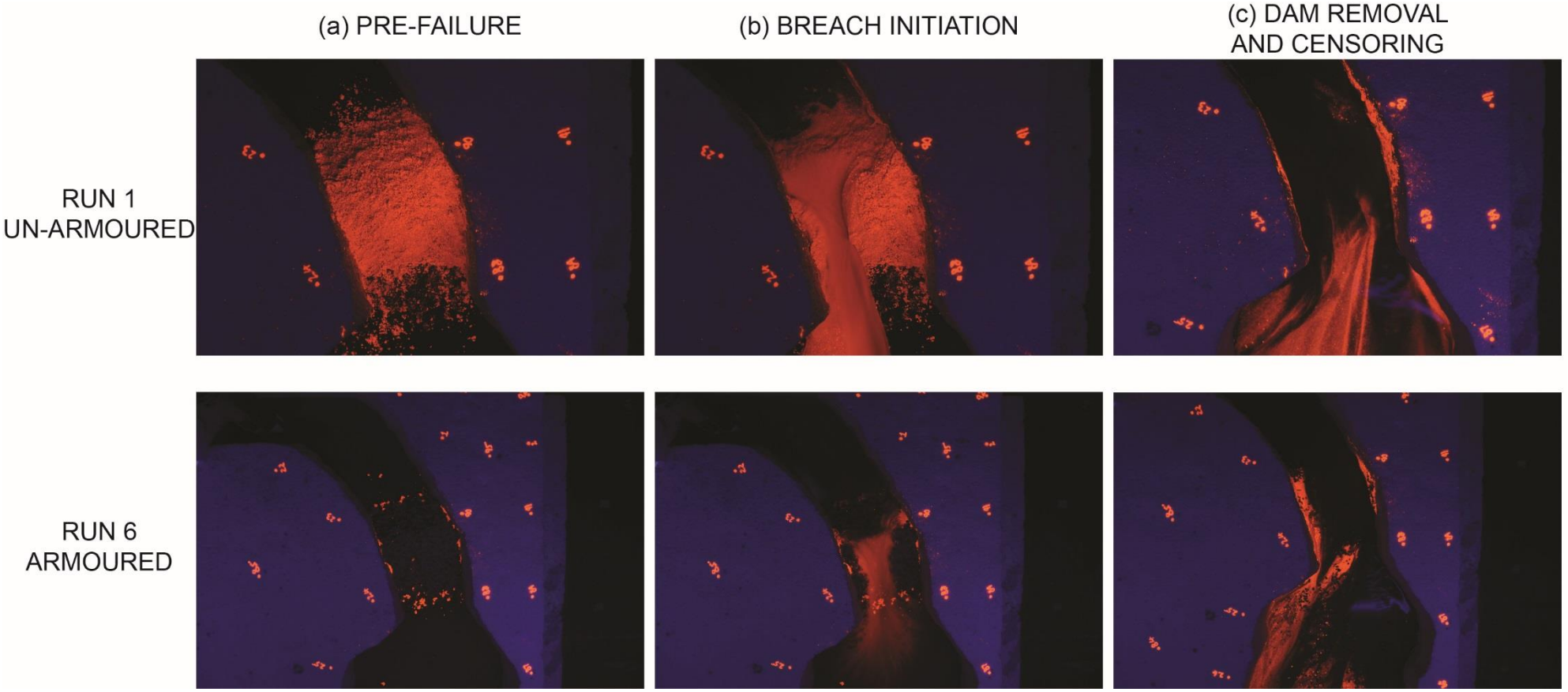

Fig. 4.23 Comparison of UV model evolution from Run 1 (un-armoured) and Run 6 (armoured). Images show the dam pre-failure, dam breach initiation and the removal and censoring of the deposit by subsequent fluvial action.

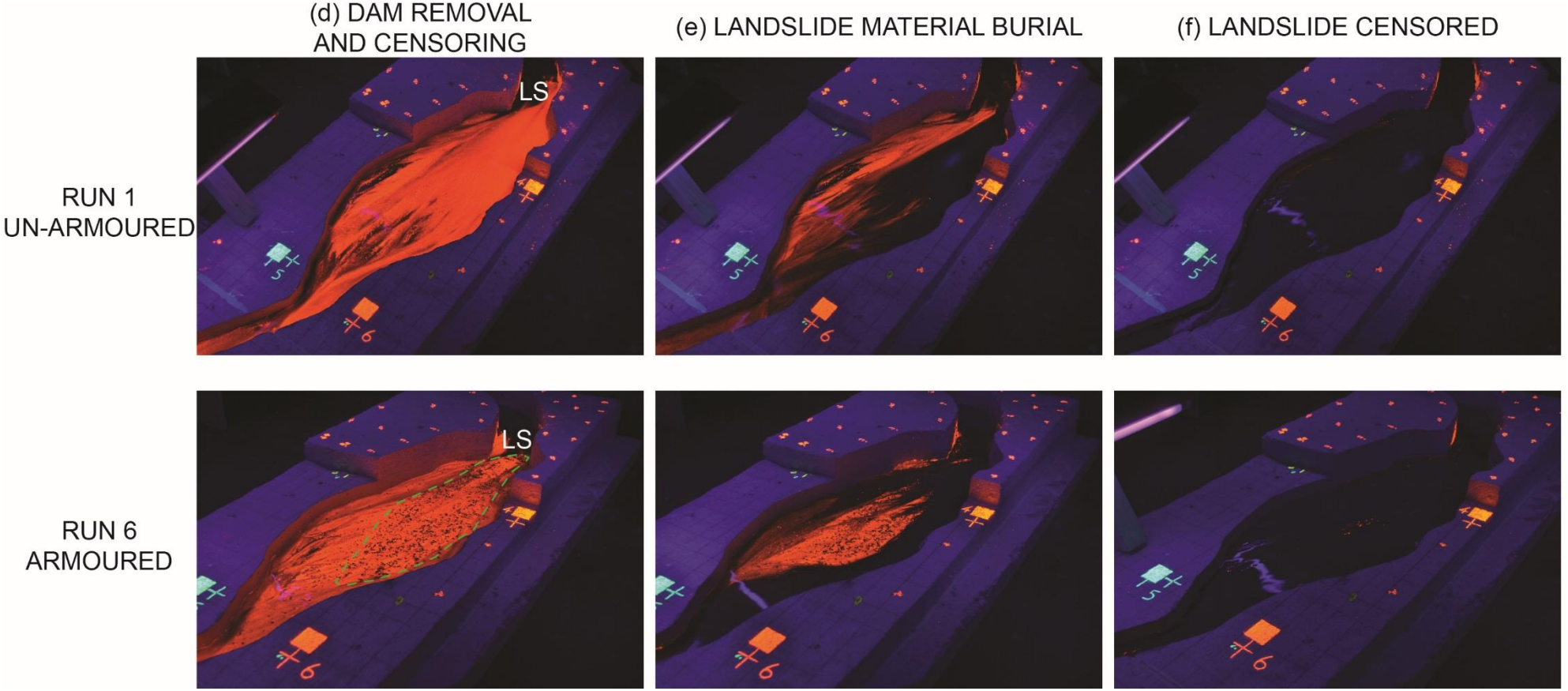

Fig. 4.23 Cont. Comparison of UV model evolution from Run 1 (un-armoured) and Run 6 (armoured). Images show the dam removal by fluvial action, the process of UV sand burial and the eventual censoring of the deposit and any reworked material from view. The green dotted line indicates an area where RAD carapace material has been deposited in Run 6.

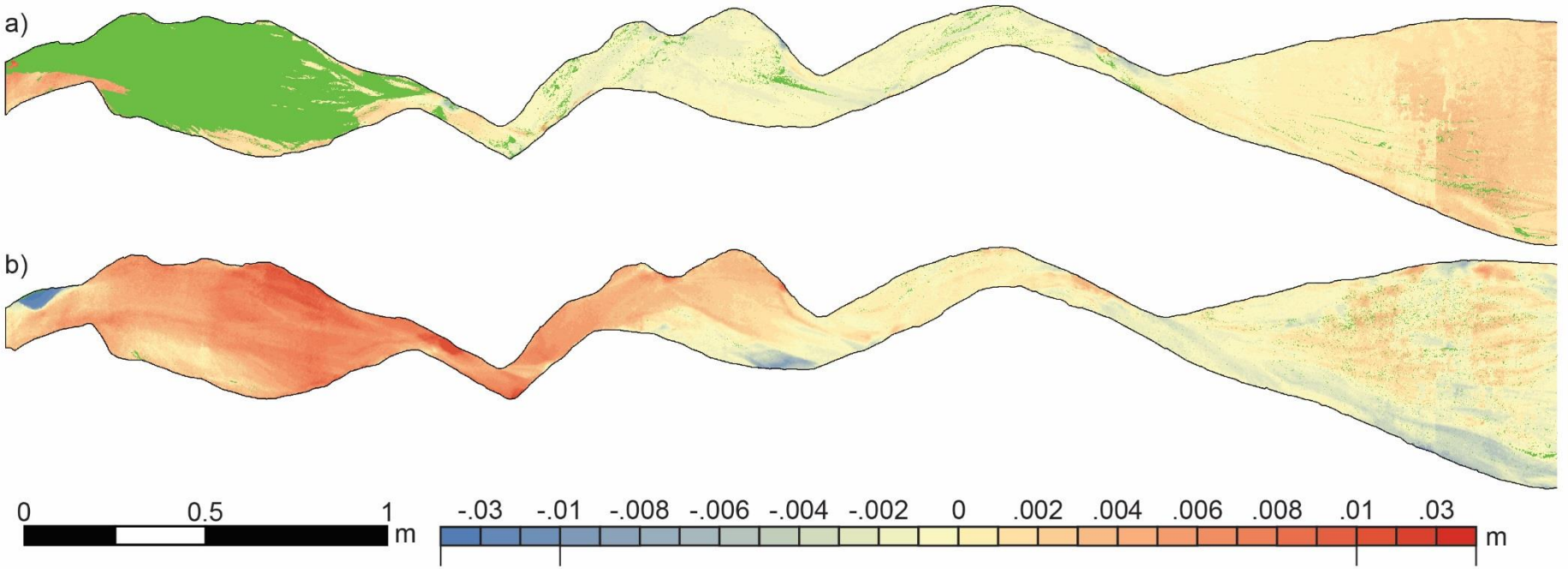

Fig. 4.24 Run 1 (a) DEM of difference between the Base Level and Dam Break time-steps with UV sand locations overlain; (b) DEM of difference between the Dam Break and Post Dam Break time-steps with UV sand locations overlain.

Silica sand. The Lower Gorge and Braidplain show evidence of highly dispersed UV sand in the lower reaches of the model, a similar pattern to what was observed in the Dam Break model. This indicates that material is being reworked down the system even by the end of the model run but never in large quantities to create concentrated deposits.

The sub-surface stratigraphy of Run 1 (Fig. 4.25) shows the pervasive burial of concentrated UV material throughout the upper, dam proximal reaches of the model. Cores indicate that a layer of highly concentrated UV material is buried under the surface of the Upper Flat. In parts this concentrated layer is capped by plain Silica sand or by Silica sand with low UV sand concentrations. Cross-model cores show that a concentrated UV or 50/50 UV/Silica mix of sand exists as a sub-surface layer across the Upper Flat. The concentrated sub-surface UV layer transitions into being composed of ~50/50 UV and Silica sand in the lower portion of the Upper Flat and is seen to continue as a sub-surface layer to the end of the Middle Gorge. Within the Middle Gorge the surface material is seen to transition into being a low-UV, high-Silica sand mix, this surface layer continues to the Braidplain where the cores indicate that the distribution of UV sand becomes patchy; some concentrated material exists in surface layers but no material is buried.

The gross-change difference model for Run 1 (Table 4.4; Fig. 4.21) show that over the experiment aggradation was observed in all alluvial flat and gorge reaches of the model. The introduction of the dam has caused catchment scale changes in sediment distribution and deposition. Higher aggradation is seen in dam proximal reaches and lower aggradation is seen in the dam distal reaches. The initial degradation of the Middle Gorge and, Lower Flat caused by the dam break flood, is reversed with low level aggradation in the long term. Over the experimental period the Lower Gorge appears to have had little change as the initial degradational signal is counterbalanced with low level aggradation. The Braidplain reach has been removed from analysis of Run 1 due to potential bowling effects observed during DEM reconstruction (Fig. 4.22a).

The additional un-armoured models were Runs 2 and 3. Run 2 was a continuously running model and therefore has no Dam Break and Post Dam Break data to describe here. In Run 2 the landslide failed through piping under the true-left of the dam and was the only one to fail in this manner. The landslide in Run 3 failed by overtopping, the same as all other model runs. Similar dam breach characteristics are noted in Run 1 and Run 3 with partial removal of the UV dam (Table 4.4); however, there are some differences in the downstream, morphology produced. At the Dam Break time-step Run 3 produced low level aggradation throughout all model reaches in contrast to the dam-break flood scouring the lower reaches in Run 1. Run 3 also exhibits lower levels of aggradation in the Upper Flat immediately after the dam breach than Run 1. The UV sand distribution for Run 3 Dam Break (Table 4.4) indicates that much of the UV material eroded from the

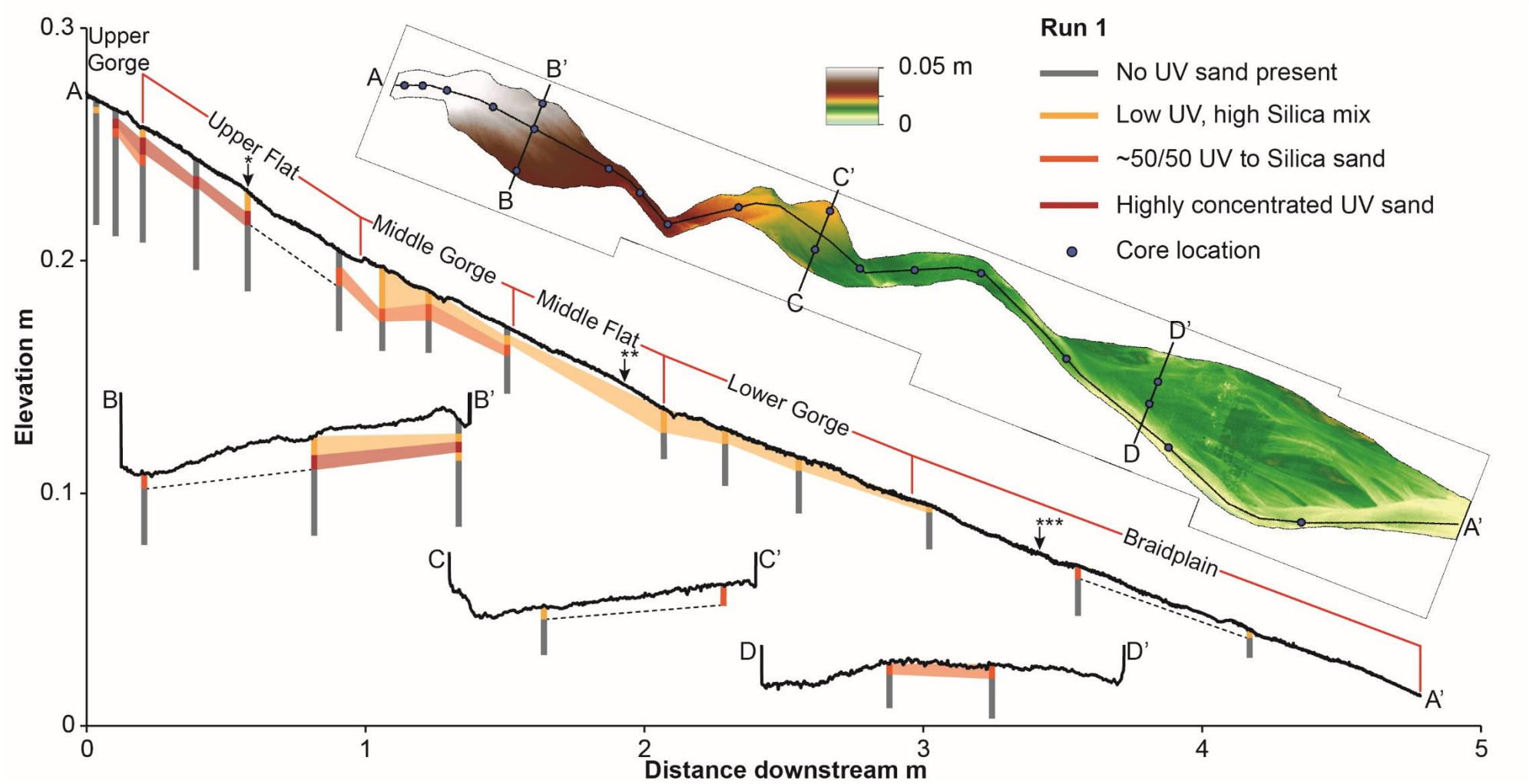

Fig. 4.25 Run 1 Flume model profile with core logs after the Post Dam Break time-step. Core colours indicate the concentration of UV sand within identifiable sediment layers. Vertical scale is 0.01:0.025, horizontal scale is 0.01:0.25.

dam during the breach was deposited in the Upper Flat but in contrast to Run 1 the dam breach flood was also able to mobilise more UV material into the Lower Flat developing a concentrated surface layer of material. Additionally, there were higher concentrations of material mobilised to the lower reaches of the model when compared to Run 1.

In the Post Dam Break time-step the UV dam in both Runs 2 and 3 has been completely removed in a similar fashion to Run 1 (Table 4.4). The Post Dam Break time-step in Run 3 shows high levels of aggradation within the Upper Flat (Fig. 4.20 4a) and as with Run 1, diminishing levels of aggradation down the system in dam distal locations. Upper flat aggradation is coupled with the complete burial of a concentrated layer of UV sand by Silica sand (Table 4.4). The Lower Flat is moderately aggraded, mostly in the area occupied by the main channel during the experiment operation. No UV sand is visible in the Upper Flat and Middle Gorge of the Run 3 model with only dispersed UV sand visible in the lower reaches. Run 1 and Run 2 have lower levels of UV sand visible in their lower reaches but the pattern of distribution is similar between the three models; burial of landslide material in the Upper Flat and Middle Gorge with dispersed surface UV material visible in the lower reaches of the model (Table 4.4; Appendix 4.4).

Table 4.5 summarises the model sub-surface stratigraphy for the three un-armoured dam models from the core diagrams in Appendix 4.5; they all display similar patterns of UV sand distribution. High concentrations of UV sand are buried in the Upper Gorge and Upper Flat of all models, For Runs 1 and 2 this layer transitions into a less concentrated ~50/50 mix of UV/Silica sand as it reaches the Middle Gorge. For Run 4 the concentrated layer of sand continues into the Middle Gorge, indicating that this is the same sediment layer that was deposited through the Dam Break flood where UV material was mobilised further down model than in Runs 1 and 2. The concentrated UV layer is buried by either plain Silica sand or a low UV concentration mix in all three models. All models see the sub-surface layer transition to a surface layer in the lower portion of the Middle Gorge or upper portion of the Lower Flat. This surface layer continues down the entire model but diminishes in concentration. In the Braidplain reach all models also have UV sand distributed across the reach indicating UV sand has been deposited in a number of avulsion channels which have captured the flow of the main active channel to the true-right of the Braidplain reach.

All three gross change models show a similar pattern of aggradation in the upper reaches of the model with greater dam proximal deposition of material. Run 2 has greater aggradation within the Lower Flat than Runs 1 and 3, however it is still not as high a level as seen in the Upper Flat in other models. The aggradational signal in the Upper Flat and Lower Flat for Run 2 has a uniform moderate aggradation signal, differing from the other two models where high-aggradation is seen in the dam proximal flat and moderate aggradation is seen in the Lower Flat (Fig. 4.21). Comparisons of a profile down the gross

Table 4.5 Summary table of sub-surface stratigraphy of all Post Dam Break flume models. Run 6 is the Post Dam Break +16 model. Colour gradients across table cells indicate that UV sand concentrations change within that reach of the model.

	Un-armoured			Armoured		
	1	2	3	4	5	6
Upper Gorge						
UV burial	✓	✓	✓	✓	✓	✓
Burial by Silica sand	✓	✓		✓	✓	
Burial by Silica/UV mix			✓			✓
Upper Flat						
Buried UV layer	✓	✓	✓	✓	✓	✓
Burial by Silica sand		✓		✓		
Burial by Silica/UV mix	✓		✓		✓	✓
UV buried across cross-section	✓	✓	✓	✓	✓	✓
Middle Gorge						
Surface Silica sand						✓
Surface UV visible	✓	✓	✓	✓	✓	
Buried UV layer	✓	✓	✓	✓	✓	✓
Lower Flat						
Surface UV visible	✓	✓	✓	✓	✓	
Buried UV layer				✓	✓	✓
Higher conc. of material in true-left of cross-section	✓		✓	✓		
Lower Gorge						
Continuous surface layer of UV	✓	✓	✓	✓	✓	
Buried UV layer						✓
Braidplain						
Continuous layer of UV in main channel (true-right)		✓	✓	✓	✓	✓
Semi-continuous UV layer in main channel (true-right)	✓					
Surface UV layer in avulsion channels	✓	✓	✓		✓	✓

Key for core profile log features	
High-concentration of UV sand	
~50/50 Silica to UV sand	
Mostly Silica sand, some UV sand	
Not visible	

change models highlights the more uniform aggradation observed in Run 3 and the higher levels of aggradation in Run 1 and 3 (Fig. 4.22). All models show a gradual decline in the level of aggradation down the model with degradation observed within the braidplain. The Braidplain in Runs 2 and 3 has seen low level degradation across the reach (Table 4.4; Appendix 4.4) where the main channel on the true-right and avulsion channels over the true-left of the reach have eroded through bank material and 'floodplain' material respectively.

4.3.4 Morphology of armoured dam models

Runs 4-6 are the armoured landslide dam models which will be discussed in this section. Run 6 will first be discussed as a representative armoured dam model, which was run for an extended running period beyond the Post Dam Break time-step. Runs 4 and 5 will then be compared to Run 6 to determine if there is model similarity within the experimental set.

Run 6 was conducted in the same way as the other start-stop model runs in that it has a Dam Break and Post Dam Break time step. However, the model was run beyond the 6 hour Post Dam Break time-step to include further +8 hour and +16 hour time-steps. The dam in Run 6 was breached through overtopping, was incised by the dam breach flood and further eroded by fluvial erosion of the breach walls (Fig. 4.23 6b). Table 4.4 shows that there was low-level aggradation throughout all model reaches. Fig. 4.26 and looks at the long term evolution of the Upper Flat in Run 6. Initially at the Dam Break time-step (Fig. 4.26a) the remaining sections of dam after it has failed are visible in towards the left of the reach, indicated by the dark red. Fig. 4.26 6d shows that the aggradation seen in the Upper Flat during the Dam Break time-step was coupled with the deposition of large quantities of UV material as well as many scattered larger carapace grains. The larger carapace grains are largely confined to the true-left of the Upper Flat, indicating a focussed dam breach flood flow path. The aggradation seen within the other gorge and flat reaches are also coupled with the presence of UV sand material deposited during the dam break flood (Table 4.4). There is a concentration gradient of UV sand from the upper model where there is highly concentrated material to dispersed UV material within the Braidplain reach.

There are small remnants of the UV sand dam at the Post Dam Break time-step, however much of the material surviving the dam break flood has been removed, this is shown in Fig. 4.26b by the blue areas of degradation to the left of the figure. Aggradation has continued to occur throughout all reaches of the model with the exception of the Braidplain (Table 4.4) which exhibits some aggradation on overbank areas to the true-left of the reach and degradation within the observed main channel in the reach to the true-right (Fig. 4.27b). The aggradation seen in the Upper Flat (Fig. 4.27) is coupled with burial of the UV landslide material with Silica sand, however a section of UV sand remained unburied up to the Post Dam Break time-step in this reach (Fig. 4.23 6e). This appears to be a result of the aggradation in the Dam Break model where the deposition of courser carapace material was located (Fig. 4.23 6d). The area with the reworked carapace material had aggraded higher in the Dam Break model than the surrounding area of the Upper Flat, this forced the aggradation of the area surrounding the Dam Break deposition during the Post Dam Break time-step. This is visible when comparing the patterns of aggradation in the Upper Flat in Fig. 4.26a and b. Surface UV sand is not visible in the

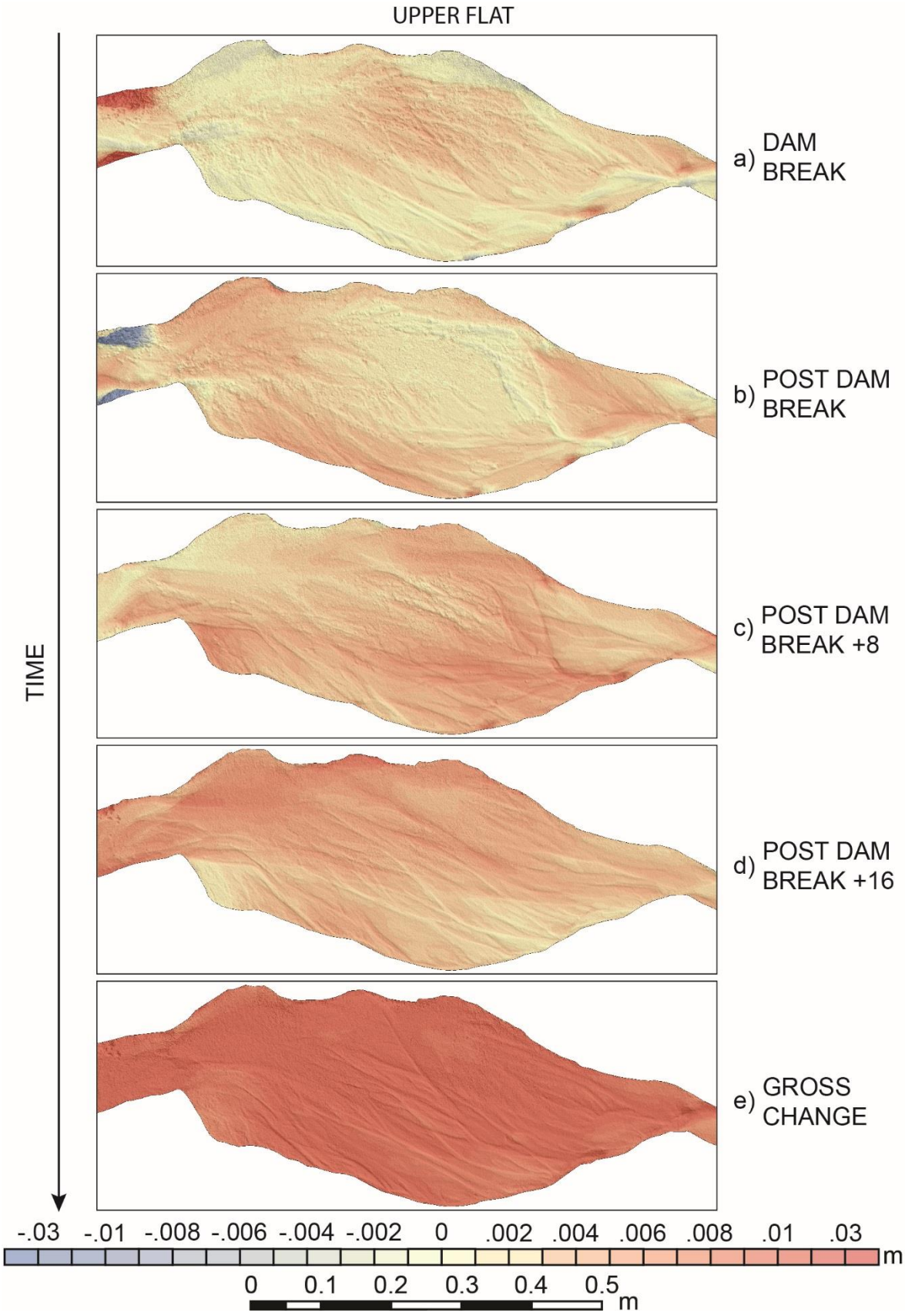

Fig. 4.26 Comparison time series of the Upper Flat from Run 6 showing aggradation and degradation between each time-step shown on the right hand side

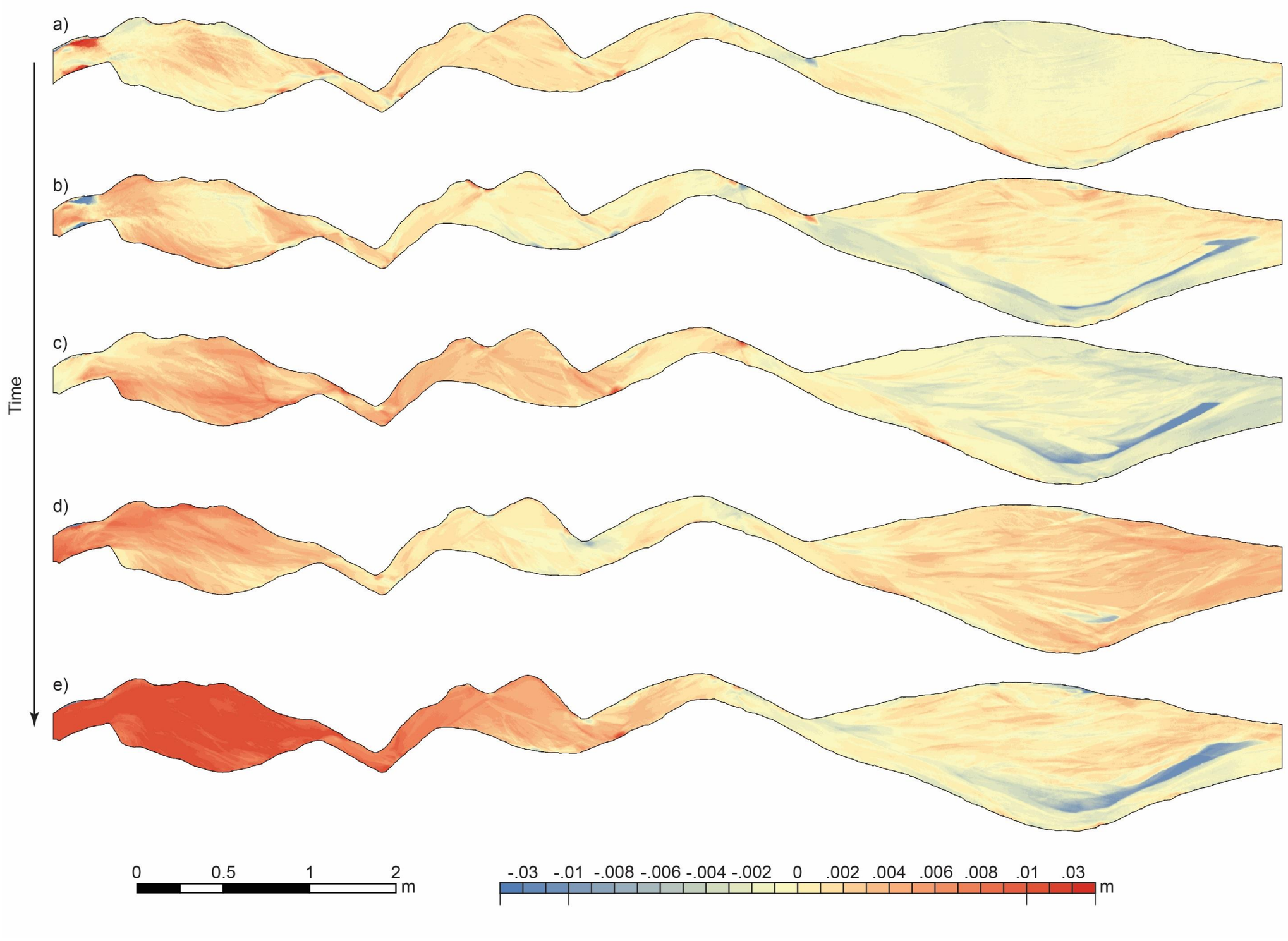

Fig. 4.27 Run 6 (a) Change DEM between the Base Level and Dam Break time-steps; (b) Change DEM between the Dam Break and Post Dam Break time-steps; (c) Change model between the Post Dam Break and Post Dam Break +8 time-steps indicating longer term change; (d) Change DEM between the Post Dam Break +8 and Post Dam Break +16 time-steps (b) Gross change in the model between the Base Level DEM and the final morphology of the Post Dam Break +16 DEM.

Middle Gorge of the model and only dispersed or highly dispersed UV sand is visible in the lower model reaches.

After the Post Dam Break time-step Run 6 had two additional model runs, Post Dam Break +8 hours and Post Dam Break +16 hours. The Post Dam Break +8 and Post Dam Break +16 time-steps show further, progressive aggradation of the Upper Flat over the extended model run period (Fig. 4.26c and d). The exposed area of UV sand from the Post Dam Break time-step was rapidly buried at the start of the Post Dam Break +8 experiment. The +8 and +16 difference DEMs show differing levels of aggradation in opposing areas across the reach between the two time-steps. This indicates the continuation of avulsion activity within the flat. It appears that the dam emplacement, breach and sediment deposition significantly disturbed the Upper Flat and over the time scale of the experiment this reach did not achieve equilibrium again. Fig. 4.28 shows a time sequence for the Lower Flat which appears to be more dynamic than the Upper Flat over the experiment running time. Initial aggradation is observed in the Dam Break time-step, but very little morphological change is observed in the Post Dam Break time-step. Within the Post Dam Break time-step localised scour is observed on channel edges and bar surfaces on the true-right hand side of the reach. The +8 hour model shows a significant increase in aggradation throughout the reach. This is contrasted by another phase of low aggradation and some localised scour in the +16 hour model. Fig. 4.29 shows that very little UV material is visible on the surface of the models after the +8 hour and +16 hour models, more than likely due to the shutdown of UV sediment sources with the removal of most of the dam material and burial of the reworked landslide material in the Upper Flat. The extra running period for Run 6 allowed the compilation of cumulative visible UV sand over each time-step (Fig. 4.28e). It shows that the majority of redistribution work is done within the Dam Break and Post Dam Break time-steps and that as time goes on less and less material is visible. This censoring of the visible UV material is either a product of burial or flushing of material through the system.

The sub-surface stratigraphy of Run 6 is shown in Fig. 4.30 and summarised in Table 4.5. Unlike the other un-armoured and armoured model runs the cores for Run 7 were taken after the +16 time-step. A thick layer of highly concentred material is buried within the Upper Gorge, this is the location of the landslide dam and possibly indicates that the base of the landslide survived reworking and is buried in-situ. The concentrated layer of material thins into the Upper Flat and transitions into a less concentrated ~50/50 UV/Silica sand mix (Fig. 4.30). The ~50/50 layer continues as a subsurface layer throughout the Middle Gorge and Lower Flat; a cross-profile in the Lower Flat (Fig. 4.30c) indicates that this layer continues to be present in material deposited in the main channel to the true-left of the Lower Flat but not into the true-right which was rarely occupied by a

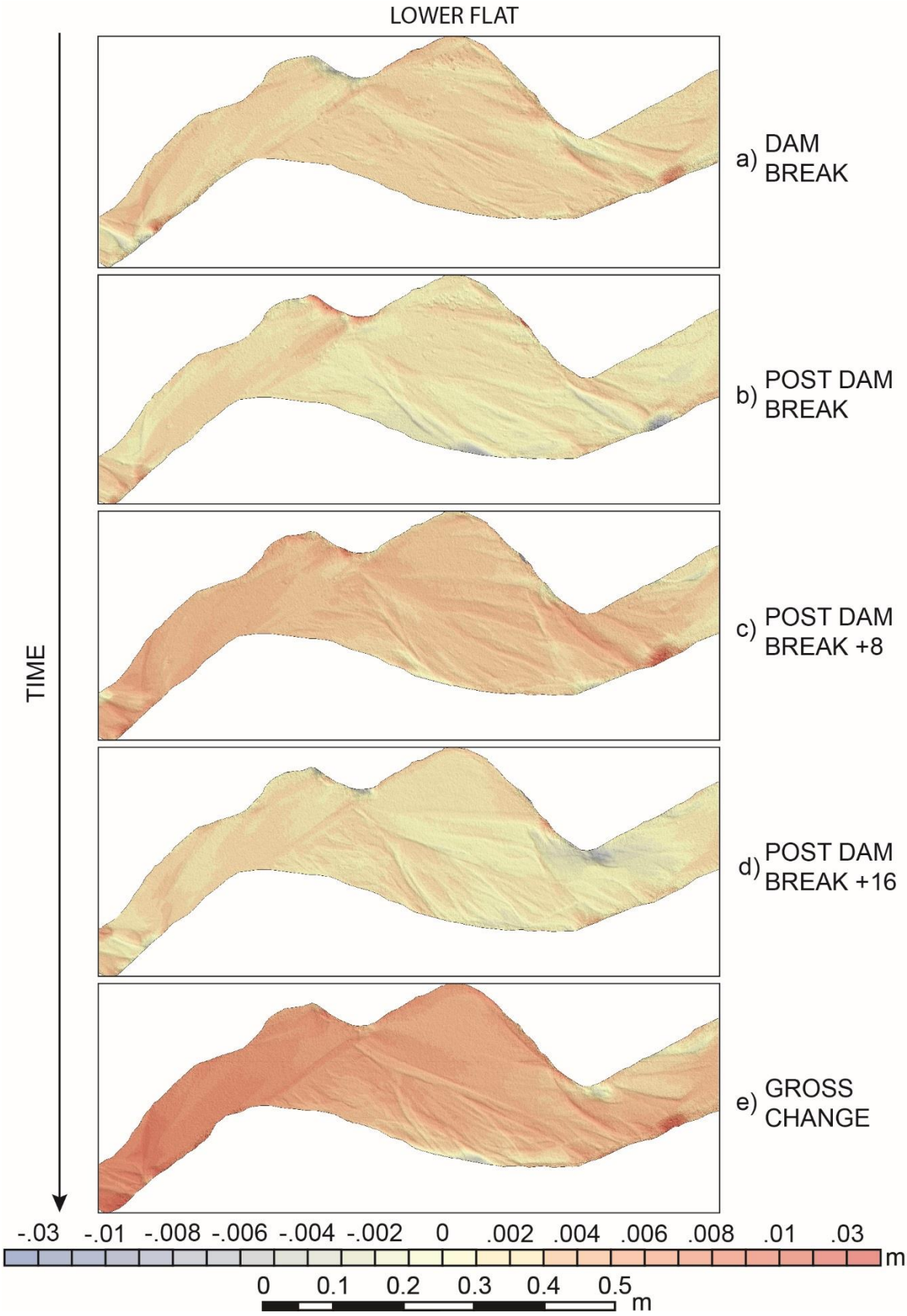

Fig. 4.28 Comparison time series of the Lower Flat from Run 6 showing aggradation and degradation between each time-step shown on the right hand side.

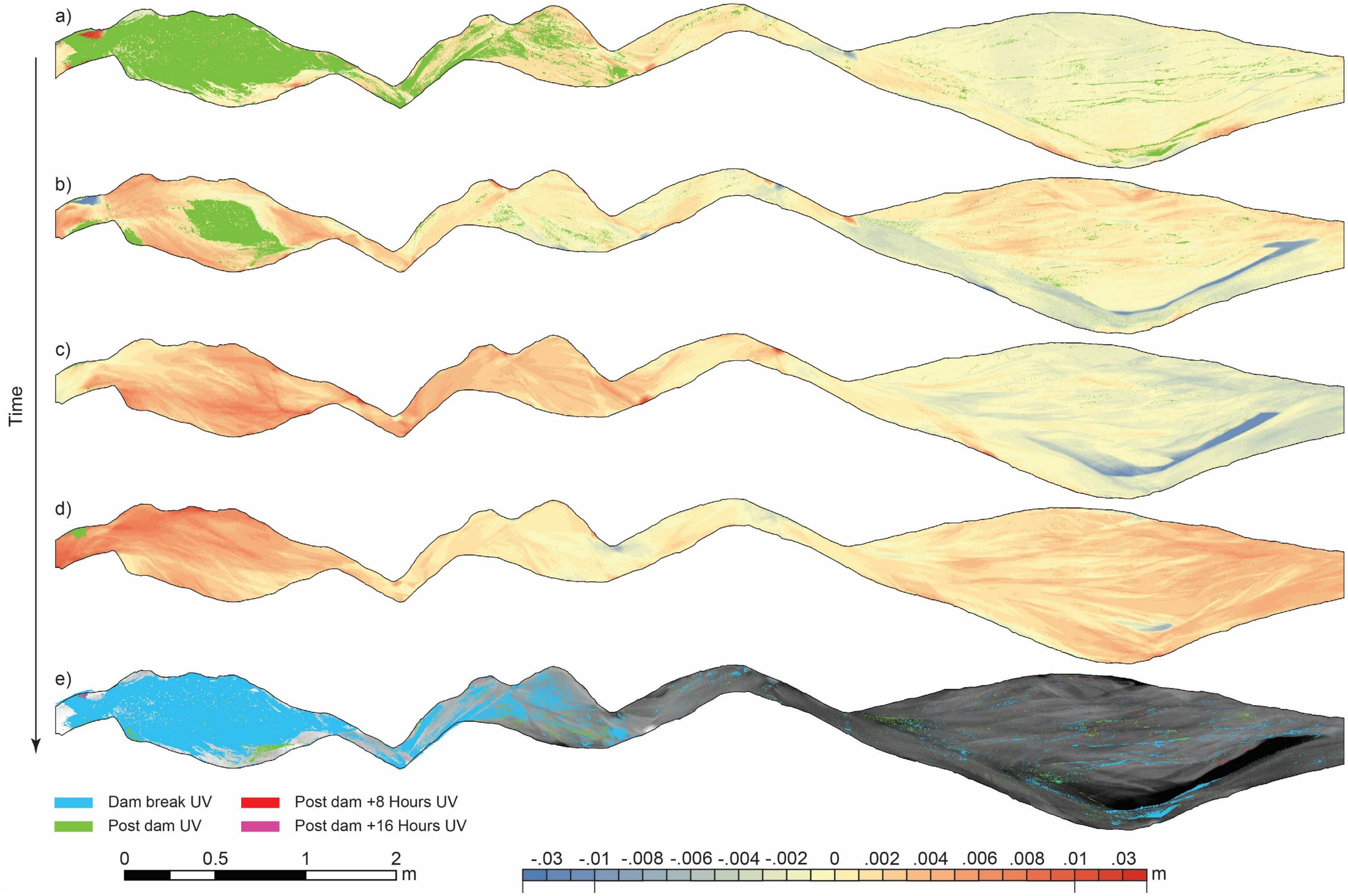

Fig. 4.29 Run 6 (a) DEM of difference between the Base Level and Dam Break time-steps with UV sand locations overlain; (b) DEM of difference between the Dam Break and Post Dam Break time-steps; (c) DEM of difference between the Post Dam Break and Post Dam Break +8 time-steps with UV sand locations overlain, at this point very little evidence of the dam exists on the model surface.; (d) DEM of difference after the Post Dam Break +16 time-step with UV sand locations overlain; (e) Cumulative UV sand locations from all models in Run 6. The Dam Break model shows the largest dispersion of sediment and some mobilisation of UV sand occurs in the Post Dam Break phase. Very little sand is visible in the Post Dam Break +8 hours and Post Dam Break +16 hour models

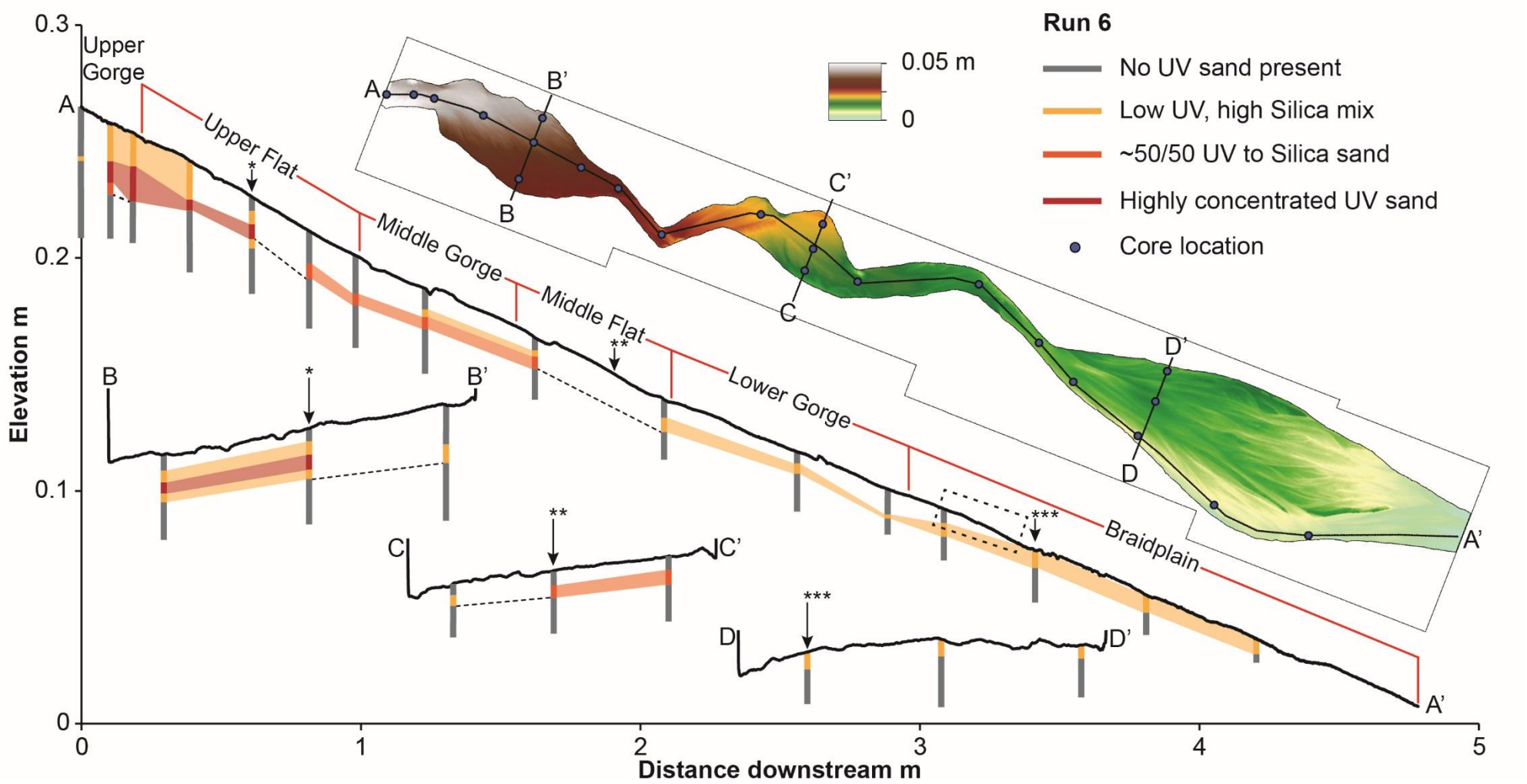

Fig. 4.30 Run 6 Flume model profile with core logs after the Post Dam Break +16 time-step. Core colours indicate the concentration of UV sand within identifiable sediment layers. Vertical scale is 0.01:0.025, horizontal scale is 0.01:0.25. The dashed box indicates the front of the aggradational sediment slug.

channel. This sub-surface layer continues but transitions to having a lower UV concentration at the bottom of the Lower Flat. The lower concentration, mostly Silica sand layer continues down to the end of the model, however becomes a surface layer once it enters the Braidplain reach. The surface layer of UV/silica mixed sand in Run 6, that is visible from the centre of the Braidplain reach, is thicker than in other models, potentially as a result of the longer +16 hour running time. This longer running period with increased depth of low-UV concentration sand could indicate that as the time-steps progress more of this material is transported from the upper reaches of the model and stored within the braidplain reach.

This transport and deposition of UV material is likely to have occurred in conjunction or just after the burial of the UV sand sources in the upper reaches of the model. This is because a Silica sand sediment slug is visible in the Braidplain reach, evidenced by the elevation profile in Fig. 4.30. This means that the UV sand layer must precede this aggradational sediment slug. The sediment slug is only visible after prolonged running of the model. The elevation profile in Fig. 4.30 shows clear burial of UV material by Silica sand in all reaches down to the Braidplain. Here a visible drop in channel elevation is displayed. It is hypothesised that this sediment slug has propagated down the model slowly over the 22 hour running period from the dam failure to the end of Post Dam Break +16. The propagation of this sediment slug would explain the aggradation observed in the Lower Flat of the Post Dam Break +8 model (Fig. 4.28) that was followed by little to no aggradation in the Post Dam Break +16 model (Fig. 4.28). Essentially the wave propagated through this reach in the Post Dam Break +8 causing the aggradation observed. It is likely that this sediment slug would have continued down the Braidplain reach had the model been run for a longer time period. The gross change model for Run 6 (Fig. 4.26e) shows that aggradation occurs across the Upper Flat over the whole experiment time period. Aggradation in time-steps a and b (Fig. 4.26) are associated with the deposition of UV sand whereas the signal in time-steps d and e (Fig. 4.26) indicate that the majority of aggradational work shown in the gross change model was done in the +8 and +16 model runs when the Silica rich aggradational pulse was migrating down the model system.

Runs 4 and 5 were the additional armoured dam models, with Run 5 being a continuously running model which therefore does not have Dam Break and Post Dam Break difference models. Run 4 and 6 display morphological and UV dispersion similarity in the Dam Break model (Table 4.4), with the exception of slightly higher aggradation in the Upper Flat in Run 4 associated with an area of increased deposition in front of the dam breach (Fig. 4.19 4a). Unlike other models, Run 4 displays greater erosion into the substrate within the breach channel of the dam (Fig. 4.19 4a). Aggradation in the Upper and Lower Flats (Fig. 4.19) shows that aggradation occurred across the entire reach for

both of these sections during the dam break flood. The aggradation is coupled with highly concentrated UV sand deposition in the Upper Flat and Middle Gorge with a diminishing concentration of visible surface UV sand down through the lower reaches of the model.

All of the armoured model runs have surviving dam remnants in the Upper Gorge by the Post Dam Break time-step (Table 4.4). Runs 4 and 6 had small remnants with sporadic carapace cover whilst Run 6 had a larger proportion of the dam surviving, possibly due to the protection provided by a collapsed section of the carapace which was protecting the up-stream flank. Despite remnants of the dams surviving, relatively speaking very little evidence for the original deposit is visible in any of the models and would be less visible without the aid of the UV sand and lighting. Aggradation at the Post Dam Break time-step is similar in pattern between Runs 4 and 6 in that both show higher aggradation in the dam proximal Upper Flat and Middle Gorge reaches, this is associated with the burial of UV material by a layer of Silica sand (Table 4.4); the same is seen for Run 5, although there is no Post Dam Break difference model to display for that run. There is a diminishing level of aggradation down model Runs 4 and 6 through the Lower Flat and Lower Gorge before a mix of low level aggradation and low-level degradation is seen in differing parts of the Braidplain. The low aggradation in the Lower Flat of Run 4 is seen across the entire reach (Fig. 4.20). The distribution of UV sand within this reach (Appendix 4.4 Run 4b) indicates that flows had avulsed across the true-right of the flat, deposited UV sand and moved back to the main channel on the true-left of the reach. Run 6 displays a similar pattern but with a less concentrated volume of UV sand present (Fig. 4.29b). In the lower reaches of the model for Runs 4, 5 and 6 there appears to be differences in the surface distribution of UV material (Table 4.4). Runs 4 and 5 appear to have been able to mobilise UV material into the lower reaches and preserve that material within the Lower Gorge and Braidplain (Table 4.4; Appendix 4.4 Runs 4 and 5); whilst Run 6 has much more highly dispersed UV sand within the model reaches.

The sub-surface distribution of UV material between Runs 4, 5 and 6 (Table 4.5) indicates some similar patterns of deposition occurring within each model run. Each model has a buried layer of highly concentrated UV sand within the Upper Flat (Table 4.5), which transitions into a 50/50 concentrated layer mid-way down the flat (Fig. 4.30; Appendix 4.5). Core profiles for Runs 4 and 5 show that this less concentrated layer continues down through the Middle Gorge and Lower Flat, buried under a low UV concentration Silica sand mix. The 50/50 concentrated layer is likely associated with the original dam break flood as the armoured models were capable of mobilising more concentrated UV material into the Lower Flat during the Dam Break time-step. The low concentration sand mix capping the model is likely a product of continued reworking of UV material throughout the Post Dam Break time-step; this is visible in the aggradation seen in the difference models for these runs. Cores indicate that the 50/50 concentrated layer becomes a surface layer

at the bottom of the Lower Flat into the top of the Middle Gorge and continues as such down the rest of the model reaches. In Runs 5 and 6 this layer becomes less concentrated down the model, whereas in Run 4 the layer switches between zones of more and less concentrated material (Table 4.5 Lower Gorge and Braidplain). Within Run 4 there is also no UV material visible within the avulsion channels on the Braidplain (Table 4.5; Appendix 4.5 Run 4d). This could explain the larger quantities of UV material within the main channel of Run 4 when compared to the other armoured models (Table 4.4 Post Dam Break model), as very little UV material is deposited out of the main channel. Run 6 shows a similar sub-surface pattern of UV sand distribution; however the cores were taken after the +16 hour time-step for this model and therefore have a thicker layer of Silica sand burial material.

Gross change models between the Base Level and Post Dam Break models for Runs 4, 5 and 6 indicate that Run 5 has a larger amount of aggradation in the Upper Flat than the other two models (Fig. 4.21 5a). This aggradation is confined to the dam proximal end of the reach. Regardless of the different levels of aggradation within the Upper Flat between the models, there is agreement that aggradation has occurred. The Lower Flat for all three models shows more similarity than the Upper Flat with moderate level aggradation occurring over the Base Level to Post Dam Break time-step. Overall there is a diminishing level of aggradation down the model in each of the runs with overall degradation occurring within the main channel of the Braidplain (Table 4.4; Fig. 4.22).

4.3.5 Comparison of un-armoured and armoured dam models

The majority of the landslide dams failed through the same overtopping mechanism. In all start-stop models there was partial removal of the dam through erosional processes at the Dam Break time-step. There is aggradation of the Upper Fat and Middle Gorge in every model run after the Dam Break irrespective of an armoured or un-armoured landslide dam. In each case this is associated with the deposition of dam material by the dam breach flood. Run 1 displays low level degradation of the Lower Flat and Lower Gorge; however, the other unarmoured model, Run 3, displays similar characteristics to the armoured models. In Run 3 low level aggradation occurs in these reaches associated with the mobilisation of UV material further down the model in the dam breach flood. This can be seen in Table 4.4 where the Dam Break UV sand distribution in Run 3 is similar to that of Runs 4 and 6.

In the Post Dam Break time-step there is complete removal of the landslide dam in the un-armoured model runs whilst the armoured model runs have carapace protected remnants of deposits on the channel margins. Upper model reaches have higher levels of aggradation to middle and lower reaches. Table 4.4 shows higher aggradation proximal to the dam location compared to distal reaches. Examining the Upper Flat in more detail

through the DEMs of difference (Fig. 4.20) it can be seen that Runs 1, 3 and 4 have similar levels of aggradation regardless of their un-armoured/armoured nature. In contrast Run 6 has aggraded but to a lesser degree (Fig. 4.20 6a). The aggradation in the Upper Flat in the un-armoured and armoured model runs is developed through the progressive burial of UV sand material deposited in the Dam Break time-step by a layer composed predominantly of Silica sand. This burial process took between 1-2 hours during model runs.

The landslide dam and the layer of UV sand in the upper flat were the major sources of UV sand to the rest of the model in armoured and un-armoured landslide runs. These sources of material were shut down once they became buried by Silica sand. This prevented any further mobilisation and transport of UV sand down the system. Occasionally model flow would incise through the protective Silica sand layer to remobilise some UV material but these incised channels would often be short-lived as new Silica sand infilled them.

Runs 1 and 3 display higher aggradation in the Lower Flat to that of the armoured experiments (Fig. 4.20, 1b and 3b); this aggradation is confined to the area occupied by the main channel to the true left of the model throughout experimental runs. Armoured experiments Runs 4 and 6 display low-level aggradation or no change across the reach (Fig. 4.20 4b, and 6b). Higher concentrations of UV material present in the lower reaches of the model (Table 4.4) indicate that UV material has been mobilised from the upper reaches of the model between the Dam Break and Post Dam Break for both model types.

Table 4.5 which summarises the core data for model Runs 1-6 shows that with each run there is a surface and sub-surface dam-proximal to dam-distal gradient of high-UV concentration to low-UV concentration of material respectively. This is evidenced in Table 4.5 by the changes in cell colour from high-UV concentration red colours at the top of the table (upper reaches of the model), through orange coloured ~50/50 mixed UV/Silica cells in the central reaches of the model down to yellow coloured low-UV concentrations in the lower reaches of the model. Differences in sub-surface stratigraphy occur between the armoured and unarmoured models. Within the Upper Flat more highly concentrated UV material is spread across the cross-section of the reach in un-armoured model runs whilst in the Lower Flat there is not a layer of buried UV sand (Table 4.5). This implies some morphological differences generated by armouring the landslide dam. The armoured dam break floods appear to initially be able to mobilise material further down the model system; this material is then preserved and progressively buried by a mix of Silica sand. Whilst there are these small differences in UV sand mobilisation the broad pattern of UV sand distribution is similar for all models, both in terms of surface and sub-surface distribution.

The gross-change models across all model runs display similarity over the broad scale. More aggradation is seen in dam proximal locations with diminishing aggradation down model. Most models display some degradation of the braidplain where the main channel on the true-right of the reach has eroded into bank material (e.g. Fig. 4.29c). Gross change long profiles for the models in Fig. 4.22 indicate a very similar pattern of model aggradation in the upper reaches of the system and degradation in the lower reaches of the model over the Base Level-Post Dam Break experimental time period. Ultimately it appears that with the exception of preserved dam deposits and mobilisation of material further down the system during the dam break flood, the armouring of the landslide dam does not significantly change the morphological outcomes of the flume model.

4.4 Discussion

4.4.1 Spatial and temporal distribution of UV material within the microscale model

The concept of landslide censoring is widely represented within contemporary literature (Korup et al., 2005; Allen et al., 2011; Dunning et al., 2015), and fluvial erosion has been cited as a major component of landslide removal within NZ river systems (Chevalier et al., 2009; Barth, 2014). Previous literature has focussed on the removal of the deposit itself and the censoring of the sedimentary record of landslide emplacement. The micro-scale fume modelling has identified additional processes involved with RAD censoring as well as visualising the routing of reworked landslide material within an idealised river system.

Dam failure in the flume models follows a similar precedent to that of the worldwide prototypes in that the majority (5 of 6) failed by overtopping (Ermini and Casagli, 2003). Given that dam failure is known to be a relatively rapid process for the majority of real-world landslide dams, with an estimated 40% failing in the first day of formation and 80% after one year (Costa and Schuster, 1988; Ermini and Casagli, 2003), the rapid failure of the model dams is to be expected.

Material from the model dam was redistributed down the system through dispersion from the point source rather than a direct translation of material (Cui et al., 2003). Dispersion is the process of gradual diffusion of the sediment pulse (landslide dam) downstream away from the point source (Sutherland et al., 2002). The initial model dam break reworked the majority of dam material to proximal locations but in low-concentrations down the entire length of the model. This downstream dispersion of material during the flood is analogous to studies of the dispersion of material from landslide point sources within fluvial systems (Sutherland et al., 2002). Previous studies (Cui et al., 2003) have suggested that having similar sediment pulse (UV sand) and pre-pulse substrate (Silica sand) GSDs will tend to favour the dispersal of material down a

system over translation downstream. This could also be said of prototype RADs where internal deposit material is comminuted to sizes which could mimic GSDs of river material in high mountain catchments. The flume model therefore suggests that prototype RAD material will disperse downstream from the point source.

This censoring of deposits by the fluvial erosion of material has been noted in the literature before (Korup, 2005d, 2005a; Chevalier et al., 2009; Harrison et al., 2015). Reworking of landslide material censors the absolute location of the RAD but highly-concentrated reworked dam material may be used for tracing unknown RADs through the survival of agglomerate particles in close proximity to old landslide deposits (Chapter 3) or through clast analysis (Harrison et al., 2015). It is not unusual for the majority of landslide material to become stored locally to the landslide dam. Harrison et al., (2015) document that much of the breach channel material from the Ram Creek RAD was deposited directly below the dam, whilst Hancox et al., (2005) describe the aggradation of montane flats in the Poerua River subsequent to catastrophic dam failure. The effect of the storage of UV material in the model is to 'shred' the sedimentary signature of the landslide in the rest of the system (Coulthard and Van de Wiel, 2013).

Within the model 'landslide' material was easily identifiable under even in small concentrations due to its UV reflectivity. This allowed its identification in surface deposits and sub-surface stratigraphy. However, without this diagnostic ability to distinguish landslide material from the baseline sediment flux the sedimentary signal would have been visibly unidentifiable in many locations. Likewise in prototype river systems, without a diagnostic tool for identifying landslide derived material, such as agglomerate particles or clast analysis, the RA sediment signal is essentially 'shredded' by material transport and storage within the fluvial system (Jerolmack and Paola, 2010; Coulthard and Van de Wiel, 2013). The shredding of the signal is forced by the storage of material proximal to the dam coupled with the non-linear release of material from that storage area. The non-linear nature of material release from storage can be affected by different factors such as channel placement, avulsions and flooding (Coulthard and Van de Wiel, 2013). The flume models show a further factor affecting material release in the burial of the landslide material. The flume models unfortunately did not model additional floods within the river channel, however frequent avulsion behaviour was observed. Avulsions allow the channels to move to different parts of the material storage area and remove varying quantities of sediment. Material burial effectively shuts off the removal of landslide material from the storage area, however the model did show localised channel incision into the burial material which allowed the remobilisation of stored UV material. Both of these flume model observations add to the non-linearity of material release and the shredding of the landslide sediment signal downstream. The results support the idea that a particular river system may buffer the sedimentological impacts of large landslides from

distal reaches, including if that river joins a trunk valley. This buffering depends on the location of the deposit within a system and that system's geomorphology.

Rainfall is likely to have a significant impact on the ability of any given fluvial system to remove material from river storage areas (Hicks et al., 1996). Coulthard and Van De Wiel, (2013) showed that whilst the signal of material was shredded by storage, increases in rainfall led to increases in the suspended sediment yield (SSY) output of the system. However this release can be nonlinear over short and long timescales in that given the same flood discharge the suspended sediment yield output can vary dramatically from low to high values (Van De Wiel and Coulthard, 2010).

The flume model did not include any provision for rainfall, however given that high-intensity and long-duration rainfall events are experienced in Nelson, West Coast and Fiordland and East Coast catchments (Henderson and Thompson, 1999) it is likely that pluvial flooding in these river systems would likely increase the volume of landslide derived material that is mobilised downstream. This could in effect make the distal landslide sediment signal a highly transient feature depending upon whether material has recently been reworked or not.

Cox and Nibourel, (2015) examined the modification and evolution of bedload composition with transport from source areas in Westland NZ. They found that the durability of rock-types being transported by fluvial systems varied considerably leading to some rock-types being better represented further from their source areas. They also noted that there were localised bedload changes around river tributaries where inputs of compositionally different material diluted the geological signature of the trunk river. Part of the censoring process observed throughout flume model runs was that material was stored in the upper reaches of the model and only low-UV concentrations of material were found in lower reaches of the model. This shows that fluvially reworked material that is diagnostic of RADs will most likely not be traceable in distal locations from a landslide source. If additional complexity was added to the model such as tributary rivers or the ability for clast degradation it could be seen that the UV sand signal could be essentially undetectable in the model and therefore a prototype South Island river system. Hovius et al., (1997) determined that much of the West Coast river sediment is dominated by landslide derived material. So in the case of South Island RADs fluvially reworked material is likely to be diluted by the sedimentary signatures of a host of small to large landslides within the same catchment.

4.4.2 Morphological and sedimentological response of the flume model to RA emplacement and breach

The aggradational behaviour of the model channel was repeated to a lesser or greater degree within all of the runs. After dam emplacement a lake formed upstream

which rapidly filled and breached (typically by overtopping) the RAD (Fig. 4.31 a-c). Breaching led to the incision of a channel through the RAD. Initial aggradation in the upper reaches of the model was associated with dam failure (Fig. 4.31c) followed by a phase of aggradational burial of material by baseline Silica sand sediment flux (Fig. 4.31d). Run 6 furthers the model evolution with an extended running period which shows a prograding sediment slug which has worked its way through the model river system (Fig. 4.31e). After 22 hours of model operation since the dam failure the front of the slug was situated towards the top of the Braidplain.

The sequence of events observed in the flume model is supported by the examination of some NZ prototype RADs. Immediate aggradation of the system is expected following dam failure as material removed from the breach is deposited downstream. Harrison et al., (2015) examining the Ram Creek RAD describe much of the breach material being deposited immediately in front of the dam and downstream to where the rivers enters a gorge. Knickpoint formation after dam failure increases the channel steepness downstream (Korup, 2006b; Harrison et al., 2015). Whilst knickpoints are difficult to discern in the Post Dam Break flume profiles there was increasing steepness in the Upper Flat associated with downstream aggradation similar to that displayed in Ram Creek. The disruption caused by the model landslide dam caused reach scale aggradation in proximal locations (Fig. 4.31c). In prototype systems this would completely engulf proximal montane flats with sediment and stop any bedrock incision processes (Hancox et al., 2005; Harrison et al., 2015). Only once the material has been flushed out of the system can rivers start bedrock incision processes again (Yanites et al., 2010). However this removal of sediment is only possible if river transport capacities have not been overwhelmed by the sediment volume and that sediment is available for removal (Pearce and Watson, 1986; Hovius et al., 2000; Korup and Crozier, 2002). In many cases NZ rivers are unable to remove the large volume of material deposited by catastrophic dam failure floods as normal flow conditions cannot transport the calibre of material, are overloaded with sediment or transportable sediment is stored and therefore unavailable to the contemporary river channel. This may lead to reach scale aggradation effects persisting for long time periods (Korup and Crozier, 2002).

The majority of UV sand distribution work was done by the dam failure flood, which deposited material in proximal locations (Fig. 4.31c). This material remained stored in these dam proximal locations until it was buried by the influx of material from upstream, effectively further censoring the material from the sedimentary record (Fig. 4.31d-e). Due to the effects of the landslide dam causing aggradation and excessive sediment loading the model was not able to revert back to an equilibrium state and re-incise a channel back through the Upper Flat (Korup and Crozier, 2002). This lack of re-incision is similar to that observed in Ram Creek where the volume and calibre of material combined with the small

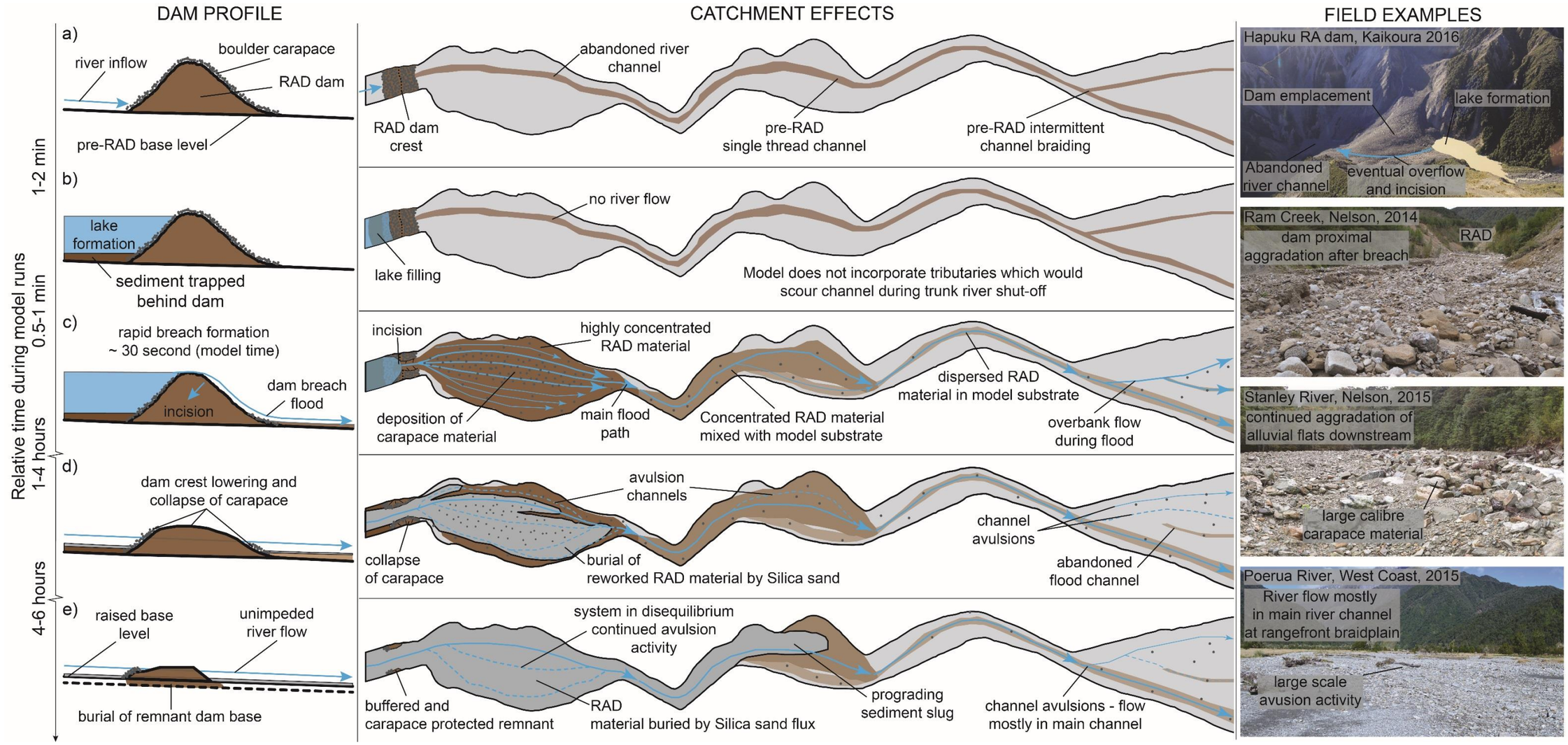

Fig. 4.31 Summary of RAD effects on fluvial system morphology and RA material distribution through a catchment. a) dam emplacement; b) lake formation behind RAD; c) overtopping of the RAD leading to the generation of a dam breach flood; d) removal of dam material and collapse of carapace material into channel, reworked dam material begins to be buried; e) partial dam remnant, prograding sediment pulse moving through system. To the right of the figure is a series of field examples of some of the catchment effects that were observed within the microscale flume model. The field location is indicated in the upper left of each image with the year the image was taken.

river discharge has hampered fluvial incision back through reworked dam material (Nash et al., 2008; Harrison et al., 2015). The model showed that reworked landslide material is stored within the 'montane' flat areas for prolonged periods of time. Prototype rivers in NZ will likely respond in a similar fashion with long term sediment storage occurring in montane/valley flats if river discharges are unable to mobilise the volume of RA material stored there (Korup and Crozier, 2002).

In the model, the basal material of the dam is eventually occluded by in-situ burial by the influx of Silica sand from upstream (Fig. 4.31e). In prototype river systems material is usually eroded to form a breach channel it may take 10^1-10^4 year timescales to remove an entire deposit from the landscape, if at all (Chevalier et al., 2009; Hancox and Perrin, 2009; Massey et al., 2013). However, when left over long timescales fluvial aggradation can bury large sections of deposits under alluvium (Hewitt, 2002; McColl and Davies, 2011; Barth, 2014). Therefore, the burial of basal material that was observed in the model may be a process that occurs in prototype deposits only once large volumes of the upper dam material have been removed and rivers can aggrade over the remnants.

Run 6 showed that after reach scale aggradation effects due to dispersion of the landslide dam (Sklar et al., 2009) and associated aggradational response (Korup and Crozier, 2002), a slow moving aggradational front, primarily composed of Silica sand, prograded through the system (Fig. 4.31e). This 'sediment slug' derived from upstream of the dam translated through the model and aggraded most reaches. The landslide deposit had at this point been censored through fluvial erosion. This indicates that internal fluvial processes rather than a sediment point source such as the landslide drive the translational movement of the sediment slug through the system (Sklar et al., 2009). The hydraulic geometry of the model will have been disturbed by the effects of the mock RAD, i.e. channel width/position and channel slope will have changed between the Base Level and Post Dam Break models. The translating sediment slug is likely a response to these changes in hydraulic geometry of downstream reaches. These changes in hydraulic geometry have been shown to produce irregular variations in transport and deposition of material, which manifests as translating sediment wave forms, in New Zealand gravel bed rivers in the past (Griffiths, 1993). By the classification of Nicholas et al., (1995) it could be termed a super-slug which has caused reach scale changes to the model morphology. It is likely that the burial phase observed in the Upper Flat, after the dam has been mostly removed, is in fact the start of the sediment slug progradation. The Post Dam Break +8 model suggests that the slug propagated through this reach during this time-step as this is when the greatest amount of aggradation was observed other than the initial dam failure response. The progradation of this sediment slug down the river system suggests that prototype rivers will have a similar response. Although time may not be upscaled from the model to prototypes directly the experiment suggests that large scale dam removal is

required before the sediment slug response is seen. In addition the slug did not make it to the end of the flume model run even after 22 hours of operation indicating that even in prototype rivers this is a slow moving aggradational pulse that may take periods of time well beyond the original event scale to propagate downstream.

The model failed to achieve an equilibrium state post dam failure for the entire model run. This can be seen from the active aggradation in alluvial flats as well as the prograding sediment slug observed over longer experimental time periods. Additionally, the Upper Flat and Braidplain reaches saw frequent channel avulsions after the landslide dam failure (Fig. 4.31e). The highly disrupted Upper Flat saw constant channel changes throughout the experiment more than likely due to contact with the landslide dam to begin with and subsequently a sedimentologically disturbed upper model reach, these are termed contact avulsions by Korup, (2004). The Braidplain avulsion behaviour was different given that it was a substantial distance from the landslide deposit. This is not unexpected and Braidplain avulsions more than likely stem from sediment loading in the reach (Korup, 2004). Avulsion and channel instability were likely initiated by the dam break flood and the transport of landslide material downstream. Surface UV sand figures do show that landslide material was deposited in avulsion channels highlighting its role in their formation. Similar avulsion effects are likely to be seen in prototype river systems at mountain range fronts where rivers exit onto large braidplains (Korup, 2004; Hancox et al., 2005).

The model does not represent tectonic uplift which is known to occur at high rates in the Southern Alps (Hovius et al., 1997). Incorporating uplift into the model may have driven some channel incision and remobilisation of buried landslide material in the upper reaches. However, this model shortfall does not discredit the initial deposition and long term storage of this sediment within dam-proximal locations.

4.5 Summary and conclusions

This chapter has discussed a series of six flume model experiments designed to examine the redistribution of RA material through and idealised South Island river system. The river system consisted of valley confined gorges, montane flats and a braidplain. The model also examined the morphological changes that occur as a result of landslide sediment redistribution by fluvial systems. The redistribution and morphological changes are important for our understanding of RA material may be stored within NZ river systems and how RADs may be censored by fluvial erosion. This could inform future research on the likelihood of finding traces of RA material within a given valley confined environment.

A micro-scale modelling approach was used for the experiment which whilst sacrificing dynamic similarity with prototype river systems they do retain morphological similarity. A novel ultra-violet (UV) sand tracing technique was devised in order to trace

landslide derived sediment down the idealised river system. To the authors knowledge this is the first time UV sand has been used in micro-scale flume modelling in as a sedimentological tracer. A mock RAD was composed of UV sand and was either left un-armoured or was armoured with coarse material to establish two distinct experimental sets.

A number of UV image capture and processing techniques were developed to extract surface UV sand locations within the model at different time-steps. Additionally an SfM reconstruction technique was used to build DEMs of different time-steps within the flume model operation in order to monitor the morphological change.

The model was allowed to run for two different time-steps; (1) A Dam Break time-step which examined the immediate consequences of catastrophic dam failure for RA material distribution and channel morphology; (2) A Post Dam Break time-step which examined the long term evolution of the idealised model. Long term model evolution included the continued transport of UV dam material through the fluvial system and the morphological changes associated with dam emplacement and system disturbance.

Analysis of the morphological change of the model channel shows that the emplacement and failure of the landslide dam severely disrupts the fluvial system over long time periods. A number of morphological changes and censoring processes are identified which could be applied to NZ prototype river systems.

1. Dam failure and the ensuing flood from the impounded lake produces dam proximal aggradation almost entirely composed of landslide derived material. The dam break flood transports low concentrations of this material throughout the differing reaches and can deposit some of the material at higher stages than the base level flow. Whilst aggrading dam proximal reaches the dam break flood can scour some of the lower model reaches.
2. Over the long term continual aggradation is seen in dam proximal locations. Eventually the dam is censored by fluvial erosion and deposited dam material in proximal locations is censored through burial processes.
3. A landslide material concentration gradient is observed with dam proximal locations having high-concentrations of material and distal model reaches having low-concentrations of material.
4. Over extended time periods an aggradational sediment slug is observed to propagate down the model system.
5. Landslide derived material is preserved in the sub-surface stratigraphy and retains the high-low concentration gradient observed previously.
6. The model did not re-achieve an equilibrium state. It is unclear from the model runs whether further model operation would have allowed a return to equilibrium or whether the system would have remained in a disrupted state.

Using the information from the flume model experiment it can be concluded that fluvially reworked RA material in valley confined settings may be stored in dam proximal reaches for prolonged periods of time in NZ prototype river systems. Steepening of dam proximal reaches may occur and continued aggradation can bury deposited landslide material. This burial protects it from reworking and preserves a record of the landslide dam within the fluvial stratigraphic record. The most likely place to find evidence of this is in montane flats close to RADs. This indicates that montane flats may hold important stratigraphic and sedimentological information on the presence of unknown RADs. Further downstream the sedimentological signal of RADs is shredded and only low concentrations of material can be seen. Given the lack of a diagnostic tool for identifying fluvially reworked landslide material for all RADs it would be near impossible to identify these low concentrations of material. Future efforts for identifying censored RADs should examine alluvial sequences in valley confined settings for evidence fluvially reworked material.

Chapter 5

Discussion and conclusions

5.1 Introduction

The overarching aim of this research was to examine the processes acting to fluvially censor RADs within high-mountain environments on the South Island, NZ. As part of this, the study seeks to establish whether reworked RAD material can be traced through river systems using a diagnostic micro-sedimentological signature. This diagnostic tracer could then be used to identify previously unknown, fluvially censored, RADs and recover 'lost' deposits in the sedimentological record. Identification of censored RADs is an important avenue of research in terms of understanding the true magnitude-frequency relationships of RAs and how this relates to their potential hazard.

Initially an inventory of known RADs was compiled. The inventory was used to examine the distribution of deposits and their relationship to spatially variable triggering and censoring controls. Using the spatial, temporal and statistical distribution of the inventory, regions with a paucity of deposits were identified as areas of likely RAD censoring. Using RAD agglomerate grains as diagnostic tracers, a method was tested in South Island Rivers to attempt to identify fluvially censored RADs within regions with deposit paucity. When it was determined that agglomerate particles did not survive long distance fluvial reworking, the thesis went on to discuss possible grain morphology, fluvial morphology and sediment reworking factors that affect the traceability of RAD material. To further understand fluvial censoring processes in South Island rivers, a physical model was used to examine the redistribution of coarse grained RAD material through an idealised fluvial system. The model examined the morphological and sedimentological impacts of RADs on river systems as well as the redistribution of RAD material using a novel UV sand tracing method.

5.2 Discussion of aims

Chapters 2-4 set out the results of the thesis and discussed those results in the context of each individual chapter, addressing the specific objectives for Aims 1-4 set out in Chapter 1. This chapter draws together the major findings of each results chapter to show how they complement each other and address current research gaps. In order to do this each of the Aims 1-4 will be discussed.

Aim 1: **To examine controls on RA distribution and censoring processes in the South Island, NZ over the Holocene period.**

Spatially the distribution of RADs is heavily weighted to the SA region with ~65% of the inventory residing there; however this is split to 14.5% in the WSA and ~51% in the ESA. The inventory is split in other regions as 23% in Nelson, 8.2% in Fiordland, 1.9% in Marlborough and 1.5% in Otago (Fig. 2.2).

ESA deposits are located mostly in the northern section of the region, with sparse occurrence in the south. The scarcity of deposits in the southern ESA likely reflects three differing factors, (1) Sampling bias within the literature, (2) a seismic gap where no >M6 earthquakes have occurred between 1800-present (Fig. 2.6) and (3) a series of large lakes with the potential to sub-aqueously occlude RADs. Certainly the literature has no large inventory covering the southern section of the ESA, therefore a sampling bias likely exists. The seismic gap is conspicuous, especially being coincident with the lack of RADs within the region and could certainly have influenced the number of RA generated. This is especially relevant given the importance of earthquakes in generating RAs in other regions of the South Island, such as Nelson. The ESA also has a large number of RAs with no known triggers indicating that earthquakes are not required for RAs to occur here (McSaveney et al., 2014). Additionally in the southern ESA there are changes from prevalent sandstones in the northern ESA to metamorphic schist that is partly coincident with the paucity of RADs (Fig. 2.9). The schists in this region typically have low dip angles and therefore may not generate steep failure planes which will precondition slopes for RA generation (Fig. 2.11; McColl, 2015).

45% of WSA RADs are located above glaciers and have occurred in the historical past between 1850 to 2013. The only indication of previous RADs that have had glacial interaction on the WSA is the identification of the Waiho Loop as a glacially rafted RAD that has been deposited as a moraine (Tovar et al., 2008b; Shulmeister et al., 2009). Contemporary RADs on glaciers will start to transit through the glacial system (Allen et al., 2011; Dunning et al., 2015), whilst only the Waiho Loop has been identified as a WSA palaeo-RAD that has already done so. This indicates that many more palaeo-deposits are likely missing from the compiled inventory, locked in glacial transit. The WSA would therefore appear to be a prime location for the glacial censoring of deposits via entrainment and deposition as moraines.

A further 22 deposits are located within river valleys in the WSA, however these deposits are sparsely distributed with some catchments not containing any known deposits (Fig. 2.15). The AF which is situated along the WSA range front and is capable of generating M_w7 to M_w>8 earthquakes (Berryman et al., 2012), well above the ≥M6 threshold necessary for RA generation (Hancox et al., 1997, 2002). AF ruptures are thought to be responsible for the Round Top (Dufresne et al., 2009) and Cascade (Barth,

2014) RADs within this region. However few valley confined deposits have really been associated with AF ruptures which are thought to recur every ~329±68 years (Berryman et al., 2012). Modelling of a M_w8 earthquake in the central section of the AF by Robinson and Davies, (2013) has shown that MM9-10 intensity shaking would be expected to occur along the entire length of the fault to the bifurcation with the Wairau and Awatere Faults in the north of the island. These shaking intensities are heavily associated with RA occurrence (Hancox et al., 2002). Using the modelled MM shaking predictions from Robinson and Davies, (2013), Robinson et al., (2016) produce landslide hazard predictions for a M_w8 earthquake along the AF, indicating that extensive landsliding, including rock-avalanching, would occur along the entire rupture length of the AF, predominantly in catchments along the WSA (Robinson and Davies, 2013). The relatively small AF rupture recurrence interval of ~329 years (Berryman et al., 2012), along with likely high MM shaking indicates a paucity of deposits within the WSA region; there are very few deposits associated with ages of known fault ruptures.

The lack of smaller WSA RADs in the PDF of deposit area (Fig. 2.5) suggests that deposits below 0.3km^2 in size are missing from the regional sedimentological record. The paucity of older deposits in the WSA, coupled with high rainfall and rapid uplift for this region suggests that fluvial censoring could have a significant role in censoring deposits over 10^2-10^4 year timescales.

The Marlborough region is a stark outlier given its geological and tectonic similarities to the ESA and high mountain terrain between (Fig. 2.2 and Fig. 2.6). This could indicate three potential processes controlling the RA distribution in the Marlborough region; (1) A large bias in the study in the inventory meaning deposits have not been looked for, (2) An as yet unexamined control exists which is preventing RADs from occurring during known triggering events, (3) Censoring of deposits is occurring on a massive scale. We know that the first is true given the examination of the literature and the identification of an additional 12 possible deposits in aerial imagery. Additionally we know that large earthquakes generate RAs in New Zealand (Hancox et al., 1997; Nash et al., 2008; Parker et al., 2015) and ≥M6 earthquakes have occurred within the historical record from 1800-present within the Marlborough region. Notably the two largest of these Marlborough earthquakes, the 1848 M~7.4 on the Awatere Fault (Downes, 1995) has no associated RADs and the M_w7.8 2016 Kaikoura earthquake has one possible RAD associated with it (Little, 2016). This suggests that there is another control in the region preventing the production of RAs. Given the potential for large RA generating earthquakes in the Marlborough region it is possible an unexamined geologic control is present.

The proximity of known Marlborough RADs to active faults suggests that earthquake generated deposits have occurred in the past. Therefore the paucity of deposits observed in the region can also be explained by a lack of RA generation in

interseismic periods. If no RADs are generated during the interseismic periods, through aseismic triggering mechanisms, it leaves only a small accumulation of deposits generated via relatively rare, large magnitude earthquakes. In contrast the SA has co-seismic and aseismically generated RADs, constantly accumulating the population of deposits through time, rather than in rare peaks. The relatively low AAR and thinner vegetation cover make deposit censoring by these processes a less likely factor for the observed paucity of deposits. However, extensive scree cover in the region could censor deposits from view or obscure surface morphology, making deposit identification difficult. The 12 possible deposits identified through aerial imagery would help to fill the gap in the record of RADs within the region.

The majority of known Fiordland deposits occurred pre-1800 and have unknown trigger mechanisms (Fig. 2.2). A further 18 possible RA deposits were located in Fiordland under extensive vegetation cover, this is more deposits than are currently identified as RADs in this region. Similar to the 1848 and 2016 events in Marlborough, where >M7 earthquakes occurred but only one RA was generated, in Fiordland the 2003 M_w7.3 event only produced one RA (Hancox et al., 2003) whilst the 2009 M_w7.8 did not produce any RAs (Fry et al., 2010). The 2009 earthquake produced far fewer landslides than expected across all size ranges in part due to the low ≤MM8 shaking intensities (Fry et al., 2010). Low shaking intensities were caused by the physical characteristics of the earthquake which allowed energy to be released more slowly during the event (Fry et al., 2010; Mahesh et al., 2011). This shows that not all >M6 earthquakes will generate RAs, however this is not the typical outcome and earthquake magnitude is usually linked to RA occurrence. Three factors suggest that RAs should be more prevalent in Fiordland; 1) The offshore position of the AF with the sporadic occurrence of high magnitude earthquakes capable of generating RADs, 2) Steep, high relief slopes over 32°, the threshold identified in this thesis over which RAs can be generated, 3) Geologic conditions similar to that of other RA generating regions (Nelson). The lack of deposits found in Fiordland is indicative of deposit censoring. Vegetation cover in the region is dense and does easily obscure sub-aerial RADs. Similar rainfall patterns to the WSA suggests it is likely that fluvial censoring is also occurring within this region. Sub-aqueous censoring has been shown to occur in Fiordland at Milford Sound (Dykstra, 2012; Taig and Mcsaveney, 2015). With similar geologic and tectonic settings it is likely that other sounds and lakes in the region will hold similar archives.

It is clear from the distribution of deposits and their triggers that Nelson is highly susceptible to the generation of RADs by earthquakes. 90% of the regions RAs are associated with the 1929 and 1968 earthquakes (Fig. 2.2; Hancox et al., 1997; Nash et al., 2008; Parker et al., 2015). Only six deposits remain within Nelson which have not been associated with these earthquakes. Given the likelihood of previous Nelson

earthquakes over the Holocene period, the presence of only six pre-1929 deposits appears to be low in comparison to what can be produced and has been produced by successive earthquakes. Granted it is possible that RAs seen in the 1968 earthquake was in part due to preconditioning by the 1929 earthquake (Parker et al., 2015), there still appears to be a paucity of pre-1929 deposits within the region. The high, orographically enhanced, rainfall present in this region would allow for enhanced fluvial censoring of deposits. Fluvial censoring has been observed on some larger RADs within Nelson, such as the 1929 Buller River deposit, which has now almost been completely removed (Nash, 2003). This implies that pre-1929 Nelson RADs are likely to have been fluvially censored from the record.

The temporal distribution of the South Island RAD inventory suggests that deposit censoring has occurred over the Holocene (Fig. 2.13). Larger intervals between RA occurrence are observed in the early Holocene, whilst the record of modern deposits from 1976 is assumed to be complete (McSaveney et al., 2014). There are no temporal clusters of deposits within the inventory between ~12,000 to ~100 years ago, just individual events. Peaks in RA occurrence would be expected in the temporal record associated with preparatory and trigger factors such as deglaciation and the occurrence of high-magnitude earthquakes respectively. The current interglacial cycle and associated deglaciation began at ~11,500BP in New Zealand (Barrell, 2011). In a non-tectonic setting Ballantyne et al., (2014) have shown that there is a lag between deglaciation and the maxima in in rock-slope failure of up to ~5,000 years. However no peaked signal of RA occurrence is present within the South Island data. Additionally high-magnitude ($>M_w7$) AF ruptures are thought to recur every ~329 years (Berryman et al., 2012) and be associated with large scale landsliding, including rock-avalanching (Robinson and Davies, 2013). However, no signal of large scale rock-avalanching recurring over a similar timescale to AF ruptures is observed. The oldest co-seismic RAD in the inventory is at ~6144BP indicating that records of co-seismically generated RADs are missing from the early Holocene.

There is an increase in RA activity over the modern period 2004-2014 (McSaveney et al., 2014). McSaveney et al., (2014) have showed that RA recurrence intervals were 4 per decade for the period 1976-1999 but have increased to 20 per decade for the last decade. The contemporary increase in RA occurrence has been linked to shear strain accumulation (McSaveney et al., 2014) and possibly permafrost degradation (Allen et al., 2011). Some of the 91 deposits with no known age would help to fill gaps within the temporal record, possibly in the early Holocene. However, it is unlikely that they would account for the paucity of deposits in the early record where more RADs would be expected. The implication is that deposit censoring has likely occurred over the early-mid

Holocene period and could include a number of deglaciation and co-seismic peaks in RA occurrence.

The analysis of preconditioning, preparatory and triggering factors within the different identified mountainous regions of the South Island indicates that differing regions are controlled by differing factors. Nelson and Fiordland have the conditions necessary for RA generation in terms of preconditioning and preparatory lithological, bedding and slope factors; however the deposits are almost solely earthquake generated indicating that large ≥M_w6 earthquakes may be needed in order to generate RADs in these regions. 2,500 year return PGA values indicate that these regions are also likely to receive earthquakes which can generate RAs.

The WSA and ESA have the highest incidence of RADs with unknown trigger mechanisms. (n=149). These regions have very high shear strain measurements which is thought to be responsible for the increase in the occurrence of modern (1979-2014) RADs within the SA (McSaveney et al., 2014). However, some of the RADs with no known triggers lie towards the eastern range front of the ESA, a region with significantly lower shear strain rates than the SA interior. 2,500 year PGA models suggest that seismic activity is capable of generating many of the RADs seen in the ESA region that have no discernible trigger.

All high-mountain regions within the South Island have been shown to be able to generate RAs. The distribution of RADs, when viewed within discrete catchments shows that there are many catchments with headwaters in high-mountain regions that do not have any known RADs within them. Nelson, Marlborough and the WSA have 1-2 catchments like this within each region, whilst Fiordland has large numbers of very small catchments with the same paucity of deposits. This indicates that these catchments are good locations to search for censored RADs.

The collation of the inventory has identified Marlborough and the southern sections of the ESA and WSA as areas with no literature based coverage. Censoring of deposits has likely occurred within all mountainous regions of the South Island. The main censoring processes are different between regions (Table 5.1) but the WSA, Nelson and Fiordland are likely to be most affected by fluvial censoring processes. The identification of censoring processes throughout the regions of the South Island allows targeted research to identify new deposits based on how they have most likely been censored. Earthquake triggers are important for generating RAs within all regions and could account for many of the deposits which remain without any associated trigger mechanism, particularly for the ESA where the majority of deposits do not have an ascribed trigger. Table 5.1 provides an overview of the most likely triggering mechanisms and censoring processes operating within each region that could be used to guide future research. This table is based upon

Table 5.1 Summary table of the main triggering controls on RA generation and the main processes operating to censor deposits from the record.

Region	Main triggering control on RA occurrence	Main deposit censoring processes
Nelson	Earthquakes	Fluvial
Marlborough	Earthquakes	Fluvial, scree cover
ESA	Shear strain accumulation (modern), earthquakes	Glacial, sub-aqueous occlusion
WSA	Earthquakes, shear strain accumulation (modern)	Fluvial, vegetation cover
Fiordland	Earthquakes	Vegetation cover, sub-aqueous occlusion, fluvial

the results of Chapter 2; whilst not fully statistically quantified it provides an indication based upon the spatial distribution of trigger mechanisms and censoring processes.

Aim 2: **To examine the potential for routing and storage of fluvially reworked RAD material in South Island river catchments**

The examination of routing characteristics and storage of material within South Island catchments is useful for determining catchments where RADs may have been fluvially censored and where that material would be stored. The distribution of RADs within South Island catchments, as well as the volumetric data calculated for deposits within the inventory, indicates that relatively equal volumes of RAD material are present within the ESA, WSA and Fiordland at 3.41, 3.48 and 3.87 km^3 respectively (Fig. 2.15); however this material is distributed very differently in each region and likely has differing impacts on those systems.

The NIWA SSY model (Fig. 2.14; Hicks et al., 2011) indicates that Fiordland catchments have very low SSYs reaching the coast of ~1.3Mt/y, whilst WSA catchments produce ~62.3Mt/yr and ESA catchments ~11.4Mt/y. Hovius et al., (1997) show that for the period 1948-1986, WSA sediment discharge is dominated by landslide-derived material and that the majority of mountain denudation is done by high-magnitude, low-frequency events. This time period only includes one RA within the WSA. However the trend of highest sediment discharge being attributed to larger, less frequent events will likely be continued outside of the time period studied by Hovius et al., (1997). It can therefore be hypothesised that much of the sediment yield (suspended and bedload) observed from the WSA would be large-landslide and RAD sourced. This further

indicates, as with Aim 1, that WSA RADs are highly likely to be fluvially censored and highlights that it is more likely to be prevalent in this region than other censoring processes given the rate of sediment export within catchments. Sediment routing within the WSA shows that the majority of material has a direct conduit for fluvial transport to the ocean, this indicates that fluvially reworked RAD material within the WSA could either be deposited in fluvial aggradational material or transported to the ocean and deposited in pelagic sediments. Likely locations of reworked RAD material deposition are important for attempting to trace the existence of fluvially censored RADs.

The SSY model (Hicks et al., 2011) for the ESA suggests differing catchment routing characteristics to that of the WSA. Many of the RADs in the central and southern parts of the ESA encounter rivers which flow directly into large lakes. Sediment entering the lakes is trapped and stored as lacustrine sediment, not transported further downstream (Hicks et al., 2003). Therefore for much of the ESA region where natural and artificial dams block rivers fine-grained suspended sediment, including agglomerates, as well as coarser bedload will be captured within these lakes. Some catchments in the northern section of the ESA have similar lake barriers to the transport of suspended sediment downstream, such as Lake Coleridge on the Rakaia River or Lake Sumner on the Hurunui River. However some display similar characteristics to the WSA with clear pathways to the ocean (Fig. 2.18). Instead of large sediment yields making it to the ocean in the ESA the signal is attenuated before the coast by a reduction in river slope (Hicks et al., 2011) over the SA mountain range front and the Canterbury Plains. This infers that the majority of fluvially reworked RAD material in the ESA is going to either be captured in lakes or deposited in fluvial aggradational material upstream of lakes; except for those few catchments in the north of the region where material will likely be deposited on the Canterbury Plains.

Based upon the examination of SSY and sediment routing characteristics from the ESA and WSA it is likely that RAD material will have longer residence times within the Nelson and Marlborough regions. SSYs are orders of magnitude lower in these regions than that of the ESA and WSA indicating a reduced export of material out of catchments, owing to lower AAR (Wratt et al., 2006; NIWA, 2015). Therefore RAD material would be expected to remain in-situ for a long time or slowly be reworked down fluvial systems. Although Fiordland has higher AAR than Nelson and Marlborough residence times of material would still be high due to the dense rainforest vegetation cover on deposits which acts to stabilise material and prevent fluvial erosion. Hicks et al., (1996) cite the rainforest cover as a factor in lower SSYs for the Fiordland region. Material that is able to be reworked by fluvial processes does in most cases, for Nelson, Marlborough and Fiordland, have clear routing pathways to the ocean or fiords.

The area of Quaternary deposition within the catchment (Edbrooke et al., 2014) can be used as an indicator of the available space into which RAD material can be reworked to (Robinson et al., 2016). Analysis of the area available for terrestrial deposition of material before reaching oceans along with the initial volume of RAD material available shows that smaller WSA, Fiordland and some Nelson catchments would store higher concentrations of material as the ratio of available RAD material to area of depositional area is higher. Given the analysis of SSYs and the remobilisation of material within catchments this data implies that the likelihood of detecting fluvially reworked RAD material would likely be highest in WSA catchments and potentially parts of Nelson.

Aim 3: **To ascertain whether agglomerates can be effectively utilised to trace fluvially reworked RA material through river systems as a diagnostic tool for detecting fluvially censored RADs.**

Examination of material from in-situ RADs as well as detailed and random spot sampling of fluvial material in Nelson and WSA river catchments indicates that agglomerates, in the 63µm-1mm grain size fraction, can be located within aggradational dam breach flood deposits proximal to source RADs up to ~0.8km downstream (Fig. 3.14 and Fig. 3.15). Further to this, agglomerates are not present in contemporary fluvial deposits in the sampled catchments, reducing their effectiveness as a long distance sedimentological tracer of RADs in the size ranges analysed.

Samples for examination were collected in the Nelson and WSA regions, both of which have been shown in Aim 2 to be good candidates for RAD sediment storage. However the sedimentology suggests it is difficult to ascertain if this is the case. Agglomerates appear to be preserved during short term fluvial transport processes as they are deposited in dam-break flood materials. No evidence of them was detected in fluvial material downstream indicating that a number of processes could be at work to make the agglomerate signal undetectable: (1) The strong electrostatic bonding that binds agglomerate grains together could be broken by shear stresses or water penetration in turbulent flows causing grain dis-agglomeration and loss of the sedimentological signal; (2) Limitations to the sediment being supplied to the studied river systems as they are not always actively eroding RADs. Additionally material being eroded from RADs is not completely comprised of agglomerates. SEM samples analysed in this project show that agglomerates are not present within all parts of the sampled deposits as they are likely created and destroyed during RA motion (Mauri McSaveney, 2016 pers. comm.); (3) Dilution of river bedload and suspended load downstream of RADs by sediment from upstream as well as the input from tributary rivers downstream. Tributary rivers have been shown to significantly alter the composition of fluvially transported material in trunk rivers (Cox and Nibourel, 2015; Harrison et al., 2015), which could aid to rapidly dilute any

agglomerate signal; (4) Agglomerate rich fluvial aggradational layers can be buried under subsequent aggradational events, in this case archives of material will likely be present in valley confined, mountain river systems around the world.

Processes occurring during the fluvial reworking and censoring of RA material may have significant impacts on the detectability of material. Agglomerate particles are produced in fine-grained, dry, granular material under intense overburdening pressure where electrostatic and Van de Waals forces can 'agglomerate' material together (Jones and Hodges, 2004; Castellanos, 2005; Reznichenko et al., 2012). SEM micrographs indicate that agglomerates can have small microscopic spaces within the matrix material or at the contact between larger grains and the matrix. These spaces are important in terms of the disaggregation of material if water can penetrate the interior of the grain. Water entering both relatively large and small pore spaces can diminish the electrostatic force between particles replacing them with capillary and liquid-bridging forces (Zhu, 2004). Here it is hypothesised that this change of interparticulate forces, plus the shear placed on the agglomerate grain during fluvial transport is able to dis-agglomerate the material, removing the diagnostic signal from the sedimentary record. It is possible that the areas inside agglomerates where this would be of greatest effect is pore spaces between large grains and the fine-grained matrix; here the surface-area available for bonding is relatively low compared to that of just small sub-micron particles within the matrix, therefore becoming a weakness within the agglomerate particle.

Additionally to dis-agglomeration other fluvial processes serve to shred the agglomerate signal through the river systems. Storage of reworked RAD material in aggradational sedimentary sequences, which can remain un-reworked or subsequently be buried, will remove the sedimentary signature. Coulthard and Van de Wiel (2013) have previously shown that storage of material within catchments can dampen the downstream sedimentary signal of basin uplift in small catchments, whilst further dilution of material can occur through sediment delivery from tributary streams. This 'shredding' of the agglomerate signal in fluvial environments makes the identification of fluvially censored RADs through this method of diagnostic particle tracing very difficult. Aggradational terraces associated with dam breaches as well as buried sedimentary sequences present the best locations for identifying agglomerate particles within fluvial material.

Aim 4: **To examine the redistribution and storage of RA material in NZ river systems by modelling an idealised river system in a laboratory based micro-scale flume**

Examination of the morphological and sedimentological impacts of RAD dam breach floods in the idealised river system has shown that large quantities of dam material are fluvially reworked during the initial failure of the dam (Fig. 4.23). This is not unexpected when dealing with catastrophic failure of RAD dams and has shown to be the

case for numerous dams in valley confined NZ catchments such as the Poerua River (Hancox et al., 2005) and Ram Creek (Nash et al., 2008). Similarly the immediate deposition of the eroded dam material within dam proximal locations occurs both in the model and can be supported by field evidence from Ram Creek (Harrison et al., 2015) and the Stanley river catchments in NZ where aggradational terraces exist at the base of breach and overflow channels respectively. Similarly much of the eroded material from the Poerua dam breach flood was deposited as deep aggradational deposits in the alluvial flats and gorges downstream of the dam (Hancox et al., 2005).

The initial dam break deposits proximal to the dam as well as material that was deposited at higher elevation by the dam break flood further down the flume model were for the most part preserved throughout model runs. The exception to this being when avulsion activity on the braidplain of the model was able to erode into higher preserved terraces. This storage of material in the upper portion of the model preserves the RAD signature in the sedimentary architecture but also 'shreds' the signal further downstream (Table 4.4). In the model reaches that are distal to the RAD were deprived of much of the RA sediment and a concentration gradient from highly concentrated RA material to very low concentrations is shown from dam proximal to dam distal locations. This is much like the processes modelled by Coulthard and Van de Wiel (2013) where sedimentary signals of uplift and climate that are detectable in upper reaches of catchments are diminished downstream due to storage of material within certain reaches of the system.

This storage and preservation of reworked material in the model, which is clearly sourced from the RAD due to the visible UV sand, indicates that the highest concentrations of RA material in NZ prototype rivers systems are likely to be in gorge and alluvial flat reaches downstream of dams. However, the signal further downstream is likely to become rapidly shredded by storage effects and dilution from tributary material (Coulthard and Van de Wiel, 2013; Cox and Nibourel, 2015). Further observations from the end of each model run showed that burial of the majority of reworked RAD derived material occurred in the dam proximal alluvial flat and gorge reaches; preserving concentrated layers of RAD material in the sub-surface sedimentary architecture (Fig. 4.25 and Table 4.5). This indicates that the visible fluvially reworked RAD material currently seen in NZ prototype catchments, such as Ram Creek and the Stanley River, are likely to be buried in the future. However, the process of burial only occurred in the model once the dam had been removed from the system. An indication of the model timescale is not possible with the micro-scale flume, therefore this process is only hypothesised here to take place on a 10^2-10^3 year timescale in NZ prototype rivers. This hypothesis is surmised as the Poerua River, Ram Creek and Stanley River dams are all between 18-49 years old and still have large quantities of RAD material that needs to be

removed before reaching the next phase of channel development shown in the flume model.

Ultimately, the flume modelling shows that the best preserved evidence for reworked RAD material is in dam proximal locations and likely derived from dam break floods. Dam break deposits from historic RADs in NZ prototype rivers will be relatively fresh and available for sampling. However, modelling suggests that in terms of detecting fluvially reworked RAD material from pre-historic deposits the sedimentary evidence is likely buried in valley confined alluvial flats and gorges. Therefore, in order to detect fluvially censored RADs and begin to use the agglomerate tracing methodology presented in Chapter 3 samples need to be exhumed from underneath coarsely armoured aggradational reaches in prototype rivers.

The research suggests a number of criteria for use in the field, on aerial photo analysis and in the laboratory that would help inform the search for sedimentological evidence of fluvially censored RADs in the future:

1. Potential RADs may be identified as large, hummocky, lobate, cross-valley deposits. They may be breached and therefore a river will likely run through the deposit on the opposite side of the valley to the deposit source where the dam is lower (Fig. 4.6). RADs often have small ponds on the deposit surface.
2. Valley confined alluvial flats and gorges are likely to store coarse RAD material. Higher concentrations are likely to be proximal to any censored RAD. RAD material is likely to be highly fractured in dam proximal locations. Under a SEM coarse material from an RAD may be highly fractured (i.e. Poerua River grains in Fig. 3.16).
3. Fine-grained material containing agglomerates is likely to be stored in lower energy environments such as backwaters, lakes and the ocean. These types of environment should be targeted for sampling. Agglomerates may also be found in in-situ RAD material and material in deposit proximal locations.
4. The presence of incised outwash-fan terrace sequences, raised above the river level, in valley-confined alluvial flats may suggest the presence of a breached natural dam upstream, such as an RAD (e.g. Stanley River and Ram Creek).
5. Preserved flood and/or debris flow deposits, in valley-confined reaches, may also be indicative of large dam breach floods. Debris flows indicate large scale sediment availability at the time of deposition, which could be easily sourced from a RAD breach. These deposits may have varying stands of vegetation which could indicate relative timescales of deposition. RAD breach flood derived facies could be buried underneath subsequent deposition from normal fluvial processes.
6. Aggradation of river channels with large calibre material. This could lead to frequent channel avulsions driven by the excess of sediment within the fluvial

system. Channel avulsions could be seen in valley-confined reaches or on mountain rangefront braidplains.

5.3 Conclusions

The following section will discuss how the material from each of the thesis chapters is related to each other and how they can be used together to inform our understanding of RAD distribution and censoring.

1. The spatial and temporal distribution or RADs within the South Island, NZ suggests that censoring of deposits has occurred. The WSA, Marlborough, Fiordland, Nelson and southern ESA regions all display signs of RAD censoring within the deposit distributions in some form or other. All of these regions have the topography, relief and triggering mechanisms which would be expected to produce greater numbers of RAs than are observed. Rainfall, narrow valleys and steep relief make the mountainous regions of South Island susceptible to fluvial censoring of RADs. This could explain the paucity of deposits, not over ice, that exist in the WSA as well as why the Nelson region displays a majority of recent, post-1929 earthquake generated RADs and very little evidence for earlier deposits.

2. Analysis of agglomerate samples and flume based modelling show that the sedimentological signal of RADs is rapidly shredded within the fluvial environment.

    - In terms of traceability of RADs in fluvial systems, agglomerates are key to identifying reworked RAD material. The results from Chapter 3 indicate there are several factors that make the agglomerate signal very difficult to trace except in dam proximal deposits linked to dam breach outburst floods; the supply of RAD sediment to the fluvial system, dis-agglomeration, dilution of the RAD material and burial of discrete layers of RAD rich material by fluvial aggradational processes.
    - The micro-scale model shows the preservation of a dam proximal sedimentary signal in an alluvial flat as well as the catchment scale shredding of the RAD signal downstream. These results further support the agglomerate results that sediment supply, dilution and burial processes are at work and could account for the difficulty in tracing fluvially reworked RAD derived sediment.

3. Glacial and fluvial processes are the only censoring mechanisms that actively remove the deposit away from the area of deposition. Furthermore, fluvial censoring is the only process that actively erodes in-situ RADs. This suggests that fluvially censored RADs will be much more difficult to locate than their glacially reworked and alternatively censored counterparts. Fluvial censoring of RADs has not received research attention

in terms of how to trace and quantify the loss of these deposits. Knickpoints in river long profiles can give an indication to the presence of large, censored landslide deposits that has previously dammed a river (Korup, 2006b); however these profile features can be developed by different processes and do not necessarily represent the occurrence of a RA specifically. This thesis is the first to try and develop a diagnostic method for tracing RAD material through the fluvial system. Whilst acknowledging that the method requires further work it has been shown that agglomerates from RADs can be traced for short distances downstream of RAD deposits.

4. Fluvial censoring has been shown to be more complex than simply eroding a RAD and depositing material elsewhere.

    - Firstly agglomerate grains were found in dam proximal deposits that are thought to be associated with dam-breach floods (Fig. 5.1b-c), the flume modelling supports this by showing that the majority of RA dam material was deposited immediately downstream of the deposit in alluvial flats rather than being transported large distances downstream (Fig. 5.1d).

    - Secondly, field studies had hypothesised that burial of concentrated RAD derived material would be an important factor in the non-detection of agglomerates within fluvial sediment (Fig. 5.1e). To support this the flume model showed that dam proximal deposition could be rapidly buried by base-level sediment flux of fluvially derived material from upstream of the breached dam.

    - Thirdly, field studies hypothesised that dilution of reworked RAD material would occur and obscure the agglomerate tracer signal. The flume model supports this hypothesis as dam proximal locations showed high concentrations of material immediately after breaching of the dam whereas dam distal locations showed a dilution of the signal. As the flume model progressed more RAD material was transported downstream, however not in high concentrations.

5. The analysis of sediment routing of RAD material within the South Island shows that there was potential for large sedimentary archives of material stored within lake environments. The examination of agglomerate grains within South Island rivers suggests that although fine-grained RAD material will likely be transported to these lakes it would be difficult to identify the material as being RA in origin due to the dilution and dis-agglomeration of the sedimentary signal. It is possible that agglomerates may survive within smaller grain size fractions and be more resistant to

dis-agglomeration but this has yet to be shown. Field and laboratory results have shown that fluvial aggradational features within valley confined reaches are also likely to hold viable sedimentary archives of fluvially censored RADs, where agglomerates may be identified (Fig. 5.1f).

6. The majority of fluvial material sampled does not contain RA agglomerate grains. Instead agglomerates appear to be present in discrete aggradational regions of sampled river systems. This means that the agglomerate signal is useful in finding discrete layers of sediment (Fig. 5.1f) which can be dated and then associated with a particular RA breaching event. Given the 80% likelihood of an RA dam breach occurring within the first year of its emplacement, an age calculated for fluvial aggradational material through radiocarbon or optically stimulated luminescence (OSL), is likely to be similar to that of the occurrence of the RA.

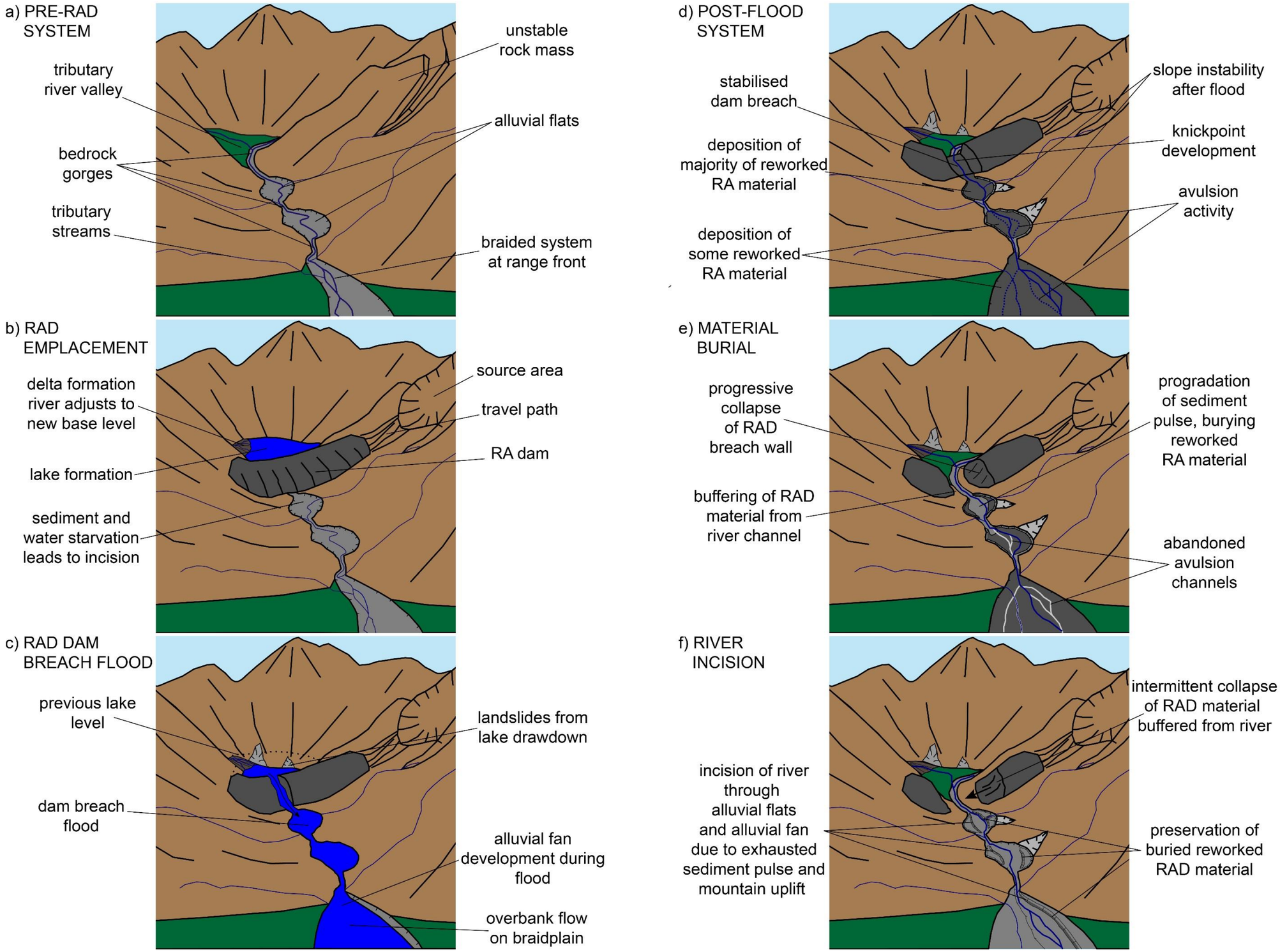

Fig. 5.1 Conceptual model of river evolution and reworked RAD material storage within a high mountain fluvial system

5.4 Limitations of this research

Although this thesis has attempted to mitigate potential limitations of the research there are some inherent limitations within the areas covered.

1. The inventory that was produced for the thesis is presumed to be incomplete, as no landslide database can ever be fully complete. Given the time covered by the inventory it is expected that deposits will have been censored from the sedimentological record, therefore not allowing a full examination of the RA distribution of the South Island. The issue of inventory completeness is further compounded by the research bias towards certain high mountain regions within the South Island which have received greater attention. The literature used to compile the inventory for this study was centred around two main regions, firstly the high Southern Alps where much of the modern RA activity is located and has relevance to contemporary societal issues such as climate change. Secondly the Nelson region is extensively covered as event based inventories were collated subsequent to the 1929 Murchison and 1968 Inangahua earthquakes. This bias exists as in the short term these regions require rapid hazard assessment when these events occur. However, this leaves notable high-mountain regions in the lower ESA/WSA and Marlborough, where modern RA generating events have not occurred, with little to no research attention in terms of the occurrence of prehistoric RADs.
2. Values for deposit area and volumes are difficult to quantify and it is often unclear how values in the literature have been calculated. An attempt was made in this thesis to rectify this by remapping deposit areas and calculating volumes from these areas. However, this does not account for the potential of valley confinement of deposits and pre-RAD valley topography; both of which have an impact on the mapped deposit areas and therefore volumes. An error margin has been calculated within the RAD inventory in order to try and account for this.
3. Within the analysis of fluvial sediment for the identification of agglomerate grains only the 63µm-1mm grain size fraction was examined and therefore the existence of modified <63µm agglomerate grains cannot be ruled out.
4. The flume modelling aimed to represent, within reason, prototype South Island river systems. However, the model was unable to include the rapid uplift experienced on South Island as well as perturbations in climate, river discharge and sediment flux. This means that some fluvial processes are not represented in the model. This includes seasonal flooding, reworking of sediment from other landslide events and river incision due to progressive base level changes driven by mountain uplift.

5. Although micro-scale modelling is practical in terms of examining broad-scale morphological changes there are a number of limitations from both a model dynamics and real-world prototype perspective. Firstly, a relative timescale for model to prototype comparisons cannot be reliably derived. Secondly, the micro-scale flume model is unable to provide quantitative data on the aggradation of the model which can then be reliably upscaled to NZ prototype rivers (Davies et al., 2003). Thirdly, the experiment described here only deals with a single large landslide dam into the idealised river system. The dam is also only positioned in the upper gorge section. Observations and data from NZ indicate that multiple landslide dams may be expected from either a single RA (i.e. Poerua) or from the triggering of many RAs in the same event (i.e. earthquakes). Finally, the configuration of the model, in terms of the succession of environments (gorge, alluvial flat, gorge etc.) was the same for all model runs, there would need to be further model runs with differing landscape configurations to determine how this might affect the impacts of RAD emplacement on fluvial systems.

5.5 Suggestions for future research

This research has focussed on the distribution of RADs within the South Island and has made progress into understanding the censoring processes acting within differing regions of the South Island, NZ. Additionally it has explored the potential for using a micro-sedimentological tracing technique in order to trace fluvially censored RADs in aggradational material. The following section will outline some avenues for future work based on this research.

1. The inventory compiled for the examination of the distribution of RADs within the South Island has incomplete attributes for some of the deposits listed. It would be beneficial to have age information for all deposits in order to build up a better understanding of the temporal gaps within the RAD distribution. Ages for deposits could be attained from Cosmogenic Nuclide dating of deposit surfaces, Radiocarbon dating of organic material or OSL dating of quartz material buried in deposits. Floral and faunal remains have been located within many deposits which would allow Radiocarbon dating of RAD emplacement. Additionally more deposits could be ground-truthed to confirm their status as RADs. This is especially true of the 47 potential RADs located through aerial image analysis in this thesis.
2. Further work could be conducted on the presence of agglomerates within fluvial environments. As this thesis has established locations where agglomerates rich material is likely to be present, specifically targeted sample collection could be conducted in alluvial flats and gorges to locate dam break flood deposits which may have evidence of fluvially censored RADs. If targeting certain aggradational

deposits it is possible that Radiocarbon, Cosmogenic Nuclide or OSL dating could be conducted to estimate an age for material containing agglomerates and constrain dates for dam break floods from RADs.

3. More analysis needs to be undertaken of the <63µm GSF for the presence of dis-agglomerated grains. This GSF was not analysed within this project, If agglomerate grains dis-agglomerate during fluvial transport, as has been hypothesised within this thesis, smaller fragments may survive in fluvial backwater, lacustrine or pelagic sediment downstream than could be detected with the <63µm GSF. These environments are more likely to contain dis-agglomerated grains as <63µm material would likely be carried in suspension by rivers away from the source deposit.
4. The flume modelling could be used to examine scaled versions of prototype NZ rivers such as the Poerua River or Ram Creek. The novel UV sand method could then be employed to examine the redistribution of material within specific river systems and model potential future impacts of the RAD input.
5. One aspect of the flume modelling that was not addressed was the presence of multiple deposits residing within the same river system; a situation which is relatively common in the ESA region of the South Island. Using the UV sand technique multiple deposits could be modelled using differing colours of UV sand. The UV sand location extraction technique applied in this thesis could be adapted to detect differing sand colours and infer the impact of multiple deposits within the same fluvial system.

References

Allen S., Owens I., and Huggel C., (2008) A first estimate of mountain permafrost distribution in the Mount Cook region of New Zealand's Southern Alps, In: Kane D, Hinkel K (eds) *9th International Conference on Permafrost, Fairbanks, Alaska*. Institute of Northern Engineering, pp 37–42

Allen S., Cox S., and Owens I., (2011) Rock avalanches and other landslides in the central Southern Alps of New Zealand: a regional study considering possible climate change impacts, *Landslides*, **8**, 33–48. doi: 10.1007/s10346-010-0222-z

Allen S. and Huggel C., (2013) Extremely warm temperatures as a potential cause of recent high mountain rockfall, *Global and Planetary Change*, **107**, 59–69. doi: 10.1016/j.gloplacha.2013.04.007

Ballantyne C., Sandeman G., Stone J., and Wilson P., (2014) Rock-slope failure following Late Pleistocene deglaciation on tectonically stable mountainous terrain, *Quaternary Science Reviews*, **86**, 144–157. doi: 10.1016/j.quascirev.2013.12.021

Barnard P., Owen L., Sharma M., and Finkel R., (2001) Natural and human-induced landsliding in the Garhwal Himalaya of northern India, *Geomorphology*, **40**, 21–35. doi: 10.1016/S0169-555X(01)00035-6

Barrell D., (2011) Quaternary glaciers of New Zealand, *Developments in Quaternary Science*, **15**, 1047–1064. doi: 10.1016/B978-0-444-53447-7.00075-1

Barringer J., Pairman D., and McNeill S., (2002) Development of a high-resolution digital elevation model for New Zealand, *Landcare Research Contract Report: LC0102/170*,

Barth N., (2012) A tectono-geomorphic study of the Alpine Fault, New Zealand, *PhD Thesis*, University of Otago

Barth N., (2014) The Cascade Rock Avalanche: implications of a very large Alpine Fault-triggered failure, New Zealand, *Landslides*, **11**, 327–341. doi: 10.1007/s10346-013-0389-1

Beavan J., Ellis S., Wallace L., and Denys P., (2007) Kinematic constraints from GPS on oblique convergence of the Pacific and Australian Plates, central South Island, New Zealand, In: Okaya D, Stern T, Davey F (eds) *A Continental Plate Boundary: Tectonics at South Island, New Zealand, AGU Geophysical Monograph series, Volume 175*. American Geophysical Union, Washington, D.C., pp 75–94

Bennett G., Miller S., Roering J., and Schmidt D., (2016) Landslides, threshold slopes, and the survival of relict terrain in the wake of the Mendocino Triple Junction, *Geology*, **44**, 363–366. doi: 10.1130/G37530.1

Berryman K., (1980) Late quaternary movement on White Creek Fault, South Island, New Zealand, *New Zealand Journal of Geology and Geophysics*, **23**, 93–101. doi: 10.1080/00288306.1980.10424194

Berryman K., (2005) Review of tsunami hazard and risk in New Zealand, *Institute of Geological & Nuclear Sciences client report 2005/104*,

Berryman K., Cochran U., Clark K., Biasi G., Langridge R., and Villamor P., (2012) Major earthquakes occur regularly on an isolated plate boundary fault, *Science*, **336**, 1690–1693. doi: 10.1126/science.1218959

Bessette-Kirton E. and Coe J., (2016) Inventory of rock avalanches in western Glacier Bay National Park and Preserve, Alaska, 1984-2016: a baseline data set for evaluating the impact of climate change on avalanche magnitude, mobility, and frequency, *US Geological Survey Data Release*,

Biasi G., Langridge R., Berryman K., Clark K., and Cochran U., (2015) Maximum-likelihood recurrence parameters and conditional probability of a ground-rupturing earthquake on the southern Alpine Fault, South Island, New Zealand, *Bulletin of the Seismological Society of America*, **105**, 94–106. doi: 10.1785/0120130259

Blikra L., Longva O., Harbitz C., and Lovholt F., (2005) Quantification of rock-avalanche and tsunami hazard in Storfjorden , western Norway, In: Senneset K, Flaate K and Larsen J (eds) *Landslides and Avalanches: ICFL 2005, Norway*. pp 57–64

Blikra L., Longva O., Braathen A., Anda E., Dehls J., and Stalsberg K., (2006) Rock slope failures in Norwegian fjord areas: Examples, spatial distribution and temporal pattern, In: Evans S, Scarascia Mugnozza G, Strom A, Hermanns R (eds) *Landslides from Massive Rock Slope Failure*. Springer Netherlands, Dordrecht, pp 475–496

Blöthe J., Korup O., and Schwanghart W., (2015) Large landslides lie low: Excess topography in the Himalaya-Karakoram ranges, *Geology*, **43**, 523–526. doi: 10.1130/G36527.1

Bodin X., Schoeneich P., Deline P., Ravanel L., Magnin F., Krysiecki J., and Echelard T., (2015) Mountain permafrost and associated geomorphological processes: recent changes in the French Alps, *Journal of Alpine Research | Revue de Géographie Alpine*, **103**, 2–16. doi: 10.4000/rga.2885

Bornhold B., Harper J., McLaren D., and Thomson R., (2007) Destruction of the first nations village of Kwalate by a rock avalanche-generated tsunami, *Atmosphere-Ocean*, **45**, 123–128. doi: 10.3137/ao.450205

Bornhold B. and Thomson R., (2012) Tsunami hazard assessment related to slope failures in coastal waters, In: Clague J, Stead D (eds*) Landslides: Types, Mechanisms and Modeling*. Cambridge University Press, pp 108–120

Brardinoni F. and Church M., (2004) Representing the landslide magnitude–frequency relation: Capilano River basin, British Columbia, *Earth Surface Processes and Landforms*, **29**, 115–124. doi: 10.1002/esp.1029

Brunetti M., Guzzetti F., and Rossi M., (2009) Probability distributions of landslide volumes, *Nonlinear Processes in Geophysics*, **16**, 179–188. doi: 10.5194/npg-16-179-2009

Brunetti M., Guzzetti F., Cardinali M., Fiorucci F., Santangelo M., Mancinelli P., Komatsu G., and Borselli L., (2014) Analysis of a new geomorphological inventory of landslides in Valles Marineris, Mars, *Earth and Planetary Science Letters*, **405**, 156–168. doi: 10.1016/j.epsl.2014.08.025

Burbank D. and Anderson R., (2011) *Tectonic geomorphology*. Wiley-Blackwell

Castellanos A., (2005) The relationship between attractive interparticle forces and bulk behaviour in dry and uncharged fine powders, *Advances in Physics*, **54**, 263–376. doi: 10.1080/17461390500402657

Castleton J., Moore J., Aaron J., Christl M., and Ivy-Ochs S., (2016) Dynamics and legacy of 4.8 ka rock avalanche that dammed Zion Canyon, Utah, USA, *GSA Today*, **26**, 4–9. doi: 10.1130/GSATG269A.1

Cenderelli D., (2000) Floods from natural and artificial dam failure, In: Wohl E (ed) *Inland Flood Hazards: Human, Riparian, and Aquatic Communities*. Cambridge University Press, pp 73–103

Chevalier G., (2008) The Wanganui-Wilberg Rock Avalanche: deposit, dynamics and dating, *MSc Thesis*, University of Canterbury

Chevalier G., Davies T., and McSaveney M., (2009) The prehistoric Mt Wilberg Rock Avalanche, Westland, New Zealand, *Landslides*, **6**, 253–262. doi: 10.1007/s10346-009-0156-5

Clague J., (2013) Landslide, In: Bobrowsky P (ed) *Encyclopedia of Earth Sciences Series - Encyclopedia of Natural Hazards*. Springer Netherlands, pp 594–602

Clarke B. and Burbank D., (2010) Bedrock fracturing, threshold hillslopes, and limits to the magnitude of bedrock landslides, *Earth and Planetary Science Letters*, **297**, 577–586. doi: 10.1016/j.epsl.2010.07.011

Costa J. and Schuster R., (1988) The formation and failure of natural dams, *Geological Society of America Bulletin*, **100**, 1054–1068. doi: 10.1130/0016-7606(1988)100<1054

Coulthard T. and Van de Wiel M., (2013) Climate, tectonics or morphology: what signals can we see in drainage basin sediment yields?, *Earth Surface Dynamics*, **1**, 13–27. doi: 10.5194/esurf-1-13-2013

Cowan H., Nicol A., and Tonkin P., (1996) A comparison of historical and paleoseismicity in a newly formed fault zone and a mature fault zone, North Canterbury, New Zealand, *Journal of Geophysical Research*, **101**, 6021–6036. doi: 10.1029/95JB01588

Cox S. and Barrell D., (2007) Geology of the Aoraki area, *Institute of Geological & Nuclear Sciences 1:250 000 geological map 15*,

Cox S., McSaveney M., Spencer J., Allen S., Ashraf S., Hancox G., Sirguey P., Salichon J., and Ferris B., (2015) Rock avalanche on 14 July 2014 from Hillary Ridge, Aoraki/Mount Cook, New Zealand, *Landslides*, **12**, 395–402. doi: 10.1007/s10346-015-0556-7

Cox S. and Nibourel L., (2015) Bedload composition, transport and modification in rivers of Westland, New Zealand, with implications for the distribution of alluvial pounamu (jade), *New Zealand Journal of Geology and Geophysics*, **58**, 154–175. doi: 10.1080/00288306.2015.1025799

Cui Y., Parker G., Lisle T., Gott J., Hansler-Ball M., Pizzuto J., Allmendinger N., and Reed J., (2003) Sediment pulses in mountain rivers: 1. Experiments, *Water Resources Research*, **39**, doi: 10.1029/2002WR001803

Davies T., (2007) Shotover river sediment management: Microscale modelling, *Final report to Otago Regional Council*,

Davies T. and McSaveney M., (1999) Runout of dry granular avalanches, *Canadian Geotechnical Journal*, **36**, 313–320. doi: 10.1139/t98-108

Davies T., McSaveney M., and Hodgson K., (1999) A fragmentation-spreading model for long-runout rock avalanches, *Canadian Geotechnical Journal*, **36**, 1096–1110. doi: 10.1139/t99-067

Davies T. and Korup O., (2007) Persistent alluvial fanhead trenching resulting from large, infrequent sediment inputs, *Earth Surface Processes and Landforms*, **32**, 725–742. doi: 10.1002/esp.1410

Davies T. and McSaveney M., (2002) Dynamic simulation of the motion of fragmenting rock avalanches, *Canadian Geotechnical Journal*, **39**, 789–798. doi: 10.1139/t02-035

Davies T., McSaveney M., and Clarkson P., (2003) Anthropic aggradation of the Waiho River, Westland, New Zealand: microscale modelling, *Earth Surface Processes and Landforms*, **28**, 209–218. doi: 10.1002/esp.449

Davies T. and McSaveney M., (2007) Dynamic rock fragmentation in grain flow: application to large mass movements, *Geophysical Research Abstracts*, **9**, **3133**,

Davies T., McSaveney M., and Deganutti A., (2007) Dynamic fragmentation causes low rock-on-rock friction, In: Eberhardt E, Stead D, Morrison T (eds) *Rock Mechanics-Meeting Society's Challenges and Demands*. Taylor and Francis, pp 959–966

Davies T. and McSaveney M., (2009) The role of rock fragmentation in the motion of large landslides, *Engineering Geology*, **109**, 67–79. doi: 10.1016/j.enggeo.2008.11.004

Davies T. and Korup O., (2010) Sediment cascades in active landscapes, In: Burt T, Allison R (eds) *Sediment Cascades: An Integrated Approach*. John Wiley and Sons, pp 89–115

Davies T. and McSaveney M., (2011) Rock-avalanche size and runout–implications for landslide dams, In: Evans S, Hermanns R, Strom A, Scarasda-Mugnozza G (eds) *Natural and Artificial Rockslide Dams - Lecture Notes in Earth Science*. Springer Berlin Heidelberg, pp 441–462

Davies T., Campbell B., Hall B., and Gomez C., (2013a) Recent behaviour and sustainable future management of the Waiho River, Westland, New Zealand, *Journal of Hydrology (NZ)*, **52**, 27–42.

Davies T., Warburton J., Dunning S., and Bubeck A., (2013b) A large landslide event in a post-glacial landscape: Rethinking glacial legacy, *Earth Surface Processes and Landforms*, **38**, 1261–1268. doi: 10.1002/esp.3377

Deganutti A., (2008) The hypermobility of rock avalanches, *PhD Thesis*, Universita' Degli Studi Di Padova

Deline P., Hewitt K., Reznichenko N., and Shugar D., (2015) Rock avalanches onto glaciers, In: Davies T, Shroder J (eds) *Landslide Hazards, Risks and Disasters*. Elsevier, pp 263–319

Digital-Globe., (2013) Digital Globe Foundation 2009 & 2013 map imagery - Poerua River, Accessed: 09/2013

Dortch J., Owen L., Haneberg W., Caffee M., Dietsch C., and Kamp U., (2009) Nature and timing of large landslides in the Himalaya and Transhimalaya of northern India, *Quaternary Science Reviews*, **28**, 1037–1054. doi: 10.1016/j.quascirev.2008.05.002

Downes G., (1995) Atlas of isoseismal maps of New Zealand earthquakes, *Institute of Geological & Nuclear Sciences monograph 11*. Institute of Geological and Nuclear Sciences Limited

Dufresne A., Davies T., and McSaveney M., (2009) Influence of runout-path material on emplacement of the Round Top Rock Avalanche, New Zealand, *Earth Surface Processes and Landforms*, **35**, 190–201. doi: 10.1002/esp.1900

Dufresne A., Bösmeier A., and Prager C., (2016a) Sedimentology of rock avalanche deposits–case study and review, *Earth-Science Reviews*, **163**, 234–259. doi: 10.1016/j.earscirev.2016.10.002

Dufresne A., Prager C., and Bösmeier A., (2016b) Insights into rock avalanche emplacement processes from detailed morpho-lithological studies of the Tschirgant deposit (Tyrol, Austria), *Earth Surface Processes and Landforms*, **41**, 587–602. doi: 10.1002/esp.3847

Dunning S., (2006) The grain-size distribution of rock avalanche deposits in valley-confined settings, *Italian Journal of Engineering Geology and Environment*, **1**, 117–121. doi: 10.4408/IJEGE.2006-01.S-15

Dunning S., Petley D., and Rosser N., (2005) The morphology and sedimentology of valley confined rock-avalanche deposits and their effect on potential dam hazard, In: Hungr O, Fell R, Couture R, Eberhardt E (eds) *Landslide Risk Management: Proceedings of the International Conference on landslide risk management, Vancouver, Canada, 31 May-3 June 2005*. Taylor & Francis, London, pp 691–701

Dunning S., Rosser N., Petley D., and Massey C., (2006) Formation and failure of the Tsatichhu landslide dam, Bhutan, *Landslides*, **3**, 107–113. doi: 10.1007/s10346-005-0032-x

Dunning S., Mitchell W., Rosser N., and Petley D., (2007) The Hattian Bala Rock Avalanche and associated landslides triggered by the Kashmir Earthquake of 8 October 2005, *Engineering Geology*, **93**, 130–144. doi: 10.1016/j.enggeo.2007.07.003

Dunning S. and Armitage P., (2011) The grain-size distribution of rock-avalanche deposits: Implications for natural dam stability, In: Evans S, Hermanns R, Strom A, Scarascia Mugnozza G (eds) *Natural and Artificial Rockslide Dams - Lecture Notes in Earth Sciences*. Springer Berlin Heidelberg, pp 479–498

Dunning S., Rosser N., McColl S., and Reznichenko N., (2015) Rapid sequestration of rock avalanche deposits within glaciers, *Nature Communications*, **6**, 7964. doi: 10.1038/ncomms8964

Dykstra J., (2012) The post-LGM evolution of Milford Sound, Fiordland, New Zealand: Timing of ice retreat, the role of mass wasting and implications for hazards, *PhD Thesis*, University of Canterbury

Edbrooke S., Heron D., Forsyth P., and Jongens R., (2014) QMap geological map of New Zealand 1:1 000 000, In: *GNS Science Geological Map 2*. GNS Science, Lower Hutt, New Zealand,

Ermini L. and Casagli N., (2003) Prediction of the behaviour of landslide dams using a geomorphological dimensionless index, *Earth Surface Processes and Landforms*, **28**, 31–47. doi: 10.1002/esp.424

Evans D., (2008) Geomorphology: Avalanches and moraines, *Nature Geoscience*, **1**, 493–494. doi: 10.1038/ngeo255

Evans S., (1989) The 1946 Mount Colonel Foster rock avalanche and associated displacement wave, Vancouver Island, British Columbia, *Canadian Geotechnical Journal*, **26**, 447–452. doi: 10.1139/t89-057

Evans S. and Clague J., (1999) Rock avalanches on glaciers in the Coast and St. Elias Mountains, British Columbia, In: *Slope stability and landslides - Proceedings of the 13th annual Vancouver Geotechnical Society Symposium*. pp 115–123

Evans S., Mugnozza G., Strom A., Hermanns R., Ischuk A., and Vinnichenko S., (2006) Landslides from massive rock slope failure and associated phenomena, In: Evans S, Mugnozza G, Strom A, Hermanns R (eds) *Landslides from Massive Rock Slope Failure*. pp 3–52

Fischer L., Purves R., Huggel C., Noetzli J., and Haeberli W., (2012) On the influence of topographic, geological and cryospheric factors on rock avalanches and rockfalls in high-mountain areas, *Natural Hazards and Earth System Science*, **12**, 241–254. doi: 10.5194/nhess-12-241-2012

Frattini P. and Crosta G., (2013) The role of material properties and landscape morphology on landslide size distributions, *Earth and Planetary Science Letters*, **361**, 310–319. doi: 10.1016/j.epsl.2012.10.029

Fry B., Bannister S., Beavan J., Bland K., Bradley B., Cox S., Cousins J., Gale N., Hancox G., Holden C., Jongens R., Power W., Prasetya G., Reyners M., Ristau J., Robinson R., Samsonov S., and Wilson K., (2010) The Dusky Sound EQ of 2009: A preliminary report, *Bulletin of the New Zealand Society for Earthquake Engineering*, **43**, 24–40.

Gaines R. and Maynord S., (2001) Microscale loose-bed hydraulic models, *Journal of Hydraulic Engineering*, **127**, 335–338. doi: 10.1061/(ASCE)0733-9429(2001)127:5(335)

Geertsema M. and Clague J. (2006) 1,000-year record of landslide dams at Halden Creek, northeastern British Columbia, *Landslides*, 3, 217-227, doi: 10.1007/s10346-006-0039-y

GeoNet., (2015) GeoNet quake search, http://quakesearch.geonet.org.nz/., Accessed: 08/2015

Glade T. and Crozier M., (2004) The nature of landslide hazard impact, In: Glade T, Anderson M, Crozier M (eds) *Landslide Hazard and Risk*. John Wiley and Sons Ltd, pp 43–74

Google-Earth., (2011) Google Earth 2011 map imagery - Poerua River, Accessed: 04/2014

Google-Earth., (2016) Google Earth imagery, Accessed: 03/2016

Grelle G., Revellino P., Donnarumma A., and Guadagno F., (2011) Bedding control on landslides: A methodological approach for computer-aided mapping analysis, *Natural Hazards and Earth System Science*, **11**, 1395–1409. doi: 10.5194/nhess-11-1395-2011

Griffiths G., (1993) Sediment translation waves in braided gravel-bed rivers, *Journal of Hydraulic Engineering*, **119**, 924–937.

Guzzetti F., Malamud B., Turcotte D., and Reichenbach P., (2002) Power-law correlations of landslide areas in central Italy, *Earth and Planetary Science Letters*, **195**, 169–183. doi: 10.1016/S0012-821X(01)00589-1

Guzzetti F., Ardizzone F., Cardinali M., Rossi M., and Valigi D., (2009) Landslide volumes and landslide mobilization rates in Umbria, central Italy, *Earth and Planetary Science Letters*, **279**, 222–229. doi: 10.1016/j.epsl.2009.01.005

Haeberli W., Schaub Y., and Huggel C., (2015) Increasing risks related to landslides from degrading permafrost into new lakes in de-glaciating mountain ranges, *Geomorphology*, doi: 10.1016/j.geomorph.2016.02.009

Hancox G., (2010) Earthquake induced landsliding in New Zealand and potential for landslides during earthquakes in Adelaide, South Australia, *Australian Geomechanics*, **45**, 51–64.

Hancox G., Perrin N., and Dellow G., (1997) Earthquake-induced landsliding in New Zealand and implications for MM intensity and seismic hazard assessment, *Institute of Geological & Nuclear Sciences client report 43601B*,

Hancox G., Perrin N., and Dellow G., (2002) Recent studies of historical earthquake-induced in New Zealand, *Bulletin of the New Zealand Society for Earthquake Engineering*, **35**, 59–95.

Hancox G., Cox S., Turnbull I., and Crozier M., (2003) Reconnaissance studies of landslides and other ground damage caused by the Mw 7.2 Fiordland earthquake of 22 August 2003, *GNS Science Report 2003/30*,

Hancox G., McSaveney M., Manville V., and Davies T., (2005) The October 1999 Mt Adams rock avalanche and subsequent landslide dam-break flood and effects in Poerua river, Westland, New Zealand, *New Zealand Journal of Geology and Geophysics*, **48**, 683–705. doi: 10.1080/00288306.2005.9515141

Hancox G. and Perrin N., (2009) Green Lake Landslide and other giant and very large postglacial landslides in Fiordland, New Zealand, *Quaternary Science Reviews*, **28**, 1020–1036. doi: 10.1016/j.quascirev.2008.08.017

Hancox G. and Thomson R., (2013) The January 2013 Mt Haast Rock Avalanche and Ball Ridge Rock Fall in Aoraki / Mt Cook National Park , New Zealand, *GNS Science Report 2013/33*,

Harrison L., Dunning S., Woodward J., and Davies T., (2015) Post-rock-avalanche dam outburst flood sedimentation in Ram Creek, Southern Alps, New Zealand, *Geomorphology*, **241**, 135–144. doi: 10.1016/j.geomorph.2015.03.038

Havenith H., Strom A., Jongmans D., Abdrakhmatov K., Delvaux D., and Trefois P., (2003) Seismic triggering of landslides, Part A: Field evidence from the Northern Tien Shan, *Natural Hazards and Earth System Science*, **3**, 135–149.

Henderson R. and Thompson S., (1999) Extreme rainfalls in the Southern Alps of New Zealand, *Journal of Hydrology (NZ)*, **38**, 309–330.

Hermanns R., (2013) Rock avalanche (sturzstrom), In: Bobrowsky P (ed) *Encyclopedia of Earth Sciences Series - Encyclopedia of Natural Hazards*. Springer Netherlands, p 875

Hermanns R., Blikra L., Naumann M., Nilsen B., Panthi K., Stromeyer D., and Longva O., (2006) Examples of multiple rock-slope collapses from Köfels (Ötz valley, Austria) and western Norway, *Engineering Geology*, **83**, 94–108. doi: 10.1016/j.enggeo.2005.06.026

Hermanns R., Folguera A., Penna I., Fauque L., and Niedermann S., (2011) Landslide dams in the central Andes of Argentina (northern Patagonia and the Argentine northwest), In: Evans S, Hermanns R, Strom A, Scarascia Mugnozza G (eds) *Natural and Artificial Rockslide Dams - Lecture Notes in Earth Sciences*. Springer Berlin Heidelberg,

Hewitt K., (1998) Catastrophic landslides and their effects on the Upper Indus streams, Karakoram Himalaya, northern Pakistan, *Geomorphology*, **26**, 47–80.

Hewitt K., (1999) Quaternary moraines vs catastrophic rock avalanches in the Karakoram Himalaya, northern Pakistan, *Quaternary Research*, **237**, 220–237.

Hewitt K., (2001) Catastrophic rockslides and the geomorphology of the Hunza and Gilgit River Valleys , Karakoram Himalaya, *Erkunde*, **55**, 72–93.

Hewitt K., (2002) Styles of rock-avalanche depositional complexes conditioned by very rugged terrain, Karakoram Himalaya, Pakistan, *Reviews in Engineering Geology*, **XV**, 345–377. doi: 10.1130/REG15-p345

Hewitt K., (2006) Disturbance regime landscapes: mountain drainage systems interrupted by large rockslides, *Progress in Physical Geography*, **30**, 365–393. doi: 10.1191/0309133306pp486ra

Hewitt K., (2009a) Catastrophic rock slope failures and late Quaternary developments in the Nanga Parbat–Haramosh Massif, Upper Indus basin, northern Pakistan, *Quaternary Science Reviews*, **28**, 1055–1069. doi: 10.1016/j.quascirev.2008.12.019

Hewitt K., (2009b) Rock avalanches that travel onto glaciers and related developments, Karakoram Himalaya, Inner Asia, *Geomorphology*, **103**, 66–79. doi: 10.1016/j.geomorph.2007.10.017

Hewitt K., (2011) Rock avalanche dams on the Trans Himalayan Upper Indus streams: A survey of Late Quaternary events and hazard-related characteristics, In: Evans S, Hermanns R, Strom A, Scarascia Mugnozza G (eds) *Natural and Artificial Rockslide Dams - Lecture Notes in Earth Science*. Springer Berlin Heidelberg, pp 177–204

Hewitt K., Clague J., and Orwin J., (2008) Legacies of catastrophic rock slope failures in mountain landscapes, *Earth-Science Reviews*, **87**, 1–38. doi: 10.1016/j.earscirev.2007.10.002

Hewitt K., Clague J., and Deline P., (2011) Catastrophic rock slope failures and mountain glaciers, In: Singh V, Singh P, Haritashya U (eds) *Encyclopedia of Snow, Ice and Glaciers*. Springer Netherlands, pp 113–126

Hicks D., McSaveney M., and Chinn T., (1990) Sedimentation in proglacial Ivory Lake, Southern Alps, New Zealand, *Arctic and Alpine Research*, **22**, 26-42. doi: 10.2307/1551718

Hicks D., Hill J., and Shankar U., (1996) Variation of suspended sediment yields around New Zealand: the relative importance of rainfall and geology, In: Walling D, Webb B (eds) *Erosion and Sediment Yield: Global and Regional Perspectives; Proceedings of the Exeter Symposium, IAHS Publication 236*. pp 149–156

Hicks M., Shankar U., and McKerchar A., (2003) Sediment yield estimates: A GIS tool, *Water & Atmosphere*, **11**, 26–27.

Hicks D., Shankar U., McKerchar A., Basher L., Lynn I., Page M., and Jessen M., (2011) Suspended sediment yields from New Zealand rivers, *Journal of Hydrology New Zealand*, **50**, 81–142.

Hilbe M. and Anselmetti F., (2014) Signatures of slope failures and river-delta collapses in a perialpine lake (Lake Lucerne, Switzerland), *Sedimentology*, 1883–1907. doi: 10.1111/sed.12120

Hong L. and Davies T., (1979) A study of stream braiding: Summary, *Geological Society of America Bulletin*, 1094–1095. doi: 10.1130/0016-7606(1979)90<1094

Hovius N., Stark C., and Allen P., (1997) Sediment flux from a mountain belt derived by landslide mapping, *Geology*, **25**, 231–234. doi: 10.1130/0091-7613(1997)025<0231

Hovius N., Stark C., Hao-Tsu C., and Jiun-Chuan L., (2000) Supply and removal of sediment in a landslide-dominated mountain belt: Central Range, Taiwan, *The Journal of Geology*, **108**, 73–89. doi: 10.1086/314387

Hsu K., (1975) Catastrophic debris streams (sturzstroms) generated by rockfalls, *Geological Society of America Bulletin*, 86, 129-140, doi: 10.1130/0016-7606(1975)86<129:CDSSGB>2.0.CO;2

Hughes P., Fink D., Fletcher W., and Hannah G., (2014) Catastrophic rock avalanches in a glaciated valley of the High Atlas, Morocco: ^{10}Be exposure ages reveal a 4.5 ka seismic event, *Bulletin of the Geological Society of America*, **126**, 1093–1104. doi: 10.1130/B30894.1

Hungr O., (2006) Rock avalanche occurrence, process and modelling, In: Evans S, Scarascia Mugnozza G, Strom A, Hermanns R (eds) *Landslides from Massive Rock Slope Failure - NATO Science series 49*. Springer Netherlands, Dordrecht, pp 243–266

Hungr O., Leroueil S., and Picarelli L., (2013) The Varnes classification of landslide types, an update, *Landslides*, **11**, 167–194. doi: 10.1007/s10346-013-0436-y

Ibsen M. and Brunsden, D. (1996) The nature, use and problems of historical archives for the temporal occurrence of landslides, with specific reference to the south coast of Britain, Ventnor, Isle of Wight, *Geomorphology*, **15**, 241-258. doi: 10.1016/0169-555X(95)00073-E

James M. and Robson S., (2012) Straight forward reconstruction of 3D surfaces and topography with a camera: Accuracy and geoscience application, *Journal of Geophysical Research*, **117**, F03017. doi: 10.1029/2011JF002289

James M. and Robson S., (2014) Mitigating systematic error in topographic models derived from UAV and ground-based image networks, *Earth Surface Processes and Landforms*, **39**, 1413–1420. doi: 10.1002/esp.3609

Jerolmack D. and Paola C., (2010) Shredding of environmental signals by sediment transport, *Geophysical Research Letters*, **37**, 1–5. doi: 10.1029/2010GL044638

Jones R. and Hodges C., (2004) Applications of atomic force microscopy to granular materials: Inter-particle forces in air, In: Antony S, Hoyle W, Ding Y (eds) *Granular Materials: Fundamentals and applications*. Royal Society of Chemistry, Cambridge, pp 229–254

Kelly M., (1980) A prehistoric catastrophic rock avalanche at Holsteinsborg, West Greenland, *Geological Society of Denmark Bulletin*, **28**, 73–79.

Keulen N., Heilbronner R., Stünitz H., Boullier A., and Ito H., (2007) Grain size distributions of fault rocks: A comparison between experimentally and naturally deformed granitoids, *Journal of Structural Geology*, **29**, 1282–1300. doi: 10.1016/j.jsg.2007.04.003

Korup O., (2002) Recent research on landslide dams – a literature review with special attention to New Zealand, *Progress in Physical Geography*, **26**, 206–235. doi: 10.1191/0309133302pp333ra

Korup O., (2003) Landslide-induced river disruption - Geomorphic imprints and scaling effects in alpine catchments of South Westland and Fiordland, New Zealand, *PhD Thesis*, Victoria University of Wellington

Korup O., (2004) Landslide-induced river channel avulsions in mountain catchments of southwest New Zealand, *Geomorphology*, **63**, 57–80. doi: 10.1016/j.geomorph.2004.03.005

Korup O., (2005a) Large landslides and their effect on sediment flux in South Westland, New Zealand, *Earth Surface Processes and Landforms*, **30**, 305–323. doi: 10.1002/esp.1143

Korup O., (2005b) Geomorphic hazard assessment of landslide dams in South Westland, New Zealand: fundamental problems and approaches, *Geomorphology*, **66**, 167–188. doi: 10.1016/j.geomorph.2004.09.013

Korup O., (2005c) Distribution of landslides in southwest New Zealand, *Landslides*, **2**, 43–51. doi: 10.1007/s10346-004-0042-0

Korup O., (2005d) Geomorphic imprint of landslides on alpine river systems, southwest New Zealand, *Earth Surface Processes and Landforms*, **30**, 783–800. doi: 10.1002/esp.1171

Korup O., (2006a) Rockslide and rock avalanche dams in the Southern Alps, New Zealand, *Italian Journal of Engineering Geology and Environment*, **Special Is**, 33–43. doi: 10.4408/IJEGE.2006-01.S-04

Korup O., (2006b) Rock-slope failure and the river long profile, *Geology*, **34**, 45. doi: 10.1130/G21959.1

Korup O., (2011) Rockslide and rock avalanche dams in the Southern Alps, New Zealand, In: Evans S, Hermanns R, Strom A, Scarascia-Mugnozza G (eds) *Natural and Artificial Rockslide Dams - Lecture Notes in Earth Science*. Springer Berlin Heidelberg, Berlin, Heidelberg, pp 123–145

Korup O. and Crozier M., (2002) Landslide types and geomorphic impact on river channels, Southern Alps, New Zealand, In: Rybar J, Stemberk J, Wagner P (eds) *Landslides, Proceedings of the 1st European Conference on Landslides, Prague, Czech Republic*. Swets and Zeitlinger, Lisse, pp 233–238

Korup O., McSaveney M., and Davies T., (2004) Sediment generation and delivery from large historic landslides in the Southern Alps, New Zealand, *Geomorphology*, **61**, 189–207. doi: 10.1016/j.geomorph.2004.01.001

Korup O., Schmidt J., and McSaveney M., (2005) Regional relief characteristics and denudation pattern of the western Southern Alps, New Zealand, *Geomorphology*, **71**, 402–423. doi: 10.1016/j.geomorph.2005.04.013

Korup O. and Tweed F., (2007) Ice, moraine, and landslide dams in mountainous terrain, *Quaternary Science Reviews*, **26**, 3406–3422. doi: 10.1016/j.quascirev.2007.10.012

Korup O., Densmore A., and Schlunegger F., (2010) The role of landslides in mountain range evolution, *Geomorphology*, **120**, 77–90. doi: 10.1016/j.geomorph.2009.09.017

Krautblatter M. and Moore J., (2014) Rock slope instability and erosion: toward improved process understanding, *Earth Surface Processes and Landforms*, **39**, 1273–1278. doi: 10.1002/esp.3578

Lajeunesse E., Malverti L., Lancien P., Armstrong L., Metivier F., Coleman S., Smith C., Davies T., Cantelli A., and Parker G., (2010) Fluvial and submarine morphodynamics of laminar and near-laminar flows: a synthesis, *Sedimentology*, **57**, 1–26. doi: 10.1111/j.1365-3091.2009.01109.x

LINZ., (2014) Land Information New Zealand 2004-2014 aerial photos - South Island, https://data.linz.govt.nz/., Accessed: 02/2014

Little C., (2016) GeoNet, In: GeoNet Blog. http://info.geonet.org.nz/display/slide/2016/12/02/Landslides+and+Landslide+dams+caused+by+the+Kaikoura+Earthquake., Accessed: 02/2017

Lowe D. and Green J., (1992) Lakes, In: Soons J, Selby M (eds) Landforms of New Zealand. Longman Paul, Auckland, pp 107–143

LRIS-Portal., (2015) New Zealand 25m National Digital Elevation Model (South Island), Accessed: 10/2015

Lyså A., Hjelstuen B., and Larsen E., (2010) Fjord infill in a high-relief area: Rapid deposition influenced by deglaciation dynamics, glacio-isostatic rebound and gravitational activity, *Boreas*, **39**, 39–55. doi: 10.1111/j.1502-3885.2009.00117.x

Madej M., Sutherland D., Lisle T., and Pryor B., (2009) Channel responses to varying sediment input: A flume experiment modeled after Redwood Creek, California, *Geomorphology*, **103**, 507–519. doi: 10.1016/j.geomorph.2008.07.017

Mahaney W., (2002) Atlas of sand grain surface textures and applications. Oxford University Press

Mahesh P., Kundu B., Catherine J., and Gahalaut V., (2011) Anatomy of the 2009 Fiordland earthquake (Mw 7.8), South Island, New Zealand, *Geoscience Frontiers*, **2**, 17–22. doi: 10.1016/j.gsf.2010.12.002

Malamud B., Turcotte D., Guzzetti F., and Reichenbach P., (2004) Landslide inventories and their statistical properties, *Earth Surface Processes and Landforms*, **29**, 687–711. doi: 10.1002/esp.1064

Malverti L., Lajeunesse E., and Métivier F., (2008) Small is beautiful: Upscaling from microscale laminar to natural turbulent rivers, *Journal of Geophysical Research*, **113**, F04004. doi: 10.1029/2007JF000974

Massey C., McSaveney M., and Davies T., (2013) Evolution of an overflow channel across the Young River landslide dam, New Zealand, In: Margottini C, Canuti P, Sassa K (eds) *Landslide Science and Practice*. Springer, Berlin, Heidelberg, pp 43–49

Masson D., Harbitz C., Wynn R., Pedersen G., and Løvholt F., (2006) Submarine landslides: processes, triggers and hazard prediction., *Philosophical Transactions Series A, Mathematical, Physical, and Engineering Sciences*, **364**, 2009–39. doi: 10.1098/rsta.2006.1810

Max D., Gordon D., and Gaines R., (2002) Operation and calibration procedures for micro-models, In: Wahl T, Pugh C, Oberg K and Vermeyen, T (eds) *Hydraulic Measurements and Experimental Methods Speciality Conference (HMEM), 2002*. American Society of Civil Engineers, pp 1–10

Maynord S., (2006) Evaluation of the micromodel: An extremely small-scale movable bed model, *Journal of Hydraulic Engineering*, **132**, 343–353.

McColl S., (2012) Paraglacial rock-slope stability, *Geomorphology*, **153**–**154**, 1–16. doi: 10.1016/j.geomorph.2012.02.015

McColl S., (2015) Landslide causes and triggers, In: Davies T, Shroder J (eds) *Landslide Hazards, Risks and Disasters*. Elsevier, pp 17–42

McColl S. and Davies T., (2011) Evidence for a rock-avalanche origin for “The Hillocks” “moraine”, Otago, New Zealand, *Geomorphology*, **127**, 216–224. doi: 10.1016/j.geomorph.2010.12.017

McColl S. and Davies T., (2013) Large ice-contact slope movements: glacial buttressing, deformation and erosion, *Earth Surface Processes and Landforms*, **38**, 1102–1115. doi: 10.1002/esp.3346

McSaveney M., (2002) Recent rockfalls and rock avalanches in Mount Cook National Park, New Zealand, *Catastrophic landslides: effects, occurrence and mechanisms: Boulder, Colorado, Geological Society of America Reviews in Engineering Geology*, **XV**, 35–70. doi: 10.1130/REG15-p35

McSaveney M. and Davies T., (2006) Rapid rock-mass flow with dynamic fragmentation: Inferences from the morphology and internal structure of rockslides and rock avalanches, In: Evans S, Scarascia Mugnozza G, Strom A, Hermanns R (eds) *Landslides from Massive Rock Slope Failure*. IOS Press, Amsterdam; Springer; NATO Public Diplomacy Division,

McSaveney M., Cox S., and Hancox G., (2014) Seeking a credible cause of the recent increase in rock-avalanche frequency in New Zealand's Southern Alps, *AGU Poster Session NH41A-3775*,

McSaveney M., Cox S., and Hancox G., (2015) Increasing rock-avalanche frequency correlates with increasing seismic moment release in New Zealand's Southern Alps, *Geophysical Research Abstracts*, **17**,

Micheletti N., Chandler J., and Lane S., (2015) Investigating the geomorphological potential of freely available and accessible structure-from-motion photogrammetry using a smartphone, *Earth Surface Processes and Landforms*, **40**, 473–486. doi: 10.1002/esp.3648

Nash T., (2003) Engineering geological assessment of selected landslide dams formed from the 1929 Murchison and 1968 Inangahua Earthquakes, *MSc Thesis*, University of Canterbury

Nash T., Bell D., Davies T., and Nathan S., (2008) Analysis of the formation and failure of Ram Creek landslide dam, South Island, New Zealand, *New Zealand Journal of Geology and Geophysics*, **51**, 187–193. doi: 10.1080/00288300809509859

Nicholas A., Ashworth P., Kirkby M., Macklin M., and Murray T., (1995) Sediment slugs: large-scale fluctuations in fluvial sediment transport rates and storage volumes, *Progress in Physical Geography*, **19**, 500–519. doi: 10.1177/030913339501900404

NIWA., (2015) NIWA national and regional climate maps, https://www.niwa.co.nz/climate/research-projects/national-and-regional-climate-maps. Accessed 11 Feb 2015

Norris R. and Cooper A., (2000) Late Quaternary slip rates and slip partitioning on the Alpine Fault, New Zealand, *Journal of Structural Geology*, **23**, 507–520. doi: 10.1016/S0191-8141(00)00122-X

Ouimet W., Whipple K., Royden L., Sun Z., and Chen Z., (2007) The influence of large landslides on river incision in a transient landscape: Eastern margin of the Tibetan Plateau (Sichuan, China), *Geological Society of America Bulletin*, **119**, 1462–1476. doi: 10.1130/B26136.1

Parker R., Hancox G., Petley D., Massey C., Densmore A., and Rosser N., (2015) Spatial distributions of earthquake-induced landslides and hillslope preconditioning in the northwest South Island, New Zealand, *Earth Surface Dynamics*, **3**, 501–525. doi: 10.5194/esurf-3-501-2015

Pearce A. and Watson A., (1986) Effects of earthquake-induced landslides on sediment budget and transport over a 50-yr period, *Geology*, **14**, 52–55.

Pedersen S., Larsen L., Dahl-Jensen T., Jepsen H., Krarup G., Nielsen T., Pedersen A., Platen-hallermund F., and Weng W., (2002) Tsunami-generating rock fall and landslide on

the south coast of Nuussuaq , central West Greenland, *Geology of Greenland Survey Bulletin*, **191**, 73–83.

Plafker G. and Ericksen G., (1978) Nevados Huascaran avalanches, In: Voight B (ed) *Developments in Geotechnical Engineering 14A - Rockslides and Avalanches 1 - Natural Phenomena*. Elsevier, pp 277–314

Plafker G. and Eyzaguirre V., (1979) Rock avalanche and wave at Chungar, Peru, In: Voight B (ed) *Developments in Geotechnical Engineering 14B - Rockslides and Avalanches 2 - Engineering Sites*. Elsevier, pp 269–279

Popescu M., (1994) A suggested method for reporting landslide causes, *Bulletin of the International Association of Engineering Geology*, **50**, 71–74. doi: 10.1007/BF02594958

Postma G., Kleinhans M., Meijer PT., and Eggenhuisen J., (2008) Sediment transport in analogue flume models compared with real-world sedimentary systems: a new look at scaling evolution of sedimentary systems in a flume, *Sedimentology*, **55**, 1541–1557. doi: 10.1111/j.1365-3091.2008.00956.x

Pudasaini S. and Miller S., (2013) The hypermobility of huge landslides and avalanches, *Engineering Geology*, **157**, 124–132. doi: 10.1016/j.enggeo.2013.01.012

Rait K. and Bowman E., (2010) Dynamic fragmentation in rock avalanches: A numerical model of micromechanical behaviour, In: Benz T, Nordal S (eds*) Numerical Methods in Geotechnical Engineering: (NUMGE 2010) - 7th European Conference on Numerical Methods in Geotechnical Engineering*. Trondheim, Norway, pp 435–440

Rait K., Lambert C., and Bowman E., (2012) Dynamic fragmentation of rock clasts under normal compression in sturzstrom, *Géotechnique Letters*, **2**, 167–172. doi: 10.1680/geolett.12.00038

Rattenbury M. and Isaac M., (2012) The QMAP 1:250 000 geological map of New Zealand project, *New Zealand Journal of Geology and Geophysics*, **55**, 393–405. doi: 10.1080/00288306.2012.725417

Reed S., (2005) Electron microprobe analysis and scanning electron microscopy in geology, 2nd edn. Cambridge University Press

Reznichenko N., (2012) Rock avalanches on glaciers: Processes and implications, *PhD Thesis*, University of Canterbury

Reznichenko N., Davies T., Shulmeister J., and McSaveney M., (2010) Effects of debris on ice-surface melting rates: An experimental study, *Journal of Glaciology*, **56**, 384–394. doi: 10.3189/002214310792447725

Reznichenko N., Davies T., and Alexander D., (2011) Effects of rock avalanches on glacier behaviour and moraine formation, *Geomorphology*, **132**, 327–338. doi: 10.1016/j.geomorph.2011.05.019

Reznichenko N., Davies T., Shulmeister J., and Larsen S., (2012) A new technique for identifying rock avalanche-sourced sediment in moraines and some paleoclimatic implications, *Geology*, **40**, 319–322. doi: 10.1130/G32684.1

Reznichenko N., Davies T., and Winkler S., (2015) Revised palaeoclimatic significance of Mueller Glacier moraines, Southern Alps, New Zealand, *Earth Surface Processes and Landforms*, **41**, 196–207. doi: 10.1002/esp.3848

Robinson T. and Davies T., (2013) Review article: Potential geomorphic consequences of a future great (Mw = 8.0+) Alpine Fault earthquake, South Island, New Zealand, *Natural Hazards and Earth System Science*, **13**, 2279–2299. doi: 10.5194/nhess-13-2279-2013

Robinson T., Davies T., Reznichenko N., and De Pascale G., (2014) The extremely long-runout Komansu rock avalanche in the Trans Alai range, Pamir Mountains, southern Kyrgyzstan, *Landslides*, **12**, 523–535. doi: 10.1007/s10346-014-0492-y

Robinson T., Davies T., Wilson T., and Orchiston C., (2016) Coseismic landsliding estimates for an Alpine Fault earthquake and the consequences for erosion of the Southern Alps, New Zealand, *Geomorphology*, **263**, 71–86. doi: 10.1016/j.geomorph.2016.03.033

Rosser N., (2010) Landslides and rockfalls, In: Burt T, Allison R (eds) *Sediment Cascades: An Integrated Approach*. John Wiley & Sons, Ltd, pp 55–87

Sattler K., Anderson B., Mackintosh A., Norton K. and de Róiste M. (2016) Estimating permafrost distribution in the maritime Southern Alps, New Zealand, based on climatic conditions at rock glacier sites, *Frontiers in Earth Science*, **4**, 1-17. 10.3389/feart.2016.00004

Schoeneich P., Hantz D., Deline P., and Amelot F., (2008) A new database of Alpine rock falls and rock avalanches, *Interpraevent, 2008 - Conference Proceedings*, **2**, 243–250.

Schulz W., Harp E., and Jibson R., (2008) Characteristics of large rock avalanches triggered by the November 3, 2002 Denali Fault earthquake, Alaska, USA, *Landslides and Engineered Slopes: from the Past to the Future, Vols 1 and 2*, 1447–1453.

Sepúlveda S. and Moreiras S., (2013) Large volume landslides in the central Andes of Chile and Argentina (32º-34ºS) and related hazards, In: Genevois R, Prestininzi A (eds) *Italian Journal of Engineering Geology and Environment - Book Series*. Italian Journal of Engineering Geology and Environment, pp 287–294

Shulmeister J., Davies T., Evans D., Hyatt O., and Tovar D., (2009) Catastrophic landslides, glacier behaviour and moraine formation – A view from an active plate margin, *Quaternary Science Reviews*, **28**, 1085–1096. doi: 10.1016/j.quascirev.2008.11.015

Sklar L., Fadde J., Venditti J., Nelson P., Aleksandra Wydzga M., Cui Y., and Dietrich W., (2009) Translation and dispersion of sediment pulses in flume experiments simulating gravel augmentation below dams, *Water Resources Research*, **45**, 1–14. doi: 10.1029/2008WR007346

Smith G., Bell D., and Davies T., (2012) The Acheron rock avalanche deposit, Canterbury, New Zealand: age and implications for dating landslides, *New Zealand Journal of Geology and Geophysics*, 55, 375-391, doi: 10.1080/00288306.2012.733947

Smith M., Carrivick J., and Quincey D., (2015) Structure from motion photogrammetry in physical geography, *Progress in Physical Geography*, **40**, 247–275. doi: 10.1177/0309133315615805

Smith M. and Vericat D., (2015) From experimental plots to experimental landscapes: Topography, erosion and deposition in sub-humid badlands from structure-from-motion photogrammetry, *Earth Surface Processes and Landforms*, **40**, 1656–1671. doi: 10.1002/esp.3747

Stark C. and Hovius N., (2001) The characterization of landslide size distributions, *Geophysical Research Letters*, **28**, 1091–1094.

Stirling M., McVerry G., Gerstenberger M., Litchfield N., Van Dissen R., Berryman K., Barnes P., Wallace L., Villamor P., Langridge R., Lamarche G., Nodder S., Reyners M., Bradley B., Rhoades D., Smith W., Nicol A., Pettinga J., Clark K., et al., (2012) National Seismic Hazard Model for New Zealand: 2010 Update, *Bulletin of the Seismological Society of America*, **102**, 1514–1542. doi: 10.1785/0120110170

Stock G. and Uhrhammer R., (2010) Catastrophic rock avalanche 3600 years BP from El Capitan, Yosemite Valley, California, *Earth Surface Processes and Landforms*, **35**, 941–951. doi: 10.1002/esp.1982

Strom A. and Korup O., (2006) Extremely large rockslides and rock avalanches in the Tien Shan Mountains, Kyrgyzstan, *Landslides*, **3**, 125–136. doi: 10.1007/s10346-005-0027-7

Sutherland D., Ball M., Hilton S., and Lisle T., (2002) Evolution of a landslide-induced sediment wave in the Navarro River, California, *Geological Society of America Bulletin*, **114**, 1036–1048. doi: 10.1130/0016-7606(2002)114<1036

Sutherland R., Berryman K., and Norris R., (2006) Quaternary slip rate and geomorphology of the Alpine fault: Implications for kinematics and seismic hazard in southwest New Zealand, *Geological Society of America Bulletin*, **118**, 464–474. doi: 10.1130/B25627.1

Sutherland R., Eberhart-Phillips D., Harris R., Stern T., Beavan J., Ellis S., Henrys S., Cox S., Norris R., Berryman K., Townend J., Bannister S., Pettinga J., Leitner B., Wallace L., Little T., Cooper A., Yetton M., and Stirling M., (2007) Do great earthquakes occur on the Alpine Fault in central South Island, New Zealand?, *Geophysical Monograph, SIGHT*, 1–24.

Taig T. and Mcsaveney M., (2015) Milford Sound risk from landslide-generated tsunami, *GNS Science Consultancy Report 2014/224*,

Tovar D., Shulmeister J., and Davies T., (2008a) Evidence for a landslide origin of the Waiho Loop Moraine, New Zealand - supplementary information, *Nature Geoscience*, **1**,

Tovar D., Shulmeister J., and Davies T., (2008b) Evidence for a landslide origin of New Zealand's Waiho Loop moraine, *Nature Geoscience*, **1**, 524–526. doi: 10.1038/ngeo249

Uhlmann M., Korup O., Huggel C., Fischer L., and Kargel J., (2013) Supra-glacial deposition and flux of catastrophic rock-slope failure debris, south-central Alaska, *Earth Surface Processes and Landforms*, **38**, 675–682. doi: 10.1002/esp.3311

Van De Wiel M. and Coulthard T., (2010) Self-organized criticality in river basins: Challenging sedimentary records of environmental change, *Geology*, **38**, 87–90. doi: 10.1130/G30490.1

Van Den Eeckhaut M., and Hervás J., (2012) State of the art of national landslide databases in Europe and their potential for assessing landslide susceptibility, hazard and risk, *Geomorphology*, 139-140, 545-558, doi: 10.1016/j.geomorph.2011.12.006

Vandergoes M., Fitzsimons S., and Newnham R., (1997) Late glacial to Holocene vegetation and climate change in the eastern Takitimu Mountains, western Southland, New Zealand, *Journal of the Royal Society of New Zealand*, **27**, 53–66. doi: 10.1080/03014223.1997.9517527

Varnes D., (1978) Slope movement types and processes, In: Schuster R, Krizek R (eds) *Special report 176: Landslides: Analysis and Control, Transportation Research Board, Washington, D.C*. National Academy of Sciences, Washington DC, pp 11–33

Wang G., Huang R., Kamai T., and Zhang F., (2013) The internal structure of a rockslide dam induced by the 2008 Wenchuan (Mw7.9) earthquake, China, *Engineering Geology*, **156**, 28–36. doi: 10.1016/j.enggeo.2013.01.004

Ward S., (2001) Landslide tsunami, *Journal of Geophysical Research*, **106**, 11,201-11,215. doi: 10.1029/2000JB900450

Weidinger J., Korup O., Munack H., Altenberger U., Dunning S., Tippelt G., and Lottermoser W., (2014) Giant rockslides from the inside, *Earth and Planetary Science Letters*, **389**, 62–73. doi: 10.1016/j.epsl.2013.12.017

Westoby M., Brasington J., Glasser N., Hambrey M., and Reynolds J., (2012) "Structure-from-motion" photogrammetry: A low-cost, effective tool for geoscience applications, *Geomorphology*, **179**, 300–314. doi: 10.1016/j.geomorph.2012.08.021

Whitehouse I., (1983) Distribution of large rock avalanche deposits in the central Southern Alps, New Zealand, *New Zealand Journal of Geology and Geophysics*, **26**, 271–279. doi: 10.1080/00288306.1983.10422240

Whitehouse I. and Griffiths G., (1983) Frequency and hazard of large rock avalanches in the central Southern Alps, New Zealand, *Geology*, **11**, 331–334. doi: 10.1130/0091-7613(1983)11<331

Wild M., (2013) Growth dynamics of braided gravel-bed river deltas in New Zealand, *PhD Thesis*, University of Canterbury

Wood J., Wilmshurst J., and Rawlence N., (2011) Radiocarbon-dated faunal remains correlate very large rock avalanche deposit with prehistoric Alpine Fault rupture, *New Zealand Journal of Geology and Geophysics*, **54**, 431–434. doi: 10.1080/00288306.2011.590212

Wratt D., Tait A., Griffiths G., Espie P., Jessen M., Keys J., Ladd M., Lew D., Lowther W., Mitchell N., Morton J., Reid J., Reid S., Richardson A., Sansom J., and Shankar U., (2006) Climate for crops: integrating climate data with information about soils and crop requirements to reduce risks in agricultural decision-making, *Meteorological Applications*, **13**, 305–315. doi: 10.1017/s1350482706002416

Yanites B., Tucker G., Mueller K., and Chen Y., (2010) How rivers react to large earthquakes: Evidence from central Taiwan, *Geology*, **38**, 639–642. doi: 10.1130/G30883.1

Young W. and Warburton J., (1996) Principles and practice of hydraulic modelling of braided gravel-bed rivers, *Journal of Hydrology New Zealand*, **35**, 175–198.

Zhu J., (2004) Fluidization of fine powders, In: Antony S, Hoyle W, Ding Y (eds) *Granular Materials: Fundamentals and applications*. Royal Society of Chemistry, Cambridge, pp 270–295

Appendix 3.1

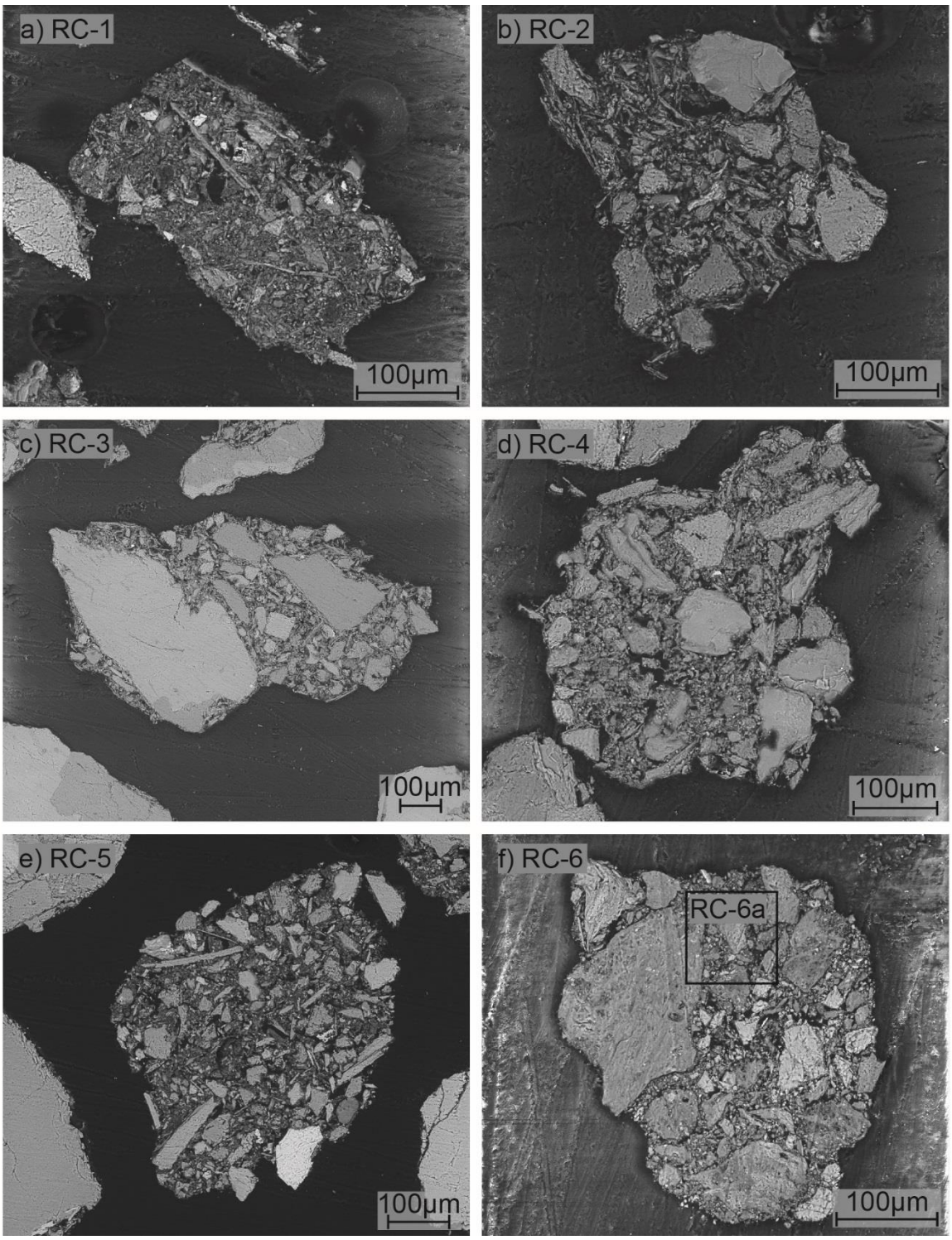

SEM micrographs of grains from the Ram Creek river system. Sample numbers refer to Fig. 3.3.

Appendix 3.1

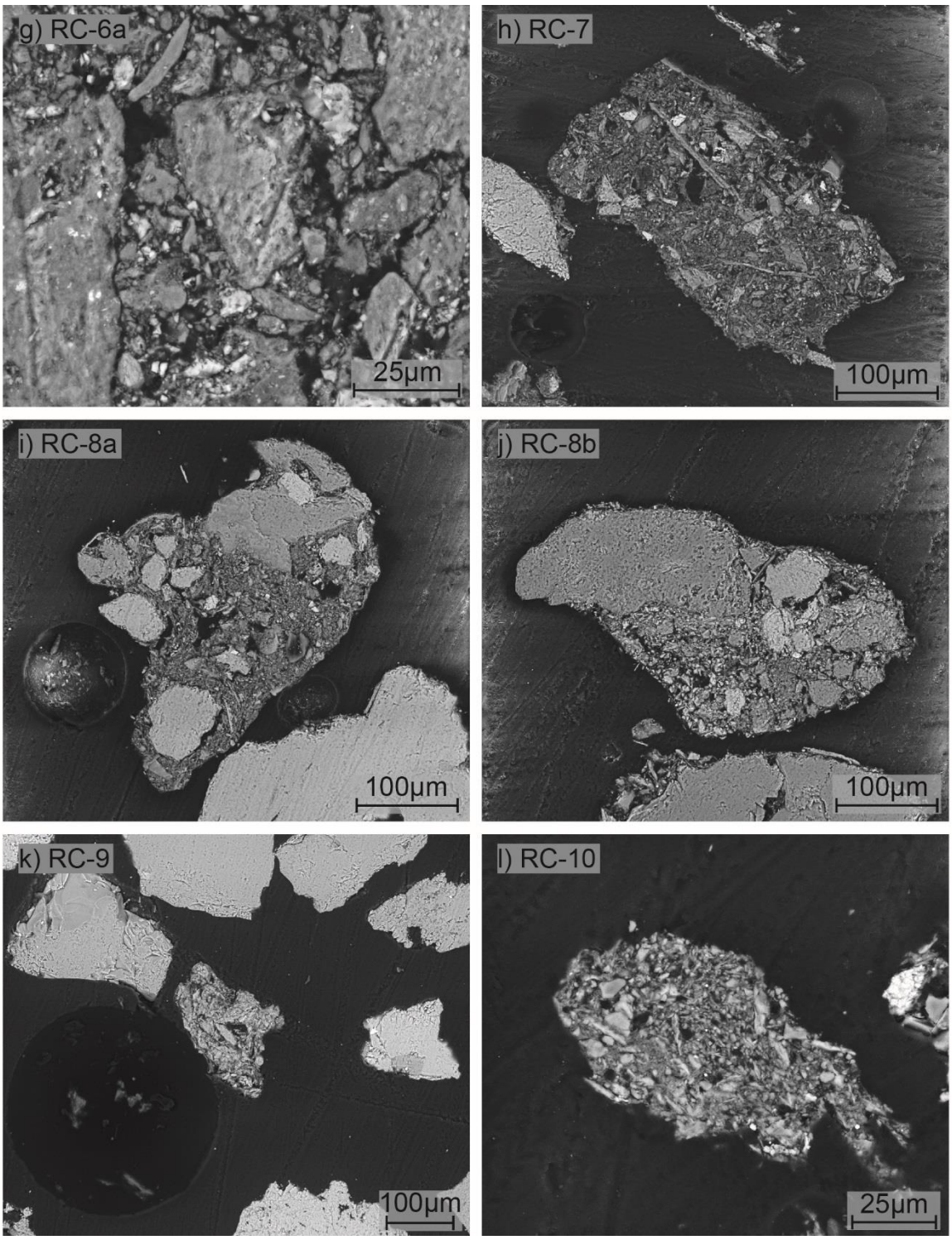

SEM micrographs of grains from the Ram Creek river system. Sample numbers refer to Fig. 3.3.

Appendix 3.2

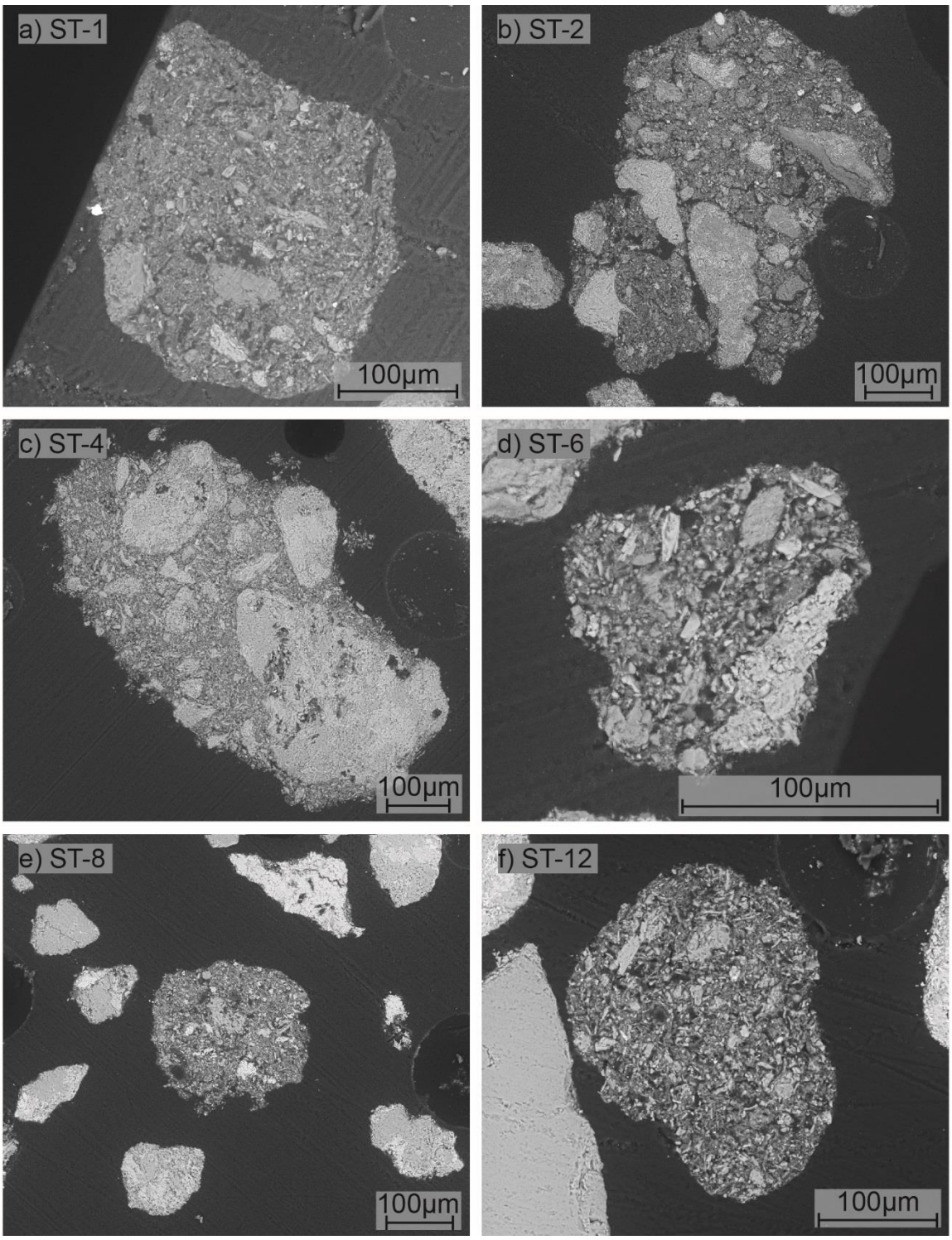

SEM micrographs of grains from the Stanley River system. Sample numbers refer to Fig. 3.5.

Appendix 3.3

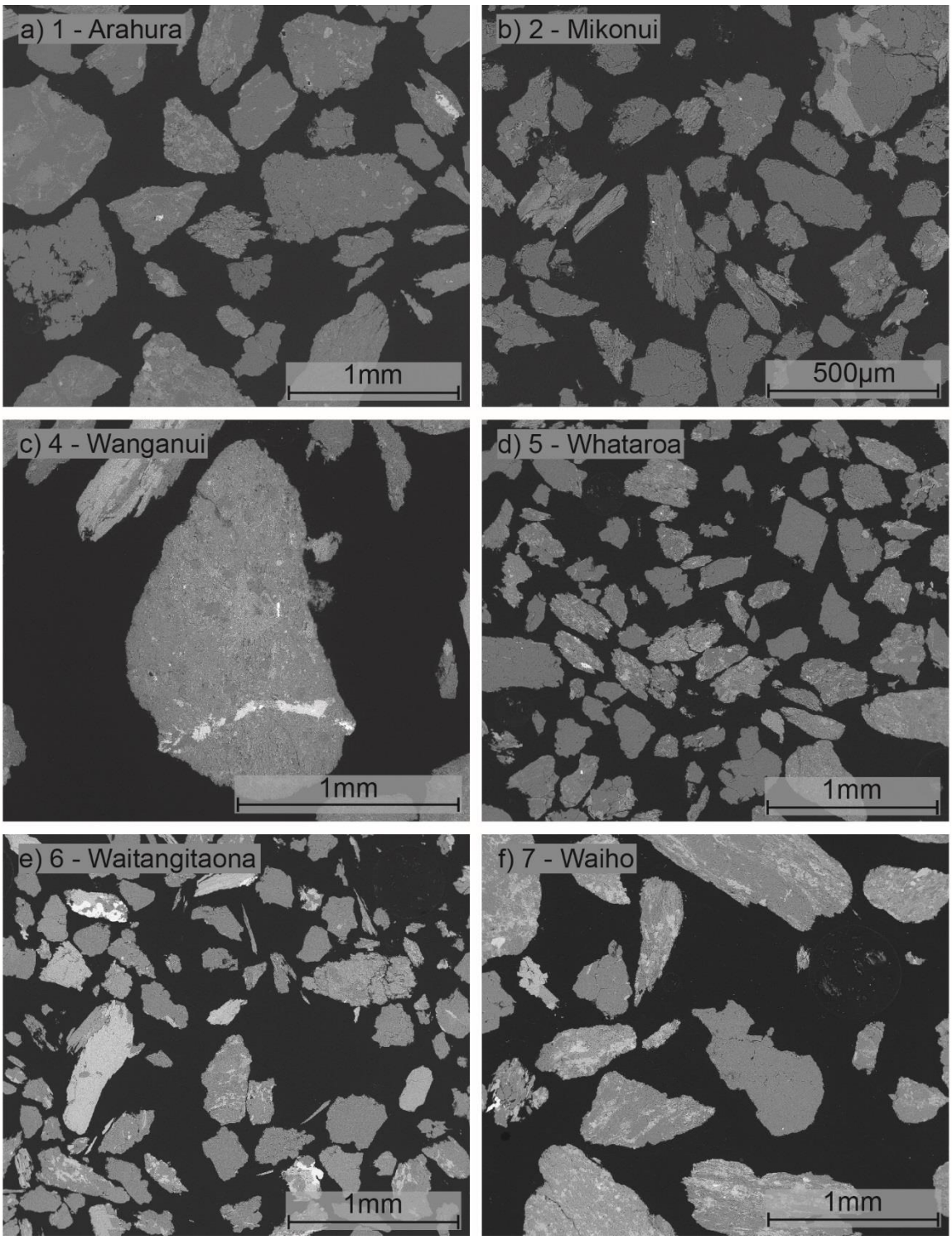

SEM micrographs of grains from named West Coast river systems. River numbers refer to Table 3.1.

Appendix 3.3

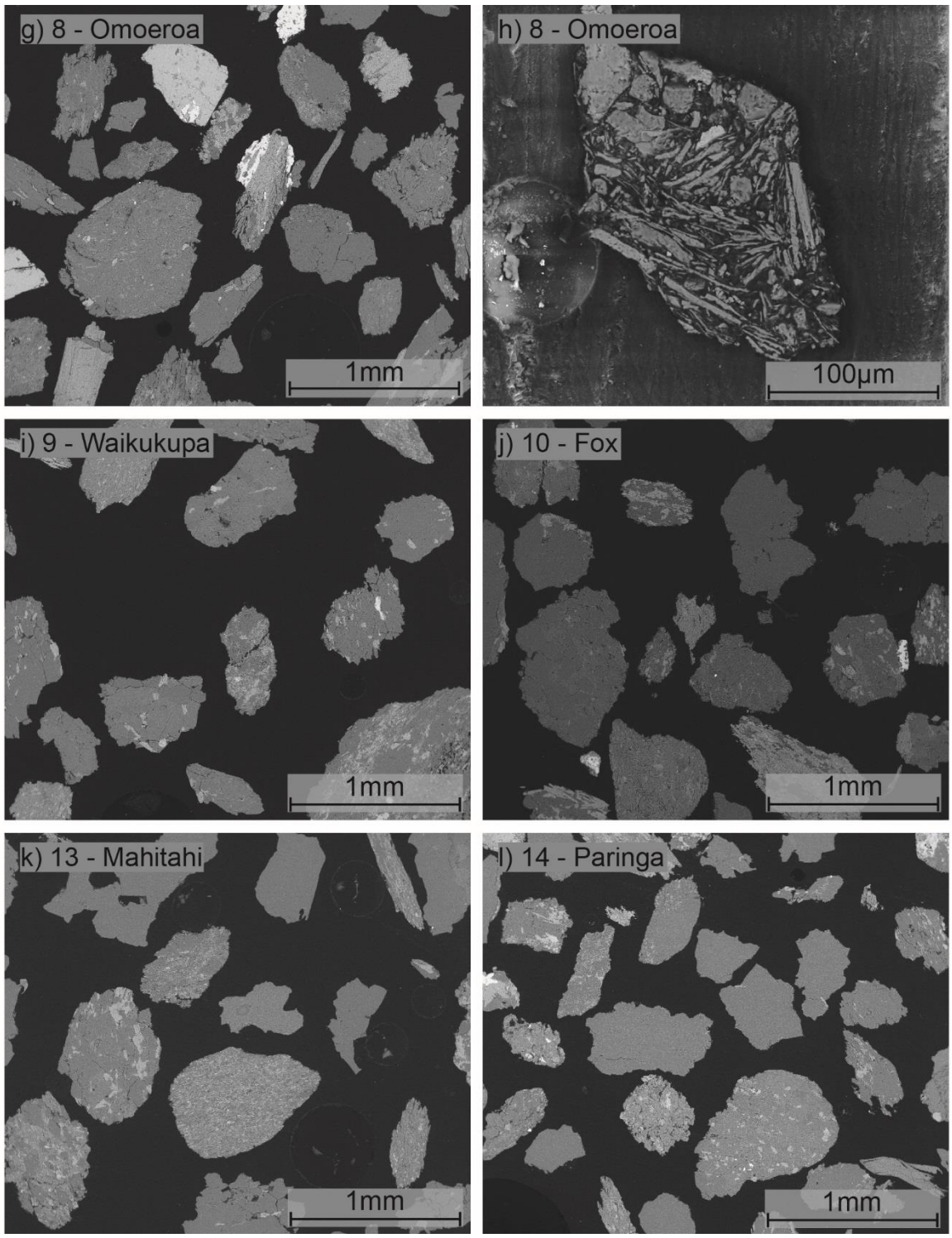

SEM micrographs of grains from named West Coast river systems. River numbers refer to Table 3.1.

Appendix 3.3

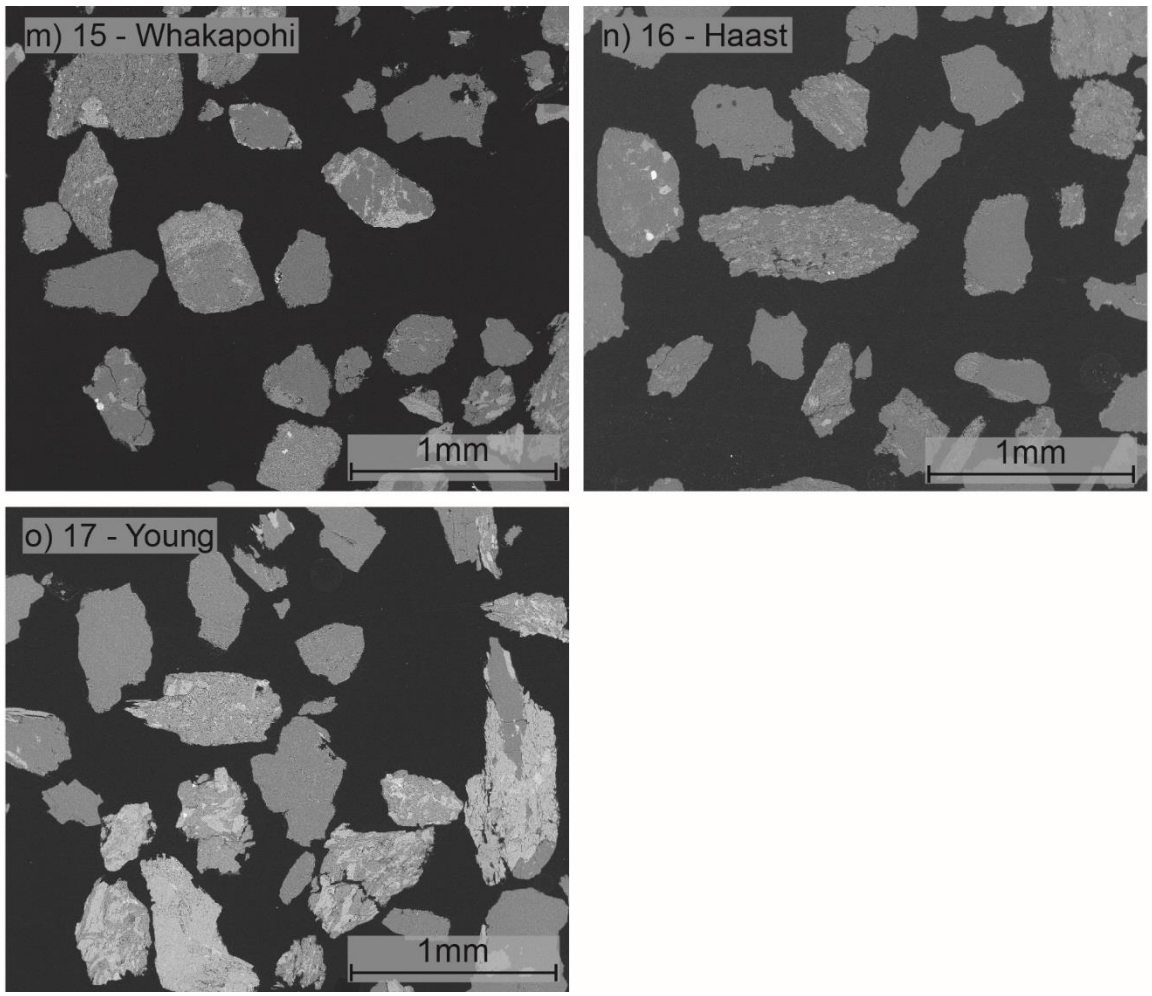

SEM micrographs of grains from named West Coast river systems. River numbers refer to Table 3.1.

Appendix 3.4

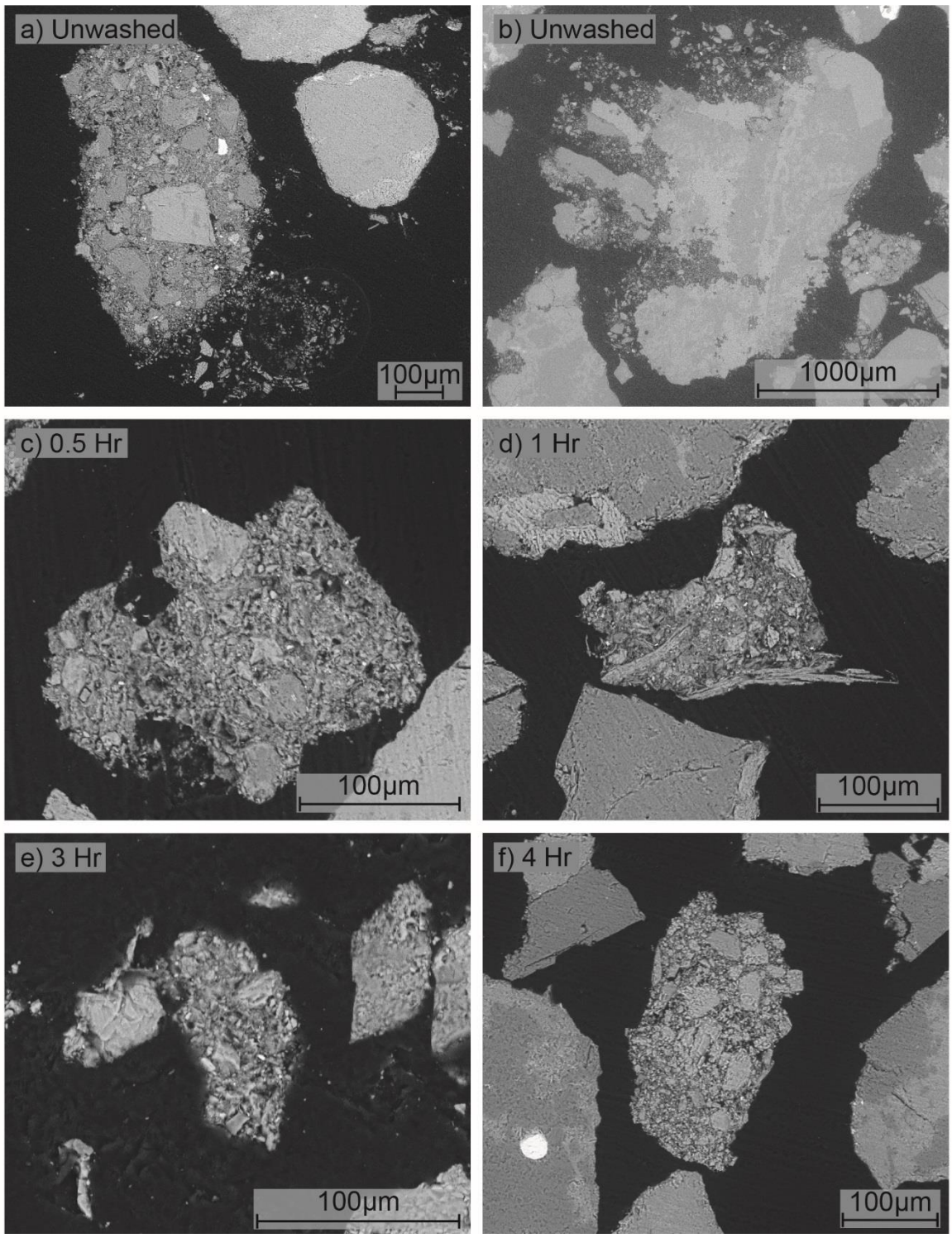

SEM micrographs of grains from the laboratory washing experiment of Kyrgyzstan RAD material. Sample collection time-steps are noted in each micrograph.

Appendix 3.4

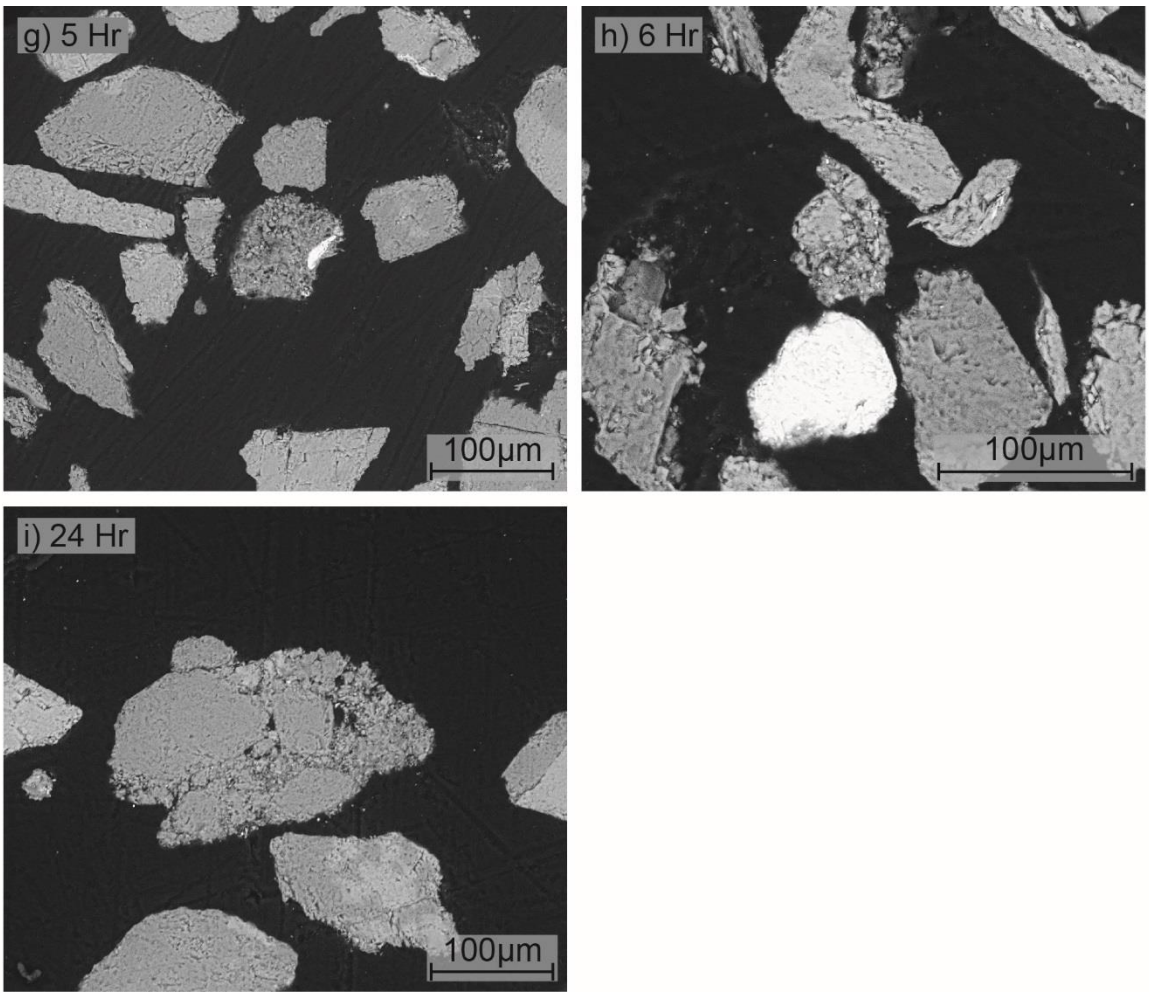

SEM micrographs of grains from the laboratory washing experiment of Kyrgyzstan RAD material. Sample collection time-steps are noted in each micrograph.

Appendix 3.5

Table of summary statistics for all agglomerates detected in samples

	Sample Name	Sampling location	Distance from RAD (km)	Agglomerate a-axis length (µm)	Agglomerate roundness	Figure in text
Ram Creek	RC-3	Dam breach outwash	0.00	1,066	Sub-rounded	3.14
	RC-4	Dam breach outwash	0.00	487	Rounded	Appendix 3.1
	RC-6	RAD/debris flow	0.48	425	Rounded	3.14
	RC-8a	Debris flow	0.77	375	Rounded	3.14
	RC-8b	Debris flow	0.77	394	Rounded	3.14
Stanley River	ST-2	RAD	0.00	610	Rounded	3.15
	ST-4	RAD	0.00	710	Rounded	3.15
	ST-6	Flood outwash	0.00	140	Rounded	3.15

Appendix 4.1

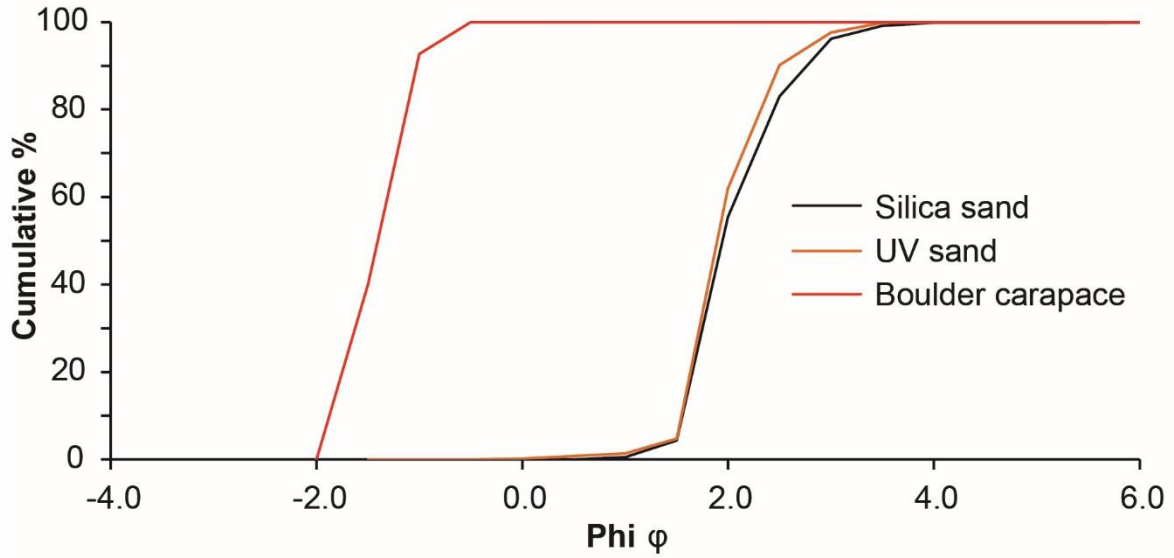

Graph of the GSD of the fine-grained Silica sand, UV sand and gravel landslide carapace used in the microscale flume model.

Appendix 4.1

GSD data for the fine Silica sand that was used in the micro-scale flume model. The starting weight of sand in the sieves was 521.65g.

Phi (φ)	Sieve Aperture (mm)	Sieve Weight (g)	Sieve + Sample (g)	Sample Weight (g)	Fractional %	Cumulative %	Cumulative % Finer
-1.5	2.8	0.00	0.00	0.00	0.00	0.00	100.00
-1.0	2	0.00	0.00	0.00	0.00	0.00	100.00
-0.5	1.5	0.00	0.00	0.00	0.00	0.00	100.00
0.0	1	349.75	349.75	0.00	0.00	0.00	100.00
0.5	0.707	323.20	323.22	0.02	0.00	0.00	100.00
1.0	0.5	308.93	311.65	2.72	0.52	0.53	99.47
1.5	0.354	295.26	315.25	19.99	3.83	4.36	95.64
2.0	0.25	281.62	547.87	266.25	51.04	55.40	44.60
2.5	0.177	288.32	432.24	143.92	27.59	82.99	17.01
3.0	0.125	280.84	349.51	68.67	13.16	96.15	3.85
3.5	0.084	265.08	280.63	15.55	2.98	99.13	0.87
4.0	0.063	272.32	275.72	3.40	0.65	99.78	0.22
10.0	0	242.89	243.35	0.46	0.09	99.87	0.13
			Sum	**520.98**	**99.87**		

Appendix 4.1

GSD data for the UV sand that was used to construct the RA dam in the micro-scale flume model. The starting weight of sand in the sieves was 496.24g.

Phi (φ)	Sieve Aperture (mm)	Sieve Weight (g)	Sieve + Sample (g)	Sample Weight (g)	Fractional %	Cumulative %	Cumulative % Finer
-1.5	2.8	0.00	0.00	0.00	0.00	0.00	100.00
-1.0	2	0.00	0.00	0.00	0.00	0.00	100.00
-0.5	1.5	0.00	0.00	0.00	0.00	0.00	100.00
0.0	1	349.75	350.93	1.18	0.24	0.24	99.76
0.5	0.707	323.20	326.09	2.89	0.58	0.82	99.18
1.0	0.5	308.93	311.64	2.71	0.55	1.37	98.63
1.5	0.354	295.24	311.98	16.74	3.37	4.74	95.26
2.0	0.25	281.65	565.60	283.95	57.22	61.96	38.04
2.5	0.177	288.32	428.09	139.77	28.17	90.13	9.87
3.0	0.125	280.84	317.77	36.93	7.44	97.57	2.43
3.5	0.084	265.07	276.00	10.93	2.20	99.77	0.23
4.0	0.063	272.32	273.36	1.04	0.21	99.98	0.02
10.0	0	242.82	242.90	0.08	0.02	100.00	0.00
			Sum	**496.22**	**100.00**		

Appendix 4.1

GSD data for the gravel that composed the RAD boulder carapace that was used in the micro-scale flume model. The starting weight of sand in the sieves was 263.25g.

Phi (φ)	Sieve Aperture (mm)	Sieve Weight (g)	Sieve + Sample (g)	Sample Weight (g)	Fractional %	Cumulative %	Cumulative % Finer
-1.5	2.8	539.46	644.88	105.42	40.05	40.05	59.95
-1.0	2	390.76	529.35	138.59	52.65	92.69	7.31
-0.5	1.5	372.64	391.79	19.15	7.27	99.97	0.03
0.0	1	349.75	349.79	0.04	0.02	99.98	0.02
0.5	0.707	323.20	323.22	0.02	0.01	99.99	0.01
1.0	0.5	308.93	308.93	0.00	0.00	99.99	0.01
1.5	0.354	295.24	295.24	0.00	0.00	99.99	0.01
2.0	0.25	281.65	281.65	0.00	0.00	99.99	0.01
2.5	0.177	288.32	288.32	0.00	0.00	99.99	0.01
3.0	0.125	280.84	280.84	0.00	0.00	99.99	0.01
3.5	0.084	265.07	265.07	0.00	0.00	99.99	0.01
4.0	0.063	272.32	272.32	0.00	0.00	99.99	0.01
10.0	0	242.82	242.82	0.00	0.00	99.99	0.01
			Sum	**263.22**	**99.99**		

Appendix 4.2

Camera and Photoscan reconstruction parameters for each of the reconstructed flume models

	Run 1	Run 2	Run 3	Run 4	Run 5	Run 6	Run 7
Base Level							
Number of images	248	244	248	248	256	268	268
Focal Length (mm)	26	26	30	30	28	28	28
f-Stop	5.6	5.6	5.6	5.6	5.6	5.6	5.6
Exposure time (sec)	1/500	1/500	1/500	1/500	1/500	1/500	1/500
ISO	200	200	200	200	200	200	200
Sparse cloud points	18778	183653	185180	184474	175854	178173	178455
Dense cloud points	104290084	103110913	127996765	127043190	108818041	116550914	115675806
RMS Error (m)	0.007352	0.006076	0.007779	0.005457	0.006089	0.005756	0.005949
Error (Pix)	0.496	0.408	0.39	0.46	0.488	0.444	0.471
DEM Resolution (m)	0.0002	0.0002	0.0002	0.0002	0.0002	0.0002	0.0002

Appendix 4.2

	Run 1	Run 2	Run 3	Run 4	Run 5	Run 6	Run 7
Dam Break – Halogen lighting							
Number of images	240	248		248	256		268
Focal Length (mm)	26	30		28	26		26
f-Stop	5.6	5.6		5.6	5.6		5.6
Exposure time (sec)	1/500	1/500		1/500	1/500		1/500
ISO	200	200		200	200		200
Sparse cloud points	122062	181345		166552	174945		169450
Dense cloud points	102702835	130588978		103102238	106308095		107873009
RMS Error (m)	0.005634	0.005363		0.006386	0.006235		0.006219
Error (Pix)	0.401	0.424		0.51	0.451		0.455
DEM Resolution (m)	0.0002	0.0002		0.0002	0.0002		0.0002

Appendix 4.2

	Run 1	Run 2	Run 3	Run 4	Run 5	Run 6	Run 7
Dam Break - UV lighting							
Number of images	244	244		249	260		268
Focal Length (mm)	26	30		28	26		26
f-Stop	5.6	5.6		5.6	5.6		5.6
Exposure time (sec)	1/3	2.5		2.5 sec	2.5 sec		2.5 sec
ISO	200	200		200	200		200
Sparse cloud points	64926	142411		149662	136880		137085
Dense cloud points	62777463	111077590		98399930	96105333		96759337
RMS Error	0.007183	0.005339		0.006523	0.005895		0.006044
Error (Pix)	0.527	0.457		0.53	0.487		0.441
Orthophoto Resolution	0.0001	0.0002		0.0002	0.0001		0.0001

Appendix 4.2

	Run 1	Run 2	Run 3	Run 4	Run 5	Run 6	Run 7
Post dam break - Halogen lighting							
Number of images	247	244	249	252	264	268	268
Focal Length (mm)	26	30	26	26	28	28	26
f-Stop	5.6	5.6	5.6	5.6	5.6	5.6	5.6
Exposure time (sec)	1/500 sec	1/500 sec	1/500 sec	1/500 sec	1/500 sec	1/500 sec	1/500 sec
ISO	200	200	200	200	200	200	200
Sparse cloud points	173170	183767	167585	175791	178518	184603	174952
Dense cloud points	105287396	123959375	106993986	104268594	107301804	108036632	100896882
RMS Error (m)	0.005581	0.005519	0.006016	0.00632	0.00641	0.006181	0.006306
Error (Pix)	0.378	0.401	0.476	0.495	0.471	0.498	0.488
DEM Resolution (m)	0.0002	0.0002	0.0002	0.0002	0.0002	0.0002	0.0002

Appendix 4.2

	Run 1	Run 2	Run 3	Run 4	Run 5	Run 6	Run 7
Post dam break - UV lighting							
Number of images	240	244	248	253	264	268	273
Focal Length (mm)	26	30	26	26	28	28	26
f-Stop	5.6	5.6	5.6	5.6	5.6	5.6	5.6
Exposure time (sec)	2.5 sec	2.5 sec	2.5 sec	2.5 sec	2.5 sec	2.5 sec	2.5 sec
ISO	200	200	200	200	200	200	200
Sparse cloud points	160850	170254	145457	134255	141332	139957	147750
Dense cloud points	87940101	107268693	94054065	91625641	93514468	100173362	92513665
RMS Error	0.006962	0.005705	0.005995	0.006238	0.005767	0.005733	0.006423
Error (Pix)	0.4	0.491	0.507	0.564	0.468	0.493	0.547
Orthophoto Resolution	0.0001	0.0002	0.0002	0.0002	0.0001	0.0001	0.0002

Appendix 4.2

	Run 1	Run 2	Run 3	Run 4	Run 5	Run 6	Run 7
Post dam break 2 - Halogen lighting							
Number of images							276
Focal Length (mm)							26
f-Stop							5.6
Exposure time (sec)							1/500 sec
ISO							200
Sparse cloud points							181873
Dense cloud points							102690184
RMS Error (m)							0.006337
Error (Pix)							0.451
DEM Resolution (m)							0.0002

Appendix 4.2

	Run 1	Run 2	Run 3	Run 4	Run 5	Run 6	Run 7
Post dam break 2 - UV lighting							
Number of images							271
Focal Length (mm)							26
f-Stop							5.6
Exposure time (sec)							2.5 sec
ISO							200
Sparse cloud points							136399
Dense cloud points							89853615
RMS Error							0.005807
Error (Pix)							0.488
Orthophoto Resolution							0.0001

Appendix 4.2

	Run 1	Run 2	Run 3	Run 4	Run 5	Run 6	Run 7
Post dam break 3 - Halogen lighting							
Number of images							269
Focal Length (mm)							26
f-Stop							5.6
Exposure time (sec)							1/500 sec
ISO							200
Sparse cloud points							166836
Dense cloud points							103178033
RMS Error (m)							0.006187
Error (Pix)							0.488
DEM Resolution (m)							0.0002

Appendix 4.2

	Run 1	Run 2	Run 3	Run 4	Run 5	Run 6	Run 7
Post dam break 3 - UV lighting							
Number of images							268
Focal Length (mm)							26
f-Stop							5.6
Exposure time (sec)							2.5 sec
ISO							200
Sparse cloud points							140322
Dense cloud points							103677521
RMS Error							0.00562
Error (Pix)							0.479
Orthophoto Resolution							0.0001

Appendix 4.3

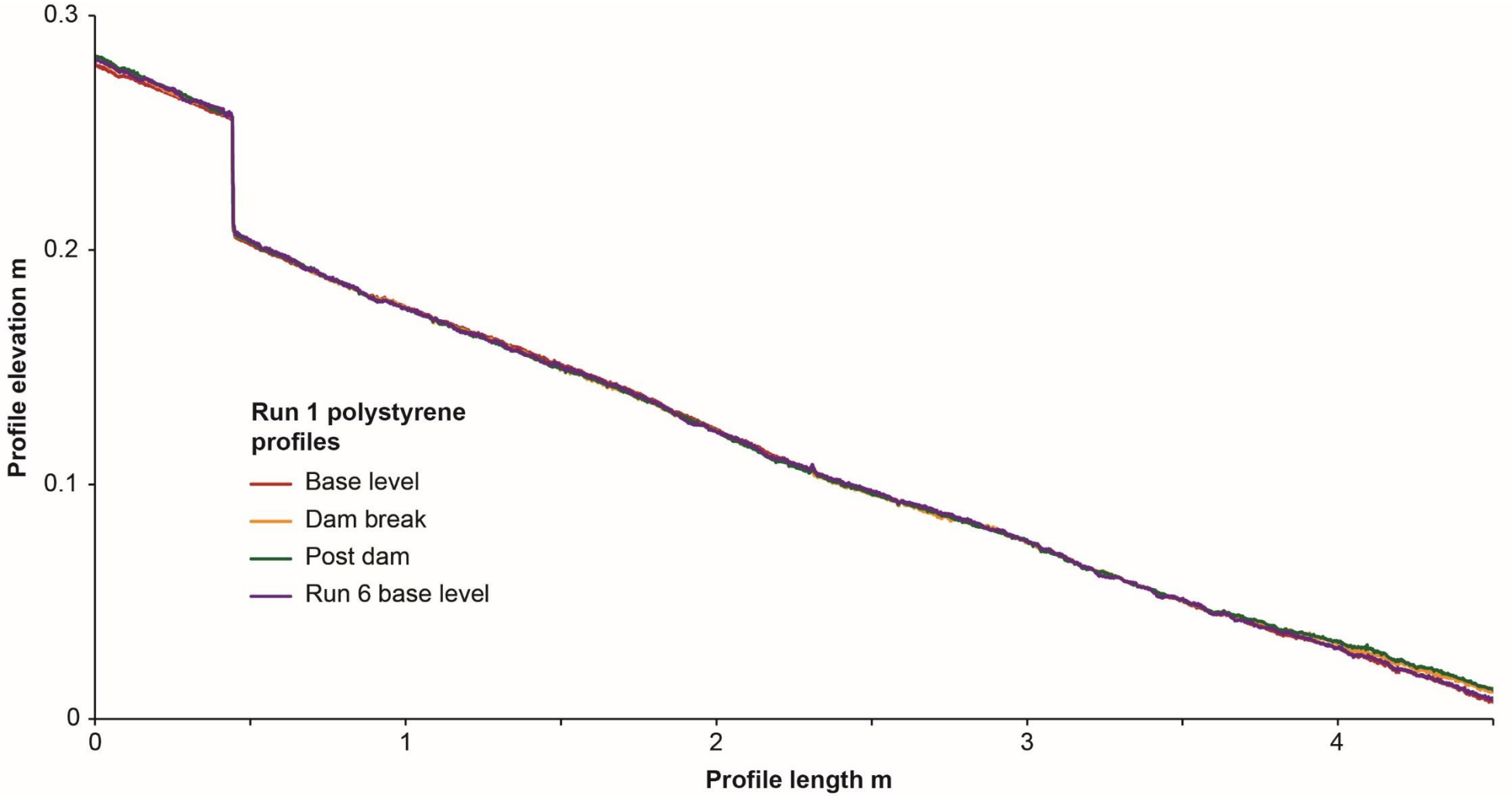

Comparison graph of a profile over the same section of polystyrene for the base level, dam break and post dam models in Run 1. The base level model for Run 6 has been added for comparison purposes as an accurate representation of the true model DEM profile.

Appendix 4.3

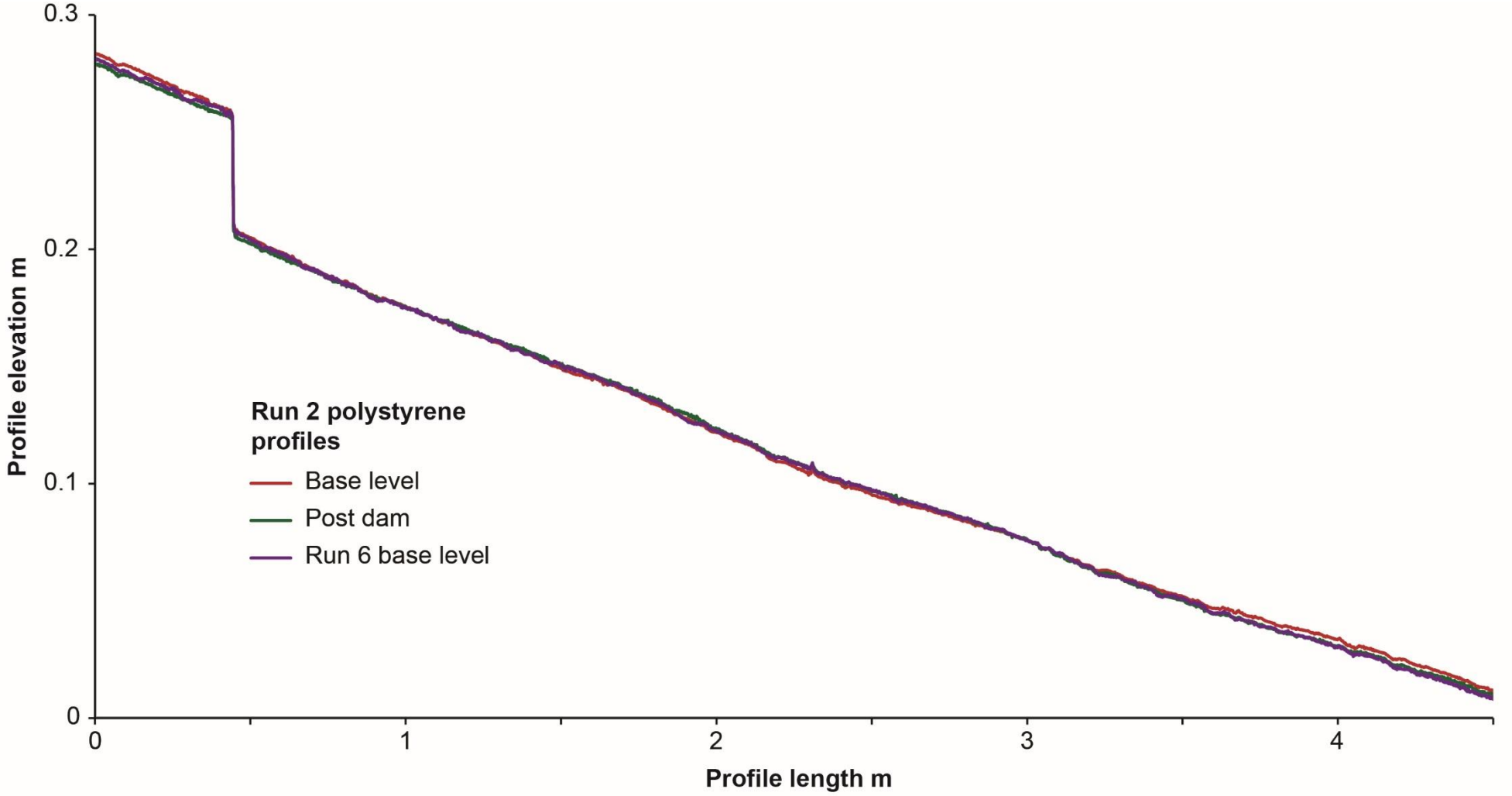

Comparison graph of a profile over the same section of polystyrene for the base level, dam break and post dam models in Run 2. The base level model for Run 6 has been added for comparison purposes as an accurate representation of the true model DEM profile.

Appendix 4.3

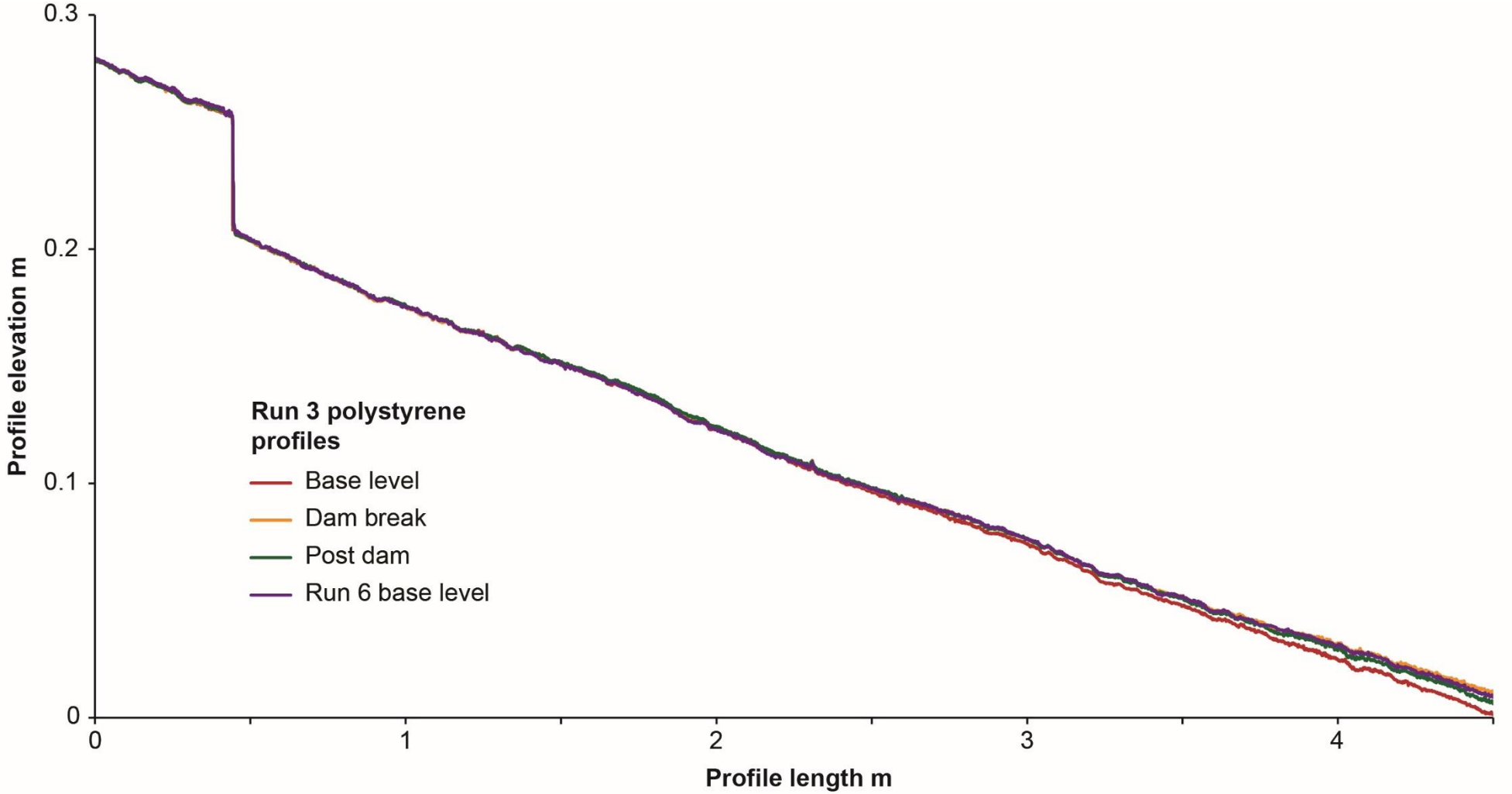

Comparison graph of a profile over the same section of polystyrene for the base level, dam break and post dam models in Run 3. The base level model for Run 6 has been added for comparison purposes as an accurate representation of the true model DEM profile.

Appendix 4.3

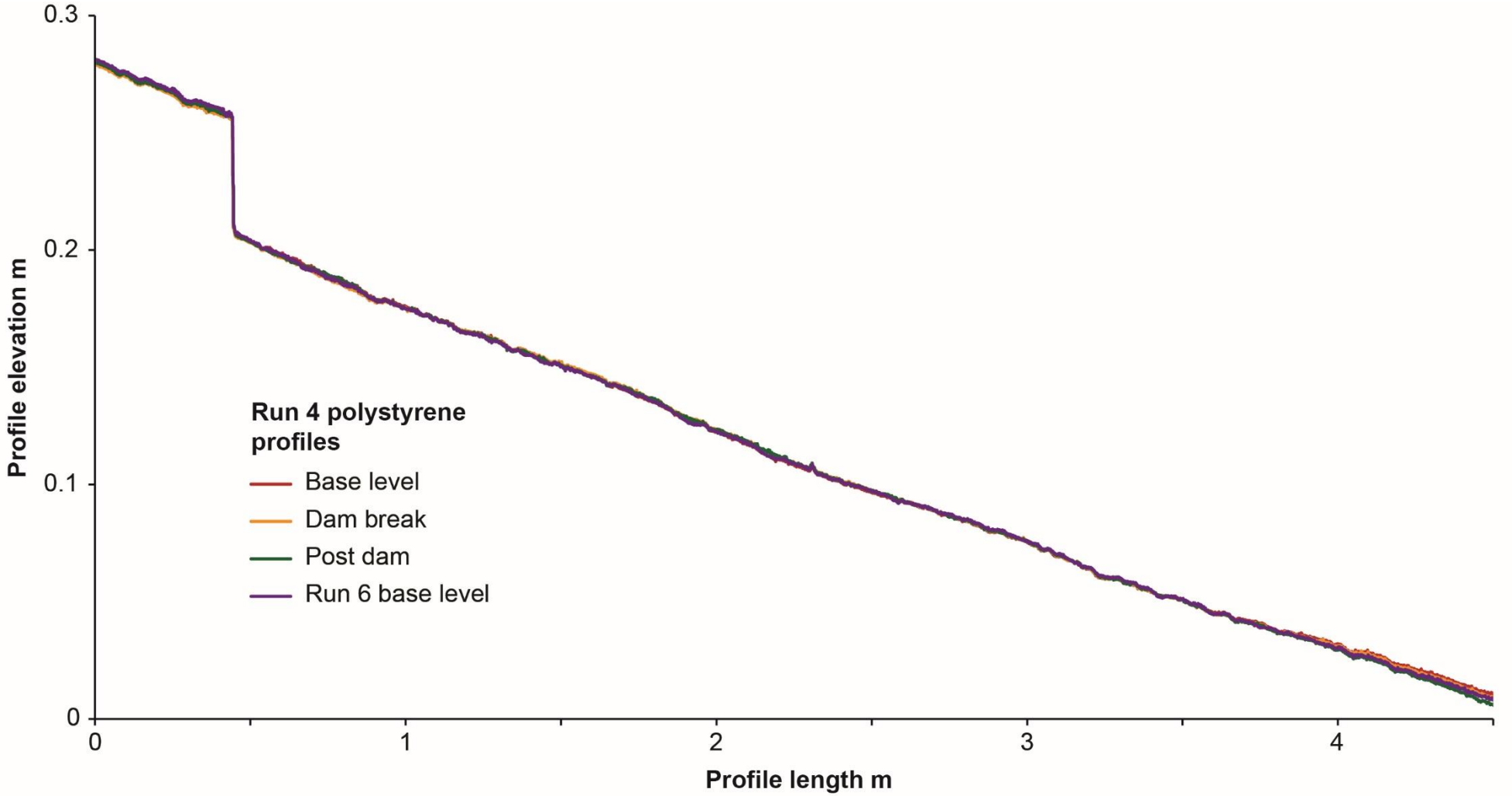

Comparison graph of a profile over the same section of polystyrene for the base level, dam break and post dam models in Run 4. The base level model for Run 6 has been added for comparison purposes as an accurate representation of the true model DEM profile.

Appendix 4.3

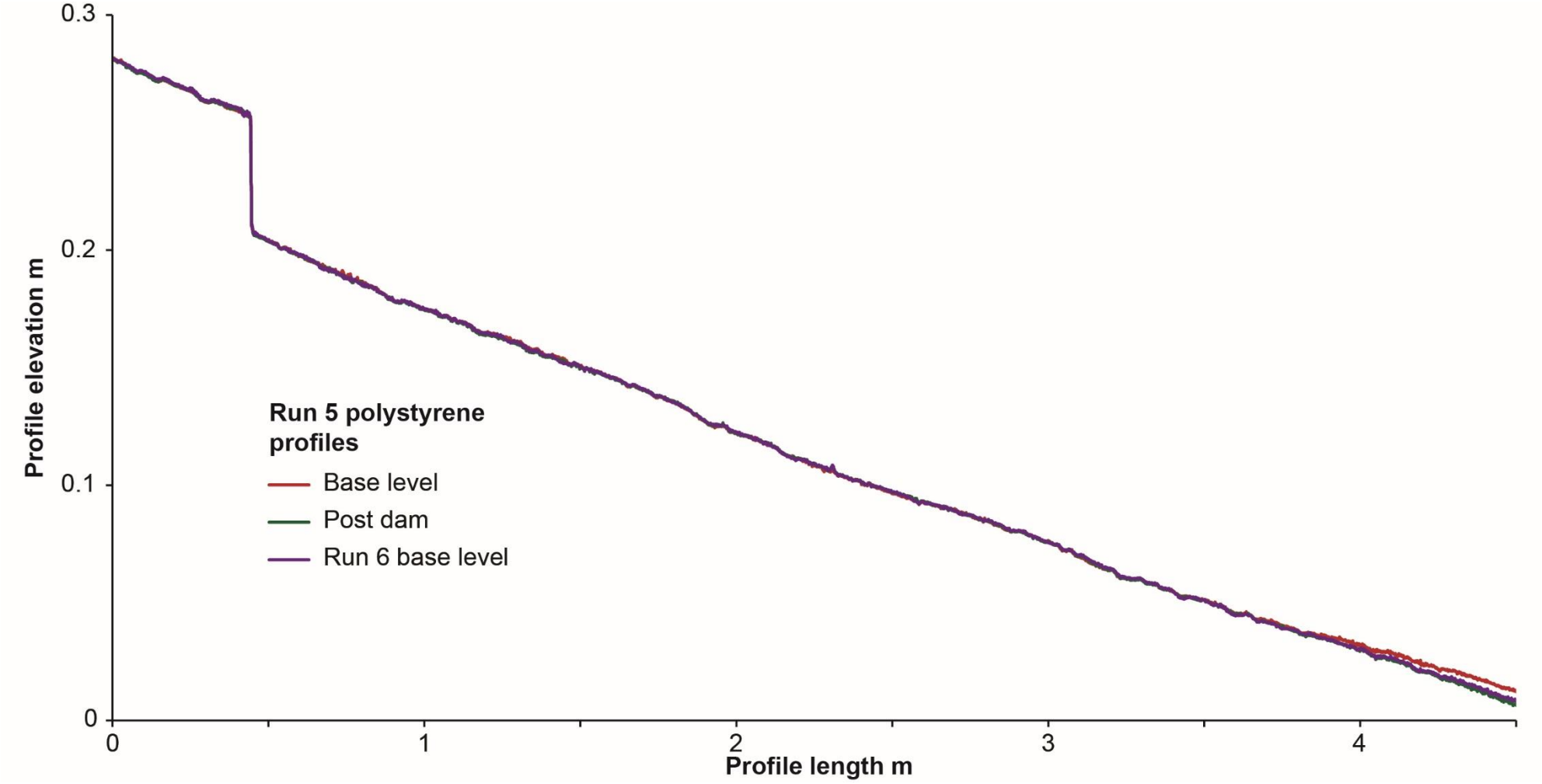

Comparison graph of a profile over the same section of polystyrene for the base level, dam break and post dam models in Run 5. The base level model for Run 6 has been added for comparison purposes as an accurate representation of the true model DEM profile.

Appendix 4.3

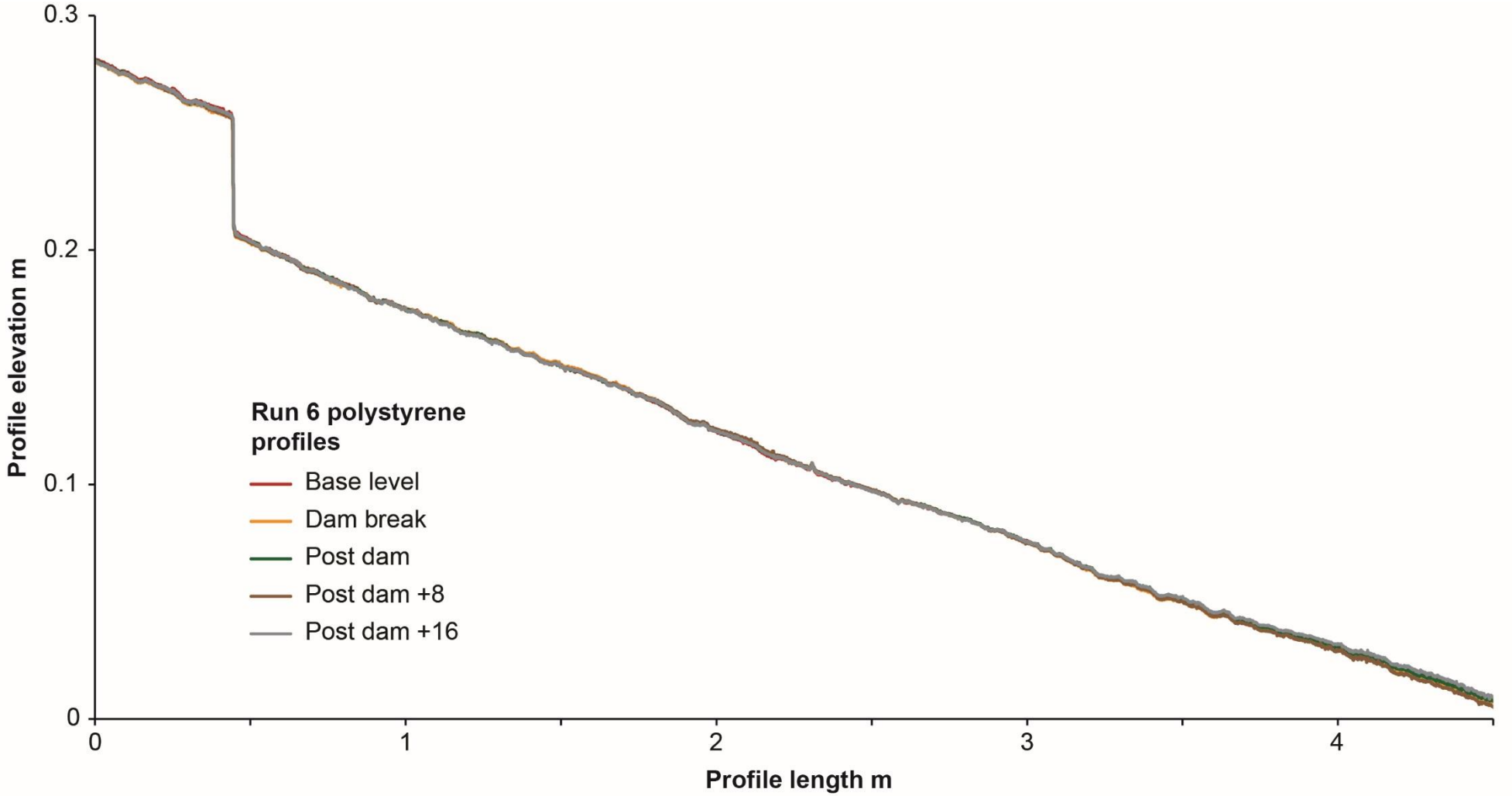

Comparison graph of a profile over the same section of polystyrene for the base level, dam break and post dam models in Run 6. Two additional post dam models are included in Run 6 as this experiment was extended to include +8 and +16 hour time-steps.

Appendix 4.4

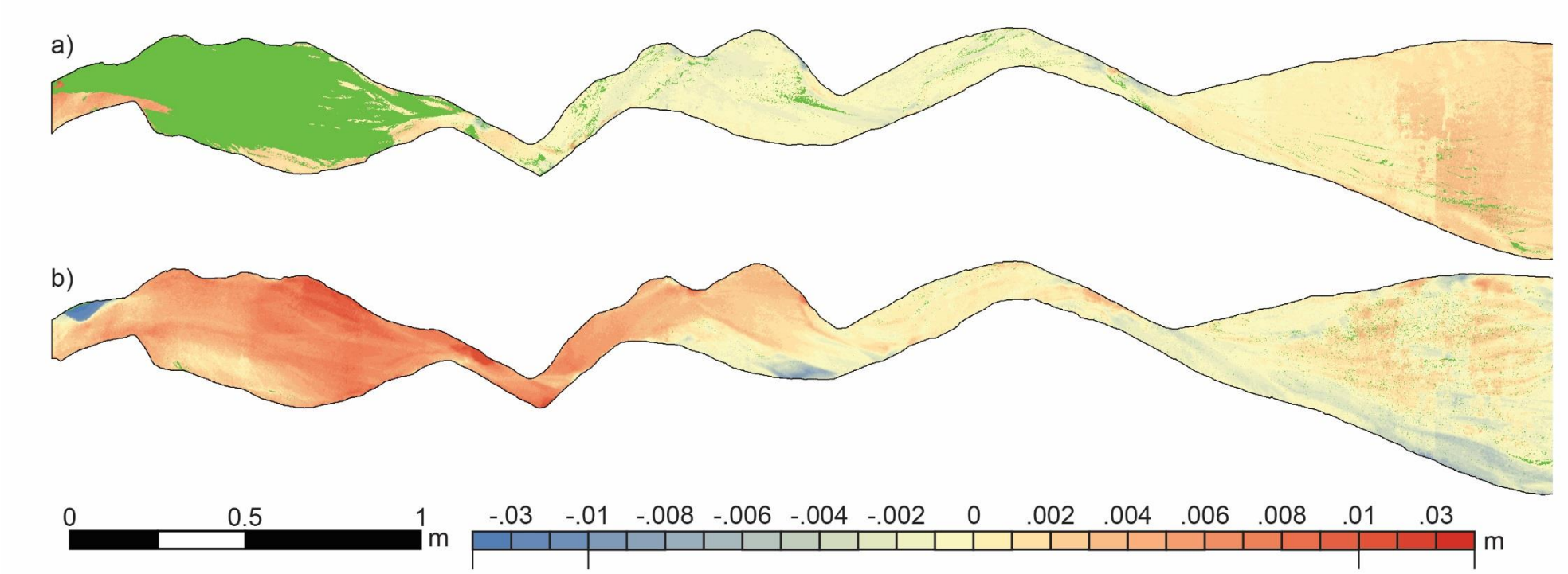

Run 1 (a) DEM of difference between the Base Level and Dam Break time-steps with UV sand locations overlain; (b) DEM of difference between Dam Break and Post Dam Break time-steps with UV sand locations overlain.

Appendix 4.4

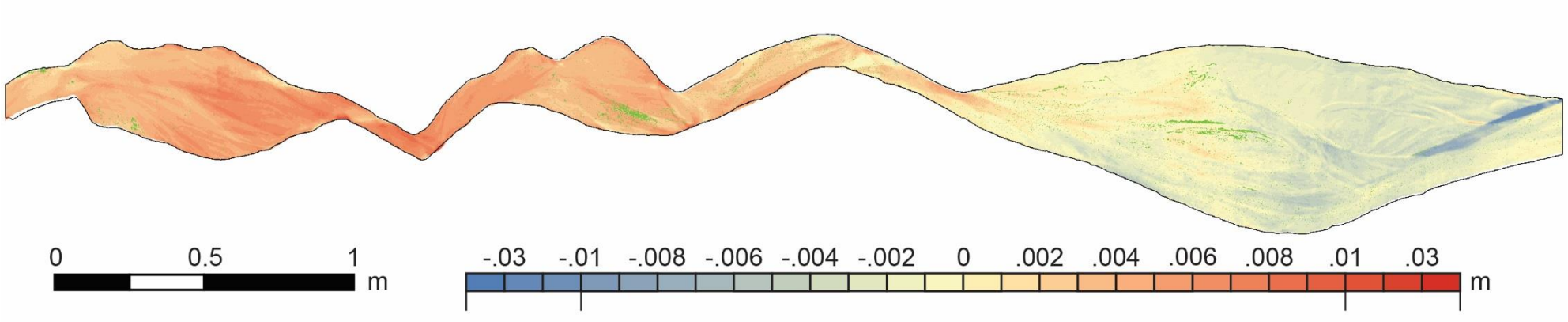

Run 2 Gross change difference model with Post Dam Break UV sand locations overlain.

Appendix 4.4

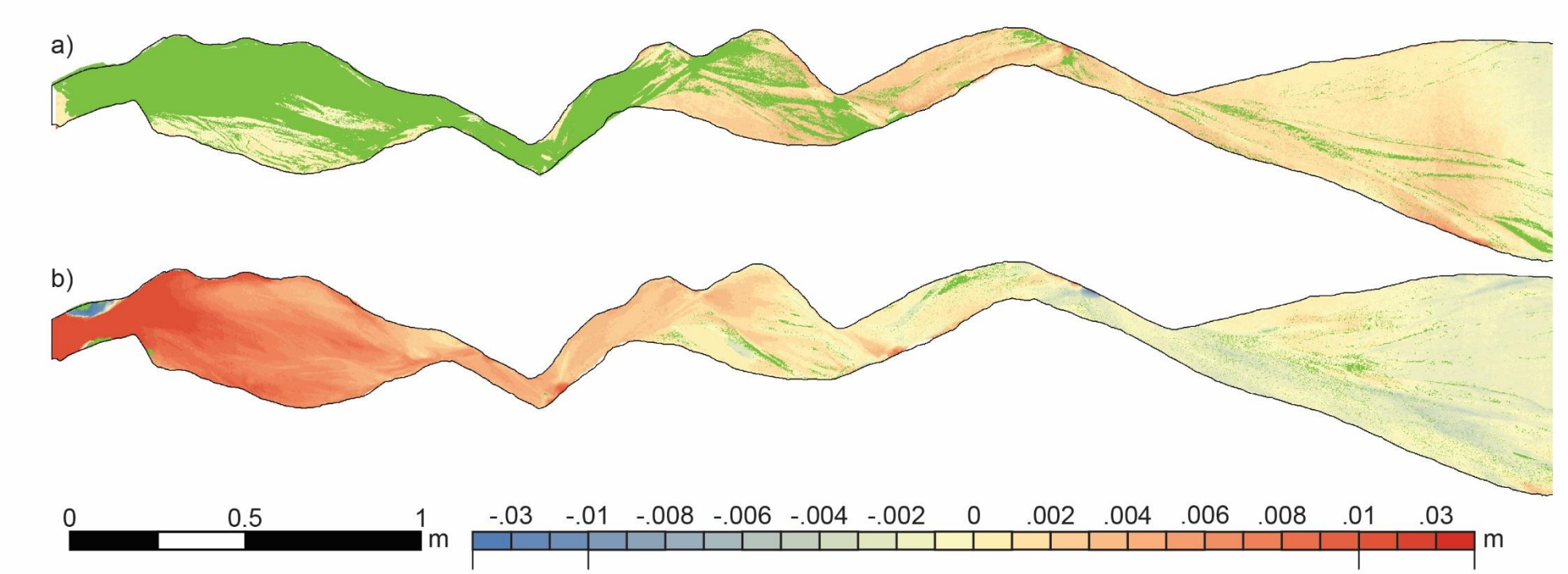

Run 3 (a) DEM of difference between the Base Level and Dam Break time-steps with UV sand locations overlain; (b) DEM of difference between Dam Break and Post Dam Break time-steps with UV sand locations overlain.

Appendix 4.4

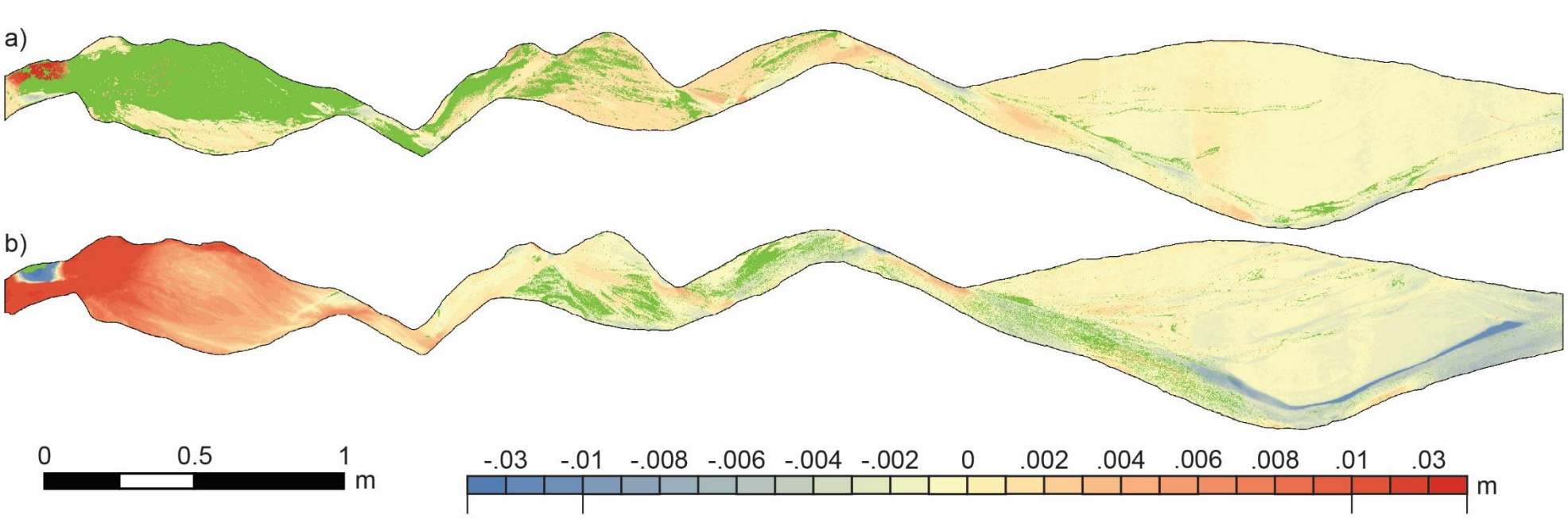

Run 4 (a) DEM of difference between the Base Level and Dam Break time-steps with UV sand locations overlain; (b) DEM of difference between Dam Break and Post Dam Break time-steps with UV sand locations overlain.

Appendix 4.4

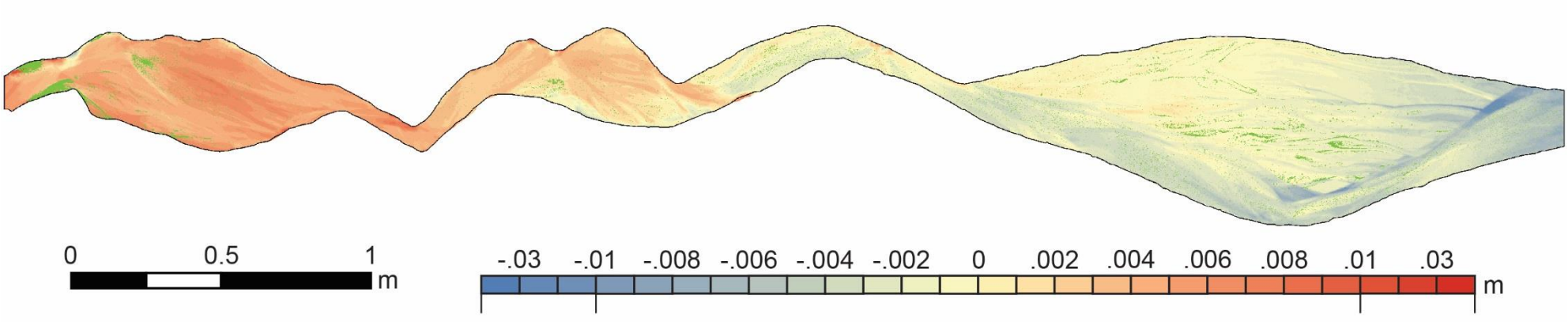

Run 5 Gross change difference model with Post Dam Break UV sand locations overlain.

Appendix 4.4

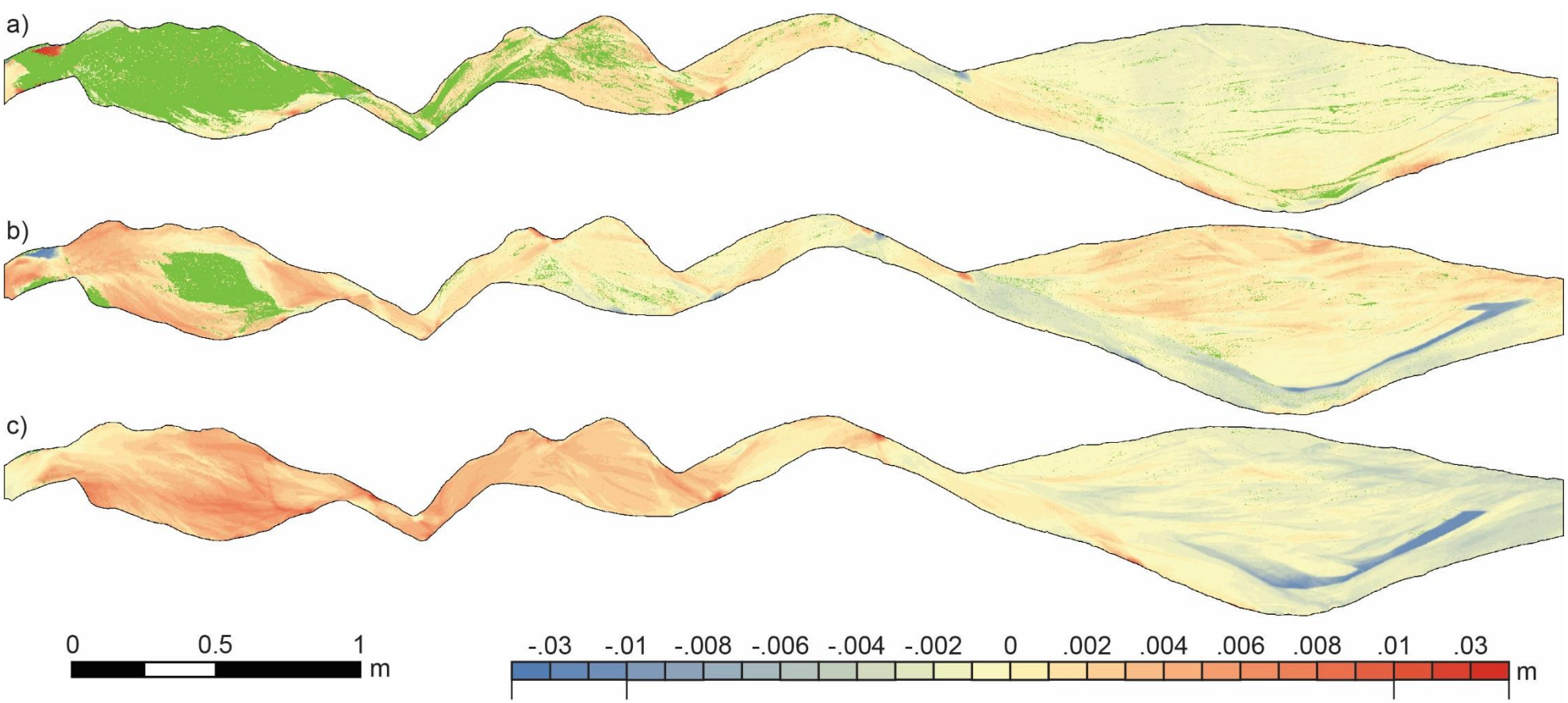

Run 6 (a) DEM of difference between the Base Level and Dam Break time-steps with UV sand locations overlain; (b) DEM of difference between Dam Break and Post Dam Break time-steps with UV sand locations overlain; (**c**) DEM of difference between the Post Dam Break and Post Dam Break +8 time-steps with UV sand locations overlain.

Appendix 4.4

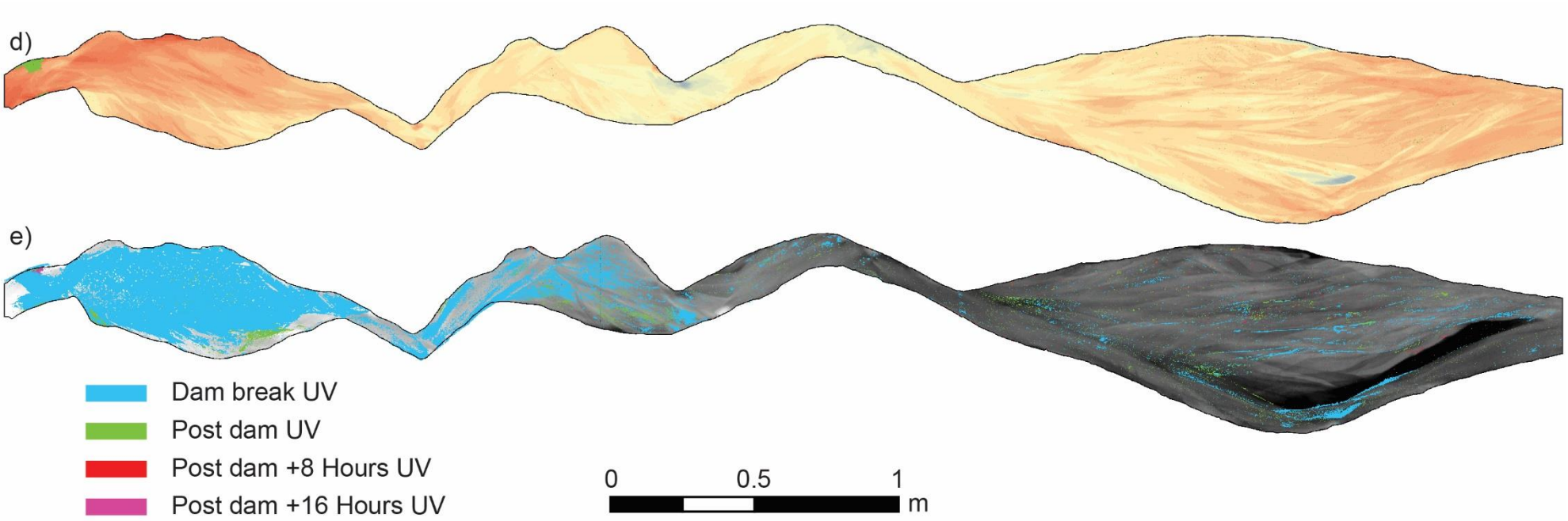

Run 6 Cont. (d) DEM of difference between the Post Dam Break +8 and Post Dam Break +16 time-steps with UV sand locations overlain. (e) Cumulative UV sand locations from all models in Run 6. The Dam Break model shows the largest dispersion of sediment and some mobilisation of UV sand occurs in the Post Dam Break phase. Very little sand is visible in the Post Dam Break +8 hours and Post Dam Break +16 models.

Appendix 4.5

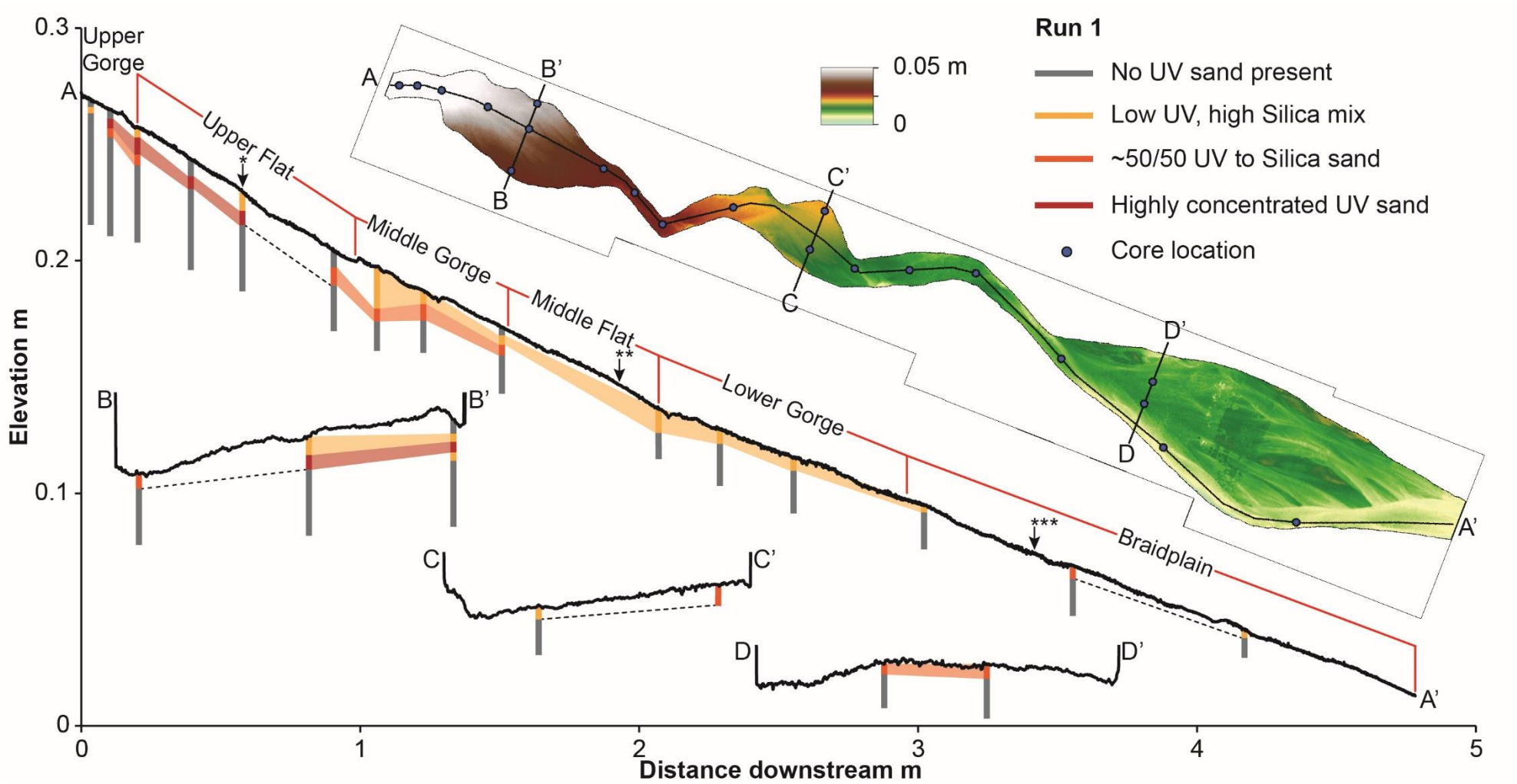

Run 1 Flume model profile with core logs after the Post Dam Break time-step. Core colours indicate the concentration of UV sand within identifiable sediment layers. Vertical scale is 1:0.025, horizontal scale is 1:0.25

Appendix 4.5

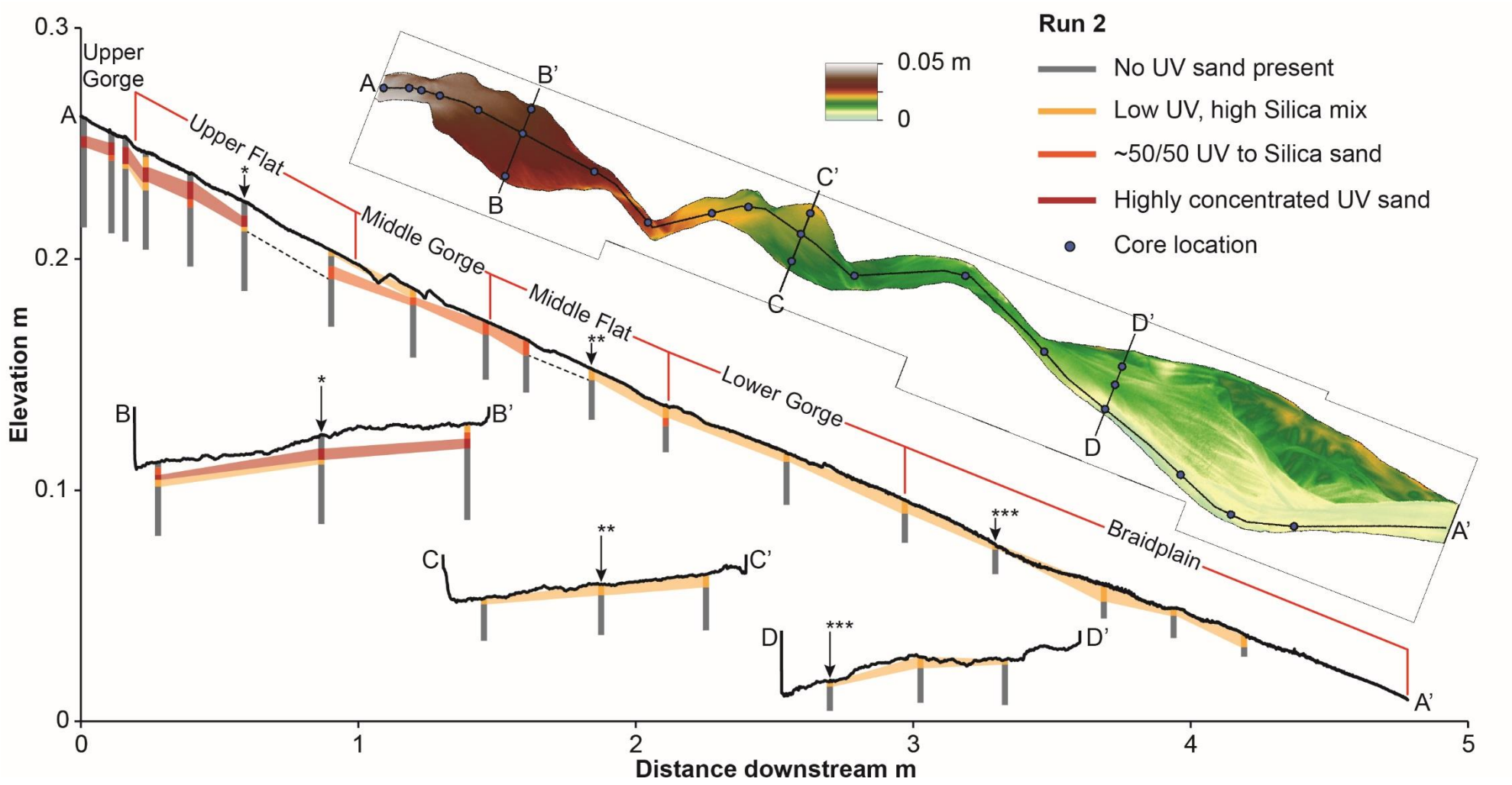

Run 2 Flume model profile with core logs after the Post Dam Break time-step. Core colours indicate the concentration of UV sand within identifiable sediment layers. Vertical scale is 1:0.025, horizontal scale is 1:0.25

Appendix 4.5

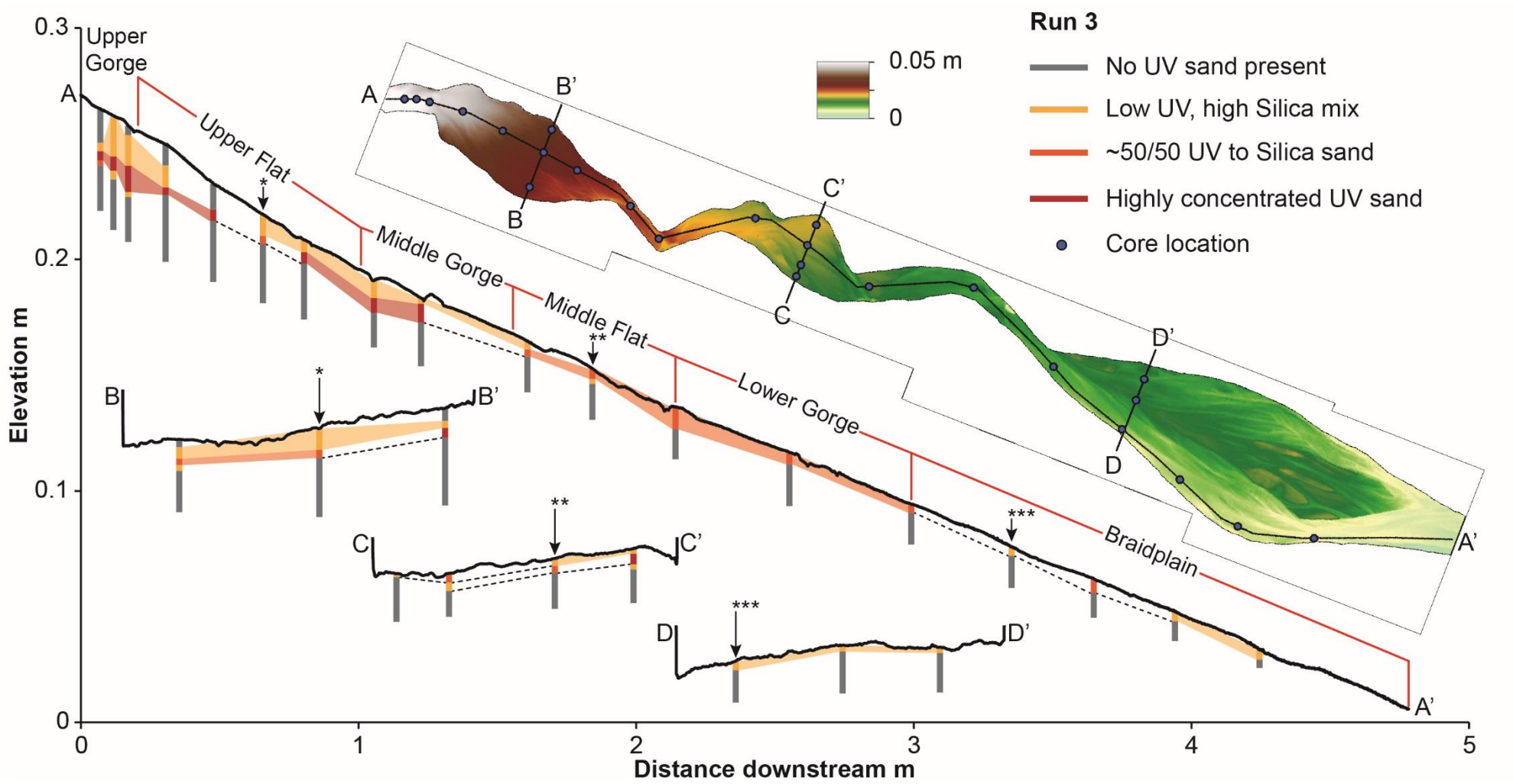

Run 3 Flume model profile with core logs after the Post Dam Break time-step. Core colours indicate the concentration of UV sand within identifiable sediment layers. Vertical scale is 1:0.025, horizontal scale is 1:0.25

Appendix 4.5

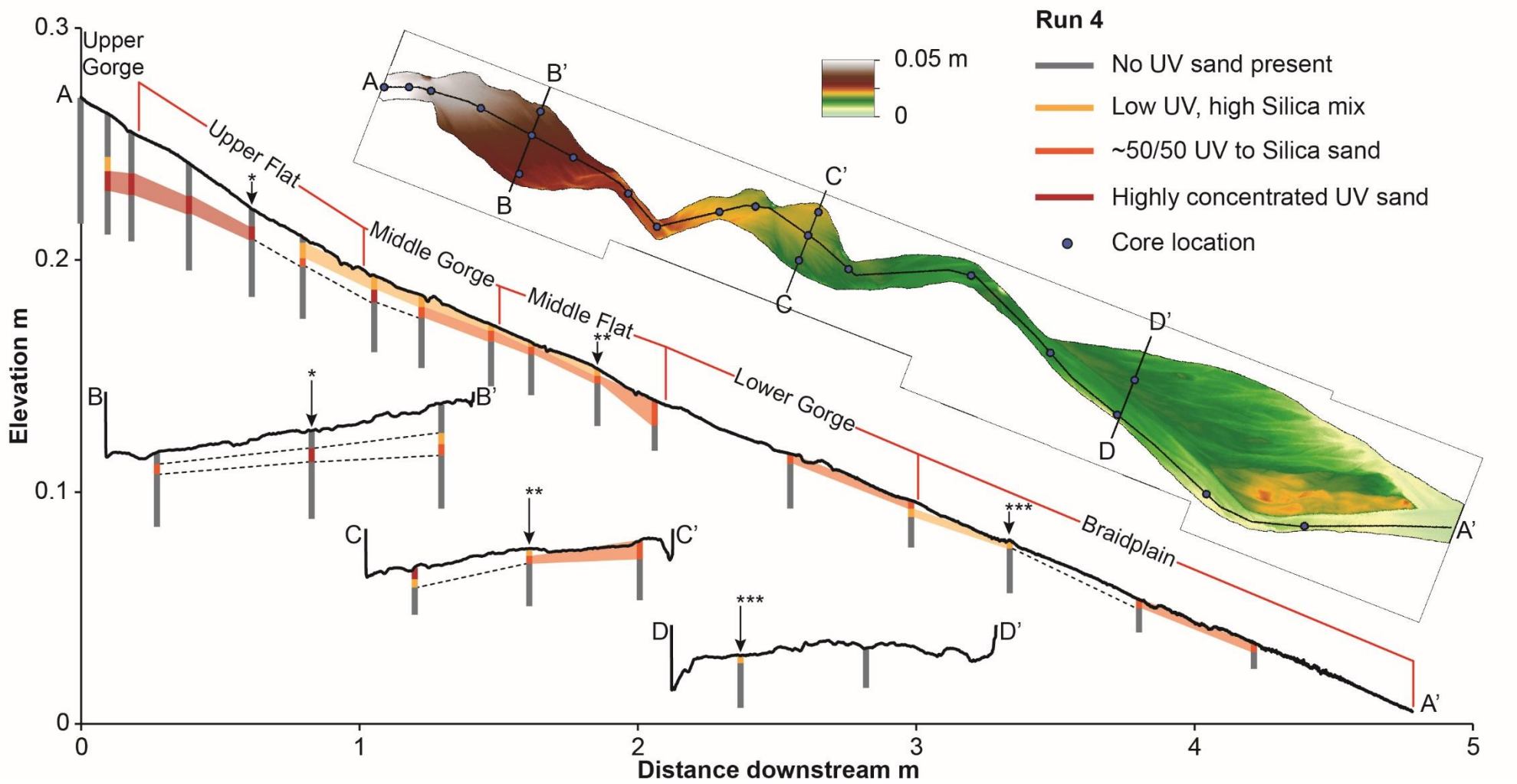

Run 4 Flume model profile with core logs after the Post Dam Break time-step. Core colours indicate the concentration of UV sand within identifiable sediment layers. Vertical scale is 1:0.025, horizontal scale is 1:0.25

Appendix 4.5

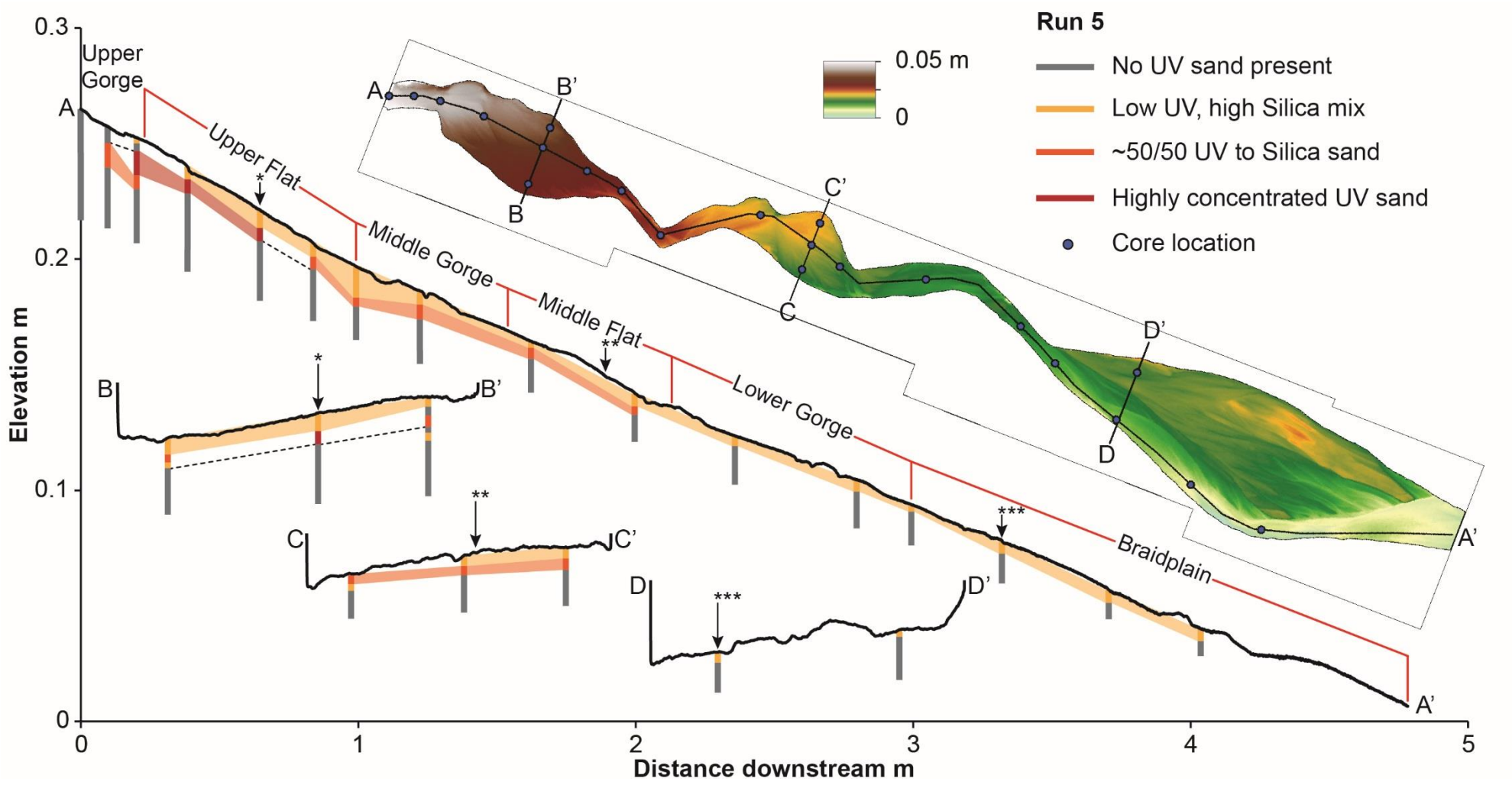

Run 5 Flume model profile with core logs after the Post Dam Break time-step. Core colours indicate the concentration of UV sand within identifiable sediment layers. Vertical scale is 1:0.025, horizontal scale is 1:0.25

Appendix 4.5

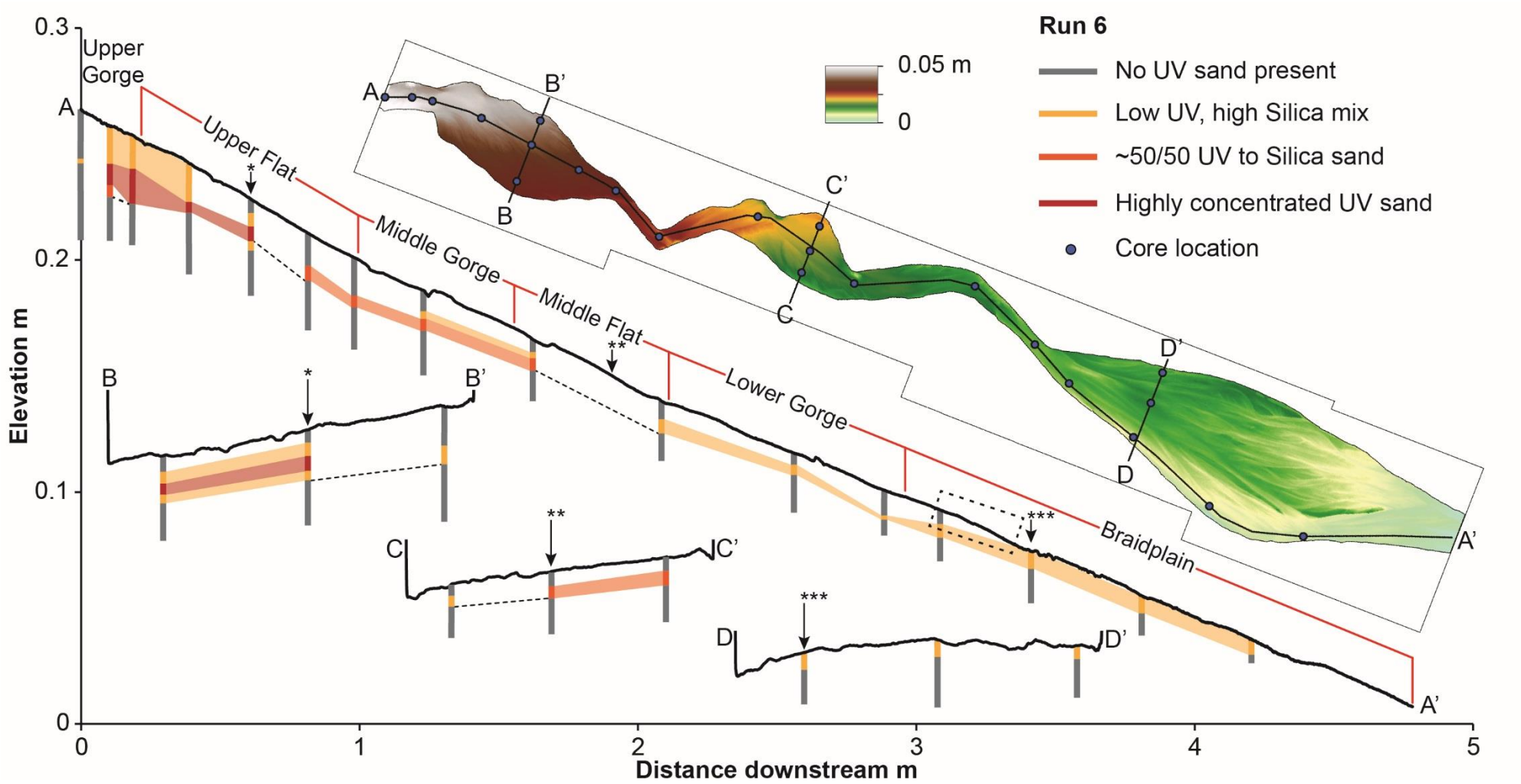

Run 6 Flume model profile with core logs after the Post Dam Break +16 time-step. Core colours indicate the concentration of UV sand within identifiable sediment layers. Vertical scale is 0.01:0.025, horizontal scale is 0.01:0.25. The dashed box indicates the front of the aggradational sediment slug.

Appendix 4.6

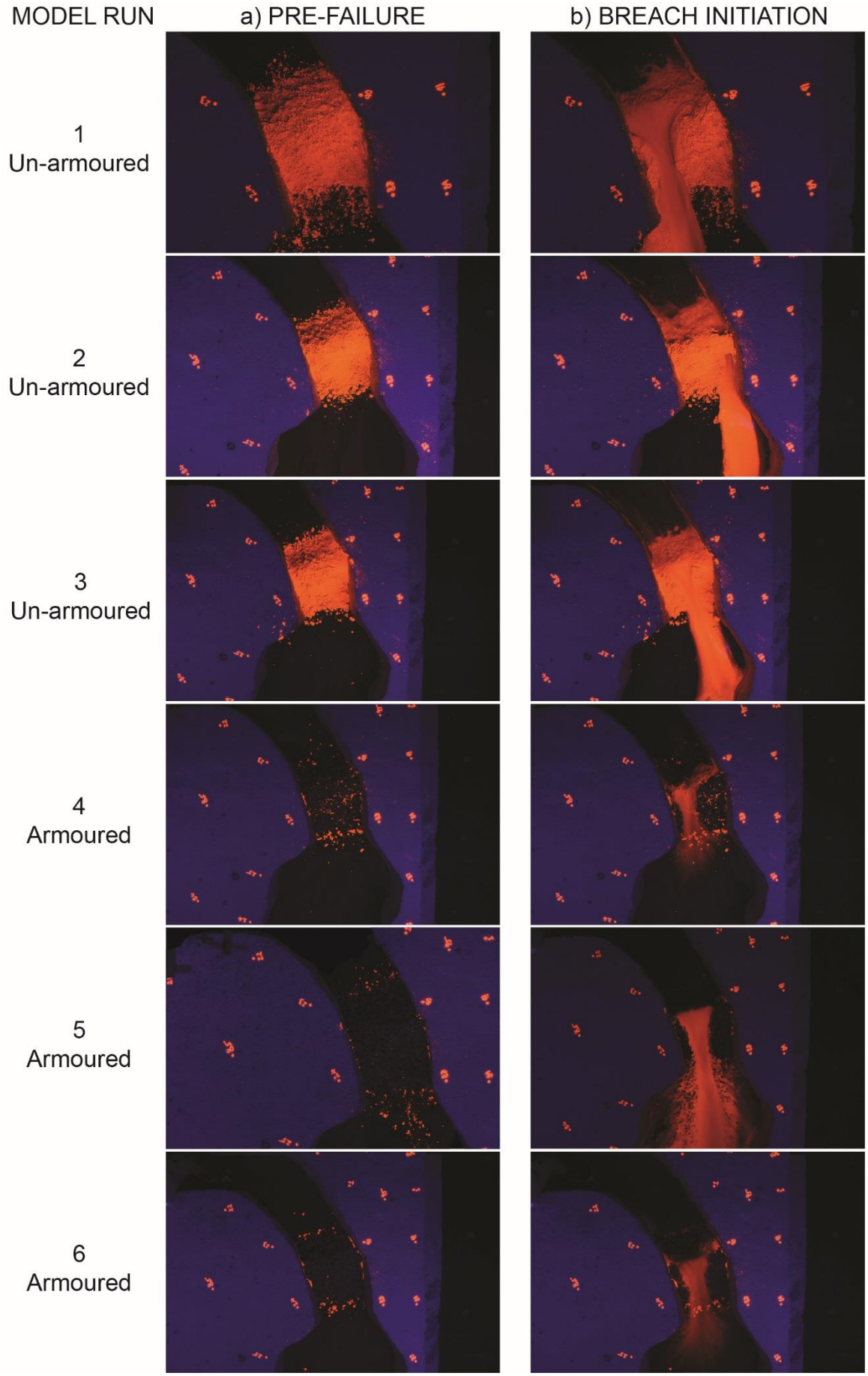

Comparisons of (**a**) model dams and (b) dam breach initiation from Runs 1-6 under UV illumination

Appendix 4.6

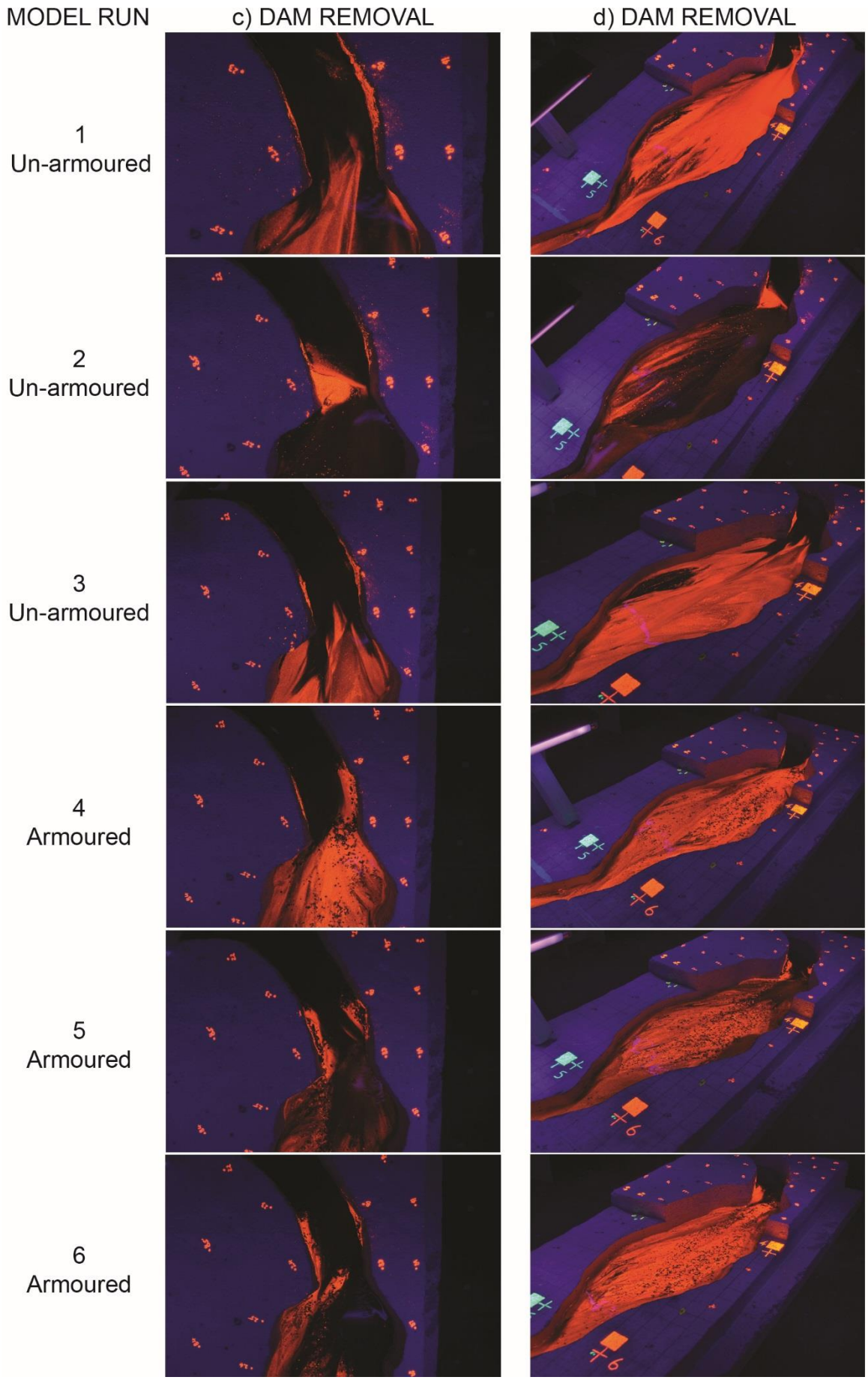

Comparisons of (c) model dam removal and (d) dam removal within the context of the Upper Flat from Runs 1-6 under UV illumination.

Appendix 4.6

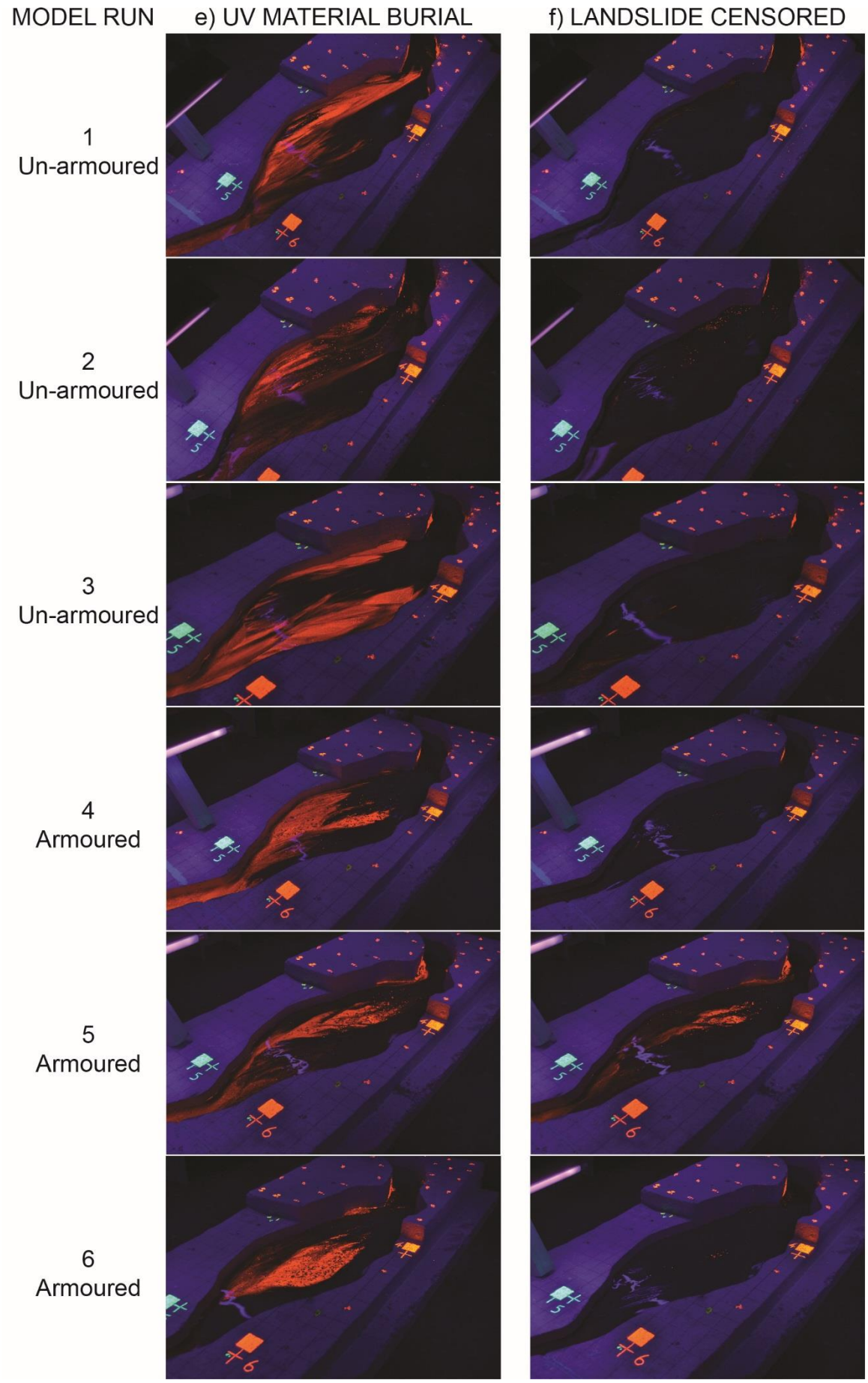

Comparisons of (e) landslide material burial and (f) dam censoring within the context of the Upper Flat from Runs 1-6 under UV illumination.